BNL 52361
(REV. 10/95)
UC-406
UC-510

SEISMIC DESIGN AND EVALUATION GUIDELINES FOR THE DEPARTMENT OF ENERGY HIGH-LEVEL WASTE STORAGE TANKS AND APPURTENANCES

K. Bandyopadhyay, A. Cornell, C. Costantino,
R. Kennedy, C. Miller and A. Veletsos*

October 1995

ENGINEERING RESEARCH AND APPLICATIONS DIVISION
DEPARTMENT OF ADVANCED TECHNOLOGY
BROOKHAVEN NATIONAL LABORATORY, ASSOCIATED UNIVERSITIES, INC.
UPTON, NEW YORK 11973-5000

Prepared for the
OFFICE OF ENVIRONMENTAL RESTORATION AND WASTE MANAGEMENT
UNITED STATES DEPARTMENT OF ENERGY
CONTRACT NO. DE-AC02-76CH00016

*Authors' names are listed in alphabetical order.

DISCLAIMER

ABSTRACT

This document provides seismic design and evaluation guidelines for underground high-level waste storage tanks. The guidelines reflect the knowledge acquired in the last two decades in defining seismic ground motion and calculating hydrodynamic loads, dynamic soil pressures and other loads for underground tank structures, piping and equipment. The application of the guidelines is illustrated with examples.

The guidelines are developed for a specific design of underground storage tanks, namely double-shell structures. However, the methodology discussed is applicable for other types of tank structures as well. The application of these and of suitably adjusted versions of these concepts to other structural types will be addressed in a future version of this document.

The original version of this document was published in January 1993. Since then, additional studies have been performed in several areas and the results are included in this revision. Comments received from the users are also addressed. Fundamental concepts supporting the basic seismic criteria contained in the original version have since then been incorporated and published in DOE-STD-1020-94 and its technical basis documents. This information has been deleted in the current revision.

TABLE OF CONTENTS

TABLE OF CONTENTS (Continued)

TABLE OF CONTENTS (Continued)

TABLE OF CONTENTS (Continued)

TABLE OF CONTENTS (Continued)

TABLE OF CONTENTS (Continued)

TABLE OF CONTENTS (Continued)

TABLE OF CONTENTS (Continued)

LIST OF TABLES

LIST OF TABLES (Continued)

LIST OF FIGURES

LIST OF FIGURES (Continued)

LIST OF FIGURES (Continued)

ACKNOWLEDGMENTS

The authors interacted with a number of individuals and organizations in the course of preparing the guidelines presented in this report. These interactions focused on the characterization of waste storage tanks, vaults and their contents; the definition of the topics to be addressed in the report; and the effect of the proposed criteria on the safety evaluation of existing tanks and the design of new tanks. The authors gratefully acknowledge the support, technical assistance and review comments received from this group. Specific contributions were received for piping criteria and tank fabrications. The following is a list of the major contributors:

John Tseng, DOE-EM
James Antizzo, DOE-EM
Howard Eckert, DOE-EM
Charles O'Dell, DOE-EM
Dinesh Gupta, DOE-EM
Jeffrey Kimball, DOE-DP
Krishan Mutreja, DOE-DP
James Hill, DOE-EH
Daniel Guzy, DOE-NS
V. Gopinath, DOE-NE
Lee Williams, DOE-ID
Sandor Silverman, DOE-ID
Ronald Rucker, DOE-ORO
Jerome Pearring, SAIC
Morris Reich
Spencer Bush
Everett Rodabaugh
Chi-Wen Lin
George Antaki
Norman Edwards
Westinghouse Hanford Co.
Westinghouse Savannah River Co.
INEL/EG&G/LINCO and Consultants
West Valley Nuclear Services and Consultants
Martin Marietta Energy Systems
Defense Nuclear Facilities Safety Board Staff and
Outside Experts

The authors also thank Walter Grossman for his dedicated effort in coordinating the report, and Marjorie Chaloupka for typing it.

CHAPTER 1

INTRODUCTION

1.1 BACKGROUND

There is a large number of high-level waste (HLW)[a] storage tanks and bins at various DOE facilities. These tanks and bins are mostly underground and contain large quantities of radionuclides. General guidelines, such as DOE Orders 6430.1A and 5480.28 (References 1.2 and 1.3), and DOE Standards 1020, 1021, 1022, 1023, 1024 and 1027 (References 1.4 through 1.9), are available for performing seismic evaluations of DOE facilities. Specific criteria are required, however, for application to the underground HLW tanks. In addition, seismic analysis procedures and acceptance criteria are needed for design of new tanks. This report has been prepared in response to these needs, and provides guidelines for seismic evaluation of existing tanks and design of new ones.

1.2 TANK FARMS

The primary purpose of the HLW tanks is to store the waste and, sometimes, support its processing for disposal. The tanks contain liquid waste of various density and viscosity levels. Underneath the liquid supernate, saturated chemicals develop "saltcakes," and settled solid particles form sludge layers.

Tanks are typically built in clusters in an area called a "tank farm." A tank farm contains a group of tanks placed side-by-side in both directions and separated from each other by a soil

---

[a]High-level waste (HLW) is defined as the highly radioactive waste material that results from the reprocessing of spent nuclear fuel, including liquid waste produced directly in reprocessing and any solid waste derived from the liquid, that contains a combination of transuranic waste and fission products in concentrations requiring permanent isolation (Reference 1.1).

barrier 15-25 feet wide. The tank structures are basically of two different designs: single-shell and double-shell. A single-shell tank is a completely enclosed cylindrical reinforced concrete structure lined with steel plates along the wetted surface (Figure 1.1). A double-shell structure consists of a steel tank enclosed within a reinforced concrete tank or vault (Figure 1.2). The steel tank contains the waste, whereas the concrete vault retains the soil pressure and may also act as a secondary confinement.

There are variations to these two basic designs. For example, instead of a domed roof, as shown in Figures 1.1 and 1.2, some tanks are designed with flat roofs supported by a single column (Figure 1.3) or a group of concentric columns (Figures 1.4 and 1.5). In one tank farm, the steel tanks containing the wastes are free-standing similar to above-ground tanks, and are enclosed by pre-cast or cast-in-situ octagonal concrete vaults (Figure 1.6). The unique details of all existing tanks are not necessarily illustrated in these figures. Moreover, the design concept of future tanks may be different. For example, in a new tank farm, the primary tanks may be built on a common footing enclosed by a large concrete vault or can have a superstructure such as a weather enclosure. In order to satisfy the confinement requirements, all new tanks are expected to be designed as double-shell structures.

The entire tank structure is covered with soil up to a depth of 10 feet. Most tanks can contain approximately one million gallons of waste. The tank diameter is in the range of 75-80 feet and the maximum height of the liquid waste is 30-40 feet. There are a few smaller tanks. For example, there are tanks with a capacity of 750,000, 300,000 or 55,000 gallons each. Tanks are interconnected with underground piping to facilitate waste transfer. Pumps, valves, monitoring instruments, cooling devices, and other equipment types are used as necessary for the

waste management.

On the other hand, bin sets are used for storage of processed granular waste such as calcined products. A bin set consists of a cluster of long steel cylinders enclosed in a partially or completely underground reinforced concrete cylindrical structure (Figure 1.7).

1.3 OVERVIEW OF SEISMIC GUIDELINES

This report presents guidelines for considering earthquake loading in the design and evaluation of HLW storage tanks. The guidelines are applicable to the primary tank, secondary liner, concrete vault, transfer piping and the other components required to maintain the confinement function of a tank farm. Certain components are specifically addressed in this report and general guidelines are provided for others. The guidelines include a definition of the design basis earthquake ground motion, simplified methods for determination of soil-structure and liquid-structure interaction effects, analytical techniques for computation of the member forces, and the structural acceptance criteria. The interpretation and use of the guidelines are illustrated through examples included in this report.

The scope and applicability of the report are discussed in Chapter 2. The guidelines are developed primarily for double-shell tanks since it is expected that all new tanks will be double-shell structures. However, these guidelines are generally applicable to single-shell tanks as well.

The general criteria are described in Chapter 3. The seismic criteria aim at achieving a desired performance goal (e.g., confinement of HLW) expressed in probabilistic terms. This performance goal is achieved by use of probabilistic seismic hazard estimates in terms of a site-specific design response spectrum. Thus, the design basis earthquake (DBE) ground motion

is determined by correlating probabilistic measures of the performance goal and the seismic hazard. Once the DBE ground motion is obtained, the remaining evaluations, such as the structural analysis and design, are based on deterministic methods. Acceptable material properties such as strength, damping and inelastic energy absorption factors are also discussed in Chapter 3. The appropriate load combinations and the corresponding acceptance criteria are also described.

The procedures for evaluating the hydrodynamic effects in tanks are described in Chapter 4. Simplified methods are presented for both rigid and flexible tanks that are excited either horizontally or vertically. Since the primary or inner steel tank for many of the double-shell tanks is supported at the top by the concrete vault structure, the response of top-constrained systems is considered in addition to that of free-standing, cantilever systems. Most of the results are for wastes that may be modeled as homogeneous and inviscid, water-like liquids of arbitrary density. However, the effects of liquid viscosity and liquid inhomogeneity are also examined.

Chapter 5 provides an approach for determining the seismic capacity of flat-bottom vertical liquid storage tanks. Formulas are presented for both anchored and unanchored tanks. Various failure mechanisms are considered for the tanks. The approach involves developing a nominal ultimate strength capacity for the tank and then applying appropriate strength reduction factors that lead to factors of safety consistent with those discussed in Chapter 3.

The criteria for the computation of the seismically induced soil pressures and of the in-vault response spectra required in the qualification of equipment are provided in Chapter 6. Both finite element and simplified methods are described for the evaluation of the soil-structure interaction effects.

The chapters referred to above deal with the response of the tank-vault system. Evaluation guidelines for underground transfer piping are provided in Chapter 7. Guidelines for assessing the potential for liquefaction are also included in this chapter.

Seismic qualification of equipment is discussed in Chapter 8. The available approaches are described and the applicable standards are cited. The qualification level required to satisfy the general seismic criteria presented in Chapter 3 is also addressed.

The supporting technical information that was used in the development of the guidelines or that is useful for their implementation is presented in the appendices. Appendix A provides guidance for estimating the inelastic energy absorption factor. Appendix B examines the infuence of liquid viscosity on the hydrodynamic effects considered in Chapter 4. Appendix C provides membrane solutions for top-constrained tanks subjected to some simple distributions of loading, and Appendix D examines the effects of the sloshing liquid impacting the roof of tanks with inadequate freeboard. The dimensional tolerance and construction details used in the tank seismic capacity calculations are presented in Appendix E. The information on buckling of cylindrical tanks presented in Chapter 5 is further supported in Appendix F by experimental data for more realistic estimation of the tank strength. The application of the guidelines for the computation of the seismic response and capacity of the tank is illustrated by an example in Appendix G. Appendix H elaborates on the lumped parameter soil-structure interaction method presented in Chapter 6 and provides a set of factors required in the implementation of the analysis. Appendix I contains an example of an analysis of an underground double-containment piping system for pressure, deadweight, thermal expansion, natural soil settlement and seismic loads.

The pipe follows a straight line between two tanks and contains expansion loops to accomodate thermal expansion in service.

1.4 NOTATION

A special effort was made in the preparation of this report to use notation consistent with that commonly used in the technical literature, particularly in national codes and standards. However, because of the wide range of topics covered and the large number of parameters involved, the use of a unique set of symbols did not prove practical for the entire report. As a result, some of the symbols used have different meanings in different chapters. The various symbols are defined where first introduced in the text, and are also summarized at the end of each chapter. Symbols used only in the sections in which they are introduced are not included in the notation lists.

REFERENCES

1.1 DOE Order 5820.2A, "Radioactive Waste Management," September 1988, Attachment 2, Definitions.

1.2 DOE Order 6430.1A, "General Design Criteria," April 1989.

1.3 DOE Order 5480.28, "Natural Phenomena Hazards Mitigation," January 1993.

1.4 DOE-STD-1020-94, "Natural Phenomena Hazards Design and Evaluation Criteria for Department of Energy Facilities," April 1994.

1.5 DOE-STD-1021-93, "Natural Phenomena Hazards Performance Categorization Guidelines for Structures, Systems, and Components," July 1993.

1.6 DOE-STD-1022-94, "Natural Phenomena Hazards Site Characterization Criteria," March 1994.

1.7 DOE-STD-1023-94, "Natural Phenomena Hazards Assessment Criteria," Draft, May 1995.

1.8 DOE-STD-1024-92, "Guidelines for Use of Probabilistic Seismic Hazard Curves at Department of Energy Sites," December 1992.

1.9 DOE-STD-1027-92, "Hazard Categorization and Accident Analysis Techniques for Compliance with DOE Order 5480.23, Nuclear Safety Analysis Reports," December 1992.

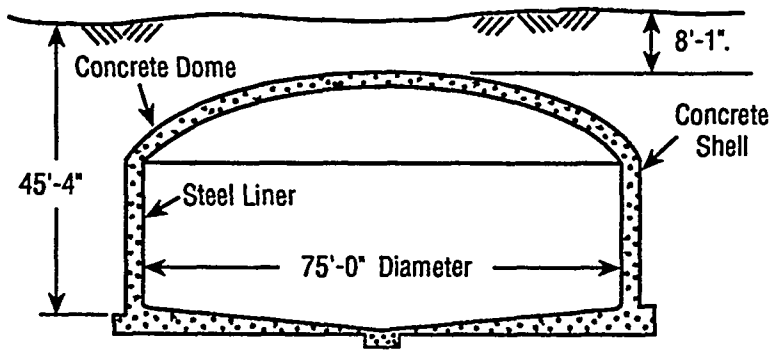

Figure 1.1 A Typical Single-Shell Tank

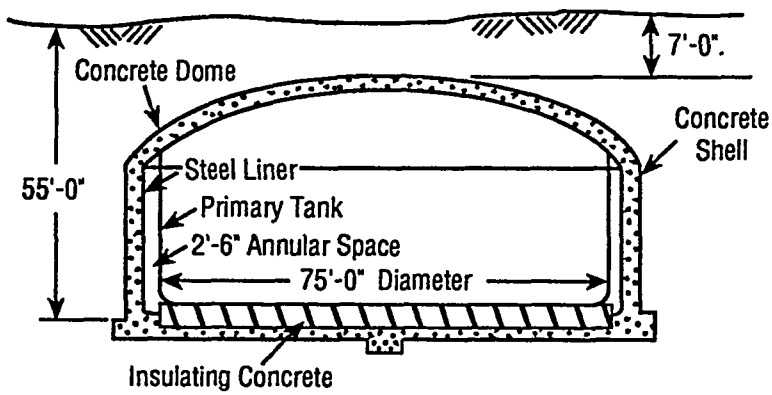

Figure 1.2 A Typical Double-Shell Tank

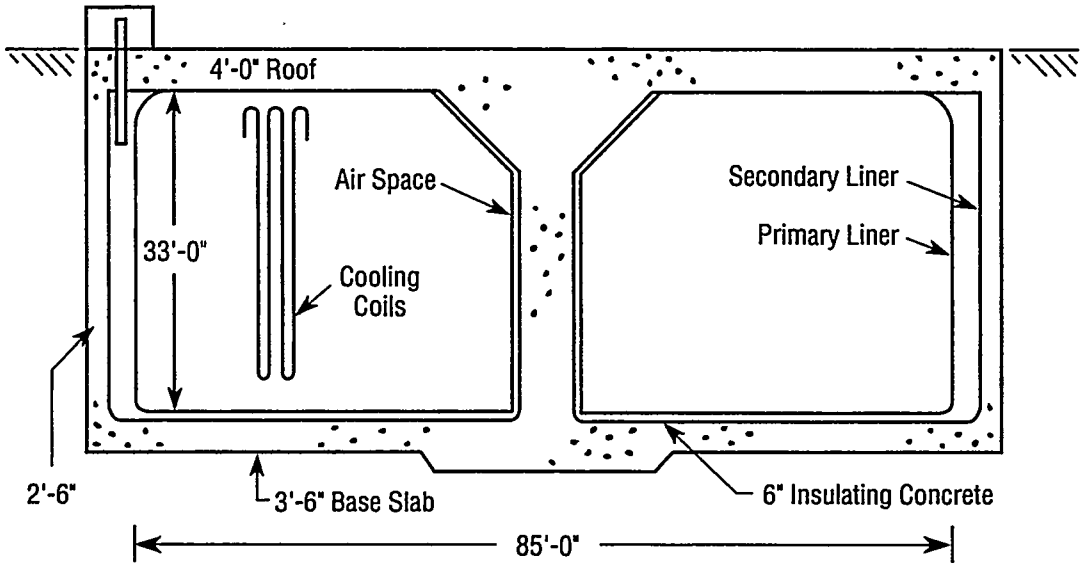

Figure 1.3 Tank with a Central Column

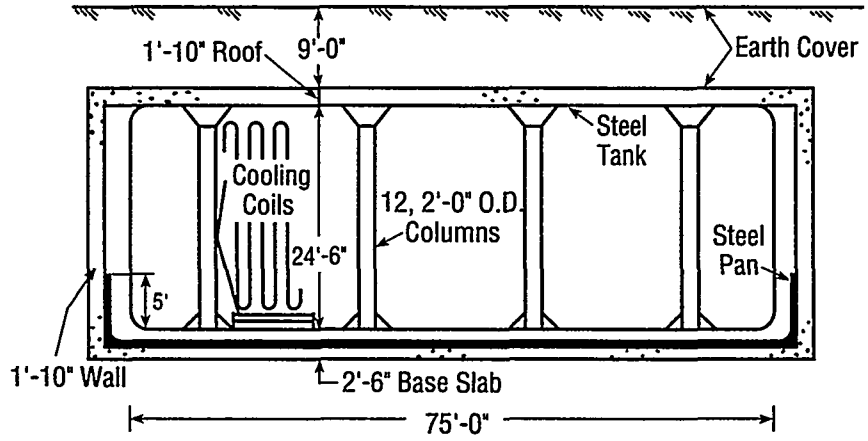

Figure 1.4 Tank with Concentric Columns

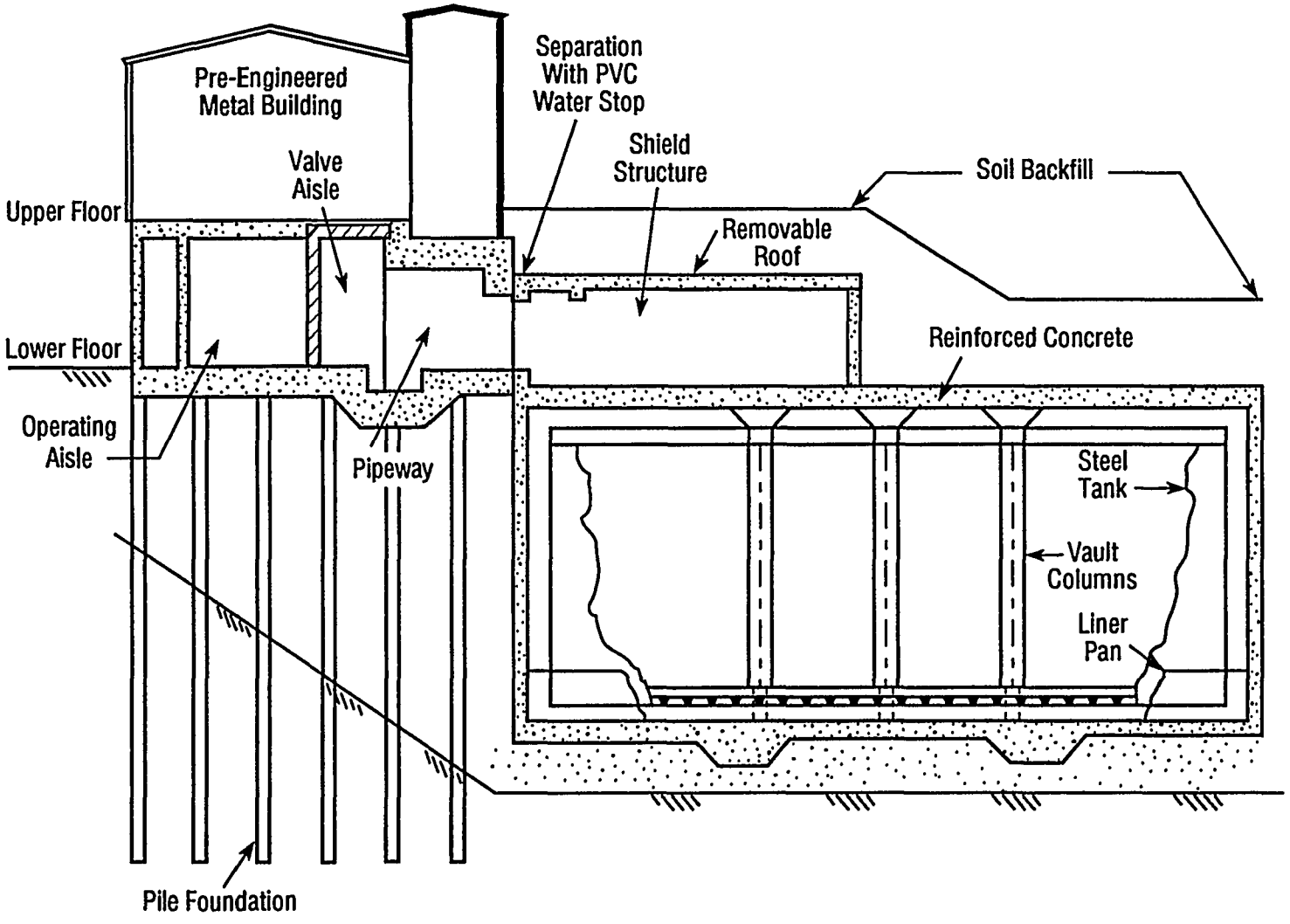

Figure 1.5 Tank with Concentric Columns and Other Superstructures

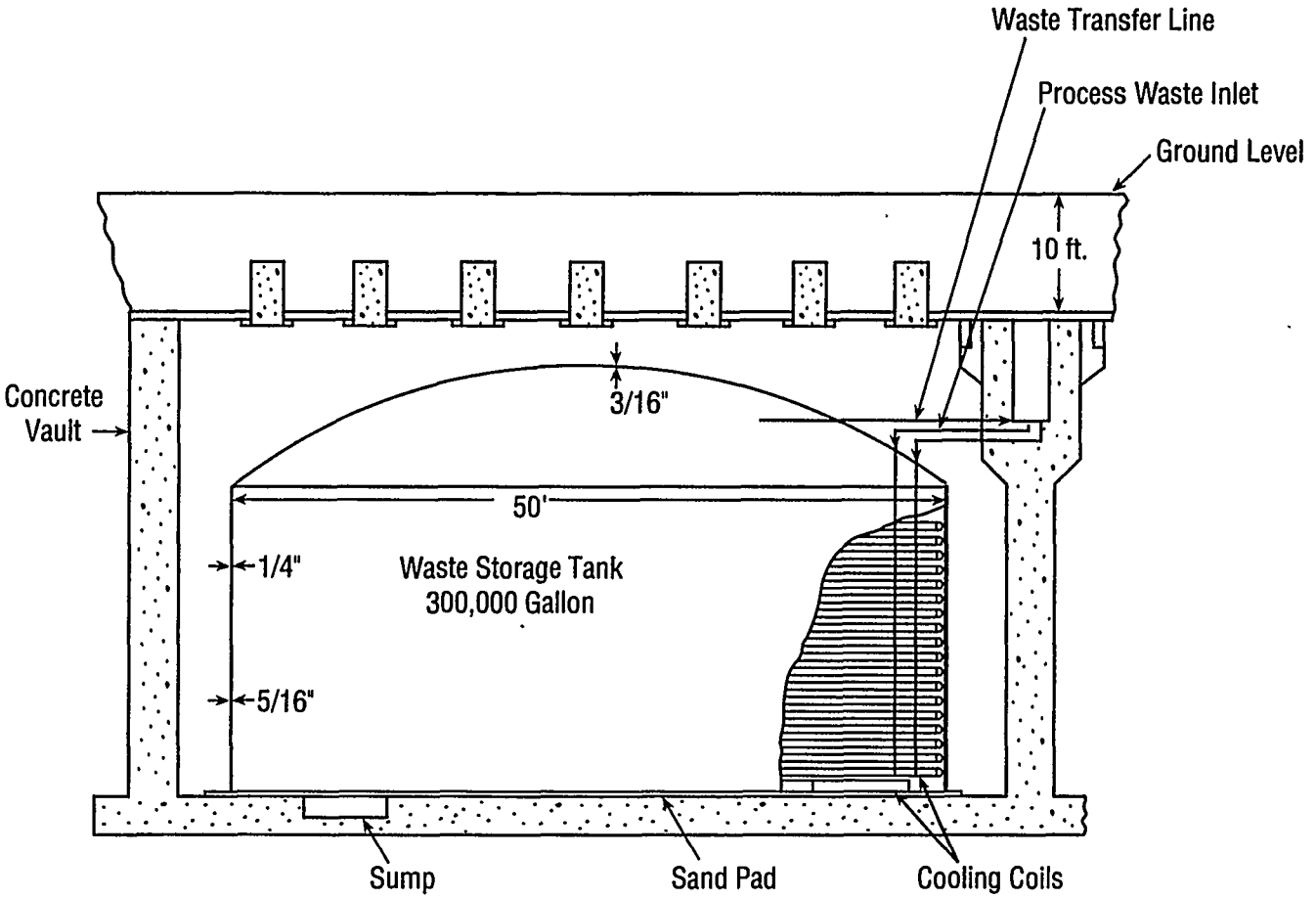

Figure 1.6 Free Standing Tank

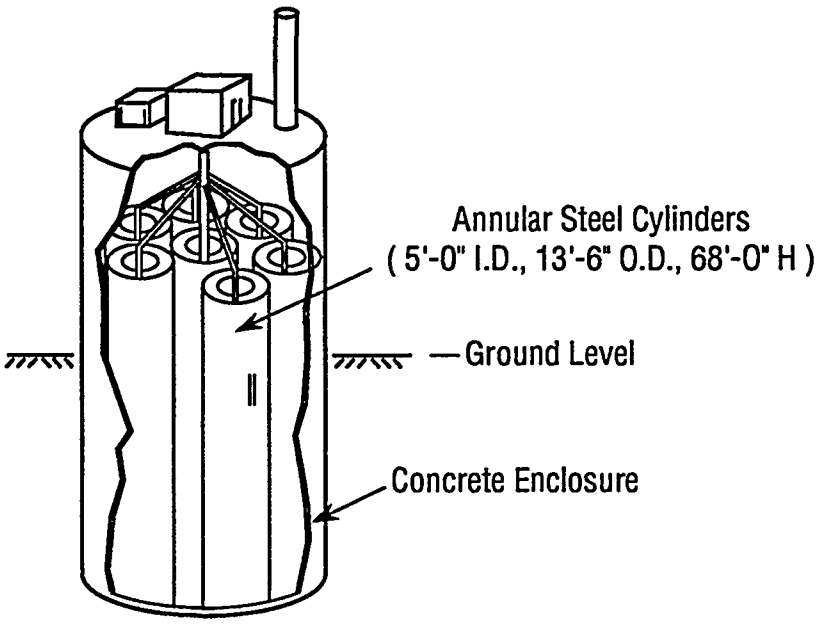

Figure 1.7 A Typical Bin Set

CHAPTER 2

SCOPE AND APPLICABILITY OF GUIDELINES

2.1 INTRODUCTION

The seismic design and evaluation guidelines for high-level waste (HLW) storage facilities presented in this report are based partly on previously available information and partly on the results of supplementary new studies. National codes and standards, NRC Regulatory Guides and Standard Review Plans, and DOE Orders and Standards have been consulted in this regard. This document is consistent with DOE Order 6430.1A (Reference 2.1) that provides a set of general design criteria for the DOE facilities and with DOE-STD-1020 (Reference 2.2) that provides guidelines for design and evaluation of DOE facilities due to earthquakes and other natural hazards such as wind and flood. Additionally, the graded approach promulgated in DOE Order 5480.28 (Reference 2.3) and DOE-STD-1020 has also been used and expanded in the formulation of the information presented here. Other analysis methods, design details and acceptance criteria delineated in DOE-STD-1020, DOE-STD-1024 (Reference 2.4), ASME Code Section III (Reference 2.5), ASCE 4-86 (Reference 2.6), AISC Manuals (References 2.7 and 2.8), NRC SRP Section 3.7 (Reference 2.9), ACI 349 (Reference 2.10) and similar documents have been used to the extent they are applicable to the topics considered.

2.2 SCOPE

This section identifies the principal elements of the HLW storage facilities covered by the guidelines, and highlights the assumptions and approximations made in the evaluation of their dynamic response so that the reader may judge the range of applicability of the information presented.

The facility elements examined include the tank-waste system,

the vault-soil system, and the underground piping. The assumptions and approximations made relate to the geometries, support conditions, and relative flexibilities of the tank and vault, and to the properties of the retained waste. In the formulation of these guidelines, a special effort has been made to ensure that they apply to most HLW storage facilities of interest. This matter is discussed further at the end of this section.

2.2.1 Tank-Waste System

The evaluation of the seismic response of the tank-waste system requires consideration of the dynamics of the retained waste and of its interaction with the flexible tank.

In the commonly used method of analysis for this problem, the tank is modeled as a free-standing, fixed-based, flexible, circular cylinder, and the waste is modeled as a homogeneous and inviscid liquid. The actual tank-waste system may differ from this description in several respects:

- The tank may not be free-standing, but supported at the top by the surrounding vault. As part of the work leading to the formulation of the guidelines, existing methods of analysis and computer programs have been generalized to account for the effects of the top constraint. The hydrodynamic pressures and associated forces are evaluated both for free-standing, cantilever tanks and for top-constrained tanks. Additionally, both fully filled and partially filled systems are examined.

- The tanks in most HLW facilities are not anchored at the base and may, therefore, slide and/or uplift during intense ground shaking. Although evaluated on the assumption of an anchored base, the results presented are believed to be sufficiently accurate for the class of tanks considered. Two factors justify this conclusion: (1) For the tank

dimensions of interest, the frictional resistance at the tank base is normally sufficient to prevent sliding; and (2) the specified stress acceptance criteria for the tank preclude uplifts of a sufficiently large magnitude to significantly affect the hydrodynamic effects computed on the assumption of an anchored base. Furthermore, although the effects of base uplifting are not included in the evaluation of the dynamic response of the tank-liquid system, they are considered in the evaluation of the tank capacity.

- The representation of the waste as an inviscid liquid may not be appropriate. Viscous wastes would be expected to manifest higher damping, lower sloshing mode response, and larger impulsive mode responses, thereby reducing the slosh heights and increasing the dynamic liquid pressures over those developed by inviscid wastes for a given seismic input.

  The effects of liquid viscosity are examined in Appendix B, where it is shown that for viscosity values up to 10,000 centipoise, the hydrodynamic effects induced by earthquake ground motions in tanks of the dimensions found in HLW facilities are essentially the same as for inviscid liquids. Accordingly, the solutions for the inviscid liquids presented in this report can be used as reasonable approximations for most viscous liquids of interest.

- The wastes in HLW tanks may not be of uniform density due to the settling of solid particles and the precipitation of chemicals. The hydrodynamic effects in tanks storing an inhomogeneous liquid with a layered or continuous variation in density have been studied only recently, and the method of analysis for these systems has not yet been reduced to the simplicity level of the corresponding method for a homogeneous liquid. A summary of the available information

on the subject, along with a technique for simplifying a major step in the analysis of such systems, are given at the end of Chapter 4. Additional studies aimed at further simplifying the method of analysis are currently in progress, and the results will be included in a future revision to the guidelines.

- All or parts of the contents of some HLW tanks may more appropriately be characterized as solids rather than liquids. The dynamic response of large-capacity tanks containing a viscoelastic solid is currently under study, and the results will be incorporated in a future revision of the guidelines. Some preliminary results from this study are identified in Appendix B.

- The basemat of the tank-vault system is assumed to be rigid. There is some indication that basemat flexibility may affect the response of the fluid to the vertical seismic input. This is discussed in Section 6.5.

- The vault is assumed to be rigid when the fluid response is determined for the top-constrained tanks. This assumption is valid for most HLW tanks.

2.2.2 Vault-Soil System

The guidelines recommend two methods for evaluating the seismic response of the vault-soil system. The first method utilizes large computer codes that can adequately handle the vault-soil systems found in HLW tank farms. However, these codes may be difficult and expensive to use and may not be particularly appropriate for the detailed parametric studies that are needed to assess the sensitivity of the response of the system to the uncertainties involved in the definitions of the soil properties and seismic hazard. As a result, a second methodology is also recommended which is much simpler to implement. This methodo-

logy is based on a lumped parameter definition of the soil-structure interaction process.

The accuracy of the lumped parameter methodology requires that the vault be rigid compared to the soil it replaces, that the depth of the soil cover over the vault be less than one half the vault radius, and that the shear wave velocity of the soil beneath the vault be no more than three times the shear wave velocity of the soil along the sidewall of the vault. These conditions are generally satisfied for the HLW tanks of interest. Work is underway to improve the lumped parameter methodology so that the third restriction identified above can be relaxed. The results of this work will be included in a future revision to the guidelines.

2.2.3 Underground Piping

Acceptance criteria for underground piping are not explicitly discussed in current versions of piping codes. Procedures for evaluation of the stresses and strains induced in underground piping and conduits by seismic effects, together with criteria for use as a basis for acceptance, are presented in this report. Analysis procedures for assessing both transient effects, due to wave passage and support point movements, and long term permanent ground displacements are considered in the evaluation. Modifications to current analytical procedures are recommended for incorporating the seismic effects in the criteria. Since stresses in underground piping induced by the ground displacements are considered to be self-limiting, these modifications are made by treating the seismically induced stresses as secondary.

2.2.4 Application to Other Waste Storage Systems

The design and evaluation guidelines in this report were specifically developed for double-shell tanks that are composed

of a steel tank within a concrete vault. Any new tanks are expected to be of this type, and so are many of the existing tanks.

The methodology presented, however, is also applicable to single-shell tanks, for which the primary confinement is the steel-lined concrete vault. The vault in this case is subjected to both the liquid and soil pressures, and in the evaluation of the component effects, it is necessary to consider the time phasing between the two pressure loadings.

Waste storage bins contain solid material so that the dynamic pressure loading for the contents cannot be accurately determined by the methods used for the liquid filled tanks. These facilities may be conservatively analyzed, however, by attaching the entire mass of the contents to the walls and analyzing the seismic response of the bin by the methods discussed in the guidelines. This may result in some conservatism because a portion of the seismic inertial loads in the solid contents may be carried down to the base through the contents rather than through the walls.

REFERENCES

2.1 DOE Order 6430.1A, "General Design Criteria," 1989.

2.2 DOE-STD-1020-94, "Natural Phenomena Hazards Design and Evaluation Criteria for Department of Energy Facilities," April 1994.

2.3 DOE Order 5480.28, "Natural Phenomena Hazards Mitigation," January 1993.

2.4 DOE-STD-1024-92, "Guidelines for Use of Probabilistic Seismic Hazard Curves at Department of Energy Sites," December 1992.

2.5 American Society of Mechanical Engineers, "ASME Boiler and Pressure Vessel Code, Section III, Rules for Construction of Nuclear Power Plant Components, Division 1," 1989.

2.6 American Society of Civil Engineers, Standard 4-86, "Seismic Analysis of Safety-Related Nuclear Structures and Commentary on Standard for Seismic Analysis of Safety-Related Nuclear Structures," September 1986.

2.7 American Institute of Steel Construction, "Manual of Steel Construction, Load & Resistance Factor Design," 2nd Ed., 1994.

2.8 American Institute of Steel Construction, "Manual of Steel Construction," Ninth Ed., 1989.

2.9 U.S. Nuclear Regulatory Commission, "Standard Review Plan, NUREG-0800," Sections 3.7.1 through 3.7.3, Rev. 2, August 1989.

2.10 American Concrete Institute, "Code Requirements for Nuclear Safety-Related Concrete Structures (ACI 349-85) and Commentary - ACI 349R-85," 1985.

CHAPTER 3

SEISMIC CRITERIA

3.1 INTRODUCTION

The objective of seismic design is to limit the likelihood of unacceptable seismic performance to a specified, low value. In this document it is presumed that such a specified value (or, possibly, suite of values for different components and structures) has been provided to the seismic design team by those responsible for overall project safety. This specified seismic performance value (performance goal) depends on factors such as the consequences of failure. Guidance on acceptable performance goal values is given in DOE Standard 1020-94 (Reference 3.1). Unfortunately, future seismic ground motions, as well as structure and component responses and capacities, are subject to varying degrees of randomness and uncertainty, complicating the development of simple, but accurate design procedures.

The engineering challenge is to achieve the performance goals, i.e., the specified low probabilities of failure, in a practical, cost-effective manner in the face of these multiple uncertainties. This chapter provides the guidance to meet this objective successfully.

After a discussion of the nature of the problem, Chapter 3 presents a design or evaluation scheme that separates the problem into its customary two phases: (1) the design basis earthquake ground motion (DBE); and (2) the response and capacity criteria. The former element is discussed in Section 3.3. Sections 3.4 to 3.9 present a set of practical response and capacity criteria that together with the DBE defined in Section 3.3 will meet any specified performance goal. Finally, Sections 3.10 and 3.11 (supported by Reference 3.2) present the basic criterion, reasoning and analysis underlying these recommendations, as well

as permissible alternatives and generalizations that will achieve the same performance goals. An application of these concepts and generalizations will not only confirm the technical soundness of the criteria and factors outlined in Sections 3.3 through 3.9, but also lead to alternative analysis procedures that prove more effective in particular circumstances. Indeed, there are certain cases (e.g., liquefaction) when these alternatives are necessary (see Section 3.10).

3.2 FUNDAMENTAL CONCEPTS

Elementary structural safety theory (e.g., Reference 3.3) as practiced, for example, in seismic probabilistic risk assessments (PRAs), requires that calculations of the failure probability for a given design be conducted by a formal integration of the probability distributions of the loads and capacities. This probability can then be compared to the specified performance goal to establish design adequacy. Such an integration will properly reflect the uncertainties in both major elements of the problem, demand and capacity. However, constraints of practical design require the use of simpler deterministic procedures. The challenge in developing complete seismic criteria is to provide this direct deterministic analysis format while recognizing both the probabilistic nature of the seismic hazard, as reflected in the site's seismic hazard curve, and the documented variability in dynamic responses, material properties, and structural capacities. This challenge has been addressed with varying degrees of success in the various available sets of seismic criteria. They have never been as explicitly developed as they are in this document.

The following criteria address directly two major potential obstacles to simple deterministic criteria: (1) the seismic hazard curve varies significantly from site-to-site, both in level and in shape, implying not only that the DBE level must be

adjusted to the site, but also that any value of load factor (or strength reduction factor) will imply different levels of risk reduction at different sites; and (2) the total degree of uncertainty in the capacity (associated with responses, material strengths, and other factors) varies from location-to-location (within a structure), from material-to-material, etc. (This degree of uncertainty is commonly measured by a coefficient of variation[1] or similar dimensionless quantity.)

The procedure outlined in this chapter requires the specification of two probability-related factors, the use of which will achieve the specified seismic performance objective. This objective is to ensure that the mean[2] annual probability of unacceptable performance of the structure does not exceed a specified value P_F (the "performance goal"). The first factor is P_H, the (mean) hazard or annual probability of exceedance associated with the design basis earthquake ground motion (DBE). The second is a risk or probability reduction factor, R_R, to be associated with the acceptance criteria. The more conservative these criteria the larger is R_R. The values of P_H and R_R should be selected such that:

$$P_H = (R_R)\ (P_F) \tag{3.1}$$

This condition states in probabilistic terms, i.e., $P_F = P_H/R_R$, the obvious fact that the same safety can be achieved by many combinations of design earthquake level and acceptance criteria,

---

[1]The coefficient of variation is defined as the standard deviation divided by the mean. In seismic PRA analysis it is common to use, instead, the standard deviation of the natural log of the variable, denoted β. For β less than about 0.3 the two coefficients are comparable in numerical value.

[2]The mean here is an average over sources of uncertainty in the estimation of the hazard curve as well as the response and capacity parameters (see References 3.2 and 3.4).

provided that, when one is made less conservative, the other is made appropriately more conservative in order to compensate.

It is presumed here, recall, that the seismic engineering team has been given a value for P_F, the performance goal. This value may depend on the implications of the failure of the component, the redundancy of the system, the marginal cost of strengthening the component (versus another parallel component in the same system), the remaining design life, etc. This performance goal ultimately reflects the safety goals of the DOE (References 3.5 and 3.6).

The procedures in this document grant the flexibility of selecting one or more pairs of values of P_H and R_R to meet the goal, P_F. Typical values of R_R considered are 5, 10, and 20. One advantage of this flexibility is that the engineer can keep the same seismic input level while consistently and easily adjusting the acceptance criteria for components with different performance goals (within a factor of 4, at least). Alternatively, one can keep the same criteria and adjust the DBE level.

Readers familiar with the DOE seismic criteria in the DOE Standard 1020-94 (Reference 3.1) will recognize this general format. In that document performance goals (P_F values) of 10^{-5} to $2x10^{-4}$ are suggested for the more critical facilities. The document then defines conservative seismic acceptance criteria aimed at achieving risk reduction factors, R_R, of about 5, 10, and 20. These variations in R_R are accommodated by variations in a factor S_F (to be introduced in Section 3.3.1). In principle, the users are free to choose whichever set of criteria they wish. Reference 3.1 then recommends establishing the DBE by entering the seismic hazard curves at an annual probability of exceedance of $P_H = (R_R)(P_F)$. For example, if the specified performance goal for a structure or component is 10^{-5} and the selected set of acceptance criteria are associated with an R_R of 10, then the DBE

should be that with an annual probability of exceedance of $1x10^{-4}$ (i.e., a mean return period of 10,000 years). The criteria in this document follow this same philosophy. They supplement DOE Standard 1020-94 by providing criteria and procedures for underground high-level waste storage tanks.

Once the values of P_H and R_R have been established, the design or evaluation of an existing component or structure follows straightforward procedures. Section 3.3 details the selection of the DBE earthquake consistent with P_H. The seismic acceptance process may have one of various forms. While more general processes are possible (see Sections 3.10 and 3.11), the bulk of this chapter (Sections 3.4 through 3.9) is dedicated to a conventional process based on deterministic factors[3] and pseudo-linear analysis. One of these factors depends explicitly on R_R. While the procedure in Sections 3.4 through 3.9 has been chosen because of its familiarity to those experienced in seismic design and evaluation of commercial nuclear power plants and other critical facilities, certain of the factors and details have been adjusted by the authors to better approximate the specified R_R factors.

The procedure is described in Sections 3.4 through 3.9, and the primary steps are summarized as follows:

A. Perform a linear elastic seismic response analysis for the DBE ground motion to determine the elastically computed seismic demand D_{se} (see Sections 3.4 and 3.5).

B. Establish the code ultimate capacities C_c for all relevant failure modes for each component being evaluated (see Sections 3.6 and 3.7).

---

[3]By "deterministic" it is meant that for simplicity the specification of the values of the coefficients of variation and even particular percentiles, for the most part, is avoided. That this can be done without significant loss of generality or accuracy is one of the facts demonstrated in Reference 3.2.

C. For each failure mode of a component, define the maximum permissible inelastic energy absorption factor $F_{\mu D}$ by which the elastically computed seismic demand may exceed the code ultimate capacity (see Section 3.9).

D. Compute a factored inelastic seismic demand D_{si} by dividing the elastically computed seismic demand D_{se} by the appropriate inelastic energy absorption factor $F_{\mu D}$ and multiplying the result by a seismic scale factor SF. This scale factor is a function of the desired risk-reduction ratio R_R. The factored inelastic seismic demand D_{si} is then combined with the "best-estimate" of the concurrent non-seismic demands D_{ns} to obtain the total factored inelastic demand D_{ti} which must be less than the code ultimate capacity C_C. This step is defined by Equations 3.4 through 3.6 of Section 3.8.

The criteria presented are based primarily on the judgment and experience of the authors and are deemed to approximately achieve the desired seismic risk reductions R_R. However, great rigor or quantitative accuracy in achieving these seismic risk reduction factors should not be inferred. These factors served merely as target goals in the development of the criteria.

The seismic criteria are also considered to be sufficiently conservative to guard against damage from subsequent aftershocks with ground motion less than the DBE.

Although it is envisioned that most users will prefer to follow the deterministic pseudo-linear seismic evaluation procedure of Sections 3.4 through 3.9 outlined in the above four steps, a more basic seismic acceptance criterion and a general approach to demonstrate compliance with it are presented in Section 3.10. This criterion is expressed in terms of an acceptable probability of failure capacity. This alternate approach is presented for two reasons:

1. to enable the user to define more sophisticated alternate acceptance criteria than those presented in Sections 3.4 through 3.9 when the user has a sufficient basis to develop and defend these alternate criteria.

2. to define the basis upon which the seismic criteria of Section 3.4 through 3.9 were developed.

Lastly, Section 3.11, together with Section 4.2 of Reference 3.2, uses this basic seismic criterion of Section 3.10 to benchmark the adequacy of the factors used in the deterministic pseudo-linear seismic evaluation procedure defined in Sections 3.4 through 3.9.

3.3 DESIGN BASIS EARTHQUAKE GROUND MOTION

3.3.1 Probabilistic Definition of Ground Motion

Given a seismic hazard curve for the site, such as those shown in Figure 3.1, it is straightforward to enter the curve at the value P_H (which equals $R_R \times P_F$) and read off the corresponding level of the ground motion parameter (which is peak ground acceleration [PGA] in Figure 3.1). For example, if P_F is specified to be 10^{-5} and R_R is selected to be 10, then P_H is 10^{-4}, and the DBE PGA is 0.3g at the site characterized by Curve B of Figure 3.1.

However, the elastically computed response to this DBE must ultimately be scaled by a scale factor SF before being compared to a seismic capacity as will be discussed in Section 3.8. This SF is a function of the desired risk reduction ratio R_R and should preferably also be a function of the hazard curve slope between the hazard probability P_H and the performance goal P_F.

If the hazard curve slope is either not available or highly uncertain for annual probabilities less than the seismic hazard exceedance probability P_H, the constant (site-independent) scale factors permitted by DOE Standard 1020-94 are given in Table

3.1a. However, if the hazard curve slope between the hazard exceedance probability P_H and the performance goal probability P_F can be reasonably estimated , a substantially improved estimate of the appropriate scale factor can be obtained from (Reference 3.2)

$$SF = \text{larger of} \begin{Bmatrix} SF_1 \\ SF_2 \end{Bmatrix} \tag{3.2a}$$

$$SF_1 = (\text{see Table } 3.1b) \tag{3.2b}$$

$$SF_2 = 0.6\ (A_R)^{\alpha} \tag{3.2c}$$

where A_R is the slope (strictly the secant) of the hazard curve (when displayed on log-log paper) in the region of interest, i.e., between the exceedance frequencies P_F and P_H. The ground motions at these frequencies are denoted by a_{PF} and a_{PH} respectively. (Note that in this document the DBE is equal to a_{PH}.) With these definitions A_R becomes

$$A_R = (a_{PF}/a_{PH})^{1/\log_{10}R_R} \tag{3.3}$$

The values for SF_1 and α are given in Table 3.1b for R_R values of 20, 10 and 5. Scale factors, based on Equations 3.2a and 3.2b, versus A_R are plotted in Figure 3.2.

When the hazard exeedance probability is defined by Equation 3.1 and the scale factor is defined by Figure 3.2, then the product of the SF and the DBE will be independent of the risk reduction ratio chosen R_R when $A_R > 2$, and will have negligible sensitivity to R_R when $A_R < 2$. For example, for hazard curves A and B in Figure 3.1 a seismic performance goal of 1×10^{-5} is achieved by any of the following:

Hazard Curve	Risk Reduction Factor R_R	Hazard Probability P_H	DBE	A_R	SF	SF x DBE
A a_{PF} = 1.00 g	20	2×10^{-4}	0.50 g	1.70	1.15	0.58 g
	10	1×10^{-4}	0.60 g	1.67	1.00	0.60 g
	5	5×10^{-5}	0.71 g	1.63	0.87	0.62 g
B a_{PF} = 0.64 g	20	2×10^{-4}	0.24 g	2.13	1.38	0.33 g
	10	1×10^{-4}	0.30 g	2.13	1.10	0.33 g
	5	5×10^{-5}	0.38 g	2.11	0.87	0.33 g

Therefore, it is practically immaterial to the scaled elastic response or to SF x DBE as to which value of R_R is chosen, so long as the DBE is defined at the hazard probability P_H given by Equation 3.1 and SF is selected from Fig.3.2.

3.3.2 Design Basis Earthquake Response Spectra

The DBE ground motion at the site shall be defined in terms of smooth and broad banded response spectra in the horizontal and vertical directions defined at a specific control point. In most cases, the control point should be on the free ground surface. However, in some cases it might be preferable to define the DBE response spectra at some other location. One such case is when a soft, shallow soil layer at the ground surface (e.g., with a shear wave velocity less than 750 feet/second and a depth less than 100 feet) is underlain by a much stiffer material. In this case, the control point should be specified at the top of the stiffer material and the input motion specified as an equivalent outcrop motion. Wherever specified, the breadth and amplification of the DBE response spectra should be either consistent with or conservative for the site soil profile and facility embedment conditions.

Ideally, it is desirable for the DBE response spectrum to be defined by the mean uniform hazard response spectrum (UHS) associated with the seismic hazard annual frequency of exceedance

P_H specified in Section 3.2 over the entire natural frequency range of interest (generally 0.5 to 40 Hz). Currently, however, some controversy exists concerning both the shape and amplitude of such mean UHS[4].

First, many mean UHS shapes are not consistent with response spectra shapes derived from ground motion recordings. This discrepancy is strongest when different portions of the UHS are dominated by earthquakes of different magnitudes. The DBE response spectrum should be consistent in shape with spectra calculated from motions recorded at similar sites for earthquakes with magnitudes and distances similar to those that dominate the seismic hazard at the specified annual frequency. This condition may require the use of two (or more) alternate spectra (or their envelope) as discussed below.

Second, even for a specified ground motion parameter such as peak ground acceleration (PGA) or the spectral acceleration (S_A) at a specified frequency, the estimate for a given mean hazard or exceedance probability, P_H, may be unstable among different predictors and can be driven by extreme models. Mean ground motion estimates should be used only when such estimates are stable. Mean estimates outside the range of 1.3 to 1.7 times the median estimate are likely to suffer from such problems.

Because of these issues with regard to both mean estimates and UHS, the Department of Energy has published DOE Standard 1024 (Reference 3.7) on the use of probabilistic seismic hazard estimates. The following recommendations have been adapted from DOE-STD-1024-92 (Reference 3.7):

---

[4]The spectral acceleration associated with a specified mean hazard is not, precisely, the mean spectral acceleration associated with a specified hazard, but this short-hand terminology will be used herein for simplicity. See Reference 3.4 for a discussion of this and related interpretation of means and factors in seismic engineering.

1. When stable mean estimates of the PGA and spectral accelerations do not exist, then one should use a surrogate mean DBE PGA and spectral acceleration set at appropriate factors times their median estimates at the appropriate seismic hazard annual frequency of exceedance. Reference 3.7 defines an approach which may be used to obtain an acceptable median estimate from existing eastern U.S. seismic hazard study results, and it defines this surrogate median-to-mean factor for PGA and PGV. This same procedure can be used if necessary for spectral accelerations as well.

2. It is recommended that spectral accelerations S_A associated with two or more frequency ranges be selected, e.g., high and moderate, 5-10 Hertz and 1-2.5 Hertz respectively. The precise frequency ranges to be used should depend on the frequencies of the structures and components at hand, on soil column response, and on the nature of the dominant seismic source zones. The values of these spectral accelerations at the mean hazard level P_H form the anchor points of the design basis spectra.

3. The DBE response spectrum is then defined by a smooth, broad-frequency-content, median[5] response spectrum shape scaled so as to be anchored to the mean DBE spectral acceleration values defined in Step 2.

Preferably, the median deterministic DBE response spectrum shape should be site-specific and consistent with the expected earthquake magnitudes and distances, and the site soil profile. Reference 3.7 provides an acceptable approach for estimation of the earthquake magnitudes and distances to be used in defining this median deterministic site-specific response spectrum shape.

---

[5]The word *median* here refers to the median with respect to a suite of records (Reference 3.4).

When a site-specific response spectrum shape is unavailable then a median standardized spectral shape such as the spectral shape defined in NUREG/CR-0098 (Reference 3.8) may be used so long as such a shape is either reasonably consistent with or conservative for the site conditions.

The median site-specific response spectrum shape may be derived from any combination of the following:

a) the median response spectrum shape from a suite of actual ground motion records associated with reasonably similar magnitudes, distances, and site soil profiles.

b) empirical regression equations defining median spectral acceleration at various natural frequencies as a function of the magnitude, distance, and soil profile.

c) stochastic ground motion models benchmarked against response spectra from actual ground motion records associated with magnitudes, distances, and soil profiles as similar to the site as practical.

For the purpose of clarity in the discussion in this paragraph, assume that there are two representative frequency ranges (e.g., 5-10 Hertz and 1-2.5 Hertz) that can be represented by two spectral accelerations, denoted SA_{HF} and SA_{MF}, respectively.

In some cases the mean DBE SA_{HF} and SA_{MF} may be associated with different controlling earthquakes, the SA_{HF} being controlled by a lower magnitude local earthquake while the SA_{MF} is controlled by a larger magnitude more distant earthquake. In these cases it is preferable to develop separate DBE response spectra for each of the two controlling earthquakes in lieu of a single enveloped DBE response spectrum. This alternative is particularly appropriate when site-specific spectral shapes are used rather than a standardized spectral shape, and when the site- specific spectral shapes differ substantially for the two

controlling earthquakes. In this case, the local earthquake spectral shape should be anchored to the mean DBE SA_{HF}, and the more distant earthquake spectral shape should be anchored to the mean DBE SA_{MF}. Both spectra may then be used separately in the seismic response analysis with the larger of the separately computed responses being used to define the seismic demand. Of course, alternatively, the two DBE response spectra may be enveloped by a single combined DBE response spectrum which is used to define the seismic demand.

Note that this envelope may then *not* be consistent with spectral shapes derived from ground motion recordings, for much the same reasons that the UHS may not. Such an envelope spectrum is likely to be inappropriate for soil convolution and deconvolution analyses.

Those responsible for the DBE should also specify a PGA, PGV, and PGD associated with the DBE spectra. These values provide valuable consistency checks with the spectral levels in the high, moderate, and lower (less than 1 Hertz) frequency ranges, respectively. Further, the PGV may be needed for the assessment of buried piping (Chapter 7). The lower frequency spectral values may be needed for low frequency response issues (such as sloshing) and for non-linear soil or structural analyses (such as soil settlement and liquefaction).

3.4 ANALYSIS OF SEISMIC DEMAND (RESPONSE)

It is anticipated that the seismic demand will generally be estimated based upon linear response analyses. Sections 3.4 through 3.9 outline a set of acceptance criteria consistent with this approach. (But see also Section 3.10.). DBE response spectra arrived at in accordance with Section 3.3 should be used as input to such analyses. Other than for the conservatism specified in the DBE response spectra, the seismic response analyses can be median centered (no intentional conservatism),

but with variation of some of the most uncertain parameters. Seismic response analyses should be conducted in accordance with the guidance contained in References 3.1 and 3.9 as amplified herein.

Best estimate structural models and material damping values should be used. Best estimate material damping values are provided in Section 3.5. However, a variation by approximately plus/minus one standard deviation in both the natural frequency of the structural model, and soil stiffness properties should be incorporated into these analyses. In general, the structural frequency uncertainty can be accommodated by use of a 30% frequency uncertainty band either centered on the best estimate frequency or skewed to the low frequency side when such skewness is considered appropriate. Guidance on the appropriate variation of soil stiffness properties is given in Section 3.3.1.7 of ASCE 4-86 (Reference 3.9) and Section 3.7.2 of the USNRC Standard Review Plan (Reference 3.10). The seismic demand, D_{se}, should be obtained from the largest computed response within these uncertainty bands. Great precision is unnecessary, and this largest response can generally be estimated by considering the following five cases:

1. Best estimate model (corresponding to best estimate structural model coupled with best estimate soil properties).

2. Best estimate model frequency shifted +15%.

3. Best estimate model frequency shifted -15%.

4. Best estimate structural model coupled with upper estimate soil stiffness properties (see Section 6.2).

5. Best estimate structural model coupled with lower estimate soil stiffness properties.

As noted above, it is sometimes preferable to skew the 30% frequency uncertainty to the low frequency side and for these situations, Cases 2 and 3 should be adjusted accordingly. Floor spectra should be smooth (i.e., valleys filled in) envelopes from these cases.

So long as the DBE Response Spectrum is smooth and has broad frequency content as is required by Section 3.3.2, it is unnecessary to consider Cases 2 and 3 for the seismic evaluation of the structure itself. As a practical guideline, so long as the input spectral acceleration at the dominant frequency of the structure is not increased by more than 15% by a ±15% frequency shift, it is not necessary to consider Cases 2 and 3 for the structure itself. Instead, it is sufficient to use only a best estimate structural model and to frequency shift the resulting in-structure (floor) spectra by ±15%. These spectra are used as input to components mounted on the structure.

Even for in-structure spectra, it is seldom necessary to analyze all five cases. When soil-structure-interaction (SSI) effects are substantial, Cases 4 and 5 will lead to broader frequency shifting than will Cases 2 and 3 so that Cases 2 and 3 can be dropped. When SSI effects are small, Cases 4 and 5 will be enveloped by Cases 2 and 3 and can then be dropped.

3.5 DAMPING

Damping values recommended for dynamic analyses are presented in Table 3.2 at three different response levels. These values may be used unless lower damping values are specified in the applicable construction code or standard specified by the Department of Energy for the facility design. Response Level 3 corresponds to inelastic response when the elastically computed total demand (seismic plus non-seismic) exceeds the capacity limits defined herein (i.e., when credit must be taken for the inelastic energy absorption factor F_μ). When evaluating the

component, Response Level 3 damping may be used in elastic response analyses independent of the state of response actually reached, because such damping is expected to be reached prior to component failure. When determining the input to subcomponents mounted on a supporting structure, the damping value to be used in elastic response analyses of the supporting structure to define input to the subcomponent should be a function of the response level reached in the majority of the seismic load resisting elements of the supporting structure. Defining D_t as the total elastically computed demand (seismic D_{se} plus non-seismic D_{ns}) for the combined (three earthquake components) and enveloped (frequency varied) results and C_c as the code strength capacity (see Section 3.7) for the supporting structure, then the appropriate Response Level damping can be estimated from the following:

Response Level	D_t/C_c
3	$\gtrsim$ 1.0
2*	$\approx$0.5 to 1.0
1*	$\lesssim$ 0.5

*Consideration of these damping levels is required only in the generation of floor or amplified response spectra to be used as input to sub-components mounted on the supporting structure.

Based on a review of the overall structural response, the seismic evaluator is expected to make a reasonable estimate of the Response Level reached for the purpose of establishing the damping levels to be used. However, it is expected that the Response Level chosen will be based on reasonable judgment rather than any prescriptive procedure, and that multiple iteration or fine-tuning of this estimate is unwarranted. This requirement to make damping a function of response level is identical in philosophy, and should be interpreted in the same way as the nuclear power industry has done with the guidance given in ASCE

4-86 (Reference 3.9) and USNRC Regulatory Guide 1.61 (Reference 3.11). No additional requirements are implied here.

The damping values presented in Table 3.2 are intended to be best-estimate (median centered) damping values with no intentional conservative bias for use in elastic response analyses. Other damping values may be used when such values are properly justified as best-estimate values. For example, in the case of very high viscosity fluid, impulsive mode damping values in excess of 4% may be permissible for tanks.

Response Level 3 damping values are intended for use in elastic response analyses coupled with the permissible inelastic energy absorption factors $F_{\mu D}$ defined later. However, when a nonlinear inelastic response analysis which explicitly incorporates the hysteretic energy dissipation is performed, no higher than Response Level 2 damping values should be used to avoid the "double-counting" of this hysteretic energy dissipation that would result from the use of Response Level 3 damping values.

3.6 MATERIAL STRENGTH PROPERTIES

For existing components, material strength properties should be established at the 95% exceedance strength levels associated with the time during the service life at which such strengths are minimum. If strengths are expected to increase during the service life, then the strength of an existing component should be its value at the time the evaluation is performed. If strengths are expected to degrade during the service life, then strengths to be used in the evaluation should be based upon estimated 95% exceedance strengths at the end of the service life. Whenever possible, material strengths should be based on 95% exceedance values estimated from tests of the actual materials used at the facility. However, when such test data are unavailable, then code minimum material strengths may be used. If degradation is anticipated during the service life, then these

code minimum strengths should be further reduced to account for such degradation (for example, due to long-term thermal effects on concrete). (See Section 3.7 for additional discussion on applicable code material strengths.)

For new designs, material strength properties should be established at the specified minimum value defined by the applicable code or material standard. If degradation is anticipated during the service life, then these code minimum strengths should be further reduced to account for such degradation.

3.7 CAPACITIES

In general, for load combinations which include the DBE loading, capacities C_c to be used should be based upon code-specific minimum ultimate or limit-state (e.g., yield or buckling) capacity approaches coupled with material strength properties specified in Section 3.6. For concrete, the ACI ultimate strength approach with the appropriate capacity reduction factor, ϕ, included as specified in either ACI318 (Reference 3.12) or ACI349 (Reference 3.13) should be used. For structural steel, the AISC-LRFD (Reference 3.14) limit-state strength approach with the appropriate capacity reduction factor, ϕ, included is preferred. However, the AISC plastic design (Part 2, Reference 3.15 or Chapter N, Reference 3.16) maximum strength approach may be used so long as the specified criteria are met. The plastic design strengths can be taken as 1.7 times the allowable stresses specified in Reference 3.15 or 3.16 unless another factor is defined in the specified code. For ASME Section III, Division 1 components, ASME Service Level D (Reference 3.17) capacities should be used. In some cases, functional failure modes may require lesser limits to be defined (e.g., ASME Mechanical Equipment Performance Standard, Reference 3.18).

For existing facilities, in most cases, the capacity evaluation equations should be based on the most current edition of the appropriate code, particularly when the current edition is more conservative than earlier editions. However, in some cases (particularly with the ACI and ASME codes), current code capacities may be more liberal than those specified at the time the component was designed and fabricated, because fabrication and material specification requirements have become more stringent. In these latter cases, current code capacities will have to be reduced to account for the more relaxed fabrication and material specifications that existed at the time of fabrication. In all cases, when material strength properties are based on code minimum material strengths, the code edition enforced at the time the component was fabricated should be used to define these code minimum material strengths.

If any material can be degraded during the service life, the degraded material size and properties should be used for estimation of the component capacity. For example, when corrosion is likely during the service life, thicknesses should be reduced by an appropriate corrosion allowance before computing the code capacity.

A capacity approach acceptable for the seismic capacity evaluation of unanchored and anchored flat-bottom liquid storage tanks at the atmospheric pressure is presented in Chapter 5. It is judged that for temperatures not exceeding 200°F, the thermal effects need not be considered explicitly in such capacity evaluations.

3.8 LOAD COMBINATIONS AND ACCEPTANCE CRITERIA

This section deals only with load combinations that include DBE loadings. In many cases, other (non-seismic) load combinations may control the design or evaluation of a component. These non-seismic load combinations should be defined by other documents.

It is assumed herein that the DBE seismic demand, D_{se}, will be computed by linear elastic analyses conducted in accordance with the response criteria defined in Sections 3.3 through 3.5. This elastically computed seismic demand D_{se} should be modified by the appropriate inelastic energy absorption factor $F_{\mu D}$ as defined in Section 3.9 and by the appropriate seismic scale factor SF from Section 3.3.1 to obtain a factored inelastic seismic demand D_{si} by:

$$D_{si} = \left(\frac{SF}{F_{\mu D}}\right) D_{se} \qquad (3.4)$$

The seismic scale factor SF is used to accommodate varying seismic risk reduction factors R_R (as discussed in Section 3.3). Note that this is the only factor that need be adjusted to modify the acceptance criteria for different specified R_R levels.

The total factored inelastic demand D_{ti} is then given by:

$$D_{ti} = D_{ns} + D_{si} \qquad (3.5)$$

where D_{ns} represents the best-estimate of all non-seismic demands expected to occur concurrently with the DBE. Equation 3.5 represents the DBE load-combination equation. The seismic capacity is adequate when the capacity C_c determined as defined in Section 3.7 exceeds D_{ti}, i.e.:

$$C_c \geq D_{ns} + \left(\frac{SF}{F_{\mu D}}\right) D_{se} \qquad (3.6)$$

Equation 3.6 represents the seismic acceptance criterion appropriate for the DBE.

The factor $(SF/F_{\mu D})$ in Equation 3.6 is outside the normal application of codes such as ACI, AISC and ASME which are used herein to establish the code capacity C_C. This factor $(SF/F_{\mu D})$ may be either greater than or less than unity depending upon the relative values of SF and $F_{\mu D}$, and is used to bring code practice in line with the desired target risk reduction factor R_R as part of the process of aiming at a desired target performance goal probability P_F. In normal code application, one may think of the factored inelastic seismic demand D_{si} as the seismic demand to be used with the code. Arbitrarily resetting $(SF/F_{\mu D})$ to unity would undesireably penalize ductile failure modes in which $F_{\mu D} >$ SF. Such modes do not need this additional conservatism. Similarly it would be unconservative to take this factor as unity for brittle failure modes (for which $F_{\mu D} <$ SF). Ignoring the factor $(SF/F_{\mu D})$ in Equation 3.6 would have the effect of placing the conservatism where it is least needed, i.e., in ductile failure modes.

No factors are needed on D_{ns} in Equation 3.5. The non-seismic demand D_{ns} should be defined at its best-estimate level as opposed to an unlikely-to-exceed or conservative level. The conservatism embodied in defining C_C, $F_{\mu D}$, and D_{se} are sufficient to achieve the specified R_R values without additional sources of conservatism being required.

In some cases, such as a column under combined axial compression and moment, the code capacity C_C is defined in terms of interaction equations. Furthermore, the $F_{\mu DP}$ for axial compression defined in Section 3.9 is less than $F_{\mu DM}$ for flexure.

To interpolate in such cases, Equations 3.4 and 3.5 are entered twice to establish the total factored inelastic demands P_{ti} and M_{ti} for axial compression and for moment respectively, i.e.:

$$P_{ti} = P_{ns} + \frac{SF}{F_{\mu DP}} \bullet P_{se} \qquad M_{ti} = M_{ns} + \frac{SF}{F_{\mu DM}} \bullet M_{se} \qquad (3.7)$$

The combination of P_{ti} and M_{ti} is entered into the code capacity interaction equation to determine the adequacy of the seismic design.

For ductile failure modes, non-seismic demands which are relieved by small levels of inelastic distortion (such as thermal and settlement stresses) do not have to be included in Equation 3.5 for combination with the factored seismic inertial force induced demand. However, for non-ductile failure modes, these inelastically-relieved non-seismic stresses must still be included. For example, if a wall capacity is controlled by flexure, these inelastically-relieved non-seismic stresses do not have to be added to the seismic demand D_{si}. However, if the wall capacity is controlled by shear, they do have to be added. In addition, seismic and non-seismic displacements and strains are additive when checking displacement or strain criteria such as for underground pipes (see Chapter 7).

As another example of non-seismic demands relieved by inelastic distortion, many vertical cylindrical flat bottom high-level waste storage tanks are restrained against longitudinal (vertical) movement at both the top and bottom of the tank walls. In many cases, the degree of longitudinal restraint is uncertain and difficult to quantify. Therefore, the longitudinal stresses set up in the tank walls are difficult to determine, but can be bounded by the cases of full longitudinal restraint and no longitudinal restraint. When fully restrained, substantial longitudinal stresses occur in the tank walls due to the following effects:

1. *Longitudinal stresses induced by Poisson's ratio effects resulting from the circumferential (hoop) stresses due to the combination of hydrostatic and hydrodynamic fluid pressures on the tank wall (See Chapter 4).* For all practical problems, these Poisson's ratio induced longitudinal stresses are tensile and are a small fraction (about 30%) of the average peak hoop stress over the height of the tank. They are easily relieved by a very small amount of longitudinal straining in the cylindrical shell or support relaxation.

2. *Thermal expansion stresses.* These longitudinal thermal expansion stresses are compressive and may be large at high temperatures. But, at metal temperatures not exceeding 200°F the corresponding longitudinal compressive strains are less than 0.15% and thus the stresses are easily relieved by small amounts of inelastic straining or bowing of the thin metal tank sidewalls.

In conclusion, for a ductile metal tank, both of the above two longitudinal stresses are secondary and easily relieved by a very small amount of nonlinear longitudinal straining (less than 0.15%). As such, neither of these computed elastic longitudinal stress will reduce the seismic capacity of the tank, and neither of them needs to be combined with the primary seismic overturning induced longitudinal stresses when defining D_{ti} by Equation 3.5.

3.9 INELASTIC ENERGY ABSORPTION FACTOR

The inelastic energy absorption factor is defined as the amount that the elastically computed seismic demand may exceed the capacity of a component without impairing the performance of the component. Thus, the elastically computed seismic demand D_{se} may be factored by an inelastic energy absorption factor $F_{\mu D}$ as shown in Equation 3.4 to obtain a factored inelastic seismic demand D_{si}. In order for the acceptance criteria to achieve a risk

reduction (R_R) value between 5 and 20, this inelastic energy absorption factor $F_{\mu D}$ should be defined by:

$$F_{\mu D} = F_{\mu 5\%} \tag{3.8}$$

where $F_{\mu 5\%}$ is the estimated inelastic energy absorption factor associated with a permissible level of inelastic distortions specified at about the 5% level, i.e., there is only a 5% chance that the actual F_μ will be less than $F_{\mu 5\%}$.

It is always preferable to perform nonlinear analysis on the structure or component being evaluated in order to estimate $F_{\mu 5\%}$ for use in Equation 3.8 to define $F_{\mu D}$. Some guidance on estimating $F_{\mu 5\%}$ is given in Appendix A. However, such analyses are often expensive and the modeling assumptions may be controversial. Therefore, standard values of $F_{\mu D}$ are provided in Table 3.3 for common elements associated with underground high-level waste storage tanks, and are discussed in the remainder of this section. Additional $F_{\mu D}$ values are provided in DOE Standard 1020-94 (Reference 3.1). The $F_{\mu D}$ values presented in Table 3.3 or from Reference 3.1 may be used in lieu of performing nonlinear analyses, so long as the cautions identified later in this section are observed.

The $F_{\mu D}$ factors in Table 3.3 for failure modes of metal liquid-storage tanks are intended to recognize that each of these failure modes is accompanied by at least some nonlinear behavior prior to failure; such action leads to a reduction in the effective frequency of the system, to increased energy dissipation, and/or to redistribution of the load. For example, the moment capacity is governed by a combination of local compressive buckling which is not catastrophic under a moment load, and (highly ductile) axial tensile behavior over the majority of the shell circumference. Similarly, the shear capacity at the tank base must be exceeded by a significant amount before non-negligible movement will occur under seismic

loading. $F_{\mu D}$ values of unity in Table 3.3 are for failure modes which can be catastrophic as soon as the capacity is exceeded.

The use of $F_{\mu D}$ values listed in Table 3.3 equal to 1.5 and greater for concrete walls is conditional on acceptable performance permitting extensive wall cracking, while requiring stable wall behavior. If only minor wall cracking is acceptable, then lesser $F_{\mu D}$ values closer to unity should be used.

The $F_{\mu D}$ values listed in Table 3.3 for ductile failure modes (i.e., values greater than 1.0) assume that steel reinforcing bars, metal tank shells and anchorage will remain ductile during the component's entire service life. It is assumed that the metal will retain at least a 6% uniaxial elongation strain capability including the effects of welding. If this metal can become embrittled at some time during the service life, $F_{\mu D}$ values should be 1.0.

In some cases reinforcement details in older facilities do not satisfy the development length requirement of current codes (References 3.12 and 3.13). In these instances the potential exists for a ductile failure mode associated with yielding of the reinforcement to become a more brittle mode associated with bond failure. Data exist (Reference 3.19), however, indicating that bond failure modes retain a reasonable amount of ductility provided that the reinforcement is suitably confined within the region of the potential bond failure. The confinement may be provided by a cover of at least 2.5 bar diameters or by ties (stirrups) spaced no further than 5 bar diameters apart. If this confinement is provided a strength of the reinforcement equal to the yield strength of the steel times the ratio of actual to required development length may be used in the capacity evaluations. In these cases the factor ($F_{\mu D}$) should be limited to 1.0. If the confinement is not provided the reinforcement should be omitted in the capacity evaluations.

The $F_{\mu D}$ values listed in Table 3.3 or from Reference 3.1 and the acceptance criteria of Section 3.8 are based on the assumption that the component will be removed from service after being subject to ground motion in excess of the DBE response spectrum. If a component is to remain in service after being subjected to a DBE, and stress corrosion cracking is a major concern, $F_{\mu D}$ should be 1.0. In addition, the capacity C_C may have to be reduced in order to maintain the seismic margin defined in Section 3.10

For low-ductility failure modes such as axial compression or shear in concrete walls or columns or wall-to-diaphragm, wall-to-column, or column-to-base connections, the $F_{\mu D}$ values listed in Table 3.3 are 1.0. In most cases, such stringent limits can be relaxed somewhat, as described below, because most such components also have a ductile failure mode which when reached is likely to limit the demand in the low-ductility failure modes. Unless the component has a seismic capacity in the ductile failure mode significantly in excess of its required capacity, inelastic distortions in this ductile failure mode will likely limit the factored seismic demand D_{si} in the low-ductility failure modes to levels less than those given by Equation 3.4 with the $F_{\mu D}$ values given by Table 3.3. Since greater conservatism exists in code capacities C_C for low-ductility failure modes than for ductile failure modes, the failure will be controlled by the ductile failure mode so long as the low-ductility failure mode code capacity is at least equal to the ductile failure mode capacity. Thus, for low-ductility failure modes, the factored seismic demand D_{si} can be limited to the *lesser* of the following:

1. D_{si} given by Equation 3.4 using $F_{\mu D}$ from Table 3.3, or

2. $D_{si} = C_C - D_{ns}$ computed for the ductile failure mode, where C_C is the ductile failure mode code capacity.

Therefore, for example, connections do not have to be designed to have code capacities C_c greater than the code capacities C_c of the members being connected, or the total factored demand D_{ti} given by Equations 3.4 and 3.5 and Table 3.3, whichever is less. Similarly, the code shear capacity of a wall does not have to exceed the total shear load which can be supported by the wall at the code flexural capacity of the wall. Finally, the horizontal seismic-induced axial force in a moment frame column can be limited to the axial force which can be transmitted to the column when a full plastic hinge mechanism develops in the frame where the plastic hinge capacities are defined by the code ultimate flexural capacities.

When the component's or structure's dominant response frequency (generally the fundamental frequency) is greater than the frequency at which the input spectral acceleration is maximum, the cautions contained in Section C.3.2.1 and illustrated in Figure C-10 of Reference 3.1 remain in effect. In this case, the factored seismic demand D_{si} may be computed from any of the following three approaches:

1. The maximum (input) spectral acceleration shall be used to compute the elastic response of the dominant response mode in lieu of the lesser input spectral acceleration corresponding to the frequency of this mode. In this case, the $F_{\mu D}$ values listed in Table 3.3 or Reference 3.1 may be used.

2. The (lesser) spectral acceleration corresponding to the modal frequency of the dominant response mode may be used together with $F_{\mu D}$ values of 1.0.

3. The spectral acceleration corresponding to the modal frequency of the dominant response may be used together with $F_{\mu D}$ values based on $F_{\mu 5\%}$ computed from nonlinear analyses in accordance with guidance given in Appendix A.

This approach is the most accurate and least conservative approach, but requires more effort.

The DBE response spectra defined in accordance with Section 3.3 are elastic response spectra which may be directly used to obtain the elastically computed seismic demand which is then divided by $F_{\mu D}$ to obtain an inelastic-factored seismic demand. However, some engineers prefer to reverse the order of these steps by first dividing the elastic response spectra by $F_{\mu D}$ to obtain inelastic response spectra which may be directly used to compute the inelastic-factored seismic demand. This approach is also permitted so long as it is performed in a manner consistant with the use of $F_{\mu D}$ as described herein.

One way to obtain this consistency is to first multiply the elastic DBE response spectra by the seismic scale factor SF defined in Section 3.3.1 to obtain the load-factored elastic DBE response spectra. Next, at all frequencies equal or less than the frequencies at which the input spectrum is maximum, these scale-factored elastic DBE response spectra are divided by $F_{\mu 5\%}$ to obtain the inelastic-factored spectra. At all higher frequencies, the inelastic-factored spectral accelerations are defined by the lesser of either the scale-factored elastic spectral acceleration at that frequency, or the maximum scale-factored elastic spectral acceleration divided by $F_{\mu 5\%}$. Alternatively, frequency dependent $F_{\mu 5\%}$ obtained in accordance with the guidance given in Appendix A and appropriate references such as References A.1 through A.6 of Appendix A may be used at all frequencies to obtain the inelastic-factored response spectra from the load-factored elastic response spectra. This method becomes more complicated when different failure modes with differing $F_{\mu 5\%}$ are present.

This completes the specification of a set of seismic criteria that will satisfy the performance goal P_F through, first, the

introduction of P_H and R_R, and then, the determination of the DBE and acceptance criteria as outlined in Sections 3.3 through 3.9.

3.10 BASIS OF PROCEDURES AND AN ALTERNATE APPROACH TO COMPLIANCE

The deterministic, pseudo-linear seismic evaluation procedures presented in Sections 3.4 through 3.9 are applicable to most problems. This section defines the fundamental basis of those procedures and provides an approach that expands the applicability of the recommendations. This information is not necessary, however, to the effective application of the previously presented procedures.

In the seismic assessment of underground tanks one may encounter problems for which deterministic, pseudo-linear procedures are insufficient. These problems include situations in which it is necessary to conduct explicitly non-linear dynamic analysis of structures or soil columns. In other cases, such as liquefaction analysis, there may not be existing capacity standards consistent with those used in the preceding sections. In such situations use of the criterion and the compliance approach below will permit assessments that meet the target safety objective and are consistent in conservatism with the procedures in Sections 3.4 through 3.9. The user will, of course, be responsible for developing, documenting, and defending the judgements made in these applications.

The procedures presented in Sections 3.4 through 3.9 are based on the more fundamental criterion and approach described in this section and implemented in Section 3.11. When future research on structural materials, behavior, or mechanisms improves the current knowledge base, it may be necessary to modify the judgments that led to the deterministic, pseudo-linear procedures described above, but it will not affect the criterion below. At that time one should return to this section to derive the appropriate changes to Sections 3.4 through 3.9. Many readers

may want to study this section to gain a deeper appreciation of the foundation of the guidelines.

3.10.1 The Basic Seismic Criterion

For probabilistic seismic hazard curves such as those shown in Figure 3.1, it is demonstrated in Reference 3.2 that risk reduction factors R_R of 20, 10 and 5 are closely obtained when:

$$C_{10\%} \geq 1.5SF(DBE) \tag{3.9}$$

In this basic seismic criterion, $C_{10\%}$ represents the 10-percentile seismic capacity level, i.e., the level at which a 10% probability of failure is estimated.

Notice that this single "basic" criterion (Equation 3.9) compares capacity and demand in ground motion terms, rather than in force, stress, or deformation terms, as is implied in Sections 3.4 to 3.9. The non-seismic demands are implicitly included here within $C_{10\%}$.

Reference 3.2 demonstrates that the basic seismic criterion defined by Equation 3.9 is appropriate for a wide range of hazard curves with different shapes, i.e., with a wide variation of ground motion ratios A_R (defined by Equation 3.3) when the DBE ground motion is defined at the hazard exceedance probability P_H and the factor SF is defined by Equation 3.2. This demonstration covers the practical range of A_R ratios from 1.5 to 3.75. However, the basic criterion Equation 3.9 can be extended beyond this range of A_R values with generally increasing conservatism for A_R less than 1.5.

3.10.2 The General Approach to Compliance

The most general approach to demonstrate compliance with the above basic seismic criterion is as follows. Given the performance criterion P_F and the selected R_R:

1. Establish the DBE ground motion in accordance with the guidance of Section 3.3.

2. Define a Scaled Design Basis Earthquake (SDBE) ground motion by increasing the DBE ground motion by an earthquake adjustment factor F_e defined by:

$$SDBE = 1.5(SF)(DBE) \qquad (3.10)$$

where SF is the appropriate seismic scale factor from Section 3.3.1 for the selected seismic risk reduction factor R_R.

3. Perform sufficient linear analyses, nonlinear analyses, testing, etc., to reasonably determine that for the combination of the SDBE with the best-estimate of the concurrent non-seismic loads there is less than about a 10% probability of unacceptable performance.

Any seismic evaluation approach which is consistent with the above three steps is acceptable.

3.11 BENCHMARKING DETERMINISTIC SEISMIC EVALUATION PROCEDURES AGAINST THE BASIC SEISMIC CRITERION

The basic criterion Equation 3.9 defines the necessary overall conservatism that must be built in any seismic evaluation procedure in order to achieve the desired performance goal probability P_F. The DBE has a P_H consistent with P_F and R_R (See Equation 3.1).

The necessary overall conservatism to satisfy Equation 3.9 could have been introduced into Steps A through D of Section 3.2 by any of a variety of combinations of values or factors in the deterministic pseudo-linear seismic evaluation procedure described in Section 3.2 and defined in detail in Sections 3.4 through 3.9. The deterministic procedure defined in Section 3.4 through 3.9 was chosen because it closely follows existing practices for the seismic design of critical facilities.

In this approach, very little conservatism has been introduced in the computation of the elastically computed seismic demand (Section 3.4). Best estimate structural models and material damping are used. It has been found that an introduction of conservatism into the calculation of elastically computed demand produces a highly variable factor of conservatism across the entire spectrum of natural frequencies and locations within a structure. This variation makes it difficult to achieve a specified target risk reduction factor, R_R. Reasonable variation in structure and soil stiffness properties are, however, considered and the maximum computed seismic demand over this uncertainty variation is used to represent the elastically computed seismic demand. It is estimated that enveloping the effects of these stiffness variations results in less than a 25% chance of the elastically computed response being exceeded given the occurrence of the DBE.

On the other hand, considerable conservatism has been introduced in the specified capacity by using minimum code ultimate capacities (including code specified strength reduction factors) coupled with 95% exceedance or code specified material strengths (Sections 3.6 and 3.7). For ductile failure modes, it is expected that the specified capacities will have at least a 98% probability of being exceeded by the actual capacities. For brittle failure modes, code capacities contain even greater conservatism, the code capacity typically being about half of the median (or "best-estimate") capacity.

Also considerable conservatism is introduced in the specified maximum permissible inelastic energy absorption factor by which the elastically computed seismic demand is divided to obtain the inelastic-factored seismic demand (Section 3.9). The permissible inelastic energy absorption factor $F_{\mu D}$ is conservatively established at its value associated with inelastic distortions corresponding to about a 5% failure probability.

In addition, a seismic scale factor SF is introduced in Equation 3.4 used to define the inelastic-factored seismic demand so as to accommodate a range of seismic risk reduction factors ranging from 20 to 5. The values of the seismic load factor SF and the required degree of conservatism for the permissible inelastic energy absorption factor $F_{\mu D}$ are based upon the benchmarking demonstration studies outlined in Section 2 of Reference 3.2. It is shown there that, taken together, the procedures and values in Sections 3.4 to 3.9 manage to achieve the target R_R levels for the wide range of response and capacity uncertainties that are encountered in practice.

Therefore, the procedures recommended in this chapter have succeeded in meeting the objectives of giving flexibility, simplicity, and opportunities for adaptation despite the complex and diverse nature of the seismic safety problem.

REFERENCES

3.1 DOE-STD-1020-94, "Natural Phenomena Hazards Design and Evaluation Criteria for Department of Energy Facilities," April 1994.

3.2 Kennedy, R.P., and Short, S.A., "Basis for Seismic Provisions of DOE Standard 1020-94," UCRL-CR-111478 and BNL-52418, Lawrence Livermore National Laboratory and Brookhaven National Laboratory, 1994.

3.3 Melchers, R.E., "Structural Reliability, Analysis and Prediction," Ellis, Horwood, Ltd., Chichester, England, 1987.

3.4 Cornell, C.A., "Which 84th Percentile Do You Mean?," Proceedings, 4th DOE Natural Phenomena Hazards Mitigation Conference, CONF-9310102, DOE/LLNL, Vol. 1, pp. 152-159, 1993.

3.5 SEN-35-91, DOE Nuclear Safety Policy, September 9, 1991.

3.6 DOE Order 5480.28, "Natural Phenomena Hazards Mitigation," January 1993.

3.7 DOE-STD-1024-92, "Guidelines for Use of Probabilistic Seismic Hazard Curves at Department of Energy Sites," December 1992.

3.8 Newmark, N.M., and Hall, W.J., "Development of Criteria for Seismic Review of Selected Nuclear Power Plants," NUREG/CR-0098, U.S. Nuclear Regulatory Commission, May 1978.

3.9 American Society of Civil Engineers, Standard 4-86, "Seismic Analysis of Safety-Related Nuclear Structures and Commentary on Standard for Seismic Analysis of Safety-Related Nuclear Structures," September 1986.

3.10 U.S. Nuclear Regulatory Commission, "Standard Review Plan, NUREG-0800," Sections 3.7.1 through 3.7.3, Rev. 2, August 1989.

3.11 U.S. Nuclear Regulatory Commission, Regulatory Guide 1.61, "Damping Values for Seismic Design of Nuclear Power Plants," October 1973.

3.12 American Concrete Institute, "Building Code Requirements for Reinforced Concrete, ACI 318-89," 1989.

3.13 American Concrete Institute, "Code Requirements for Nuclear Safety-Related Concrete Structures (ACI 349-85) and Commentary - ACI 349R-85," 1985.

3.14 American Institute of Steel Construction, "Manual of Steel Construction, Load & Resistance Factor Design," 2nd Ed., 1994.

3.15 American National Standard, "Nuclear Facilities - Steel Safety-Related Structures for Design, Fabrication and Erection," ANSI/AISC N-690, 1984.

3.16 American Institute of Steel Construction, "Manual of Steel Construction," Ninth Ed., 1989.

3.17 American Society of Mechanical Engineers, "ASME Boiler and Pressure Vessel Code, Section III, Rules for Construction of Nuclear Power Plant Components, Division 1," 1989.

3.18 "Qualification of Active Mechanical Equipment Used in Nuclear Power Plants," ASME QME-1-1994.

3.19 Eligehausen R., Popov, E.P., and Bertero, V.V., "Local Bond Stress-Slip Relationships of Deformed Bars under Generalized Excitations," Report No. DCB/EERC-82/23, University of California at Berkeley, October 1983.

3.20 "Seismic Design Guidelines for Essential Buildings, A Supplement to Seismic Design for Buildings," Army TM5-809-10.1, Navy NAVFAC P-355.1, Air Force ARM 88-3, Chapter 13.1, Departments of the Army, Navy and Air Force, Washington, D.C., February 1986.

3.21 Kennedy, R.P., et al., "Subsystem Response Review, Seismic Safety Margin Research Program," NUREG/CR-1706, UCRL-15216, October 1980.

3.22 "A Methodology for Assessment of Nuclear Power Plant Seismic Margin, NP-6041, Rev. 1," Electric Power Research Institute, June 1991.

NOTATION

A_R ground motion slope ratio as defined by Equation 3.3

C_C capacity based on code formula or stresses

$C_{p\%}$ seismic capacity estimated at a failure probability of p%

DBE design basis earthquake, defined at the seismic hazard exceedance probability.

D_{ns} non-seismic demand

D_{se} seismic demand based on elastic analysis

D_{si} factored inelastic seismic demand from Equation 3.4.

D_b total elastically computed demand

D_{ti} total factored inelastic demand from Equation 3.5.

$F_{\mu D}$ permitted inelastic energy absorption factor

$F_{\mu p\%}$ inelastic absorption factor specified at a failure probability level of p%

M_{ns} nonseismic moment

M_{se} seismic moment based on elastic analysis

M_{si} seismic moment based on inelastic analysis

PGA peak ground acceleration

PGD peak ground displacement

PGV peak ground velocity

P_F annual probability of failure or unacceptable performance (i.e. performance goal)

P_H seismic hazard (i.e., annual frequency of exceedance) associated with the DBE.

P_{ns} nonseismic axial load

P_{se} seismic axial load based on elastic analysis

P_{ti} total axial load based on inelastic analysis

R_R risk reduction factor, i.e., ratio of P_H/P_F

SDBE scaled design basis earthquake

SF seismic scale factor

β composite logarithmic standard deviation

ϕ capacity reduction factor (e.g., as per References 3.12, 3.13 and 3.14)

Table 3.1a Recommended Constant (Site-Independent) Scale Factors SF to Achieve Various Risk Reduction Factors

Risk Reduction Factor R_R	Constant Scale Factor SF
20	1.60
10	1.25
5	1.00

Table 3.1b Recommended Variable Scale Factor Parameters to Use in Equations (3.2a) and (3.2b)

Risk Reduction Factor R_R	SF_1	α
20	1.15	1.1
10	1.00	0.8
5	0.87	0.5

Table 3.2 Recommended Damping Values (Based on References 3.1, 3.8, 3.9, 3.11, 3.20, and 3.22)

Type of Component	Damping (% of Critical)		
	Response Level 1	Response Level 2	Response Level 3
Welded and friction-bolted steel structures	2	4	7
Bearing-bolted steel structures	4	7	10
Prestressed concrete structures (without complete loss of prestress)	2	5	7
Reinforced concrete structures	4	7	10
Piping	3	5	5
Massive, low-stressed components (pumps, motors, etc.)	2	3	--(1)
Light, welded instrument racks	2	3	--(1)
Electrical cabinets	3	4	5(2)
Metal liquid-storage tanks:			
Impulsive mode	2	3	4
Sloshing mode	0.5	0.5	0.5

(1) Should not be stressed to response level 3. Do not use damping values higher than those shown for Response Level 2.

(2) May be used for anchorage and structural failure modes which are accompanied by at least some inelastic response. Response Level 1 damping values should be used for functional failure modes such as relay chatter or relative displacement issues which may occur at a low cabinet stress level.

Table 3.3 Inelastic Energy Absorption Factors $F_{\mu D}$
(5% Non-Exceedance Values)

Structural System	$F_{\mu D}$
Concrete vault	
Walls:	
In-plane:	
Flexure	1.75
Shear	1.5
Out-of-plane:	
Flexure	1.75
Shear	1.0
Columns:	
Axial Compression	1.0
Flexure	1.5
Shear	1.0
Connections	1.0
Metal Liquid-Storage Tanks	
Moment and Shear Capacity	1.25
Hoop Capacity	1.5

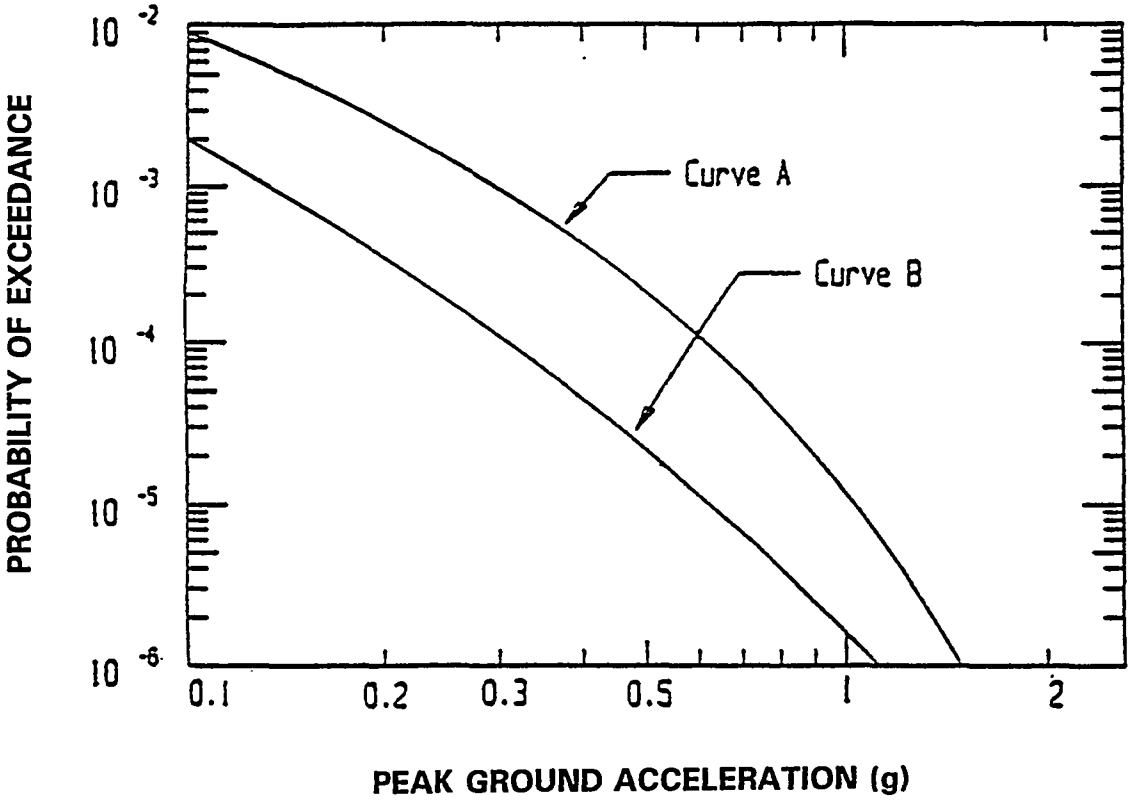

Figure 3.1 Representative Probabilistic Seismic Hazard Curves

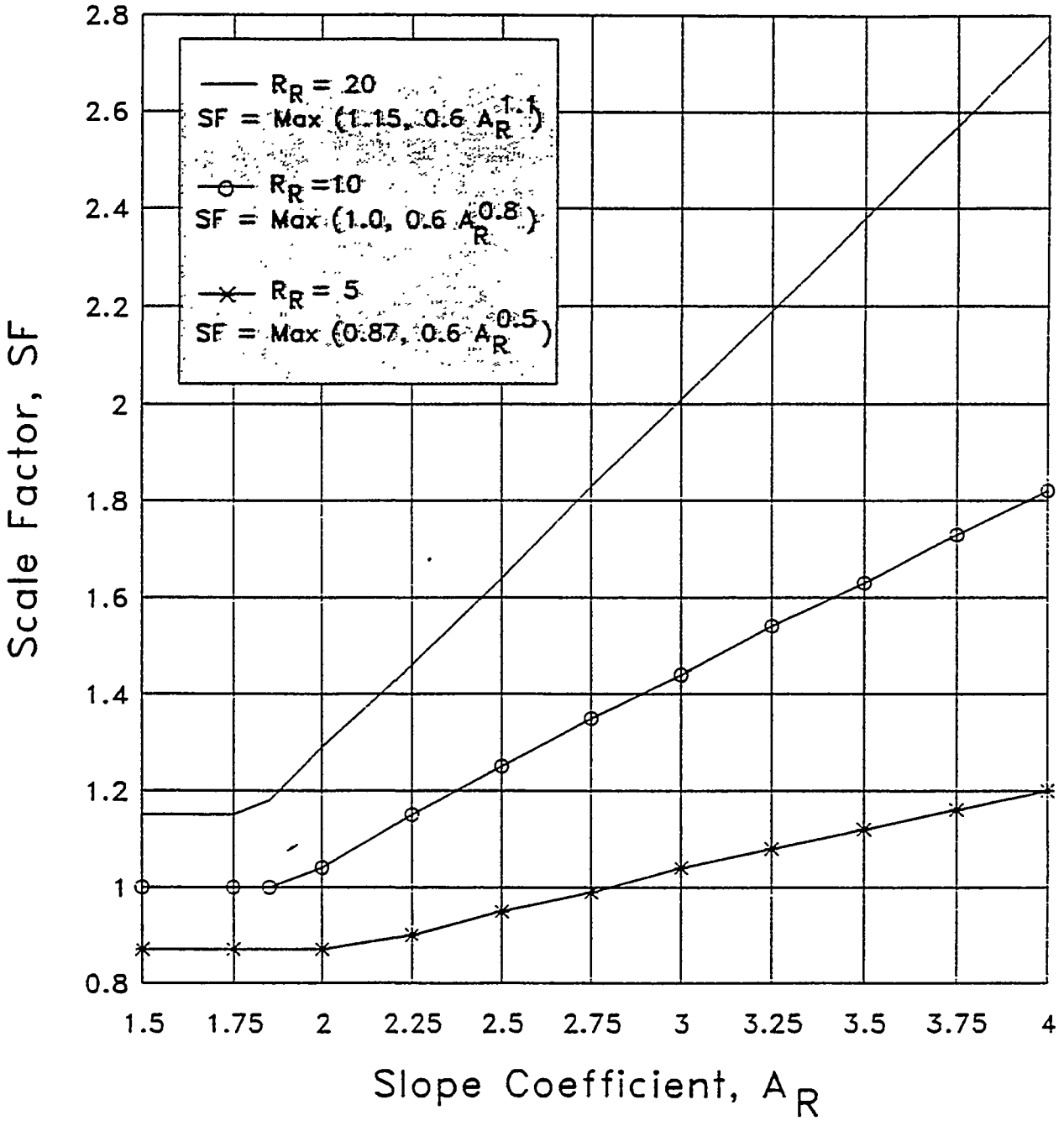

Figure 3.2 Variable Seismic Scale Factor SF

CHAPTER 4

EVALUATION OF HYDRODYNAMIC EFFECTS IN TANKS

4.1 OBJECTIVES AND SCOPE

The design guidelines in this chapter are for the evaluation of the hydrodynamic pressures and forces and of the associated liquid motions induced by earthquake ground motions in liquid-storage tanks. The term hydrodynamic is used in a generalized sense to represent the dynamic effects of any liquid.

The systems examined are shown in Figure 4.1. They are upright, circular cylindrical tanks of radius R and height H_t which are filled with liquid to a height H_ℓ. Unless otherwise indicated, the liquid is considered to be of uniform density and free at its upper surface, and only linear responses are examined. The tank wall is presumed to be clamped to a rigid moving base so that no sliding or base uplifting may occur, and to be either free or constrained at the top. The effects of both horizontal and vertical components of ground shaking are examined. Consideration also is given to the effects of a rocking component of base motion. Whereas the cantilever system is excited solely at the base, the top-constrained system is presumed to be excited simultaneously and similarly at the base and the top. Except where otherwise indicated, the liquid and tank heights may be different. The evaluation of the hydrodynamic effects in tanks containing inhomogeneous liquids is addressed briefly at the end of this chapter.

The densities of the tank wall and liquid are denoted by ρ_t and ρ_ℓ, and the modulus of elasticity and Poisson's ratio for the tank material are denoted by E_t and ν_t, respectively. Points on the tank wall are defined by the vertical distance z, measured positive upward from the tank base, and by the circumferential

angle θ, which is measured counterclockwise from the direction of the horizontal excitation. The accelerations of the horizontal, vertical and rocking components of the base motion at any time t are denoted by $\ddot{x}(t)$, $\ddot{y}(t)$ and, $\ddot{\psi}(t)$, respectively, and the absolute maximum values of these quantities are denoted by $\ddot{x}_o$, $\ddot{y}_o$ and $\ddot{\psi}_o$.

Two additional assumptions are embodied in the information presented herein: (1) The tank wall is of uniform thickness, t_{tw}; and (2) the liquid is incompressible and inviscid. For tanks of variable wall thickness, the non-uniform wall must be replaced by one of constant thickness, as indicated in a later section.

The effects of liquid viscosity are examined in Appendix B, where it is concluded that, for absolute viscosity values up to 10,000 centipoise (cP), the hydrodynamic effects may for all practical purposes be considered to be independent of the viscosity level involved. Accordingly, the information for inviscid liquids presented here may be used for viscous liquids as well. For viscosity values in excess of 10,000 cP, the representation of the waste as a liquid may not be appropriate, and it may be necessary to consider other idealizations. The studies currently being carried out in this regard are identified at the end of Appendix B.

The evaluation of the seismic response of the systems examined here does not generally warrant the use of complex, computer-based finite-difference or finite-element methods, and may be implemented reliably and cost-efficiently by the procedures described. More sophisticated methods and computer programs may naturally be used, provided their reliability is confirmed by comparing their predictions for representative cases with those obtained by the recommended procedures.

In the form presented, the design provisions are applicable only

to relatively broad tanks, for which the ratio of liquid-height to tank-radius, H_ℓ/R, is less than unity. These proportions are representative of those of waste-storage tanks normally found in DOE facilities.

For background information on the subject matter covered in this chapter, and for data on the response of tanks with values of H_ℓ/R in excess of unity, the reader is referred to the references listed at the end of this chapter.

4.2 RESPONSES OF INTEREST AND MATERIAL OUTLINE

A critical element in the analysis of the seismic response of the tank-liquid system is the evaluation of the hydrodynamic pressures exerted against the tank wall and base. Once these pressures have been established, the corresponding forces and stresses in the tank may be determined with relative ease.

Of special importance in the seismic design and safety evaluation of tanks are the maximum values of the following forces:

- The hoop forces in the tank wall;
- The total hydrodynamic force exerted on the tank wall, and the resulting end shears;
- The resulting bending moments across sections normal to the tank axis; these moments, in combination with the beam theory, are used to evaluate the axial forces in the tank wall; and
- The forces and moments transmitted to the tank support.

Also of importance is the maximum vertical or sloshing motion of the free liquid surface.

In the following sections, the hydrodynamic pressures and tank forces are evaluated first for a horizontal component of ground

shaking, then for a possible rocking motion of the tank base, and finally for a vertical motion of the ground. The sloshing motion of the free liquid surface is examined at the end of the chapter. The effects of dynamic coupling between the tank-liquid system, the supporting vault, and the surrounding soil are considered only briefly in this chapter; they are examined in detail in Chapter 6.

4.3 EFFECTS OF HORIZONTAL COMPONENT OF SHAKING

4.3.1 General

The hydrodynamic effects induced by the horizontal component of ground shaking may conveniently be expressed as the sum of two components:

- An impulsive component, which represents the effects of the part of the liquid that may be considered to move in synchronism with the tank wall as a rigidly attached mass; and

- A convective component, which represents the action of the part of the liquid near the free surface that experiences sloshing or rocking motion.

In mathematical terms, the impulsive component of the solution satisfies the actual boundary conditions along the lateral and bottom surfaces of the liquid and the condition of zero hydrostatic pressure at the mean level of the free liquid surface; accordingly, it does not account for the effects of the surface waves associated with sloshing actions. The convective component of the solution effectively corrects for the difference between the actual boundary condition at the mean liquid surface and the one considered in the development of the impulsive solution.

Because it is associated with motions of significantly lower

frequencies than the natural frequencies of the tank-liquid system or the dominant frequencies of the excitation, the convective part of the solution is practically unaffected by the flexibility of the tank wall, and may be evaluated with reasonable accuracy considering the tank to be rigid. By contrast, the impulsive part of the solution is sensitive to the tank wall flexibility, and this factor must be, and is, provided for in the analysis.

4.3.2 Hydrodynamic Wall and Base Pressures

The instantaneous value of the hydrodynamic pressure induced at an arbitrary point of the tank wall, $p = p(\eta_\ell, \theta, t)$, may be expressed as

$$p(\eta_\ell, \theta, t) = p_i(\eta_\ell, \theta, t) + p_c(\eta_\ell, \theta, t) \qquad (4.1)$$

in which $\eta_\ell = z/H_\ell$ is the normalized vertical distance measured from the base, positive upward; and p_i and p_c are, respectively, the impulsive and convective components of the pressure. The impulsive component may be expressed by the product of functions of η_ℓ, θ and t as

$$p_i(\eta_\ell, \theta, t) = c_i(\eta_\ell)\, \rho_\ell R A_i(t) \cos\theta \qquad (4.2)$$

and the convective component may be expressed by the sum of the products of such functions, as

$$p_c(\eta_\ell, \theta, t) = \sum_{n=1}^{N} [c_{cn}(\eta_\ell)\, \rho_\ell R A_{cn}(t)] \cos\theta \qquad (4.3)$$

in which N is a sufficiently large integer. In these expressions, $A_i(t)$ and $A_{cn}(t)$ are pseudoacceleration response functions for single-degree-of-freedom oscillators defined in greater detail later; $c_i(\eta_\ell)$ is a dimensionless function of η_ℓ that defines the axial or heightwise variation of the impulsive component of the wall pressure; and $c_{cn}(\eta_\ell)$ is a similar function that defines the corresponding variation of the pressure

associated with the nth sloshing mode of vibration of the liquid. The latter function is given by

$$c_{cn}(\eta_\ell) = \frac{2}{\lambda_n^2 - 1} \frac{\cosh[\lambda_n (H_\ell/R)\, \eta_\ell]}{\cosh[\lambda_n (H_\ell/R)]} \qquad (4.4)$$

in which λ_n represents the nth root of the first derivative of the Bessel function of the first kind and first order. The first three of these roots are

$$\lambda_1 = 1.841 \qquad \lambda_2 = 5.331 \qquad \lambda_3 = 8.536 \qquad (4.5)$$

Note that, in addition to the position coordinate η_ℓ, the functions $c_{cn}(\eta_\ell)$ depend on the liquid height to tank radius ratio, H_ℓ/R. The maximum values of these functions occur at the top, $\eta_\ell = 1$, are independent of H_ℓ/R, and add up to unity. The first three maxima are

$$c_{c1}(1) = 0.837 \qquad c_{c2}(1) = 0.073 \qquad c_{c3}(1) = 0.028 \qquad (4.6)$$

With the functions $c_{cn}(\eta_\ell)$ determined, the function $c_i(\eta_\ell)$ for the impulsive component of wall pressure may be determined from

$$c_i(\eta_\ell) = 1 - \sum_{n=1}^{N} c_{cn}(\eta_\ell) \qquad (4.7)$$

The values of $c_i(\eta_\ell)$ for tanks of different proportions are listed in Table 4.1. These values may also be determined approximately from

$$c_i(\eta_\ell) = D_i\left[\cos\frac{\pi}{2}\eta_\ell - 0.11\cos\frac{3\pi}{2}\eta_\ell + 0.04\cos\frac{5\pi}{2}\eta_\ell - 0.02\cos\frac{7\pi}{2}\eta_\ell + \ldots\right] \qquad (4.8)$$

in which D_i is a dimensionless function of H_ℓ/R, given in Column 2 of Table 4.2.

Equations 4.2 and 4.3 reveal that both components of the hydrodynamic wall pressure vary in the circumferential direction as

$\cos\theta$. Therefore, their peak values at an arbitrary elevation and time are attained along a diametral axis in the direction of the excitation, and the zero values are attained along a normal axis. Equations 4.4 and 4.7 further reveal that, whereas the convective pressure components decrease from top to bottom, the impulsive component increases from zero at the liquid surface to a maximum at the base.

The distribution function $c_i(\eta_\ell)$ for the impulsive component of the hydrodynamic wall pressure and the corresponding functions for the first two convective components are shown in Figure 4.2 for tanks with $H_\ell/R=0.75$.

The instantaneous value of the hydrodynamic pressure on the tank base, $p' = p'(\xi,\theta,t)$, may similarly be expressed as

$$p'(\xi,\theta,t) = p_i'(\xi,\theta,t) + p_c'(\xi,\theta,t) \qquad (4.9)$$

where $\xi = r/R$ is the normalized radial distance; and p_i' and p_c' are the impulsive and convective components of the pressure, respectively. The impulsive component may be expressed as

$$p_i'(\xi,\theta,t) = c_i'(\xi)\rho_\ell RA_i(t)\cos\theta \qquad (4.10)$$

and the convective component as

$$p_c'(\xi,\theta,t) = \sum_{n=1}^{\infty}[c_{cn}'(\xi)\rho_\ell RA_{cn}(t)]\cos\theta \qquad (4.11)$$

where $c_i'(\xi)$ and $c_{cn}'(\xi)$ are dimensionless functions of ξ. The values of $c_i'(\xi)$ for tanks of different proportions are listed in Table 4.3, and those of $c_{cn}'(\xi)$ are given by

$$c_{cn}'(\xi) = \frac{2}{\lambda_n^2 - 1}\,\frac{1}{\cosh[\lambda_n(H_\ell/R)]}\,\frac{J_1(\lambda_n\xi)}{J_1(\lambda_n)} \qquad (4.12)$$

where J_1 is the Bessel function of the first kind and first order. The values of $c_i'(\xi)$ and $c_{cn}'(\xi)$ at $\xi = 1$ are naturally equal to those of $c_i(\eta_\ell)$ and $c_{cn}(\eta_\ell)$ at $\eta_\ell = 0$, respectively. The

variations of $c_i'(\xi)$ and $c_{c1}'(\xi)$ for tanks with $H_\ell/R = 0.75$ are shown graphically in Figure 4.3.

Note should be taken of the fact that the pressures in Equations 4.1 through 4.3 and Equations 4.9 through 4.11 are expressed in terms of the tank radius, R, rather than the liquid height, H_ℓ, or the tank height, H_t. Accordingly, in comparing tanks of different proportions, their radii rather than the liquid or tank heights must be considered to be the same.

Implicit in Equations 4.2 and 4.10 is the assumption that the distributions (but not magnitudes) of the impulsive components of the wall and base pressures are independent of the tank wall flexibility and identical to the distributions of the corresponding pressures in a rigid tank of the same proportions. More precise analyses of flexible tanks with both free and constrained top boundaries (References 4.3 through 4.6) reveal that this is indeed a valid approximation for the relatively broad tanks with values of $H_\ell/R \leq 1$ considered herein. While Equations 4.2 and 4.10 for the impulsive effects are limited to such broad tanks, Equations 4.3, 4.4, 4.11 and 4.12 for the convective effects may be used for tanks of arbitrary proportions.

The functions $A_i(t)$ and $A_{cn}(t)$ in Equations 4.2, 4.3, 4.10 and 4.11 represent the instantaneous pseudoaccelerations induced by the prescribed base motion in viscously damped single-degree-of-freedom linear systems of specified damping and natural frequencies. Specifically, $A_i(t)$ refers to a system the natural frequency of which is equal to the fundamental natural frequency of the tank wall vibrating along with the impulsive component of the liquid mass, and $A_{cn}(t)$ refers to a system with a natural frequency equal to the nth sloshing frequency of vibration of the contained liquid. These frequencies are defined further in the next two sections. The damping value used in the computation of the impulsive effects should correspond to that

deemed to be appropriate for the tank wall material, whereas that for the convective effects should be taken as 0.5 percent of the critical value, unless higher values can be justified. These issues are addressed further in Chapter 5 and Appendix B.

For a single-degree-of-freedom system with a circular natural frequency ω and percentage of critical damping ζ, the pseudo-acceleration A(t) is given by

$$A(t) = \frac{\omega}{\sqrt{1-\zeta^2}} \int_0^t \ddot{x}(\tau) \exp[-\zeta\omega(t-\tau)] \sin[\omega\sqrt{1-\zeta^2}(t-\tau)]\, d\tau \qquad (4.13a)$$

and it is related to the instantaneous deformation of the system, u(t), by

$$A(t) = \omega^2 u(t) \qquad (4.13b)$$

The absolute maximum values of u(t) and A(t) are the quantities displayed in deformation and pseudoacceleration response spectra, respectively. The spectral pseudoaccelerations will be denoted by S_A, and appropriate subscripts will be used to identify the values corresponding to the impulsive and convective components of response.

4.3.2.1 Natural Sloshing Frequencies

The natural frequency in cycles per second of the nth convective or sloshing mode of vibration of the liquid, f_{cn}, is given by

$$f_{cn} = \frac{1}{2\pi}\sqrt{\lambda_n \frac{g}{R} \tanh[\lambda_n (H_\ell/R)]} \qquad (4.14)$$

in which g represents the acceleration of gravity, and λ_n has the values given in Equation 4.5.

As a measure of the values of f_{cn} that may be encountered in practice, it is noted that, for tanks with $H_\ell/R = 0.5$, Equation 4.14 leads to the following expressions for the first three

sloshing periods of vibration

$$T_{c1} = 0.958\sqrt{R} \qquad T_{c2} = 0.482\sqrt{R} \qquad T_{c3} = 0.379\sqrt{R} \qquad (4.15)$$

in which $T_{cn} = 1/f_{cn}$ is expressed in seconds, and R is expressed in feet. Observe that the sloshing periods can be quite long for tanks of large radii.

4.3.2.2 Fundamental Natural Frequency of Tank-Liquid System

The fundamental natural frequency of the impulsive mode of vibration of the tank-liquid system, in cycles per second or Hz, may conveniently be expressed in terms of the liquid height H_ℓ as

$$f_i = \frac{1}{2\pi}\frac{C_i}{H_\ell}\sqrt{\frac{E_t}{\rho_t}} \qquad (4.16)$$

where C_i is a dimensionless coefficient that depends on:

- The ratio of liquid height to tank radius, H_ℓ/R;
- The conditions of tank support at the top;
- The ratio of liquid height to tank height, H_ℓ/H_t;
- The ratio of wall thickness to tank radius, t_{tw}/R;
- The ratio of the mass densities for the liquid and tank material, ρ_ℓ/ρ_t; and
- Poisson's ratio for the tank material, ν_t.

For steel tanks for which E_t = 30,000 ksi and the unit weight $\gamma_t = \rho_t g$ = 490 lb/ft^3, Equation 4.16 may be written as

$$f_i = \frac{2{,}680\, C_i}{H_\ell} \qquad (4.17)$$

in which H_ℓ is expressed in feet. Note that H_ℓ affects Equations 4.16 and 4.17 both directly through its presence in the denominators of these expressions and indirectly through the dimensionless coefficient C_i, which is a function of H_ℓ/R.

The values of C_i for a representative group of roofless steel tanks that are filled with water to four different fractions of the tank height are listed in Table 4.4. These are reference systems with $\nu_t = 0.3$, $\rho_\ell/\rho_t = 0.127$ and $t_{tw}/R = 0.001$, and their values of C_i are identified with the subscript r.

Three conditions of support are considered for the top boundary of the shell:

- A completely free condition, for which the axial, circumferential and radial displacements are unconstrained;
- A roller support, for which only the axial displacements are unconstrained and the others vanish; and
- A hinge support, for which all three displacement components vanish.

For a clamped top boundary, for which the rotation of the tank wall vanishes in addition to all linear displacement components, the results may be taken equal to those for the hinged boundary.

With the values of C_i for the reference systems established, the corresponding values for tanks of arbitrary t_{tw}/R and ρ_ℓ/ρ_t may be determined from

$$C_i = (C_i)_r \sqrt{127\,(t_{tw}/R)\,/\,(\rho_\ell/\rho_t)} \qquad (4.18)$$

This expression is based on the assumption that the inertia effects of the tank itself are negligible compared to those of the contained liquid, a condition normally satisfied in practice.

It is worth noting in Table 4.4 that the values of $(C_i)_r$ for the top-free, cantilever systems are practically independent of the H_ℓ/H_t ratio. As a result, provided the height H_ℓ in Equations 4.16 and 4.17 is interpreted correctly as the liquid height

rather than the tank height, the results for the fully filled tanks may be used for the partially filled tanks as well. To a reasonable degree of approximation, the same is also true of the top-constrained tanks, particularly those with the roller support which, as indicated later, is the more realistic of the two constrained top boundary conditions considered.

Effects of Nonuniform Wall Thickness. Note has already been taken of the fact that, for the tank proportions considered herein, the distribution functions $c_i(\eta_\ell)$ and $c_i'(\xi)$ in Equations 4.2 and 4.10 may be considered to be independent of the thickness of the tank wall and, hence, of its possible variation with height. By contrast, the pseudoacceleration $A_i(t)$ in this equation, being a function of the natural frequency f_i, does depend on the tank wall thickness and its heightwise variation.

For tanks of nonuniform wall thickness, the natural frequency f_i may be determined from the information presented in the preceding section by replacing the variable thickness of the tank wall with an average value. The averaging should be done so as to emphasize the section of the tank for which the associated modal displacements are the largest. Inasmuch as the maximum displacements for the fundamental mode of vibration occur within the lower rather than the upper parts of the tank, the wall thickness should be averaged over the lower two-thirds of the liquid height.

Effect of Roof Mass. For tanks for which the top cannot deflect relative to its base, the roof mass will have no effect on the natural frequency of the tank-liquid system. Even for cantilever tanks, this mass is likely to be inconsequential, unless its magnitude is a sizable fraction of the liquid mass.

For systems for which the roof mass is sufficiently large to warrant consideration, the fundamental impulsive natural period, $\overline{T}_i$, may be determined from

$$\overline{T_i^2} = T_i^2 + T_f^2 + T_s^2 \tag{4.19}$$

in which $T_i = 1/f_i$ = the natural period determined from Equation 4.16 or 4.17 for the roofless tank-liquid system, and T_f and T_s are the natural periods of the empty tank computed on the assumption that the roof mass is the only structural mass. Specifically, T_f represents the natural period computed on the assumption that the empty tank responds as a cantilever flexural beam, and T_s is the corresponding period computed on the assumption that the tank behaves as a cantilever shear beam. These periods are given by

$$T_f = 2\pi\sqrt{\frac{m_r}{k_f}} \tag{4.20}$$

and

$$T_s = 2\pi\sqrt{\frac{m_r}{k_s}} \tag{4.21}$$

in which k_f = the flexural stiffness of the substitute beam, and k_s = the corresponding shearing stiffness. For a tank of uniform wall thickness, these stiffnesses are given by

$$k_f = 3\frac{E_t I_t}{H_t^3} = 3\pi\left(\frac{R}{H_t}\right)^3 E_t t_{tw} \tag{4.22}$$

and

$$k_s = \frac{1}{2}\frac{G_t A_{tw}}{H_t} = \frac{\pi}{2(1+\nu_t)}\frac{R}{H_t}E_t t_{tw} \tag{4.23}$$

In these expressions, $G_t = E_t/[2(1+\nu_t)]$ = the shear modulus of elasticity of the tank material ; $A_{tw} = 2\pi R t_{tw}$ = the cross-sectional area of the tank wall; and $I_t = \pi R^3 t_{tw}$ = the moment of inertia of the tank cross section about a horizontal centroidal axis.

4.3.2.3 Maximum Values of Wall and Base Pressures

The maximum values of the impulsive and convective components of the hydrodynamic wall pressures may be determined from Equations 4.2 and 4.3 by replacing the pseudoacceleration functions $A_i(t)$ and $A_{cn}(t)$ by their maximum or spectral values, $(S_A)_i$ and $(S_A)_{cn}$, respectively. The maximum values of the total hydrodynamic wall pressures, $p_{max}(\eta_\ell, \theta)$, may then be determined from Equation 4.1 by combining the component maxima by the square-root-of-the-sum-of-the-squares rule as

$$p_{max}(\eta_\ell, \theta) = \left[\sqrt{[C_i(\eta_\ell)(S_A)_i]^2 + [C_{c1}(\eta_\ell)(S_A)_{c1}]^2 + [C_{c2}(\eta_\ell)(S_A)_{c2}]^2 + \ldots}\right]\rho_\ell R\cos\theta \quad (4.24)$$

A more conservative approach would be to add to the maximum numerical value of the impulsive pressure the square root of the sum of squares of the maximum values of the convective pressure components, i.e., express $p_{max}(\eta_\ell, \theta)$ as

$$p_{max}(\eta_\ell, \theta) = \left[C_i(\eta_\ell)(S_A)_i + \sqrt{\sum_n [C_{cn}(\eta_\ell)(S_A)_{cn}]^2}\right]\rho_\ell R\cos\theta \quad (4.25)$$

When the contribution of only the fundamental sloshing mode is considered, which would be adequate in most cases, Equations 4.24 and 4.25 reduce to

$$p_{max}(\eta_\ell, \theta) = \left[\sqrt{[C_i(\eta_\ell)(S_A)_i]^2 + [C_{c1}(\eta_\ell)(S_A)_{c1}]^2}\right]\rho_\ell R\cos\theta \quad (4.26a)$$

and

$$p_{max}(\eta_\ell, \theta) = \left[C_i(\eta_\ell)(S_A)_i + C_{c1}(\eta_\ell)(S_A)_{c1}\right]\rho_\ell R\cos\theta \quad (4.26b)$$

respectively. For the terms retained, Equation 4.26b is, of

course, the same as that obtained by taking the numerical sum of the component maxima.

The hydrodynamic pressures referred to above are in excess of the hydrostatic, and must be added to the latter to obtain the total wall pressures exerted by the liquid.

4.3.2.4 Relative Magnitudes of Impulsive and Convective Pressures

For the tank proportions normally encountered in practice, the hydrodynamic effects are dominated by the impulsive component of response. This is due mainly to the fact that the fundamental impulsive frequency of the tank-liquid system, f_i, normally falls in the amplified, nearly constant region of the pseudoacceleration response spectrum, for which the value $(S_A)_i$ is quite high. By comparison, the fundamental sloshing frequency, f_{c1}, is significantly lower and is associated with correspondingly smaller values of $(S_A)_{c1}$. While the spectral pseudoaccelerations corresponding to the higher sloshing frequencies may be substantial, they are associated with values of $c_{cn}(\eta_\ell)$ which are so much smaller than those for the fundamental sloshing mode (see, for example, Figure 4.2) that their contributions are generally unimportant. In fact, excellent approximations to the total hydrodynamic effects may generally be obtained by superposing on the impulsive effects those of the fundamental convective mode only; this approximation is adopted for several of the expressions presented in the following sections.

4.3.3 Evaluation of Critical Effects

With the maximum values of the hydrodynamic wall pressures established, the corresponding values of the tank forces may be computed by means of a **static** analysis, making use of an appropriate shell theory or any one of a number of available computer programs. However, a detailed evaluation of the state

of stress throughout the shell is generally not necessary, and it is sufficient to evaluate the effects across certain critical sections by simpler approaches. In particular, circumferential hoop stresses in the tank wall may be determined from the wall pressures considering the shell to behave as a series of isolated rings, and shearing and axial stresses across normal sections may be computed from the corresponding shearing forces and bending moments by application of the beam theory.

If $\bar{p}_{max}$ represents the maximum value of the combination of the hydrostatic and hydrodynamic wall pressure at an arbitrary level, the maximum value of the circumferential hoop stress in the tank wall at that level, $(\sigma_\theta)_{max}$, is given by

$$(\sigma_\theta)_{max} = \frac{\bar{p}_{max} R}{t_{tw}} \tag{4.27}$$

in which t_{tw} should be taken as the **actual** wall thickness at the level under consideration. The stress evaluated in this manner should be compared to the allowable stress for a normal section one foot above the base as well as for each section where t_{tw} changes.

Similarly, if V_{max} and M_{max} represent the maximum values of the shearing force and bending moment across a normal section, the maximum value of the corresponding shearing stress in the tank wall, τ_{max}, is given by

$$\tau_{max} = 2\frac{V_{max}}{A_{tw}} = \frac{1}{\pi}\frac{V_{max}}{R t_{tw}} \tag{4.28}$$

and the corresponding value of the axial force per unit of circumferential length, $(N_z)_{max}$, is given by

$$(N_z)_{max} = \frac{M_{max}}{\pi R^2} \tag{4.29}$$

Finally, the maximum axial stress, $(\sigma_z)_{max}$, is given by

$$(\sigma_z)_{max} = \frac{(N_z)_{max}}{t_{tw}} \qquad (4.30)$$

in which t_{tw} should again be taken as the thickness of the tank wall for the section under consideration. The critical sections and the evaluation of the maximum shear and bending moment are discussed in the following sections.

4.3.4 Total Hydrodynamic Force

The instantaneous value of the total hydrodynamic force induced against the tank wall, P(t), may be expressed, in a form analogous to Equation 4.1, by the sum of an impulsive component and a series of convective components as

$$P(t) = m_i A_i(t) + \sum_{n=1}^{N} m_{cn} A_{cn}(t) \qquad (4.31)$$

in which m_i = the component of the liquid mass which may be considered to move in unison with the tank wall, and m_{cn} = the mass associated with the nth sloshing mode of vibration of the liquid. Obtained by integration of the appropriate components of the hydrodynamic wall pressures, these masses are given by

$$m_{cn} = \left\{ \frac{2}{\lambda_n(\lambda_n^2-1)(H_\ell/R)} \tanh[\lambda_n(H_\ell/R)] \right\} m_\ell \qquad (4.32)$$

and

$$m_i = m_\ell - \sum_{n=1}^{N} m_{cn} \qquad (4.33)$$

in which $m_\ell = \pi R^2 H_\ell \rho_\ell$ = the total liquid mass. The values of m_i, m_{c1} and m_{c2}, normalized with respect to the total liquid mass, m_ℓ, are listed in Columns 3, 7 and 8 of Table 4.2. In view of the smallness of the values of m_{cn} for $n \geq 2$, it is normally sufficient to consider only the first term of the summation in

Equation 4.31.

4.3.5 Critical Tank Forces

4.3.5.1 Base Shear

For cantilever tanks with a free top, the base shear is clearly equal to the total hydrodynamic wall force defined by Equation 4.31.

For top-constrained tanks of the proportions considered herein, the instantaneous value of the base shear, $V(0,t) = V_b(t)$, may be expressed in a form analogous to Equation 4.31 as

$$V_b(t) = \alpha_i m_i A_i(t) + \alpha_{c1} m_{c1} A_{c1}(t) \qquad (4.34)$$

in which α_i and α_{c1} are dimensionless factors representing the contributions of the impulsive and fundamental convective modes of vibration, respectively. The effects of the higher convective modes are generally quite small, and are not provided for in this expression. The values of these factors for tanks that are constrained at the top either by roller or hinge supports are listed in Table 4.5. Both fully filled and partially filled systems are considered. The resulting shears for the fully filled systems are naturally larger than for the corresponding partially filled systems.

Examination of the data in Table 4.5 reveals that the α_i factor is practically independent of the H_ℓ/R ratio and insensitive to the type of top constraint. For the fully filled tanks, α_i varies within the narrow range of 0.56 and 0.63, indicating that, almost independently of the tank proportions and the type of top constraint, the impulsive component of the base shear is approximately 60 percent of the corresponding component of the total force exerted on the tank wall. By contrast, the fundamental convective component of the base shear is in the range of 37 to 54 percent of the corresponding component of the

total force. The ranges of variation of the α_i and α_{c1} factors are even smaller for the partially filled tanks. The shear at the top is clearly equal to the difference between the total hydrodynamic wall force and the base shear.

With the instantaneous values of the end shears established, their maximum values may be obtained by appropriate combinations of the peak values of their impulsive and convective components, as previously indicated for the corresponding wall pressures.

4.3.5.2 Bending Moments Across Normal Tank Sections

Moments for Cantilever Tanks. For a cantilever tank with a totally free top boundary, the absolute maximum bending moment occurs across a normal section immediately above the tank base, and its instantaneous value, $M(0,t) = M_b(t)$, is given approximately by

$$M_b(t) = -0.40 m_i H_\ell A_i(t) - \sum_{n=1}^{N} m_{cn} h_{cn} A_{cn}(t) \qquad (4.35)$$

in which the first term represents the impulsive component and the summation represents the convective components. The quantity h_{cn} in this equation represents the height at which the nth sloshing mass may be considered to be concentrated, and it is defined by

$$h_{cn} = \left\{ 1 - \frac{1}{\lambda_n (H_\ell/R)} \tanh\left[\frac{\lambda_n}{2} (H_\ell/R) \right] \right\} H_\ell \qquad (4.36)$$

The values of h_{c1} and h_{c2} are listed in Columns 9 and 10 of Table 4.2. Equation 4.35 reveals that the impulsive mass, m_i, is effectively concentrated at a distance of $0.40H_\ell$ from the base.

The negative signs in Equation 4.35 signify that for the part of the tank defined by values of the circumferential position coordinate θ in the range between -90° and 90°, for which the

hydrodynamic wall pressures are positive (i.e., they push against the wall), the moment induces compressive meridional axial forces. Consistent with the engineering sign convention used in the analysis of beams, a positive moment is considered to induce tensile meridional axial forces in this half of the tank. Although the sign of the moment is of no special interest in the seismic analysis of structures, it is indicated here for use later in explaining a fundamental difference between the responses of cantilever and top-constrained tanks.

For cantilever tanks for which the thickness of the tank wall decreases with height, the bending moment inducing the largest axial wall stress may well occur at some distance away from the base. It is desirable, therefore, to evaluate the heightwise variation of the moment as well.

On a normal section defined by the dimensionless distance η_ℓ, the instantaneous value of the impulsive component of the bending moment, $M_i(\eta_\ell, t)$, can most conveniently be expressed in terms of the total mass of the liquid, m_ℓ, and the liquid height, H_ℓ, as

$$M_i(\eta_\ell, t) = d_i(\eta_\ell)\, m_\ell H_\ell A_i(t) \tag{4.37}$$

and the corresponding convective component, $M_c(\eta_\ell, t)$, may be expressed similarly by the series

$$M_c(\eta_\ell, t) = \sum_{n=1}^{N} d_{cn}(\eta_\ell)\, m_\ell H_\ell A_{cn}(t) \tag{4.38}$$

in which $d_i(\eta_\ell)$ and $d_{cn}(\eta_\ell)$ are dimensionless functions. The values of $d_i(\eta_\ell)$ and $d_{cn}(\eta_\ell)$ for cantilever tanks of different proportions filled to four different fractions of the tank height are listed in Tables 4.6 and 4.7. These values, as well as the corresponding values for top-constrained tanks presented in subsequent tables, are strictly valid for steel tanks with $t_{tw}/R = 0.001$ that are filled with water. The ratio of the mass densities of the liquid and tank material in this case is ρ_ℓ/ρ_t

= 0.127, and Poisson's ratio of the tank material ν_t = 0.3. Despite this, the results may be used with good accuracy for all combinations of the parameters that are likely to be encountered in the type of applications envisioned herein. This matter is considered further in Section 4.3.5.3.

For a section immediately above the base, the values of d_i and d_{cn} are related to the quantities $0.40m_i$ and $m_{cn}h_{cn}$ in Equation 4.35 as follows:

$$d_i(0) = -0.40\frac{m_i}{m_\ell} \tag{4.39}$$

and

$$d_{cn}(0) = -\frac{h_{cn}}{H_\ell}\frac{m_{cn}}{m_\ell} \tag{4.40}$$

However, because the 0.40 factor and the values of d_i were computed by procedures of somewhat different accuracy, the values obtained from Equation 4.39 do not always agree with those listed in Table 4.6 to the number of significant figures reported. The 0.40 factor is strictly valid for rigid tanks, whereas the values of d_i in Table 4.6 are for the flexible tanks referred to earlier in this section.

Moments for Top-Constrained Tanks. For top-constrained tanks, it is desirable to normalize the vertical distance z in terms of the tank height, H_t, rather than the liquid height, H_ℓ. Equations 4.37 and 4.38 are, therefore, rewritten as

$$M_i(\eta_t, t) = d_i(\eta_t)\, m_\ell H_\ell A_i(t) \tag{4.41}$$

and

$$M_c(\eta_t, t) = \sum_{n=1}^{N} d_{cn}(\eta_t)\, m_\ell H_\ell A_{cn}(t) \tag{4.42}$$

where $\eta_t = z/H_t$. The values of $d_i(\eta_t)$ and $d_{ci}(\eta_t)$ for tanks with a roller support at the top are listed in Tables 4.8 and 4.9, respectively, and those for tanks hinged at the top are given in Tables 4.10 and 4.11. As before, a large number of H_ℓ/R values and four values of the H_ℓ/H_t ratio are considered. In addition, the functions $d_i(\eta_t)$ and $d_{ci}(\eta_t)$ for fully filled cantilever and top-constrained tanks with $H_\ell/R = 0.75$ are compared in Figure 4.4.

Examination of the plots in Figure 4.4 and of the data for fully filled tanks presented in Tables 4.6 through 4.11 reveals the following trends:

1. The maximum values of the bending moment coefficients for tanks with a roller support at the top are, as might be expected, smaller than those for similarly excited cantilever tanks of the same proportions. By contrast, the corresponding values for tanks with the hinged boundary are either of the same order of magnitude or significantly larger than those for cantilever tanks.

2. The heightwise distributions of both the impulsive and convective components of the bending moments for the top-constrained tanks are more nearly uniform than for the corresponding cantilever tanks. Furthermore, whereas the absolute maximum values of the moment for the cantilever tanks occur at the base, those for the top-constrained tanks occur at or close to midheight.

3. For a prescribed direction of the hydrodynamic wall pressure, the bending moments in top-constrained tanks act in a direction **opposite** to that for the corresponding cantilever tanks. This fact is indicated by the opposite signs of the data presented in Tables 4.6 and 4.7 and in Tables 4.8 through 4.11.

These trends are Poisson's ratio-related, and may be explained

as follows. For tanks of non-zero Poisson's ratio, a tensile circumferential (hoop) force in the tank wall tends to induce axial shortening of the wall, whereas a compressive circumferential force tends to induce axial extension. For a tank that is fully constrained against axial movements, these displacements naturally cannot occur. As a result, the circumferential tensile forces caused by the hydrodynamic wall pressures over half of the tank induce **tensile** axial forces over that half, and the circumferential compressive forces over the opposite half induce **compressive** axial forces in that half. The net effect of these axial forces is a bending moment over sections normal to the tank axis. Furthermore, the direction of this moment is **opposite** to that of the moment induced in a similarly excited cantilever tank.

The axial force per unit of circumferential length, N_z, corresponding to the moments referred to above may be determined from Equation 4.29. For fully filled tanks that are totally constrained in the axial direction, the value of N_z due to this Poisson's ratio-related effect is approximately ν_t times (for steel tanks, 30 percent of) the corresponding average hoop force over the tank height. The latter force is given roughly by

$$(N_\theta)_{av} = \left[\frac{m_i}{m_t}(S_A)_i + \frac{m_{c1}}{m_t}(S_A)_{c1}\right]\rho_t R^2 \qquad (4.43)$$

It should be realized that, for axially constrained tanks, Poisson's ratio-related axial forces also develop under hydrostatic loads, and that these forces must be considered in assessing the consequences of the corresponding forces induced by the hydrodynamic actions. For the tank proportions and intensities of ground shaking normally encountered in practice, the uniform axial tensile forces induced by the hydrostatic wall pressures are generally larger than the corresponding tensile and compressive forces induced by the hydrodynamic pressures. The net effect under these conditions would be a reduction in

the magnitudes of the compressive axial forces compared to those developed in a free-standing cantilever tank, and a consequent reduction in the tendency for wall buckling.

The Poisson's ratio-related axial forces may easily be relieved by slight movements of the supports or slight bending of the tank wall. Since such movements are almost certain to occur in practice, the roller condition of top support is believed to be a more realistic representation of actual conditions than the hinged condition.

The effect of Poisson's ratio ν_t on the bending moments induced across normal sections of tanks with a roller support at the top is illustrated in Table 4.12. Listed are the values of the moment coefficients $d_i(\eta_t)$ and $d_{c1}(\eta_t)$ for tanks with $H_\ell/R=0.75$ and values of ν_t = 0 and 0.3. It is observed that increasing ν_t increases the positive moments and decreases the negative moments. Note, in particular, that whereas the base moments are negative for $\nu_t=0$, they are positive for $\nu_t=0.3$.

Further insights into the magnitude and distribution of the axial forces induced in top-constrained tanks may be gained from the membrane solutions presented in Appendix C.

4.3.5.3 Sensitivity to Variations in System Parameters

In addition to the ratios H_ℓ/R, H_ℓ/H_t and the vertical position coordinate η_ℓ or η_t, the shear and moment coefficients listed in Tables 4.5 through 4.11 depend on Poisson's ratio for the tank material, ν_t, the ratio of the wall thickness to tank-radius, t_{tw}/R, and the mass density ratio, ρ_ℓ/ρ_t. As already noted, the tabulated data are strictly valid only for systems with ν_t = 0.3, $t_{tw}/R=0.001$ and $\rho_\ell/\rho_t=0.127$, but can also be used with reasonable accuracy for other practical combinations of the parameters involved.

As a measure of the sensitivity of the critical responses to

variations in the ratios t_{tw}/R and ρ_ℓ/ρ_t, the coefficients α_i and α_{c1} in the expression for the maximum base shear for tanks of different proportions with a roller support at the top are compared in Table 4.13, and those for tanks that are hinged at the top are compared in Table 4.14. Three values of t_{tw}/R (ranging from R/t_{tw} values of 1,500 to 500), three values of H_ℓ/R in the range between 0.3 and 1.0, and two values of ρ_ℓ/ρ_t, corresponding to steel tanks filled with liquids of specific gravities of 1 and 2, are considered.

Tables 4.15 and 4.16 give the corresponding values of the coefficients d_i and d_{c1} in the expressions for the maximum impulsive and maximum convective components of the bending moment across normal tank sections. In all cases, the tanks are presumed to be fully filled, and Poisson's ratio for the tank material is taken as $\nu_t = 0.3$.

It is observed that the deviations in the results from those obtained for the systems with $t_{tw}/R = 0.001$ and $\rho_\ell/\rho_t = 0.127$ considered in the extended tabulations are for all practical purposes negligible. The results for free-standing cantilever tanks were found to be even less sensitive than for the top-constrained tanks, and they are not included here.

4.3.6 Effects of Tank Inertia

To the hydrodynamic effects considered in the preceding sections must also be added the inertia effects of the tank itself. However, unless the mass of the roof is substantial compared to that of the contained liquid and unless the roof is free to move laterally, these effects are likely to be negligible. When their consideration is warranted, they may be evaluated conservatively by considering the tank to behave as a rigid body but taking as the maximum response acceleration the pseudo-acceleration of the system $(S_A)_i$.

In particular, for a cantilever system, the maximum value of the base shear induced by the tank inertia is given by

$$V_{max} = (m_w + m_r)(S_A)_i \qquad (4.44)$$

in which m_w and m_r are the total masses of the tank wall and roof, respectively. Similarly, the maximum base moment is given by

$$M_{max} = - (m_w H_w + m_r H_r)(S_A)_i \qquad (4.45)$$

in which H_r is the distance from the base to the centroid of the roof mass, and H_w is the corresponding distance to the center of gravity of the inertia forces of the tank wall.

4.3.7 Hydrodynamic Forces Transmitted to Tank Support

The horizontal shear transmitted through the base plate of the tank to its support is clearly equal to the shear $V_b(t)$ induced across a section immediately above the plate. By contrast, the bending moments across sections just above and below the base plate are different; the moment beneath the base plate also includes the effect of the radially varying hydrodynamic pressures exerted on the plate itself (see Figure 4.3).

The instantaneous value of the moment increment $\Delta M_b(t)$ due to the hydrodynamic base pressures may be expressed, in a form analogous to Equations 4.37 and 4.38 or Equations 4.41 and 4.42, as

$$\Delta M_b(t) = - \left[e_i m_l H_l A_i(t) + e_{c1} m_l H_l A_{c1}(t) \right] \qquad (4.46)$$

in which the first term represents the contribution of the impulsive component, and the second term represents the contribution of the fundamental convective component. For the sign convention considered, a positive moment on the base plate is counter-clockwise and a negative moment is clockwise. The

values of e_i for tanks of different proportions are listed in Column 4 of Table 4.2, whereas those of e_{c1} are defined by

$$e_{c1} = \frac{2(R/H_\ell)^2}{\lambda_1^2(\lambda_1^2-1)\cosh[\lambda_1(H_\ell/R)]} \qquad (4.47)$$

and they are listed in Column 11 of the table. The contributions to $\Delta M_b(t)$ of the higher convective modes of vibration are negligible and are not provided for in Equation 4.46. For tanks with the values of $H_\ell/R \leq 1$ considered herein, Equation 4.46 may be used for both cantilever and top-constrained systems that are either fully or partially filled. The functions $A_i(t)$ and $A_{c1}(t)$ in this equation are naturally different for the different conditions of support.

The total moment transmitted through the base plate of the tank to its support is obtained by adding algebraically Equation 4.46 to the base values of the moments defined by Equations 4.37 and 4.38 or Equations 4.41 and 4.42. The absolute maximum value of this moment is then obtained by combining the peak values of its impulsive and convective components in the manner indicated previously for other effects. In the implementation of these steps, care should be exercised to ensure that the correct signs are used for the component effects.

For tanks within vaults, the hydrodynamic forces and moments transmitted to the vaults are as shown in Figure 4.5. Part (a) of the figure refers to a free-standing, cantilever tank, whereas parts (b) and (c) refer to top-constrained tanks with roller and hinge supports, respectively. The forces induced by the cantilever system are merely the shear $V_b(t)$ and the bending moment $M_b(t) + \Delta M_b(t)$ transmitted through the base plate of the tank, whereas those for the top-constrained systems, also include the reactions of the tank at the top. The instantaneous value of the horizontal top reaction is clearly equal to the difference between the total hydrodynamic wall force P(t)

defined by Equation 4.31 and the base shear $V_b(t)$. Similarly, the intensity of the vertical top reaction for the tank with the hinge support may be determined from the top values of the bending moments defined by Equations 4.41 and 4.42, making use of Equation 4.29 and the top values of the factors $d_i(\eta_t)$ and $d_{c1}(\eta_t)$ listed in Tables 4.10 and 4.11.

For the evaluation of the soil-structure interaction effects considered in Chapter 6, one needs to know the **total** horizontal force, P(t), and the **total** overturning moment transmitted to the vault. Denoted by $M_b'(t)$, this moment is normally referred to a centroidal axis at the interface of the tank base and the supporting vault which is normal to the plane of the tank motion. The relevant axis is identified on the diagrams of Figure 4.5 by a heavy dot.

For a cantilever tank, the total overturning moment for the vault, $M_b'(t)$, is merely equal to the sum of the moments $M_b(t)$ + $\Delta M_b(t)$ transmitted through the base plate of the tank, whereas for the top-constrained tanks, it also includes the effects of the tank reactions at the top. While the additional moments due to the latter forces may be evaluated from information already presented, the **total** moment for both the top-constrained and cantilever tanks can more simply be expressed in a form analogous to Equation 4.35 as

$$M_b'(t) = m_i h_i' A_i(t) + m_{c1} h_{c1}' A_{c1}(t) \qquad (4.48)$$

in which the first term represents the impulsive component, and the second term represents the fundamental convective component. The contributions of the higher convective components are negligible and are not considered. In the interest of simplicity, the individual terms in this expression are taken as positive. This is possible because, unlike the base moment $M_b(t)$ which was shown to be of opposite signs for cantilever and top-constrained tanks, the moment $M_b'(t)$ is of the same sign for both

of these systems. The quantity h_i' in this equation represents the height at which m_i must be concentrated to yield the correct impulsive component of the overturning moment for the vault, and h_{c1}' represents the corresponding height for the fundamental convective mass. These heights are defined by

$$h_i' = \left[0.40 + e_i \frac{m_\ell}{m_i}\right] H_\ell \tag{4.49}$$

and

$$h_{c1}' = \left[\frac{h_{c1}}{H_\ell} + e_{c1} \frac{m_\ell}{m_{c1}}\right] H_\ell \tag{4.50}$$

and their values for tanks of different proportions are listed in Columns 5 and 12 of Table 4.2. The inertia effects of the vault itself are not included in Equation 4.48, but they can be incorporated simply by considering the vault to be rigid.

Equations 4.48 through 4.50 follow from the fact that the total overturning moment for the vault also equals the sum of the base moments induced by the hydrodynamic pressures exerted on the wall and the base plate of the tank. These equations may be used for both cantilever and top-constrained tanks, and for both full and partially filled systems. As already intimated, the pseudo-acceleration functions in these equations are, of course, different for different systems.

4.3.8 Modeling of Tank-Liquid System

For the purpose of evaluating the **total hydrodynamic force** and **the total overturning moment** exerted by the tank on the supporting vault, the tank-liquid system may be modeled by two cantilever sticks with masses m_i and m_{c1} concentrated at heights h_i' and h_{c1}' from the base, as shown in Figure 4.6. These masses and heights may be determined from Columns 3, 5, 7 and 12 of Table 4.2. The cantilever with mass m_i in this model simulates

the effects of the impulsive mass of the liquid, whereas the one with mass m_{c1} simulates the effects of the fundamental convective portion of the liquid mass. The stiffness of the cantilever with the mass m_i must be such that its natural frequency is equal to the fundamental natural frequency of the tank-liquid system defined by Equation 4.16. Similarly, the stiffness of the cantilever with the mass m_{c1} must be such that its natural frequency is equal to the fundamental sloshing frequency of the liquid defined by Equation 4.14. Being negligible, the effects of the higher convective masses are not provided for in the model.

This model may be used with good accuracy for both cantilever and top-constrained tanks, whether fully or only partially filled with liquid. The natural frequency of the model will naturally be different in the different cases. However, in the form presented so far, the model is valid only for rigidly supported systems, for which the base is subjected to a purely horizontal, translational motion. For flexibly supported systems, for which the base motion also includes a rocking component, the base of the model should be considered to possess a mass moment of inertia, I_b, about a horizontal centroidal axis. This adjustment is needed to provide for the moment of the additional hydrodynamic base pressures induced by the rocking component of the excitation. The values of I_b for tanks of different proportions are listed in Column 6 of Table 4.2; these are normalized with respect to $m_\ell R^2$.

The modeling of the tank-liquid system for the vertical component of ground shaking is considered in Section 4.5.4.

4.4 EFFECTS OF ROCKING COMPONENT OF BASE MOTION

For the responses defined so far, the tank base has been presumed to experience a purely translational, horizontal motion. The magnitudes of the rocking components of foundation

motion that may realistically be expected in practice are generally small and have a negligible effect on the convective components of response.

The impulsive effects induced by the combination of the horizontal and rocking components of base motion may be determined from the expressions presented in the preceding sections merely by redefining the response pseudoacceleration $A_i(t)$ in these expressions to correspond to an effective, horizontal base acceleration

$$\ddot{x}_e(t) = \ddot{x}(t) + h_i'\ddot{\psi}(t) \qquad (4.51)$$

This is tantamount to replacing $\ddot{x}(\tau)$ in Equation 4.13a by $\ddot{x}_e(\tau)$. The function $\ddot{\psi}(t)$ in Equation 4.51 represents the instantaneous rocking acceleration of the tank base, and h_i' represents the height defined by Equation 4.49.

Because of phase differences between $\ddot{x}(t)$ and $\ddot{\psi}(t)$, the maximum values of $\ddot{x}_e(t)$ and of the associated response pseudoacceleration are likely to be smaller than those corresponding to $\ddot{x}(t)$. As a result, the maximum response due to $\ddot{x}_e(t)$ is likely to be smaller than that due to $\ddot{x}(t)$. In the absence of the correct phase relationship between $\ddot{x}(t)$ and $\ddot{\psi}(t)$, the maximum effects of the component motions may be combined by the square-root-of-the-sum-of-squares rule, leading to a conservative estimate of the response.

4.5 EFFECTS OF VERTICAL COMPONENT OF BASE MOTION

4.5.1 Hydrodynamic Effects

Wall Pressures and Forces. The hydrodynamic wall pressures induced by the vertical component of ground shaking are uniformly distributed in the circumferential direction and may be considered to increase from top to bottom as a quarter-sine wave. The maximum value of the pressure at a level defined by

the dimensionless distance η_ℓ is given by

$$p_v(\eta_\ell) = 0.8\left[\cos\frac{\pi}{2}\eta_\ell\right]\rho_\ell H_\ell (S_A)_v \qquad (4.52)$$

in which $(S_A)_v$ represents the spectral pseudoacceleration of a similarly excited single-degree-of-freedom system, the natural frequency and damping of which are equal to those of the fundamental, axisymmetric, breathing mode of vibration of the tank-liquid system. For roofless tanks, the latter frequency, f_v, may be expressed in a form similar to Equation 4.16 as

$$f_v = \frac{1}{2\pi}\frac{C_v}{H_\ell}\sqrt{\frac{E_t}{\rho_t}} \qquad (4.53)$$

and for steel tanks with $E_t = 30{,}000$ ksi and $\gamma_t = \rho_t g = 490$ lb/ft^3, in a form similar to Equation 4.17 as

$$f_v = \frac{2{,}680C_v}{H_\ell} \qquad (4.54)$$

where C_v is a dimensionless coefficient that depends on the same dimensionless factors as the coefficient C_i in Equation 4.16 for the fundamental natural frequency of lateral mode of vibration; f_v is expressed in cycles per second; and H_ℓ in Equation 4.54 is expressed in feet. Identified with the subscript r, the values of C_v for the reference steel tanks with $t_{tw}/R = 0.001$ and $\rho_\ell/\rho_t = 0.127$ are given in Table 4.17. To a reasonable approximation, these results may be used for both partially and fully filled tanks irrespective of the condition of tank support at the top. Furthermore, the effect of the roof mass on f_v, and hence on the pseudoacceleation $(S_A)_v$, may be considered to be negligible. The results for other values of t_{tw}/R and ρ_ℓ/ρ_t may be evaluated from an expression analogous to Equation 4.18. With the hydrodynamic pressures $p_v(\eta_\ell)$ determined from Equation 4.52, the corresponding forces in the tank wall may be determined by static analysis.

For tanks that are constrained in the axial direction, in

addition to the circumferential hoop forces, there develop under vertical shaking Poisson's-ratio related axial forces analogous to those considered in Section 4.3.5.2. These forces are uniformly distributed in the circumferential direction, and their maximum intensity is approximately equal to the product of Poisson's ratio ν_t and the average intensity of the maximum hoop forces over the liquid height.

Base Pressures and Forces. The instantaneous value of the hydrodynamic pressure at an arbitrary point of the tank base, $p_v'(\xi,t)$, may be expressed as

$$p_v'(\xi,t) = c_o'(\xi)\rho_\ell H_\ell \ddot{y}(t) + c_v'(\xi)\rho_\ell H_\ell A_v(t) \tag{4.55}$$

where $c_o'(\xi)$ and $c_v'(\xi)$ are dimensionless functions of the horizontal position coordinate ξ; $\ddot{y}(t)$ is the instantaneous acceleration of the vertical component of base shaking; and $A_v(t)$ is the instantaneous pseudoacceleration of a single-degree-of-freedom system with a natural frequency and damping equal to those of the tank-liquid system when vibrating in its fundamental breathing mode. The first term in this equation represents the contribution of the part of the liquid mass that may be considered to move in synchronism with the tank base, whereas the second term represents the contribution of the part participating in the breathing action of the wall.

The $c_o'(\xi)$ and $c_v'(\xi)$ functions are shown in Figure 4.7 for the reference steel tanks with several different values of H_ℓ/R. Included for the purpose of indicating the limiting behavior of these functions, are also the results for the extreme values of H_ℓ/R = 0.1 and 5. It is observed that, irrespective of the H_ℓ/R ratio,

$$c_o'(\xi) + c_v'(\xi) = 1 \tag{4.56}$$

It should further be noted that these functions may be considered to be independent of the system parameters t_{tw}/R and

ρ_ℓ/ρ_t. The effect of changes in these parameters is reflected mainly through the natural frequency of the system f_v pseudoaccleration function $A_v(t)$. For the limiting case of a rigid tank, for which $A_v(t) = \ddot{y}(t)$, Equation 4.55 reduces, as it should, to $p_v'(\xi,t) = \rho_\ell H_\ell \ddot{y}(t)$.

The instantaneous value of the total hydrodynamic force on the tank base, $P_v'(t)$, may be expressed as (Reference 4.7)

$$P_v'(t) = m_o\ddot{y}(t) + m_v A_v(t) \qquad (4.57)$$

where m_o and m_v are the components of the total liquid mass participating in the motions of the tank base and wall, respectively. The values of these masses, normalized with respect to the total liquid mass, are listed in Table 4.17. Although strictly valid for fully filled, clamped-based cantilever tanks, these results may be used with reasonable accuracy for partially filled tanks and tanks with other support conditions as well.

The maximum values of p_v' and P_v' are obtained from Equations 4.55 and 4.57 by replacing the functions $\ddot{y}(t)$ and $A_v(t)$ in these expressions by their maximum values ($\ddot{y}_o$ and $(S_A)_v$, respectively) and combining the component terms by the square-root-of-the-sum-of-squares rule.

4.5.2 Effects of Tank Inertia

For the vertical component of shaking considered in this section, the inertia of the tank wall and roof lead to oscillatory axial forces which are uniformly distributed in the circumferential direction and attain their maximum values at the base. These forces are normally small and may be neglected. However, they may be evaluated simply by considering the tank wall to be rigid. This approach is justified by the fact that the fundamental natural frequency of the tank-roof system in the axial, column-like mode of vibration is generally much higher

than the dominant frequencies of the waves in the base motion.

For cantilever tanks and for tanks with a roller support at the top, the maximum axial force per unit of circumferential length, $(N_z)_{max}$, may be determined from

$$(N_z)_{max} = \frac{1}{2\pi R}(m_w + m_r)\ddot{y}_o \qquad (4.58)$$

For tanks that are hinged at the top, the inertia force of the roof will be resisted by the top support, and the maximum axial force at the base will be one-half of the force defined by the first term of Equation 4.58.

4.5.3 Combination with Other Effects

The effects of the vertical component of base shaking should be combined with those of the horizontal and rocking components by the square-root-of-the-sum-of-squares rule.

For axially constrained tanks, it should be recalled that Poisson's ratio related axial forces are induced under both hydrodynamic and hydrostatic conditions of loading. As a matter of fact, for realistic intensities of ground shaking, the maximum compressive axial forces due to the hydrodynamic effects will normally be counter-balanced by the axial tensile forces due to the hydrostatic effects.

4.5.4 Modeling of Tank-Liquid System

For the purpose of evaluating the total vertical hydrodynamic force transmitted through the tank base to the foundation or supporting vault, the tank-liquid system may be modeled by the two-mass system shown in Figure 4.8(a), in which the lower mass, m_o, is rigidly attached to the oscillating base, and the upper mass, m_v, is supported by a spring of stiffness

$$k_v = 4\pi^2 f_v^2 m_v \qquad (4.59)$$

and a dashpot with a damping coefficient c_v. The value of c_v is such that the percentage of critical damping for the model is the same as that for the actual tank-liquid in its fundamental axisymmetric mode of vibration.

For a rigidly supported tank, the base motion is the same as the free-field ground motion, $\ddot{y}_g(t)$, whereas for an elastically supported system, the two motions are different, their interrelationship being a function of the characteristics of the excitation and of the properties of the system itself. The action of the elastically supported system may be modeled by the two-degree-of-freedom shown in Figure 4.8(b), in which the base mass m_o' includes, in addition to the rigidly attached component of the liquid mass m_o, the masses of the foundation, tank, surrounding vault and participating soil. The bottom spring and dashpot in the model provide for the flexibility of the supporting medium and its capacity to dissipate energy by radiation and hysteretic action. The properties of these elements are identified in Chapter 6.

4.6 EFFECTS OF SOIL-STRUCTURE INTERACTION

In the approach outlined herein, the effects of soil-structure interaction are provided for in the evaluation of the acceleration histories $\ddot{x}(t)$, $\ddot{\psi}(t)$ and $\ddot{y}(t)$, and need not be reconsidered. It should be noted that these accelerations are of the motions actually experienced by the tank base and not those experienced by the ground under free-field conditions. Similarly, the pseudoaccelerations $A_i(t)$, $A_{cn}(t)$ and $A_v(t)$ are for the actual motions of the tank base. These input and response quantities may be determined directly from the analysis of the tank-vault-soil system considered in Chapter 6, and need not be evaluated independently. The effects of potential variations in the free-field ground motions between the top and bottom of the vault are accounted for in the analysis of the vault-soil system.

If the tank-liquid system is analyzed for the free-field ground motion, the effects of soil-structure interaction on the tank response may be approximated by the procedures described in References 4.7 through 4.11 by appropriately reducing the fundamental natural frequency of the tank-liquid system and increasing its damping. These effects need be considered only for the impulsive components of response, as the effects on the convective components are negligible.

4.7 SURFACE DISPLACEMENTS OF LIQUID

The maximum vertical displacement of the liquid surface, the so-called slosh height h_s, is needed to define the freeboard that must be provided to prevent the liquid from impacting the roof. This displacement may be determined from

$$h_s = R\sqrt{\left(0.837\frac{(S_A)_{c1}}{g}\right)^2 + \left(0.073\frac{(S_A)_{c2}}{g}\right)^2 + \left(0.028\frac{(S_A)_{c3}}{g}\right)^2 + \cdots} \qquad (4.60)$$

Equation 4.60 accounts for the effect of the horizontal component of base shaking only. The magnitude and frequency characteristics of the rocking component of base motion for the tanks examined herein are normally such that the contribution of this component to the surface displacement of the liquid is negligible (Reference 4.10). When both components of base motion are sufficiently important to warrant their consideration, the **combined** effect may be evaluated from Equation 4.60 by interpreting the pseudoaccelerations $(S_A)_{cn}$ to correspond to the effective horizontal base acceleration defined by

$$[\ddot{x}_e(t)]_{cn} = \ddot{x}(t) + h'_{cn}\ddot{\psi}(t) \qquad (4.61)$$

in which h'_{cn} represents the height of the nth convective liquid mass (see Reference 4.12). The values of h'_{c1} for tanks of different proportions are listed in Table 4.2, and those of h'_{c2} and h'_{c3} may, if needed, be determined from generalized versions

of Equations 4.47 and 4.50 by replacing λ_1 by λ_n and $(S_A)_{c1}$ by $(S_A)_{cn}$.

If the available freeboard is not adequate for the computed sloshing height, either the liquid level must be lowered or the tank roof and wall must be designed to withstand the impact of the sloshing liquid. These issues are addressed further in Chapter 5, and more detailed guidance is provided in Appendix D.

In assessing the capacity of the tank wall immediately above the liquid surface at rest, the maximum hydrodynamic pressure computed from Equation 4.3 for η_ℓ=1 must be applied at the highest elevation of the water surface, i.e., at $z = H_\ell + h_s$.

4.8 EFFECTS FOR TANKS WITH INHOMOGENEOUS LIQUIDS

4.8.1 General

The information presented so far in this chapter is limited to tanks containing uniform, homogeneous liquids.

The response to horizontal ground shaking of tanks containing inhomogeneous liquids has been the subject of numerous recent studies (References 4.13-4.20) which dealt with the evaluation of both the impulsive and convective effects. Both layered liquids, with two or more uniform layers of different thicknesses and densities, and liquids with a continuous variation in density have been examined. General expressions for the critical responses of the system have been formulated, and comprehensive numerical solutions have been reported for two-layered and some three-layered liquids, as well as for liquids with mass density that increases exponentially from top to bottom. This information, however, is limited to tanks that are rigid.

Some studies of the response of flexible tanks containing a two-layered liquid have been reported in References 4.19 and 4.20,

and additional studies for still more complex systems have been carried out in connection with the formulation of the simple method of analysis presented in the following sections.

4.8.2 Impulsive Effects

As is true of tanks with a homogeneous liquid, the more critical component of the response to horizontal ground shaking of tanks containing inhomogeneous liquids is the impulsive, for which a part of the contained liquid may be considered to move in synchronism with the tank wall as a rigid mass. The impulsive effects are affected significantly by the flexibility of the tank wall, whereas the convective effects are insensitive to this flexibility and may be evaluated considering the tank wall to be rigid.

For the relatively broad tanks considered in this document, the maximum hydrodynamic effects for a flexible tank may be obtained from the relevant expressions for a rigid tank simply by replacing the maximum ground acceleration in these expressions by the spectral value of the pseudoacceleration corresponding to the fundamental natural frequency of the tank-liquid system. This approach, which is fundamental to the analysis of the homogeneous systems examined so far, is also valid for the inhomogeneous systems considered in this section. It follows that the crucial step in the extension to flexible tanks of the available information on impulsive effects in rigid tanks with inhomogeneous liquids is the evaluation of the fundamental natural frequency of the tank-liquid system. This section presents a simple practical procedure for evaluating this frequency.

For a system with N uniform liquid layers of different thicknesses and mass densities, the desired frequency is determined from the corresponding frequencies of N subsystems, each containing a homogeneous liquid. The procedure is de-

scribed by reference to a three-layered system, for which the variation in liquid density is shown by the sketch at the extreme left of Figure 4.9. The individual layers are considered to be uniform but their thicknesses and densities to vary from one layer to the next. The layers are numbered sequentially starting with 1 at the bottom layer, with the density of the j th layer denoted by $\rho_{\ell j}$, and the height from the tank-base to the top of that layer denoted by $H_{\ell j}$. The total liquid height, H_ℓ, is thus also equal to $H_{\ell 3}$. The layer densities are presumed to increase from top to bottom.

Referred to as subsystems A, B and C, the three replacement systems are identified by the three rightmost diagrams in Figure 4.7. For subsystem A, a homogeneous liquid of the density of the top layer, $\rho_{\ell 3}$, extends to the total height $H_\ell = H_{\ell 3}$; for subsystem B, a homogeneous liquid of a density equal to the difference in the densities of the second and top layers, $\rho_{\ell 2}-\rho_{\ell 3}$, extends to the top of the second layer, $H_{\ell 2}$; and for subsystem C, a homogeneous liquid of a density equal to the difference in the densities of the bottom and middle layers, $\rho_{\ell 1}-\rho_{\ell 2}$, extends to the top of the bottom layer, $H_{\ell 1}$. The tank and end support conditions for each subsystem are considered to be the same as those for the actual system.

Let f_A, f_B and f_C be the fundamental natural frequencies of the impulsive modes of vibration of subsystems A, B and C, respectively, and let T_A, T_B and T_C be the corresponding periods. These quantities may be determined from the information for tanks with homogeneous liquids presented in Section 4.3.2.2. The fundamental natural frequency of the actual system, f_i, may then be determined by application of a Dunkerley-type approximation from

$$\frac{1}{f_i^2} = \frac{1}{f_A^2} + \frac{1}{f_B^2} + \frac{1}{f_C^2} \qquad (4.62)$$

and the corresponding natural period, T_i, may be determined from

$$T_i^2 = T_A^2 + T_B^2 + T_C^2 \qquad (4.63)$$

Inasmuch as these expressions do not follow from an exact application of the Dunkerley approximation, the results obtained do not necessarily constitute a low-bound estimate of the desired frequency. However, they do lead to values that are sufficiently accurate for all practical purposes. Detailed comparisons with the results obtained by a more rigorous analysis will be reported separately.

4.8.3 A Further Simplification

For a layered system with moderate variations in liquid density, the base shear and base moments for a rigid tank may also be determined from the corresponding solutions for a tank containing some 'equivalent' homogeneous liquid.

In evaluating the base shear, the density of the equivalent liquid should be such that, when computed on the assumption that the entire liquid acts impulsively as a rigid mass, the base shears for the actual layered liquid and the equivalent homogeneous liquid are the same. This is tantamount to taking the density of the equivalent liquid equal to the average density of the layered liquid.

Similarly, in evaluating the overturning moment immediately above the tank base or the total foundation moment, the densities of the equivalent uniform liquids in each case should be such that the results computed on the assumption that the entire liquid acts impulsively are identical for the actual and the equivalent systems. More specifically, the densities of the equivalent uniform liquid, $(\rho_\ell)_{eq}$, may be determined as follows.

For the computation of the base shear,

$$(\rho_\ell)_{eq} = \left(\frac{H_{\ell 1}}{H_\ell}\right)\rho_{\ell 1} + \left(\frac{H_{\ell 2} - H_{\ell 1}}{H_\ell}\right)\rho_{\ell 2} + \left(\frac{H_{\ell 3} - H_{\ell 2}}{H_\ell}\right)\rho_{\ell 3} \qquad (4.64)$$

For the computation of the overturning moment immediately above the base,

$$(\rho_\ell)_{eq} = \left(\frac{H_{\ell 1}^2}{H_\ell^2}\right)\rho_{\ell 1} + \left(\frac{H_{\ell 2}^2 - H_{\ell 1}^2}{H_\ell^2}\right)\rho_{\ell 2} + \left(\frac{H_{\ell 3}^2 - H_{\ell 2}^2}{H_\ell^2}\right)\rho_{\ell 3} \qquad (4.65)$$

and for the computation of the foundation moment

$$(\rho_\ell)_{eq} = \left(\frac{H_{\ell 1}^2 + R^2/2}{H_\ell^2 + R^2/2}\right)\rho_{\ell 1} + \left(\frac{H_{\ell 2}^2 - H_{\ell 1}^2}{H_\ell^2 + R^2/2}\right)\rho_{\ell 2} + \left(\frac{H_{\ell 3}^2 - H_{\ell 2}^2}{H_\ell^2 + R^2/2}\right)\rho_{\ell 3} \qquad (4.66)$$

Taking the density of the equivalent liquid equal to the average density of the layered liquid will yield unduly conservative results for the overturning bending moment M_b immediately above the base. For a more precise definition of the accuracy and range of applicability of these approximations, the reader is referred to Reference 4.17.

4.9 COMBINATION OF EFFECTS OF HORIZONTAL COMPONENTS OF GROUND MOTION

The maximum responses of the systems in this chapter were evaluated for only one of the two normal horizontal components of ground shaking. The component considered is naturally the more intense of those deemed to be appropriate for the site under consideration.

As indicated by Equations 4.1 to 4.3 and 4.27 to 4.29, the hydrodynamic wall pressures for a horizontal component of shaking and the resulting circumferential and axial stresses in the tank wall are proportional to $\cos\theta$ and attain their maximum values at $\theta = 0$ and 180 degrees. By contrast, the horizontal shearing stresses are proportional to $\sin\theta$ and attain their

maximum values at $\theta = \pm 90$ degrees. At these locations of maximum effects, the contribution of the second or normal component of shaking vanishes and the maximum values of the combined effects are the same as those induced by the more intense of the two components.

Even for an arbitrary point on the tank wall, it can be shown that, when computed from the component maxima by the square root of the sum of squares rule, the maximum effects due to the combination of the two horizontal components of ground shaking are no larger than the absolute maximum values of the corresponding effects induced solely by the more intense component. It follows that for the evaluation of the absolute maximum wall pressures and of the associated wall stresses, it suffices to consider the effects of only the more intense horizontal component.

This conclusion also applies to the maximum normal stresses induced at the interface of a circular foundation and the supporting soil, but not to the maximum shearing force or overturning moment induced on a foundation of arbitrary shape. In the latter case, the effects of both components of horizontal ground shaking must be considered, and the maximum values of these forces must be computed with due regard for the fact that their component maxima generally occur at different times. Specifically, it is recommended that the maximum foundation forces induced by the more intense of the two normal horizontal components of shaking be combined with 40 percent of the corresponding forces induced by the less intense component.

REFERENCES

4.1 Veletsos, A.S., and Yang, J.Y., "Earthquake Response of Liquid Storage Tanks," Advances in Civil Engineering Through Engineering Mechanics, ASCE, Proceedings ASCE/EMD Specialty Conference, Raleigh, North Carolina, pp. 1-24, 1977.

4.2 Haroun, M.A., and Housner, G.W., "Seismic Design of Liquid Storage Tanks," Journal of Technical Councils, ASCE, Volume 107, No. 1, pp. 191-207, 1981.

4.3 Haroun, M.A., and Housner, G.W., "Dynamic Characteristics of Liquid Storage Tanks," Journal of the Engineering Mechanics Division, ASCE, Volume 108, No. EM5, pp. 783-800, 1982.

4.4 Veletsos, A.S., "Seismic Response and Design of Liquid Storage Tanks," Guidelines for the Seismic Design of Oil and Gas Pipeline Systems, Technical Council on Lifeline Earthquake Engineering, ASCE, New York, pp. 255-370 and 443-461, 1984.

4.5 Veletsos, A.S., Shivakumar, P., Tang, Y. and Tang, H.T., "Seismic Response of Anchored Steel Tanks," Proceedings, Third Symposium on Current Issues Related to Nuclear Plant Structures, Equipment and Piping, A. J. Gupta, Editor, North Carolina State University, Raleigh, NC, pp. X/2-2 to X/2-15, 1990.

4.6 Veletsos, A.S., and Shivakumar, P., "Hydrodynamic Effects in Tanks with Different Conditions of Support," Proceedings, Third DOE Natural Phenomena Hazards Mitigation Conference, St. Louis, MI, pp. 578-587, October 1991.

4.7 Veletsos, A.S., and Tang, Y., "Dynamics of Vertically Excited Liquid Storage Tanks," Journal of Structural Division, ASCE, Volume 112, pp. 1228-1246, 1986.

4.8 Veletsos, A.S., and Tang, Y., "Interaction Effects in Vertically Excited Steel Tanks," Dynamic Response of Structures (Eds. G.C. Hart and R.B. Nelson), ASCE, pp. 636-643, 1986.

4.9 Haroun, M.A., and Abdel-Hafiz, E.A., "A Simplified Seismic Analysis of Rigid Base Liquid Storage Tanks Under Vertical Excitation With Soil-Structure Interaction," Journal of Soil Dynamics and Earthquake Engineering, Volume 5, pp. 217-225, 1986.

4.10 Veletsos, A.S., and Tang, Y., "Soil-Structure Interaction Effects for Laterally Excited Liquid Storage Tanks," Journal of Earthquake Engineering and Structural Dynamics, Volume 19, pp. 473-496, 1990.

4.11 Veletsos, A.S., Tang, Y., and Tang, H.T., "Dynamic Response of Flexibly Supported Liquid-Storage Tanks," Journal of Structural Engineering, ASCE, Volume 118, No. 1, pp. 264-283, 1992.

4.12 Veletsos, A.S., and Tang, Y., "Rocking Response of Liquid Storage Tanks," Journal of Engineering Mechanics, ASCE, Volume 113, pp. 1774-1792, November 1987.

4.13 Tang, Y., "Dynamic Response of a Tank Containing Two Liquids," Journal of Engineering Mechanics, ASCE, Vol. 119, No. 3, pp. 531-548, 1993; see also Discussion by Veletsos, A.S., and Shivakumar, P., and Author's Closure in Journal of Engineerign Mechanics, ASCE, Volume 120, No. 7, pp. 1598-1603, 1994.

4.14 Tang, Y., and Chang, Y.W., "The Exact Solutions to the Dynamic Response of Tanks Containing Two Liquids," Report ANL/RE-93/2, Argonne National Laboratory, Argonne, Ill, 1993.

4.15 Tang, Y., and Chang, Y.W., "Rocking Response of Tanks Containing Two Liquids," ANL/RE-93/5, Argonne National Laboratory, Argonne, Ill, 1993.

4.16 Veletsos, A.S., and Shivakumar, P., "Sloshing Response of Layered Liquids in Rigid Tanks," Journal of Earthquake Engineering and Structural Dynamics, Volume 22, pp. 801-821, 1993.

4.17 Veletsos, A.S., and Shivakumar, P., "Hydrodynamic Effects in Rigid Tanks Containing Layered Liquids," Journal of Earthquake Engineering and Structural Dynamics, Volume 24, pp. 835-860, 1995.

4.18 Shivakumar, P., and Veletsos, A.S., "Dynamic Response of Rigid Tanks with Inhomogeneous Liquids," Journal of Earthquake Engineering and Structural Dynamics, Volume 24, pp. 991-1015, 1995.

4.19 Tang, Y., "Free Vibration Analysis of a Tank Containing Two Liquids," Journal of Engineering Mechnics, ASCE, Volume 120, No. 3, pp. 618-638, 1994.

4.20 Tang, Y., "Computing Response of Tanks with Two Liquids," Technical Note, Journal of Structural Engineering, ASCE, Volume 120, No. 12, pp. 3668-3674, 1994.

NOTATION

$A(t)$ instantaneous pseudoacceleration for a simple oscillator

$A_{cn}(t)$ instantaneous pseudoacceleration for nth convective or sloshing mode of response

$A_i(t)$ instantaneous pseudoacceleraton for impulsive component of response

$A_v(t)$ instantaneous pseudoacceleration for response to vertical component of ground shaking

$c_{cn}(\eta_\ell)$ dimensionless function defining axial variation of wall pressure associated with the nth convective or sloshing mode of vibration of liquid

$c_i(\eta_\ell)$ dimensionless function defining axial variation of impulsive component of wall pressure

$c'_{cn}(\xi)$ dimensionless function defining radial variation of base pressure associated with the nth convective or sloshing mode of vibration of liquid

$c'_i(\xi)$ dimensionless function defining radial variation of impulsive component of base pressure

$c'_o(\xi)$ dimensionless function defining radial variation of component of base pressure p'_v that is proportional to $\ddot{y}(t)$

$c'_v(\xi)$ dimensionless function defining radial variation of component of base pressure p'_v that is proportional to $A_v(t)$

C_i dimensionless coefficient in expression for f_i

$(C_i)_r$ value of C_i for reference values of tank parameters considered in Table 4.4

C_v dimensionless coefficient in expression for f_v

$d_{cn}(\eta)$ dimensionless function of η in expression for nth convective component of overturning bending moment M_{cn}; η is taken as either η_ℓ or η_t

d_{cn} value of $d_{cn}(\eta)$ for $\eta = 0$

d_i value of $d_i(\eta)$ for $\eta = 0$

$d_i(\eta)$ dimensionless function of η in expression for impulsive component of overturning bending moment M_i; η is taken as either η_ℓ or η_t

D_i dimensionless function of H/R in approximate expression for $c_i(\eta_\ell)$

e_{cn} dimensionless factor in expression for nth convective component of base moment increment ΔM_b

e_i dimensionless factor in expression for impulsive component of base moment increment ΔM_b

E_t modulus of elasticity of tank material

f_{cn} natural frequency, in cycles per unit of time, of nth convective or sloshing mode of vibration of liquid in tank

f_i fundamental natural frequency of impulsive mode of vibration of tank-liquid system

f_v fundamental natural frequency for axisymmetric, breathing mode of vibration of tank-liquid system

g acceleration due to gravity

G_t shear modulus of elasticity of tank material

h_{cn} height at which m_{cn} must be concentrated to yield the correct base moment for nth convective component of response

h'_{cn} height at which m_{cn} must be concentrated to yield the correct nth convective component of the overturning moment transmitted by the tank-liquid system to the supporting vault

h'_i height at which m_i must be concentrated to yield the correct impulsive component of the overturning moment transmitted by the tank-liquid system to the supporting vault.

h_s maximum vertical displacement or slosh height of liquid surface

H_ℓ height of liquid

$H_{\ell j}$ distance from tank base to top of jth layer of a layered liquid

H_r distance from tank base to centroid of roof mass

H_t height of tank

H_w distance from tank base to point of application of resultant of lateral inertia forces for tank wall

k_f, k_s stiffness of tank when assumed to behave as a flexural beam and a shear-beam, respectively

k_v stiffness of spring in model for vertically excited system

m_{cn} liquid mass participating in nth convective mode of vibration

m_i impulsive component of liquid mass, i.e., portion of m_ℓ which may be considered to act in synchronism with tank wall

m_ℓ total liquid mass

m_o component of liquid mass participating in uniform vertical motion of tank base

m_o' total base mass for model of elastically supported, vertically excited tank-liquid system

m_r total mass of tank roof

m_v component of liquid mass of vertically excited system participating in breathing action of tank wall

m_w total mass of tank wall

M overturning bending moment across a section normal to tank axis

M_b value of M for a section immediately above tank base

M_b' total overturning bending moment transmitted from the tank to the supporting vault

ΔM_b base moment increment induced by hydrodynamic pressures exerted on tank base

M_c convective component of M

M_i impulsive component of M

N_z axial force per unit circumferential length of tank wall

N_θ	circumferential or hoop force in tank wall per unit of tank height
$(N_\theta)_{av}$	average value of N_θ over liquid height, H_ℓ
p	hydrodynamic pressure induced at an arbitrary point of the tank wall by horizontal component of shaking
p_c	convective or sloshing component of p
p_i	impulsive component of p
p_{max}	absolute maximum value of p
p_v	hydrodynamic wall pressure induced by vertical component of shaking
p'	hydrodynamic pressure induced at an arbitrary point of the tank base by horizontal component of shaking
p'_c	convective or sloshing component of p'
p'_i	impulsive component of p'
p'_v	hydrodynamic base pressure induced by vertical component of shaking
$\overline{p}_{max}$	maximum value of combination of hydrostatic and hydrodynamic wall pressures at an arbitrary point
P(t)	instantaneous value of total hydrodynamic force induced on tank wall by horizontal component of shaking
$P'_v(t)$	instantaneous value of total hydrodynamic force induced on tank base by vertical component of shaking
R	radius of tank
$(S_A)_{cn}$	absolute maximum or spectral value of $A_{cn}(t)$
$(S_A)_i$	absolute maximum or spectral value of $A_i(t)$
$(S_A)_v$	absolute maximum or spectral value of $A_v(t)$
t	time
t_{tw}	thickness of tank wall
T_{cn}	$1/f_{cn}$ = natural period of nth convective or sloshing mode of vibration of liquid in tank

T_f natural period of vibration of empty tank computed on assumption that roof mass is the only mass and that tank behaves as a flexural beam

T_i $1/f_i$ = fundamental natural period of impulsive mode of vibration

T_s natural period of vibration of empty tank computed on assumption that roof mass is the only mass and that tank behaves as a shear-beam

V horizontal shearing force

V_b value of V at tank base

$\ddot{x}$ acceleration of horizontal component of base motion

$\ddot{x}_e$ effective horizontal acceleration of base motion defined by Equation 4.51

$(\ddot{x}_e)_{cn}$ effective horizontal acceleration of base motion defined by Equation 4.61

$\ddot{y}$ acceleration of vertical component of base motion

$\ddot{y}_o$ absolute maximum value of $\ddot{y}$

z vertical distance measured upward from tank base

α_{c1} dimensionless factor in expression for base shear induced by fundamental convective component of response

α_i dimensionless factor in expression for impulsive component of base shear

ζ percentage of critical damping

η_ℓ z/H_ℓ = dimensionless vertical position coordinate

η_t z/H_t = dimensionless vertical position coordinate

θ circumferential angle

λ_n nth root of first derivative of Bessel function of first kind and first order

ν_t Poisson's ratio of tank material

ξ r/R = dimensionless horizontal position coordinate

ρ_ℓ density of liquid

$\rho_{\ell j}$	density of jth layer of a layered liquid
$(\rho_\ell)_{eq}$	density of an equivent uniform liquid approximating a layered liquid
ρ_t	density of tank material
σ_θ	circumferential or hoop stress in tank wall
σ_z	axial stress in tank wall
τ	shearing stress in tank wall
$\ddot{\psi}$	acceleration of rocking component of base motion
ω	circular natural frequency

Table 4.1 Values of Dimensionless Function $c_i(\eta_\ell)$ in Expression for Impulsive Component of Wall Pressure

$\eta_\ell = z/H_\ell$	Value of $c_i(\eta_\ell)$									
	$\frac{H_\ell}{R}=0.1$	$\frac{H_\ell}{R}=0.2$	$\frac{H_\ell}{R}=0.3$	$\frac{H_\ell}{R}=0.4$	$\frac{H_\ell}{R}=0.5$	$\frac{H_\ell}{R}=0.6$	$\frac{H_\ell}{R}=0.7$	$\frac{H_\ell}{R}=0.8$	$\frac{H_\ell}{R}=0.9$	$\frac{H_\ell}{R}=1.0$
1.0	0	0	0	0	0	0	0	0	0	0
0.9	0.023	0.047	0.072	0.097	0.122	0.146	0.170	0.192	0.213	0.233
0.8	0.037	0.076	0.116	0.157	0.197	0.237	0.274	0.310	0.343	0.373
0.7	0.048	0.098	0.150	0.203	0.256	0.306	0.354	0.399	0.440	0.477
0.6	0.056	0.115	0.177	0.239	0.301	0.361	0.417	0.468	0.515	0.556
0.5	0.063	0.129	0.198	0.268	0.338	0.404	0.466	0.522	0.573	0.618
0.4	0.068	0.140	0.215	0.291	0.366	0.438	0.504	0.564	0.617	0.664
0.3	0.072	0.148	0.227	0.308	0.387	0.463	0.533	0.595	0.650	0.699
0.2	0.075	0.154	0.236	0.320	0.402	0.480	0.552	0.617	0.673	0.722
0.1	0.076	0.157	0.241	0.327	0.411	0.491	0.564	0.629	0.687	0.736
0.0	0.077	0.158	0.243	0.329	0.414	0.494	0.568	0.633	0.691	0.740

Table 4.2 Values of Factors in Expressions for Impulsive and Convective Components of Hydrodynamic Effects in Tanks

H_ℓ/R	Impulsive Effects					Convective Effects					
	D_i	$\frac{m_i}{m_\ell}$	e_i	$\frac{h_i'}{H}$	$\frac{I_b}{m_\ell R^2}$	$\frac{m_{c1}}{m_\ell}$	$\frac{m_{c2}}{m_\ell}$	$\frac{h_{c1}}{H}$	$\frac{h_{c2}}{H}$	e_{c1}	$\frac{h_{c1}'}{H}$
(1)	(2)	(3)	(4)	(5)	(6)	(7)	(8)	(9)	(10)	(11)	(12)
0.10	0.084	0.056	0.466	8.745	0.201	0.828	0.067	0.501	0.512	24.273	29.834
0.15	0.127	0.085	0.449	5.681	0.180	0.816	0.061	0.503	0.525	10.566	13.449
0.20	0.172	0.115	0.431	4.154	0.161	0.801	0.054	0.506	0.543	5.775	7.716
0.25	0.217	0.145	0.413	3.241	0.144	0.782	0.048	0.509	0.563	3.565	5.066
0.30	0.264	0.176	0.394	2.637	0.129	0.761	0.042	0.512	0.585	2.372	3.629
0.35	0.311	0.207	0.376	2.210	0.117	0.737	0.037	0.517	0.608	1.659	2.766
0.40	0.357	0.239	0.357	1.894	0.106	0.712	0.033	0.521	0.630	1.202	2.208
0.45	0.404	0.270	0.338	1.653	0.096	0.687	0.030	0.527	0.653	0.894	1.829
0.50	0.450	0.300	0.320	1.464	0.088	0.660	0.027	0.533	0.674	0.679	1.561
0.55	0.494	0.330	0.302	1.314	0.081	0.634	0.025	0.539	0.693	0.524	1.365
0.60	0.538	0.359	0.284	1.192	0.075	0.608	0.023	0.545	0.712	0.409	1.219
0.65	0.579	0.387	0.268	1.092	0.069	0.582	0.021	0.552	0.729	0.324	1.108
0.70	0.619	0.414	0.252	1.009	0.065	0.558	0.020	0.559	0.745	0.258	1.022
0.75	0.657	0.439	0.237	0.940	0.060	0.534	0.018	0.567	0.759	0.208	0.955
0.80	0.692	0.464	0.223	0.881	0.057	0.511	0.017	0.574	0.772	0.168	0.903
0.85	0.726	0.487	0.209	0.832	0.053	0.490	0.016	0.582	0.784	0.137	0.861
0.90	0.758	0.508	0.196	0.789	0.050	0.470	0.015	0.590	0.795	0.112	0.829
0.95	0.787	0.529	0.185	0.753	0.048	0.451	0.014	0.598	0.805	0.092	0.803
1.00	0.815	0.548	0.174	0.721	0.045	0.432	0.014	0.606	0.814	0.076	0.782

Table 4.3 Values of Dimensionless Function $c_i'(\xi)$ in Expression for Impulsive Component of Base Pressure

H_ℓ/R	Value of $c_i'(\xi)$										
	ξ=0.	ξ=0.1	ξ=0.2	ξ=0.3	ξ=0.4	ξ=0.5	ξ=0.6	ξ=0.7	ξ=0.8	ξ=0.9	ξ=1.0
0.1	0	0.000	0.000	0.000	0.000	0.000	0.000	0.001	0.004	0.018	0.077
0.2	0	0.000	0.001	0.001	0.002	0.005	0.009	0.019	0.039	0.080	0.158
0.3	0	0.002	0.005	0.009	0.015	0.024	0.039	0.063	0.100	0.158	0.243
0.4	0	0.008	0.017	0.027	0.041	0.060	0.086	0.122	0.172	0.240	0.329
0.5	0	0.016	0.033	0.053	0.076	0.105	0.142	0.188	0.248	0.322	0.414
0.6	0	0.025	0.052	0.081	0.114	0.153	0.199	0.255	0.322	0.401	0.494
0.7	0	0.035	0.071	0.110	0.152	0.200	0.255	0.318	0.390	0.473	0.568
0.8	0	0.044	0.089	0.137	0.188	0.244	0.306	0.375	0.452	0.538	0.633
0.9	0	0.052	0.106	0.161	0.220	0.283	0.351	0.425	0.506	0.595	0.691
1.0	0	0.060	0.120	0.183	0.248	0.317	0.390	0.469	0.553	0.644	0.740

Table 4.4 Values of Coefficient $(C_i)_r$ in Expression for Fundamental Impulsive Frequency of Lateral Mode of Vibration of Roofless Steel Tanks Filled with Water; Reference Systems with $\nu_t = 0.3$, $\rho_\ell/\rho_t = 0.127$ and $t_{tw}/R = 0.001$

H_ℓ/R	Value of $(C_i)_r$					
	Top Support Condition					
	Free	Roller	Hinge	Free	Roller	Hinge
	(a) $H_\ell/H_t = 1.0$			(b) $H_\ell/H_t = 0.75$		
0.10	0.0412	0.0417	0.0429	0.0415	0.0417	0.0429
0.15	0.0465	0.0468	0.0484	0.0466	0.0468	0.0481
0.20	0.0516	0.0521	0.0539	0.0516	0.0521	0.0534
0.25	0.0561	0.0569	0.0589	0.0561	0.0569	0.0583
0.30	0.0600	0.0613	0.0634	0.0601	0.0611	0.0626
0.35	0.0635	0.0653	0.0675	0.0635	0.0651	0.0666
0.40	0.0666	0.0690	0.0712	0.0666	0.0687	0.0702
0.45	0.0694	0.0724	0.0747	0.0694	0.0721	0.0735
0.50	0.0719	0.0758	0.0781	0.0719	0.0753	0.0767
0.55	0.0742	0.0789	0.0812	0.0742	0.0783	0.0797
0.60	0.0762	0.0820	0.0843	0.0763	0.0813	0.0826
0.65	0.0781	0.0850	0.0873	0.0782	0.0841	0.0853
0.70	0.0799	0.0880	0.0901	0.0800	0.0869	0.0880
0.75	0.0815	0.0909	0.0939	0.0816	0.0896	0.0906
0.80	0.0829	0.0937	0.0957			
0.85	0.0843	0.0966	0.0984			
0.90	0.0855	0.0993	0.1011			
0.95	0.0865	0.1020	0.1037			
1.00	0.0875	0.1047	0.1062			
	(c) $H_\ell/H_t = 0.5$			(d) $H_\ell/H_t = 0.25$		
0.10	0.0416	0.0417	0.0424	0.0417	0.0417	0.0421
0.15	0.0466	0.0468	0.0476	0.0466	0.0468	0.0472
0.20	0.0517	0.0520	0.0528	0.0518	0.0522	0.0525
0.25	0.0561	0.0568	0.0576	0.0565	0.0571	0.0574
0.30	0.0601	0.0610	0.0619			
0.35	0.0636	0.0649	0.0657			
0.40	0.0667	0.0685	0.0693			
0.45	0.0695	0.0718	0.0725			
0.50	0.0721	0.0750	0.0756			

Table 4.5 Values of Coefficients α_i and α_{cl} in Expressions for Impulsive and Convective Components of Base Shear in Top-Constrained Steel Tanks

H_ℓ/R	Top Support Condition							
	Roller		Hinge		Roller		Hinge	
	α_i	α_{cl}	α_i	α_{cl}	α_i	α_{cl}	α_i	α_{cl}
	(a) H_ℓ/H_t = 1.0				(b) H_ℓ/H_t = 0.75			
0.10	0.578	0.500	0.617	0.536	0.659	0.605	0.704	0.650
0.15	0.564	0.473	0.613	0.517	0.653	0.583	0.702	0.633
0.20	0.565	0.462	0.617	0.509	0.652	0.574	0.703	0.626
0.25	0.566	0.455	0.620	0.504	0.653	0.569	0.704	0.620
0.30	0.567	0.449	0.622	0.499	0.654	0.565	0.705	0.616
0.35	0.568	0.443	0.623	0.494	0.655	0.562	0.706	0.612
0.40	0.569	0.438	0.623	0.489	0.656	0.559	0.706	0.608
0.45	0.570	0.433	0.624	0.483	0.657	0.556	0.706	0.604
0.50	0.571	0.428	0.624	0.478	0.659	0.553	0.705	0.600
0.55	0.572	0.423	0.624	0.471	0.660	0.551	0.705	0.595
0.60	0.573	0.418	0.624	0.465	0.662	0.548	0.705	0.590
0.65	0.574	0.412	0.624	0.459	0.664	0.546	0.704	0.586
0.70	0.575	0.407	0.623	0.452	0.665	0.543	0.703	0.581
0.75	0.576	0.401	0.622	0.445	0.667	0.541	0.702	0.575
0.80	0.577	0.395	0.622	0.437				
0.85	0.578	0.389	0.621	0.430				
0.90	0.579	0.383	0.620	0.423				
0.95	0.580	0.378	0.619	0.415				
1.00	0.581	0.372	0.618	0.408				
	(c) H_ℓ/H_t = 0.5				(d) H_ℓ/H_t = 0.25			
0.10	0.748	0.710	0.791	0.754	0.839	0.818	0.879	0.860
0.15	0.741	0.694	0.788	0.742	0.833	0.809	0.876	0.853
0.20	0.741	0.689	0.789	0.737	0.835	0.809	0.876	0.850
0.25	0.741	0.685	0.789	0.734	0.840	0.812	0.876	0.849
0.30	0.743	0.684	0.790	0.731				
0.35	0.745	0.683	0.790	0.728				
0.40	0.748	0.684	0.790	0.726				
0.45	0.751	0.685	0.790	0.723				
0.50	0.754	0.686	0.790	0.721				

Table 4.6 Values of Dimensionless Function $d_i(\eta_\ell)$ in Expression for **Impulsive** Component of Bending Moment Across Normal Sections for **Cantilever** Tanks

$\eta_\ell = z/H_\ell$	Values of $d_i(\eta_\ell)$									
	$\frac{H_\ell}{R}$=0.1	$\frac{H_\ell}{R}$=0.15	$\frac{H_\ell}{R}$=0.2	$\frac{H_\ell}{R}$=0.25	$\frac{H_\ell}{R}$=0.3	$\frac{H_\ell}{R}$=0.35	$\frac{H_\ell}{R}$=0.4	$\frac{H_\ell}{R}$=0.45	$\frac{H_\ell}{R}$=0.5	
1.0	0	0	0	0	0	0	0	0	0	
0.9	-0.0000	-0.0000	-0.0001	-0.0001	-0.0001	-0.0001	-0.0001	-0.0001	-0.0002	
0.8	-0.0003	-0.0003	-0.0004	-0.0006	-0.0007	-0.0008	-0.0009	-0.0011	-0.0012	
0.7	-0.0009	-0.0012	-0.0015	-0.0018	-0.0022	-0.0026	-0.0031	-0.0035	-0.0040	
0.6	-0.0021	-0.0027	-0.0034	-0.0042	-0.0051	-0.0061	-0.0071	-0.0081	-0.0092	
0.5	-0.0038	-0.0051	-0.0065	-0.0081	-0.0098	-0.0116	-0.0134	-0.0153	-0.0173	
0.4	-0.0062	-0.0085	-0.0109	-0.0136	-0.0164	-0.0193	-0.0224	-0.0255	-0.0287	
0.3	-0.0093	-0.0130	-0.0169	-0.0210	-0.0253	-0.0298	-0.0344	-0.0392	-0.0441	
0.2	-0.0129	-0.0186	-0.0243	-0.0303	-0.0366	-0.0431	-0.0497	-0.0565	-0.0634	
0.1	-0.0172	-0.0251	-0.0332	-0.0416	-0.0503	-0.0592	-0.0683	-0.0775	-0.0869	
0.0	-0.0220	-0.0327	-0.0436	-0.0547	-0.0663	-0.0781	-0.0901	-0.1023	-0.1145	

$\eta_\ell = z/H_\ell$	$\frac{H_\ell}{R}$=0.55	$\frac{H_\ell}{R}$=0.6	$\frac{H_\ell}{R}$=0.65	$\frac{H_\ell}{R}$=0.7	$\frac{H_\ell}{R}$=0.75	$\frac{H_\ell}{R}$=0.8	$\frac{H_\ell}{R}$=0.85	$\frac{H_\ell}{R}$=0.9	$\frac{H_\ell}{R}$=0.95	$\frac{H_\ell}{R}$=1.0
1.0	0	0	0	0	0	0	0	0	0	0
0.9	-0.0002	-0.0002	-0.0002	-0.0003	-0.0003	-0.0003	-0.0003	-0.0004	-0.0004	-0.0004
0.8	-0.0014	-0.0016	-0.0017	-0.0019	-0.0021	-0.0023	-0.0025	-0.0027	-0.0029	-0.0031
0.7	-0.0045	-0.0050	-0.0056	-0.0061	-0.0067	-0.0073	-0.0079	-0.0084	-0.0090	-0.0096
0.6	-0.0103	-0.0114	-0.0126	-0.0138	-0.0150	-0.0162	-0.0174	-0.0186	-0.0199	-0.0211
0.5	-0.0193	-0.0214	-0.0235	-0.0256	-0.0278	-0.0299	-0.0320	-0.0342	-0.0363	-0.0383
0.4	-0.0320	-0.0354	-0.0387	-0.0421	-0.0455	-0.0488	-0.0521	-0.0554	-0.0586	-0.0618
0.3	-0.0490	-0.0540	-0.0589	-0.0639	-0.0688	-0.0736	-0.0784	-0.0831	-0.0877	-0.0921
0.2	-0.0704	-0.0773	-0.0843	-0.0911	-0.0979	-0.1045	-0.1110	-0.1173	-0.1234	-0.1294
0.1	-0.0963	-0.1056	-0.1149	-0.1240	-0.1328	-0.1415	-0.1499	-0.1581	-0.1659	-0.1734
0.0	-0.1267	-0.1388	-0.1508	-0.1624	-0.1737	-0.1846	-0.1952	-0.2054	-0.2151	-0.2243

Table 4.7 Values of Dimensionless Function $d_{c1}(\eta_\ell)$ in Expression for **Convective** Component of Bending Moment Across Normal Sections for **Cantilever** Tanks

$\eta_\ell = z/H_\ell$	Values of $d_{c1}(\eta_\ell)$								
	$\frac{H_\ell}{R}$=0.1	$\frac{H_\ell}{R}$=0.15	$\frac{H_\ell}{R}$=0.2	$\frac{H_\ell}{R}$=0.25	$\frac{H_\ell}{R}$=0.3	$\frac{H_\ell}{R}$=0.35	$\frac{H_\ell}{R}$=0.4	$\frac{H_\ell}{R}$=0.45	$\frac{H_\ell}{R}$=0.5
1.0	0	0	0	0	0	0	0	0	0
0.9	-0.0042	-0.0042	-0.0042	-0.0042	-0.0041	-0.0041	-0.0041	-0.0041	-0.0041
0.8	-0.0167	-0.0167	-0.0166	-0.0165	-0.0164	-0.0164	-0.0163	-0.0161	-0.0160
0.7	-0.0375	-0.0374	-0.0372	-0.0370	-0.0367	-0.0364	-0.0361	-0.0357	-0.0354
0.6	-0.0667	-0.0664	-0.0659	-0.0654	-0.0647	-0.0640	-0.0633	-0.0625	-0.0617
0.5	-0.1041	-0.1035	-0.1026	-0.1016	-0.1004	-0.0991	-0.0977	-0.0962	-0.0947
0.4	-0.1495	-0.1485	-0.1471	-0.1454	-0.1434	-0.1412	-0.1388	-0.1364	-0.1339
0.3	-0.2034	-0.2018	-0.1997	-0.1970	-0.1940	-0.1906	-0.1870	-0.1832	-0.1794
0.2	-0.2656	-0.2633	-0.2602	-0.2564	-0.2519	-0.2471	-0.2419	-0.2364	-0.2309
0.1	-0.3360	-0.3328	-0.3285	-0.3232	-0.3172	-0.3105	-0.3033	-0.2959	-0.2882
0.0	-0.4149	-0.4107	-0.4049	-0.3979	-0.3899	-0.3810	-0.3715	-0.3616	-0.3516

$\eta_\ell = z/H_\ell$	$\frac{H_\ell}{R}$=0.55	$\frac{H_\ell}{R}$=0.6	$\frac{H_\ell}{R}$=0.65	$\frac{H_\ell}{R}$=0.7	$\frac{H_\ell}{R}$=0.75	$\frac{H_\ell}{R}$=0.8	$\frac{H_\ell}{R}$=0.85	$\frac{H_\ell}{R}$=0.9	$\frac{H_\ell}{R}$=0.95	$\frac{H_\ell}{R}$=1.0
1.0	0	0	0	0	0	0	0	0	0	0
0.9	-0.0041	-0.0041	-0.0041	-0.0040	-0.0040	-0.0040	-0.0040	-0.0040	-0.0040	-0.0040
0.8	-0.0159	-0.0158	-0.0157	-0.0156	-0.0155	-0.0154	-0.0153	-0.0152	-0.0151	-0.0150
0.7	-0.0350	-0.0347	-0.0343	-0.0339	-0.0336	-0.0332	-0.0329	-0.0326	-0.0322	-0.0319
0.6	-0.0609	-0.0601	-0.0592	-0.0584	-0.0576	-0.0569	-0.0561	-0.0554	-0.0547	-0.0540
0.5	-0.0932	-0.0916	-0.0901	-0.0886	-0.0871	-0.0857	-0.0843	-0.0829	-0.0816	-0.0804
0.4	-0.1313	-0.1288	-0.1263	-0.1238	-0.1214	-0.1190	-0.1168	-0.1146	-0.1125	-0.1104
0.3	-0.1755	-0.1716	-0.1678	-0.1640	-0.1604	-0.1569	-0.1534	-0.1502	-0.1470	-0.1440
0.2	-0.2253	-0.2197	-0.2143	-0.2089	-0.2037	-0.1987	-0.1938	-0.1892	-0.1847	-0.1805
0.1	-0.2806	-0.2730	-0.2655	-0.2582	-0.2511	-0.2443	-0.2378	-0.2315	-0.2255	-0.2198
0.0	-0.3414	-0.3314	-0.3215	-0.3120	-0.3027	-0.2937	-0.2852	-0.2770	-0.2692	-0.2618

Table 4.8 Values of Dimensionless Function $d_i(\eta_t)$ in Expression for **Impulsive** Component of Bending Moment Across Normal Sections for Steel Tanks with **Roller** Support at Top

$\eta_t = z/H_t$	(a) Values of $d_i(\eta_t)$ for $H_\ell/H_t=1$								
	$\frac{H_\ell}{R}$=0.2	$\frac{H_\ell}{R}$=0.25	$\frac{H_\ell}{R}$=0.3	$\frac{H_\ell}{R}$=0.35	$\frac{H_\ell}{R}$=0.4	$\frac{H_\ell}{R}$=0.45	$\frac{H_\ell}{R}$=0.5	$\frac{H_\ell}{R}$=0.55	
1.0	0	0	0	0	0	0	0	0	
0.9	0.0047	0.0060	0.0072	0.0085	0.0098	0.0111	0.0123	0.0135	
0.8	0.0090	0.0115	0.0140	0.0165	0.0190	0.0214	0.0238	0.0262	
0.7	0.0128	0.0163	0.0199	0.0234	0.0269	0.0304	0.0338	0.0371	
0.6	0.0156	0.0200	0.0244	0.0288	0.0331	0.0374	0.0416	0.0457	
0.5	0.0173	0.0223	0.0272	0.0322	0.0371	0.0419	0.0466	0.0512	
0.4	0.0177	0.0229	0.0281	0.0333	0.0384	0.0435	0.0484	0.0531	
0.3	0.0165	0.0216	0.0267	0.0317	0.0367	0.0415	0.0462	0.0507	
0.2	0.0139	0.0184	0.0229	0.0273	0.0317	0.0359	0.0400	0.0439	
0.1	0.0097	0.0132	0.0167	0.0201	0.0234	0.0266	0.0296	0.0325	
0.0	0.0042	0.0062	0.0081	0.0100	0.0117	0.0134	0.0149	0.0163	
$\eta_t = z/H_t$	$\frac{H_\ell}{R}$=0.6	$\frac{H_\ell}{R}$=0.65	$\frac{H_\ell}{R}$=0.7	$\frac{H_\ell}{R}$=0.75	$\frac{H_\ell}{R}$=0.8	$\frac{H_\ell}{R}$=0.85	$\frac{H_\ell}{R}$=0.9	$\frac{H_\ell}{R}$=0.95	$\frac{H_\ell}{R}$=1.0
1.0	0	0	0	0	0	0	0	0	0
0.9	0.0147	0.0158	0.0168	0.0178	0.0188	0.0196	0.0205	0.0213	0.0220
0.8	0.0284	0.0305	0.0326	0.0345	0.0363	0.0380	0.0396	0.0411	0.0425
0.7	0.0403	0.0434	0.0463	0.0490	0.0515	0.0539	0.0562	0.0583	0.0602
0.6	0.0496	0.0534	0.0569	0.0602	0.0633	0.0662	0.0689	0.0714	0.0738
0.5	0.0556	0.0597	0.0636	0.0673	0.0707	0.0739	0.0769	0.0796	0.0821
0.4	0.0576	0.0619	0.0659	0.0697	0.0731	0.0763	0.0793	0.0820	0.0844
0.3	0.0550	0.0591	0.0629	0.0664	0.0696	0.0725	0.0752	0.0775	0.0796
0.2	0.0476	0.0510	0.0542	0.0571	0.0598	0.0621	0.0642	0.0660	0.0676
0.1	0.0351	0.0376	0.0398	0.0417	0.0434	0.0449	0.0461	0.0471	0.0479
0.0	0.0175	0.0185	0.0194	0.0200	0.0205	0.0208	0.0209	0.0208	0.0205

Table 4.8 Continued. Values of Dimensionless Function $d_i(\eta_t)$ in Expression for **Impulsive** Component of Bending Moment Across Normal Sections for Steel Tanks with **Roller** Support at Top

$\eta_t = z/H_t$	(b) Values of $d_i(\eta_t)$ for $H_\ell/H_t=0.75$					
	$\frac{H_\ell}{R}=0.2$	$\frac{H_\ell}{R}=0.25$	$\frac{H_\ell}{R}=0.3$	$\frac{H_\ell}{R}=0.35$	$\frac{H_\ell}{R}=0.4$	$\frac{H_\ell}{R}=0.45$
1.0	0	0	0	0	0	0
0.9	0.0051	0.0064	0.0078	0.0092	0.0106	0.0119
0.8	0.0101	0.0129	0.0156	0.0184	0.0211	0.0238
0.7	0.0151	0.0193	0.0234	0.0276	0.0317	0.0357
0.6	0.0198	0.0252	0.0306	0.0361	0.0414	0.0467
0.5	0.0233	0.0298	0.0362	0.0426	0.0490	0.0553
0.4	0.0251	0.0322	0.0392	0.0462	0.0531	0.0599
0.3	0.0246	0.0317	0.0388	0.0458	0.0527	0.0594
0.2	0.0214	0.0280	0.0344	0.0407	0.0469	0.0529
0.1	0.0156	0.0207	0.0258	0.0306	0.0353	0.0398
0.0	0.0073	0.0102	0.0129	0.0155	0.0179	0.0201
$\eta_t = z/H_t$	$\frac{H_\ell}{R}=0.5$	$\frac{H_\ell}{R}=0.55$	$\frac{H_\ell}{R}=0.6$	$\frac{H_\ell}{R}=0.65$	$\frac{H_\ell}{R}=0.7$	$\frac{H_\ell}{R}=0.75$
1.0	0	0	0	0	0	0
0.9	0.0132	0.0145	0.0157	0.0169	0.0180	0.0190
0.8	0.0265	0.0290	0.0314	0.0338	0.0359	0.0380
0.7	0.0397	0.0435	0.0471	0.0506	0.0539	0.0569
0.6	0.0519	0.0568	0.0616	0.0661	0.0704	0.0744
0.5	0.0613	0.0672	0.0728	0.0780	0.0830	0.0876
0.4	0.0665	0.0728	0.0787	0.0843	0.0896	0.0945
0.3	0.0659	0.0720	0.0778	0.0832	0.0882	0.0928
0.2	0.0586	0.0639	0.0689	0.0735	0.0776	0.0813
0.1	0.0440	0.0478	0.0513	0.0544	0.0571	0.0593
0.0	0.0219	0.0235	0.0248	0.0257	0.0262	0.0264

Table 4.8 Continued. Values of Dimensionless Function $d_i(\eta_t)$ in Expression for **Impulsive** Component of Bending Moment Across Normal Sections for Steel Tanks with **Roller** Support at Top

$\eta_t = z/H_t$	(c) Values of $d_i(\eta_t)$ for $H_\ell/H_t=0.5$								
	$\frac{H_\ell}{R}=0.1$	$\frac{H_\ell}{R}=0.15$	$\frac{H_\ell}{R}=0.2$	$\frac{H_\ell}{R}=0.25$	$\frac{H_\ell}{R}=0.3$	$\frac{H_\ell}{R}=0.35$	$\frac{H_\ell}{R}=0.4$	$\frac{H_\ell}{R}=0.45$	$\frac{H_\ell}{R}=0.5$
1.0	0	0	0	0	0	0	0	0	0
0.9	0.0026	0.0041	0.0057	0.0072	0.0087	0.0102	0.0117	0.0130	0.0144
0.8	0.0512	0.0083	0.0113	0.0144	0.0174	0.0204	0.0233	0.0261	0.0287
0.7	0.0077	0.0124	0.0170	0.0216	0.0261	0.0306	0.0350	0.0391	0.0431
0.6	0.0102	0.0165	0.0226	0.0288	0.0348	0.0408	0.0466	0.0522	0.0575
0.5	0.0128	0.0206	0.0283	0.0360	0.0436	0.0510	0.0583	0.0652	0.0718
0.4	0.0151	0.0244	0.0335	0.0427	0.0517	0.0605	0.0691	0.0773	0.0852
0.3	0.0159	0.0263	0.0363	0.0463	0.0561	0.0658	0.0751	0.0840	0.0924
0.2	0.0143	0.0246	0.0345	0.0443	0.0538	0.0631	0.0720	0.0804	0.0883
0.1	0.0101	0.0187	0.0269	0.0349	0.0427	0.0500	0.0570	0.0634	0.0691
0.0	0.0035	0.0087	0.0134	0.0178	0.0219	0.0256	0.0287	0.0313	0.0333

$\eta_t = z/H_t$	(d) Values of $d_i(\eta_t)$ for $H_\ell/H_t=0.25$			
	$\frac{H_\ell}{R}=0.1$	$\frac{H_\ell}{R}=0.15$	$\frac{H_\ell}{R}=0.2$	$\frac{H_\ell}{R}=0.25$
1.0	0	0	0	0
0.9	0.0033	0.0053	0.0072	0.0089
0.8	0.0066	0.0106	0.0144	0.0178
0.7	0.0099	0.0159	0.0215	0.0267
0.6	0.0132	0.0212	0.0287	0.0356
0.5	0.0165	0.0266	0.0359	0.0445
0.4	0.0197	0.0319	0.0431	0.0534
0.3	0.0230	0.0372	0.0503	0.0622
0.2	0.0260	0.0422	0.0570	0.0706
0.1	0.0235	0.0393	0.0537	0.0665
0.0	0.0109	0.0205	0.0284	0.0344

Table 4.9 Values of Dimensionless Function $d_{c1}(\eta_t)$ in Expression for **Convective** Component of Bending Moment Across Normal Sections for Steel Tanks with **Roller** Support at Top

η_t= z/H_t	(a) Values of $d_{c1}(\eta_t)$ for H_ℓ/H_t=1								
	$\frac{H_\ell}{R}$=0.2	$\frac{H_\ell}{R}$=0.25	$\frac{H_\ell}{R}$=0.3	$\frac{H_\ell}{R}$=0.35	$\frac{H_\ell}{R}$=0.4	$\frac{H_\ell}{R}$=0.45	$\frac{H_\ell}{R}$=0.5	$\frac{H_\ell}{R}$=0.55	
1.0	0	0	0	0	0	0	0	0	
0.9	0.0389	0.0385	0.0378	0.0369	0.0359	0.0348	0.0336	0.0325	
0.8	0.0696	0.0688	0.0675	0.0657	0.0638	0.0617	0.-594	0.0572	
0.7	0.0921	0.0911	0.0892	0.0867	0.0840	0.0810	0.0779	0.0747	
0.6	0.1065	0.1053	0.1031	0.1001	0.0968	0.0931	0.0893	0.0854	
0.5	0.1129	0.1118	0.1094	0.1061	0.1024	0.0983	0.0940	0.0897	
0.4	0.1115	0.1107	0.1083	0.1051	0.1012	0.0970	0.0926	0.0881	
0.3	0.1020	0.1017	0.0997	0.0967	0.0931	0.0891	0.0848	0.0805	
0.2	0.0846	0.0850	0.0837	0.0813	0.0782	0.0748	0.0710	0.0672	
0.1	0.0594	0.0608	0.0604	0.0589	0.0568	0.0542	0.0514	0.0485	
0.0	0.0260	0.0288	0.0297	0.0295	0.0286	0.0274	0.0259	0.0242	
η_t= z/H_t	$\frac{H_\ell}{R}$=0.6	$\frac{H_\ell}{R}$=0.65	$\frac{H_\ell}{R}$=0.7	$\frac{H_\ell}{R}$=0.75	$\frac{H_\ell}{R}$=0.8	$\frac{H_\ell}{R}$=0.85	$\frac{H_\ell}{R}$=0.9	$\frac{H_\ell}{R}$=0.95	$\frac{H_\ell}{R}$=1.0
1.0	0	0	0	0	0	0	0	0	0
0.9	0.0313	0.0302	0.0291	0.0280	0.0269	0.0259	0.0250	0.0241	0.0232
0.8	0.0550	0.0527	0.0506	0.0485	0.0465	0.0446	0.0427	0.0410	0.0394
0.7	0.0715	0.0684	0.0653	0.0624	0.0596	0.0569	0.0543	0.0519	0.0495
0.6	0.0815	0.0777	0.0739	0.0703	0.0669	0.0636	0.0604	0.0575	0.0547
0.5	0.0853	0.0810	0.0769	0.0729	0.0690	0.0653	0.0618	0.0585	0.0554
0.4	0.0835	0.0791	0.0748	0.0706	0.0666	0.0628	0.0591	0.0557	0.0525
0.3	0.0761	0.0718	0.0676	0.0636	0.0597	0.0560	0.0525	0.0492	0.0461
0.2	0.0634	0.0596	0.0558	0.0522	0.0488	0.0455	0.0424	0.0395	0.0368
0.1	0.0455	0.0425	0.0396	0.0368	0.0341	0.0315	0.0291	0.0268	0.0247
0.0	0.0225	0.0207	0.0190	0.0173	0.0156	0.0140	0.0125	0.0111	0.0098

Table 4.9 Continued. Values of Dimensionless Function $d_{c1}(\eta_t)$ in Expression for **Convective** Component of Bending Moment Across Normal Sections for Steel Tanks with **Roller** Support at Top

$\eta_t = z/H_t$	(b) Values of $d_i(\eta_t)$ for $H_\ell/H_t=0.75$					
	$\frac{H_\ell}{R}=0.2$	$\frac{H_\ell}{R}=0.25$	$\frac{H_\ell}{R}=0.3$	$\frac{H_\ell}{R}=0.35$	$\frac{H_\ell}{R}=0.4$	$\frac{H_\ell}{R}=0.45$
1.0	0	0	0	0	0	0
0.9	0.0456	0.0450	0.0442	0.0432	0.0420	0.0407
0.8	0.0911	0.0901	0.0884	0.0865	0.0840	0.0813
0.7	0.1349	0.1334	0.1308	0.1280	0.1243	0.1203
0.6	0.1657	0.1637	0.1603	0.1567	0.1518	0.1466
0.5	0.1819	0.1797	0.1758	0.1715	0.1657	0.1595
0.4	0.1839	0.1817	0.1775	0.1729	0.1667	0.1599
0.3	0.1715	0.1697	0.1657	0.1612	0.1549	0.1482
0.2	0.1450	0.1441	0.1408	0.1368	0.1312	0.1250
0.1	0.1046	0.1049	0.1029	0.0999	0.0955	0.0906
0.0	0.0500	0.0521	0.0519	0.0506	0.0481	0.0451
$\eta_t = z/H_t$	$\frac{H_\ell}{R}=0.5$	$\frac{H_\ell}{R}=0.55$	$\frac{H_\ell}{R}=0.6$	$\frac{H_\ell}{R}=0.65$	$\frac{H_\ell}{R}=0.7$	$\frac{H_\ell}{R}=0.75$
1.0	0	0	0	0	0	0
0.9	0.0395	0.0380	0.0366	0.0354	0.0340	0.0327
0.8	0.0789	0.0761	0.0733	0.0708	0.0681	0.0654
0.7	0.1167	0.1124	0.1082	0.1045	0.1004	0.0965
0.6	0.1418	0.1363	0.1307	0.1259	0.1206	0.1154
0.5	0.1539	0.1473	0.1408	0.1351	0.1288	0.1227
0.4	0.1538	0.1466	0.1394	0.1332	0.1263	0.1197
0.3	0.1420	0.1347	0.1275	0.1212	0.1142	0.1075
0.2	0.1192	0.1125	0.1058	0.0999	0.0935	0.0873
0.1	0.0859	0.0804	0.0749	0.0700	0.0647	0.0595
0.0	0.0420	0.0385	0.0349	0.0315	0.0279	0.0245

Table 4.9 Continued. Values of Dimensionless Function $d_{c1}(\eta_t)$ in Expression for **Convective** Component of Bending Moment Across Normal Sections for Steel Tanks with **Roller** Support at Top

$\eta_t = z/H_t$	(c) Values of $d_{c1}(\eta_t)$ for $H_\ell/H_t=0.5$								
	$\frac{H_\ell}{R}=0.1$	$\frac{H_\ell}{R}=0.15$	$\frac{H_\ell}{R}=0.2$	$\frac{H_\ell}{R}=0.25$	$\frac{H_\ell}{R}=0.3$	$\frac{H_\ell}{R}=0.35$	$\frac{H_\ell}{R}=0.4$	$\frac{H_\ell}{R}=0.45$	$\frac{H_\ell}{R}=0.5$
1.0	0	0	0	0	0	0	0	0	0
0.9	0.0479	0.0500	0.0500	0.0493	0.0481	0.0467	0.0450	0.0433	0.0415
0.8	0.0958	0.0999	0.1000	0.0986	0.0963	0.0934	0.0901	0.0866	0.0829
0.7	0.1438	0.1499	0.1501	0.1479	0.1444	0.1401	0.1351	0.1299	0.1244
0.6	0.1917	0.1998	0.2001	0.1972	0.1926	0.1868	0.1802	0.1732	0.1659
0.5	0.2396	0.2498	0.2501	0.2465	0.2407	0.2335	0.2252	0.2164	0.2073
0.4	0.2711	0.2833	0.2838	0.2796	0.2727	0.2640	0.2543	0.2438	0.2330
0.3	0.2690	0.2836	0.2845	0.2800	0.2725	0.2630	0.2523	0.2407	0.2288
0.2	0.2339	0.2511	0.2531	0.2491	0.2418	0.2323	0.2215	0.2099	0.1979
0.1	0.1657	0.1863	0.1900	0.1874	0.1814	0.1731	0.1636	0.1532	0.1423
0.0	0.0643	0.0888	0.0952	0.0951	0.0916	0.0859	0.0790	0.0712	0.0631

$\eta_t = z/H_t$	(d) Values of $d_{c1}(\eta_t)$ for $H_\ell/H_t=0.25$			
	$\frac{H_\ell}{R}=0.1$	$\frac{H_\ell}{R}=0.15$	$\frac{H_\ell}{R}=0.2$	$\frac{H_\ell}{R}=0.25$
1.0	0	0	0	0
0.9	0.0603	0.0624	0.0613	0.0587
0.8	0.1206	0.1248	0.1225	0.1174
0.7	0.1810	0.1873	0.1838	0.1761
0.6	0.2413	0.2497	0.2450	0.2347
0.5	0.3016	0.3121	0.3063	0.2934
0.4	0.3619	0.3745	0.3675	0.3521
0.3	0.4222	0.4369	0.4288	0.4108
0.2	0.4659	0.4827	0.4734	0.4529
0.1	0.3931	0.4131	0.4040	0.3826
0.0	0.1883	0.2135	0.2076	0.1889

Table 4.10 Values of Dimensionless Function $d_i(\eta_t)$ in Expression for **Impulsive** Component of Bending Moment Across Normal Sections for Steel Tanks **Hinged** at Top

$\eta_t = z/H_t$	(a) Values of $d_i(\eta_t)$ for $H_\ell/H_t=1$								
	$\frac{H_\ell}{R}$=0.2	$\frac{H_\ell}{R}$=0.25	$\frac{H_\ell}{R}$=0.3	$\frac{H_\ell}{R}$=0.35	$\frac{H_\ell}{R}$=0.4	$\frac{H_\ell}{R}$=0.45	$\frac{H_\ell}{R}$=0.2	$\frac{H_\ell}{R}$=0.55	
1.0	0.717	0.596	0.509	0.442	0.389	0.346	0.310	0.278	
0.9	0.721	0.601	0.515	0.450	0.398	0.356	0.320	0.290	
0.8	0.725	0.606	0.521	0.456	0.406	0.365	0.330	0.301	
0.7	0.728	0.610	0.526	0.462	0.413	0.372	0.339	0.310	
0.6	0.730	0.613	0.529	0.467	0.418	0.378	0.345	0.317	
0.5	0.731	0.615	0.531	0.469	0.420	0.381	0.349	0.321	
0.4	0.731	0.614	0.531	0.469	0.421	0.382	0.349	0.322	
0.3	0.729	0.613	0.529	0.467	0.418	0.378	0.346	0.318	
0.2	0.726	0.609	0.525	0.461	0.412	0.372	0.338	0.310	
0.1	0.721	0.603	0.517	0.453	0.402	0.361	0.326	0.297	
0.0	0.715	0.595	0.508	0.442	0.389	0.346	0.310	0.279	
$\eta_t = z/H_t$	$\frac{H_\ell}{R}$=0.6	$\frac{H_\ell}{R}$=0.65	$\frac{H_\ell}{R}$=0.7	$\frac{H_\ell}{R}$=0.75	$\frac{H_\ell}{R}$=0.8	$\frac{H_\ell}{R}$=0.85	$\frac{H_\ell}{R}$=0.9	$\frac{H_\ell}{R}$=0.95	$\frac{H_\ell}{R}$=1.0
1.0	0.251	0.226	0.204	0.185	0.167	0.151	0.136	0.122	0.110
0.9	0.264	0.240	0.219	0.201	0.184	0.168	0.154	0.141	0.130
0.8	0.276	0.253	0.233	0.215	0.199	0.185	0.171	0.159	0.148
0.7	0.286	0.264	0.245	0.228	0.212	0.198	0.186	0.174	0.164
0.6	0.293	0.272	0.254	0.237	0.222	0.209	0.187	0.186	0.176
0.5	0.298	0.277	0.259	0.242	0.228	0.215	0.203	0.192	0.182
0.4	0.298	0.277	0.259	0.243	0.228	0.215	0.203	0.192	0.183
0.3	0.294	0.273	0.254	0.238	0.223	0.209	0.197	0.186	0.176
0.2	0.285	0.263	0.244	0.227	0.211	0.197	0.184	0.173	0.162
0.1	0.271	0.248	0.228	0.210	0.193	0.178	0.164	0.152	0.141
0.0	0.252	0.227	0.206	0.186	0.168	0.152	0.137	0.124	0.111

Table 4.10 Continued. Values of Dimensionless Function $d_i(\eta_t)$ in Expression for **Impulsive** Component of Bending Moment Across Normal Sections for Steel Tanks **Hinged** at Top

$\eta_t = z/H_t$	(b) Values of $d_i(\eta_t)$ for $H_\ell/H_t=0.75$					
	$\frac{H_\ell}{R}=0.2$	$\frac{H_\ell}{R}=0.25$	$\frac{H_\ell}{R}=0.3$	$\frac{H_\ell}{R}=0.35$	$\frac{H_\ell}{R}=0.4$	$\frac{H_\ell}{R}=0.45$
1.0	0.530	0.439	0.373	0.322	0.281	0.247
0.9	0.535	0.445	0.379	0.330	0.290	0.257
0.8	0.539	0.450	0.386	0.337	0.299	0.267
0.7	0.543	0.455	0.393	0.345	0.308	0.277
0.6	0.547	0.460	0.399	0.352	0.316	0.287
0.5	0.550	0.464	0.403	0.358	0.322	0.294
0.4	0.551	0.466	0.405	0.360	0.325	0.297
0.3	0.550	0.464	0.404	0.358	0.323	0.295
0.2	0.546	0.460	0.398	0.352	0.316	0.287
0.1	0.540	0.451	0.388	0.341	0.303	0.272
0.0	0.531	0.440	0.374	0.324	0.284	0.251
$\eta_t = z/H_t$	$\frac{H_\ell}{R}=0.5$	$\frac{H_\ell}{R}=0.55$	$\frac{H_\ell}{R}=0.6$	$\frac{H_\ell}{R}=0.65$	$\frac{H_\ell}{R}=0.7$	$\frac{H_\ell}{R}=0.75$
1.0	0.218	0.193	0.170	0.150	0.132	0.116
0.9	0.229	0.205	0.184	0.165	0.148	0.133
0.8	0.241	0.218	0.198	0.180	0.164	0.150
0.7	0.252	0.230	0.211	0.195	0.180	0.167
0.6	0.262	0.242	0.224	0.208	0.195	0.182
0.5	0.270	0.250	0.233	0.218	0.205	0.194
0.4	0.274	0.254	0.237	0.223	0.210	0.198
0.3	0.271	0.251	0.234	0.220	0.206	0.195
0.2	0.262	0.242	0.224	0.208	0.194	0.181
0.1	0.246	0.224	0.204	0.187	0.171	0.157
0.0	0.222	0.197	0.176	0.156	0.139	0.123

Table 4.10 Continued. Values of Dimensionless Function $d_i(\eta_t)$ in Expression for **Impulsive** Component of Bending Moment Across Normal Sections for Steel Tanks **Hinged** at Top

$\eta_t = z/H_t$	(c) Values of $d_i(\eta_t)$ for $H_\ell/H_t=0.5$								
	$\frac{H_\ell}{R}=0.1$	$\frac{H_\ell}{R}=0.15$	$\frac{H_\ell}{R}=0.2$	$\frac{H_\ell}{R}=0.25$	$\frac{H_\ell}{R}=0.3$	$\frac{H_\ell}{R}=0.35$	$\frac{H_\ell}{R}=0.4$	$\frac{H_\ell}{R}=0.45$	$\frac{H_\ell}{R}=0.5$
1.0	0.563	0.433	0.344	0.282	0.235	0.199	0.169	0.144	0.122
0.9	0.565	0.437	0.348	0.287	0.242	0.207	0.179	0.154	0.134
0.8	0.567	0.440	0.353	0.293	0.249	0.215	0.188	0.165	0.146
0.7	0.569	0.443	0.358	0.299	0.256	0.224	0.198	0.176	0.158
0.6	0.571	0.447	0.362	0.305	0.264	0.232	0.208	0.187	0.171
0.5	0.573	0.450	0.367	0.311	0.271	0.241	0.217	0.198	0.183
0.4	0.575	0.453	0.371	0.316	0.277	0.248	0.226	0.208	0.194
0.3	0.576	0.454	0.373	0.318	0.280	0.252	0.230	0.213	0.199
0.2	0.574	0.452	0.370	0.315	0.276	0.247	0.225	0.207	0.192
0.1	0.569	0.445	0.361	0.304	0.263	0.232	0.208	0.188	0.171
0.0	0.562	0.435	0.347	0.286	0.241	0.206	0.178	0.154	0.133

$\eta_t = z/H_t$	(d) Values of $d_i(\eta_t)$ for $H_\ell/H_t=0.25$			
	$\frac{H_\ell}{R}=0.1$	$\frac{H_\ell}{R}=0.15$	$\frac{H_\ell}{R}=0.2$	$\frac{H_\ell}{R}=0.25$
1.0	0.272	0.204	0.155	0.119
0.9	0.274	0.208	0.161	0.126
0.8	0.276	0.212	0.166	0.133
0.7	0.279	0.216	0.171	0.140
0.6	0.281	0.220	0.177	0.146
0.5	0.284	0.224	0.182	0.153
0.4	0.286	0.228	0.188	0.160
0.3	0.289	0.232	0.193	0.167
0.2	0.291	0.235	0.198	0.173
0.1	0.287	0.231	0.193	0.167
0.0	0.274	0.211	0.166	0.133

Table 4.11 Values of Dimensionless Function $d_{c1}(\eta_t)$ in Expression for **Convective** Component of Bending Moment Across Normal Sections for Steel Tanks **Hinged** at Top

$\eta_t = z/H_t$	(a) Values of $d_{c1}(\eta_t)$ for $H_\ell/H_t=1$								
	$\frac{H_\ell}{R}=0.2$	$\frac{H_\ell}{R}=0.25$	$\frac{H_\ell}{R}=0.3$	$\frac{H_\ell}{R}=0.35$	$\frac{H_\ell}{R}=0.4$	$\frac{H_\ell}{R}=0.45$	$\frac{H_\ell}{R}=0.5$	$\frac{H_\ell}{R}=0.55$	
1.0	5.076	3.279	2.251	1.614	1.194	0.905	0.699	0.548	
0.9	5.111	3.313	2.285	1.647	1.226	0.936	0.729	0.578	
0.8	5.138	3.340	2.311	1.672	1.251	0.960	0.752	0.599	
0.7	5.157	3.358	2.329	1.689	1.267	0.976	0.767	0.614	
0.6	5.168	3.368	2.339	1.699	1.276	0.984	0.775	0.621	
0.5	5.170	3.371	2.341	1.701	1.278	0.986	0.777	0.622	
0.4	5.165	3.366	2.337	1.697	1.274	0.981	0.772	0.618	
0.3	5.152	3.353	2.324	1.684	1.262	0.970	0.761	0.607	
0.2	5.131	3.333	2.304	1.665	1.244	0.952	0.744	0.591	
0.1	5.101	3.305	2.277	1.639	1.219	0.928	0.721	0.569	
0.0	5.064	3.269	2.243	1.606	1.187	0.898	0.692	0.542	
$\eta_t = z/H_t$	$\frac{H_\ell}{R}=0.6$	$\frac{H_\ell}{R}=0.65$	$\frac{H_\ell}{R}=0.7$	$\frac{H_\ell}{R}=0.75$	$\frac{H_\ell}{R}=0.8$	$\frac{H_\ell}{R}=0.85$	$\frac{H_\ell}{R}=0.9$	$\frac{H_\ell}{R}=0.95$	$\frac{H_\ell}{R}=1.0$
1.0	0.435	0.349	0.283	0.231	0.190	0.157	0.130	0.109	0.091
0.9	0.464	0.377	0.309	0.256	0.214	0.181	0.153	0.131	0.113
0.8	0.485	0.397	0.328	0.275	0.232	0.197	0.169	0.146	0.127
0.7	0.498	0.410	0.341	0.286	0.243	0.208	0.179	0.155	0.136
0.6	0.505	0.416	0.347	0.292	0.248	0.212	0.183	0.159	0.139
0.5	0.506	0.417	0.347	0.292	0.248	0.212	0.183	0.159	0.139
0.4	0.502	0.412	0.343	0.287	0.243	0.207	0.178	0.154	0.134
0.3	0.491	0.402	0.333	0.278	0.234	0.199	0.170	0.146	0.126
0.2	0.476	0.387	0.319	0.264	0.221	0.186	0.158	0.135	0.115
0.1	0.455	0.368	0.300	0.247	0.204	0.170	0.143	0.120	0.102
0.0	0.429	0.343	0.277	0.225	0.184	0.151	0.124	0.103	0.085

Table 4.11 Continued. Values of Dimensionless Function $d_{c1}(\eta_t)$ in Expression for **Convective** Component of Bending Moment Across Normal Sections for Steel Tanks **Hinged** at Top

$\eta_t = z/H_t$	(b) Values of $d_{c1}(\eta_t)$ for H_ℓ/H_t=0.75					
	$\frac{H_\ell}{R}$=0.2	$\frac{H_\ell}{R}$=0.25	$\frac{H_\ell}{R}$=0.3	$\frac{H_\ell}{R}$=0.35	$\frac{H_\ell}{R}$=0.4	$\frac{H_\ell}{R}$=0.45
1.0	4.105	2.583	1.740	1.233	0.897	0.688
0.9	4.145	2.623	1.779	1.271	0.934	0.704
0.8	4.186	2.663	1.818	1.309	0.972	0.741
0.7	4.224	2.701	1.855	1.346	1.007	0.775
0.6	4.249	2.726	1.880	1.369	1.030	0.797
0.5	4.260	2.736	1.890	1.379	1.039	0.806
0.4	4.256	2.733	1.886	1.375	1.035	0.801
0.3	4.238	2.715	1.869	1.359	1.019	0.785
0.2	4.206	2.684	1.839	1.329	0.990	0.758
0.1	4.160	2.640	1.796	1.287	0.950	0.719
0.0	4.100	2.582	1.740	1.233	0.898	0.669
$\eta_t = z/H_t$	$\frac{H_\ell}{R}$=0.5	$\frac{H_\ell}{R}$=0.55	$\frac{H_\ell}{R}$=0.6	$\frac{H_\ell}{R}$=0.65	$\frac{H_\ell}{R}$=0.7	$\frac{H_\ell}{R}$=0.75
1.0	0.509	0.390	0.302	0.237	0.185	0.145
0.9	0.544	0.425	0.335	0.269	0.216	0.175
0.8	0.580	0.459	0.368	0.301	0.248	0.206
0.7	0.613	0.491	0.400	0.332	0.277	0.234
0.6	0.634	0.511	0.419	0.350	0.295	0.251
0.5	0.642	0.519	0.426	0.356	0.300	0.255
0.4	0.638	0.514	0.421	0.351	0.295	0.250
0.3	0.622	0.499	0.405	0.336	0.280	0.235
0.2	0.595	0.473	0.380	0.312	0.256	0.213
0.1	0.558	0.437	0.346	0.279	0.225	0.182
0.0	0.510	0.391	0.303	0.237	0.185	0.145

Table 4.11 Continued. Values of Dimensionless Function $d_{c1}(\eta_t)$ in Expression for **Convective** Component of Bending Moment Across Normal Sections for Steel Tanks **Hinged** at Top

$\eta_t = z/H_t$	(c) Values of $d_{c1}(\eta_t)$ for $H_\ell/H_t=0.5$								
	$\frac{H_\ell}{R}=0.1$	$\frac{H_\ell}{R}=0.15$	$\frac{H_\ell}{R}=0.2$	$\frac{H_\ell}{R}=0.25$	$\frac{H_\ell}{R}=0.3$	$\frac{H_\ell}{R}=0.35$	$\frac{H_\ell}{R}=0.4$	$\frac{H_\ell}{R}=0.45$	$\frac{H_\ell}{R}=0.5$
1.0	9.731	4.646	2.624	1.635	1.082	0.743	0.523	0.373	0.268
0.9	9.771	4.688	2.666	1.677	1.123	0.783	0.562	0.411	0.305
0.8	9.812	4.731	2.708	1.718	1.164	0.823	0.601	0.449	0.341
0.7	9.852	4.773	2.750	1.760	1.205	0.864	0.640	0.487	0.378
0.6	9.893	4.815	2.792	1.802	1.246	0.904	0.679	0.525	0.415
0.5	9.934	4.857	2.835	1.843	1.287	0.944	0.718	0.563	0.452
0.4	9.958	4.882	2.860	1.869	1.311	0.968	0.742	0.585	0.473
0.3	9.949	4.875	2.853	1.862	1.304	0.960	0.734	0.577	0.464
0.2	9.906	4.835	2.814	1.823	1.266	0.923	0.697	0.541	0.429
0.1	9.831	4.762	2.743	1.754	1.199	0.857	0.633	0.479	0.369
0.0	9.722	4.656	2.640	1.654	1.102	0.763	0.542	0.392	0.285

$\eta_t = z/H_t$	(d) Values of $d_{c1}(\eta_t)$ for $H_\ell/H_t=0.25$			
	$\frac{H_\ell}{R}=0.1$	$\frac{H_\ell}{R}=0.15$	$\frac{H_\ell}{R}=0.2$	$\frac{H_\ell}{R}=0.25$
1.0	4.686	2.165	1.157	0.665
0.9	4.732	2.213	1.205	0.712
0.8	4.778	2.262	1.253	0.759
0.7	4.825	2.310	1.301	0.807
0.6	4.871	2.358	1.349	0.854
0.5	4.917	2.406	1.397	0.901
0.4	4.963	2.454	1.445	0.949
0.3	5.010	2.502	1.493	0.996
0.2	5.039	2.533	1.525	1.027
0.1	4.952	2.449	1.442	0.945
0.0	4.734	2.236	1.232	0.740

Table 4.12 Effect of Poisson's Ratio of Tank Material on Values of Dimensionless Functions in Expressions for Impulsive and Convective Components of Moment Across Normal Sections for Tanks with $H_\ell/R = 0.75$ and **Roller** Support at Top

η_t	Value of $d_i(\eta_t)$		Value of $d_{c1}(\eta_t)$	
	ν_t=0	ν_t=0.3	ν_t=0	ν_t=0.3
1.0	0	0	0	0
0.9	0.016	0.019	0.026	0.028
0.8	0.031	0.037	0.044	0.049
0.7	0.043	0.051	0.055	0.062
0.6	0.051	0.062	0.061	0.070
0.5	0.055	0.068	0.061	0.073
0.4	0.053	0.070	0.056	0.071
0.3	0.047	0.066	0.046	0.064
0.2	0.034	0.056	0.032	0.052
0.1	0.016	0.041	0.015	0.037
0.0	-0.008	0.020	-0.007	0.017

Table 4.13 Effect of Thickness-to-Radius Ratio on Values of Dimensionless Factors α_i and α_{c1} in Expression for Base Shear of Fully Filled Steel Tanks with **Roller** Support at Top

$\frac{t_{tw}}{R}$	Values for ρ_ℓ/ρ_t=0.127			Values for ρ_ℓ/ρ_t=0.254		
	$\frac{H_\ell}{R}$=0.3	$\frac{H_\ell}{R}$=0.5	$\frac{H_\ell}{R}$=1.0	$\frac{H_\ell}{R}$=0.3	$\frac{H_\ell}{R}$=0.3	$\frac{H_\ell}{R}$=1.0
			Values of α_i			
0.00067	0.568	0.572	0.581	0.568	0.572	0.581
0.001	0.567	0.571	0.581	0.568	0.571	0.581
0.002	0.567	0.571	0.580	0.567	0.571	0.580
			Values of α_{c1}			
0.00067	0.446	0.427	0.372	0.446	0.427	0.372
0.001	0.449	0.428	0.372	0.449	0.428	0.372
0.002	0.455	0.431	0.372	0.455	0.431	0.372

Table 4.14 Effect of Thickness-to-Radius Ratio on Values of Dimensionless Factors α_i and α_{cl} in Expression for Base Shear of Fully Filled Steel Tanks **Hinged** at Top

$\frac{t_{tw}}{R}$	Values for ρ_ℓ/ρ_t=0.127			Values for ρ_ℓ/ρ_t=0.254		
	$\frac{H_\ell}{R}$=0.3	$\frac{H_\ell}{R}$=0.5	$\frac{H_\ell}{R}$=1.0	$\frac{H_\ell}{R}$=0.3	$\frac{H_\ell}{R}$=0.3	$\frac{H_\ell}{R}$=1.0
			Values of α_i			
0.00067	0.623	0.625	0.618	0.623	0.625	0.618
0.001	0.622	0.624	0.618	0.622	0.624	0.618
0.002	0.618	0.622	0.616	0.618	0.622	0.616
			Values of α_{cl}			
0.00067	0.498	0.477	0.408	0.498	0.477	0.408
0.001	0.499	0.478	0.408	0.499	0.478	0.408
0.002	0.502	0.479	0.409	0.502	0.479	0.409

Table 4.15 Effect of Thickness-to-Radius Ratio on Maximum Values of Dimensionless Factors d_i and d_{c1} in Expression for Moment of Fully Filled Steel Tanks with **Roller** Support at Top

$\frac{t_{tw}}{R}$	Values for ρ_ℓ/ρ_t=0.127			Values for ρ_ℓ/ρ_t=0.254		
	$\frac{H_\ell}{R}$=0.3	$\frac{H_\ell}{R}$=0.5	$\frac{H_\ell}{R}$=1.0	$\frac{H_\ell}{R}$=0.3	$\frac{H_\ell}{R}$=0.3	$\frac{H_\ell}{R}$=1.0
			Max. Values of d_i			
0.00067	0.0284	0.0486	0.0845	0.0285	0.0486	0.0845
0.001	0.0281	0.0484	0.0844	0.0282	0.0484	0.0844
0.002	0.0272	0.0477	0.0840	0.0273	0.0478	0.0841
			Max. Values of d_{c1}			
0.00067	0.1103	0.0944	0.0555	0.1103	0.0944	0.0555
0.001	0.1094	0.0940	0.0554	0.1094	0.0940	0.0554
0.002	0.1070	0.0931	0.0553	0.1070	0.0931	0.0553

Table 4.16 Effect of Thickness-to-Radius Ratio on Maximum Values of Dimensionless Factors d_i and d_{c1} in Expression for Moment of Fully Filled Steel Tanks **Hinged** at Top

$\frac{t_{tw}}{R}$	Values for ρ_ℓ/ρ_t=0.127			Values for ρ_ℓ/ρ_t=0.254		
	$\frac{H_\ell}{R}$=0.3	$\frac{H_\ell}{R}$=0.5	$\frac{H_\ell}{R}$=1.0	$\frac{H_\ell}{R}$=0.3	$\frac{H_\ell}{R}$=0.5	$\frac{H_\ell}{R}$=1.0
			Max. Values of d_i			
0.00067	0.542	0.353	0.183	0.543	0.353	0.183
0.001	0.531	0.349	0.183	0.532	0.349	0.183
0.002	0.506	0.340	0.181	0.509	0.341	0.181
			Max. Values of d_{c1}			
0.00067	2.391	0.784	0.139	2.391	0.784	0.139
0.001	2.341	0.777	0.139	2.341	0.777	0.139
0.002	2.223	0.758	0.139	2.223	0.758	0.139

Table 4.17 Dimensionless Factors in Expressions for Natural Frequency of Fundamental Axisymmetric Mode of Vibration and for Total Hydrodynamic Base Force in Vertically Excited Tanks; Reference Systems with ν_t=0.3, ρ_ℓ/ρ_t=0.127 and t_{tw}/R=0.001

H_ℓ/R	Values of		
	$(C_v)_r$	m_o/m_ℓ	m_v/m_ℓ
0.10	0.0420	0.937	0.063
0.15	0.0471	0.892	0.108
0.20	0.0523	0.845	0.155
0.25	0.0570	0.801	0.199
0.30	0.0611	0.758	0.242
0.35	0.0649	0.717	0.283
0.40	0.0682	0.678	0.322
0.45	0.0712	0.642	0.358
0.50	0.0738	0.608	0.392
0.55	0.0762	0.576	0.424
0.60	0.0783	0.547	0.453
0.65	0.0802	0.521	0.479
0.70	0.0819	0.496	0.504
0.75	0.0834	0.474	0.526
0.80	0.0848	0.453	0.547
0.85	0.0860	0.434	0.566
0.90	0.0870	0.417	0.583
0.95	0.0880	0.402	0.598
1.00	0.0889	0.388	0.612

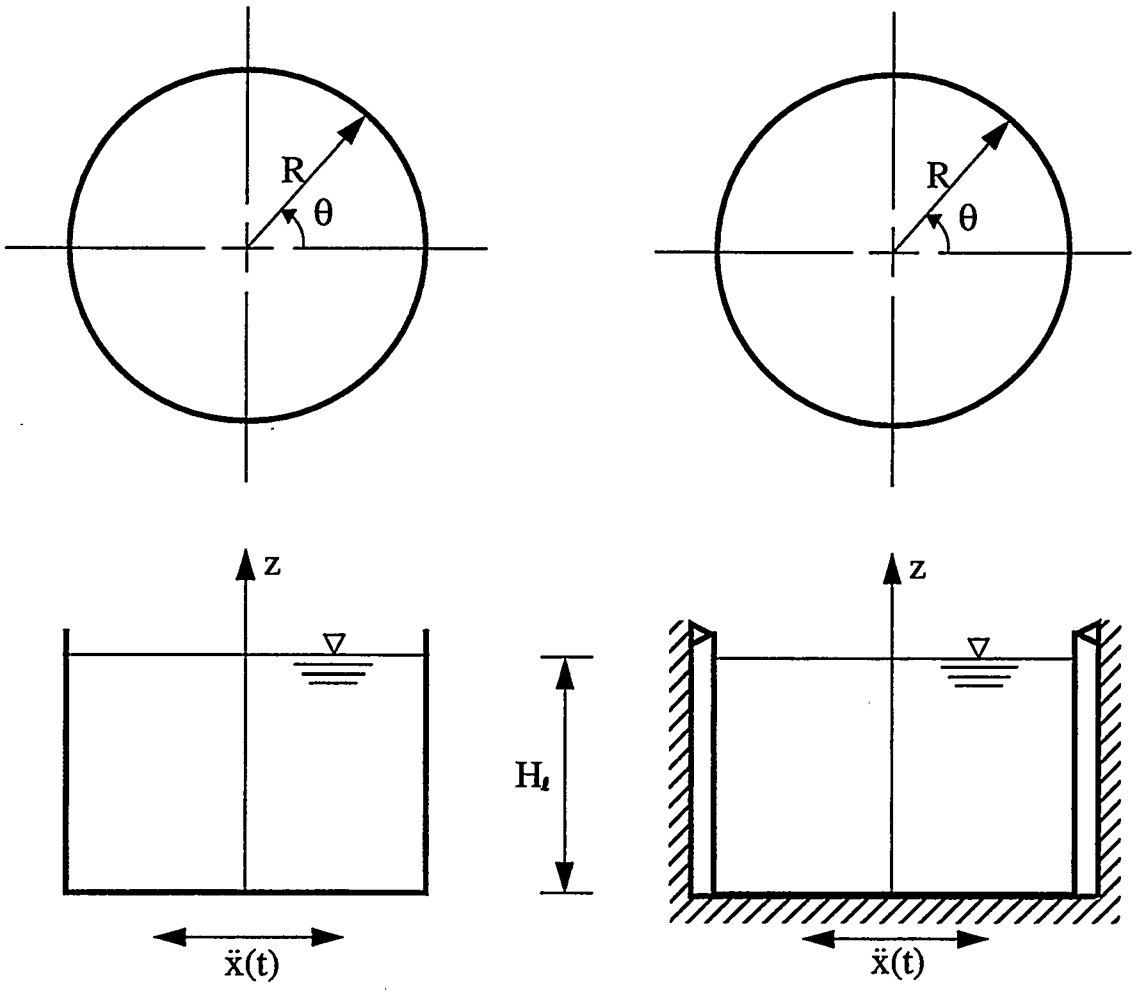

Figure 4.1 Systems Considered

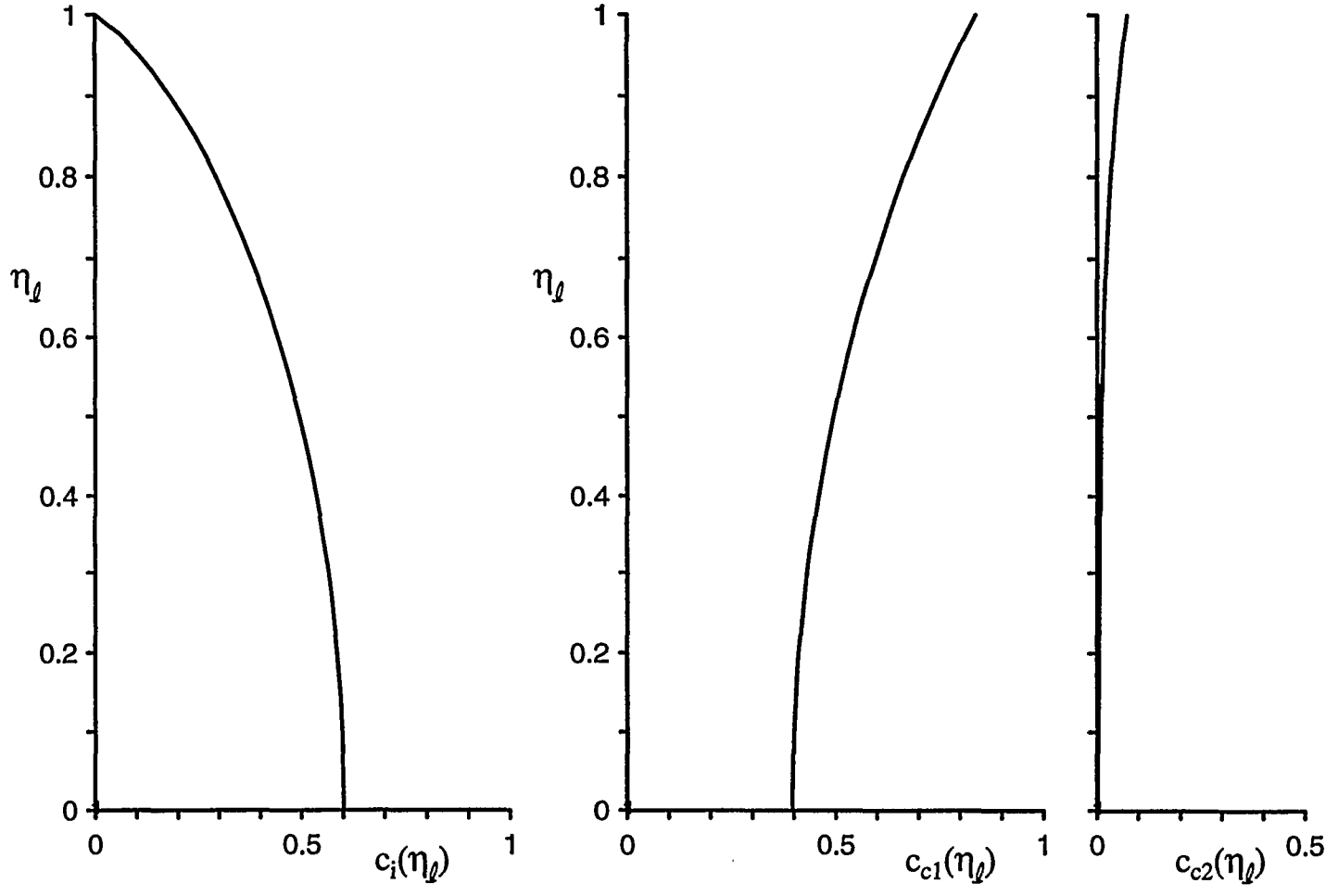

Figure 4.2 Dimensionless Functions $c_i(\eta_\ell)$ and $c_{cn}(\eta_\ell)$ in Expressions for Impulsive and Convective Components of Hydrodynamic Wall Pressures for Tanks with $H_\ell/R=0.75$

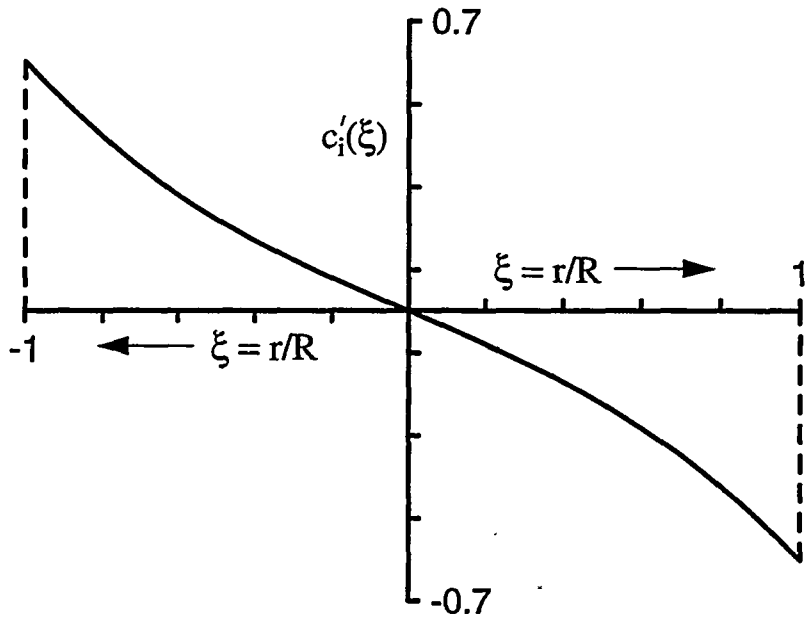

(a) Impulsive Component

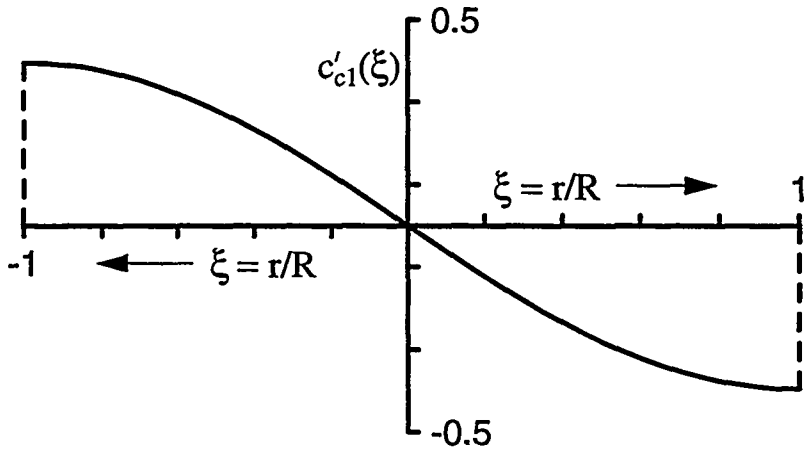

(b) Convective Component

Figure 4.3 Dimensionless Functions $c_i'(\xi)$ and $c_{c1}'(\xi)$ in Expressions for Impulsive and Fundamental Convective Components of Hydrodynamic Base Pressure for Tanks with $H_t/R=0.75$

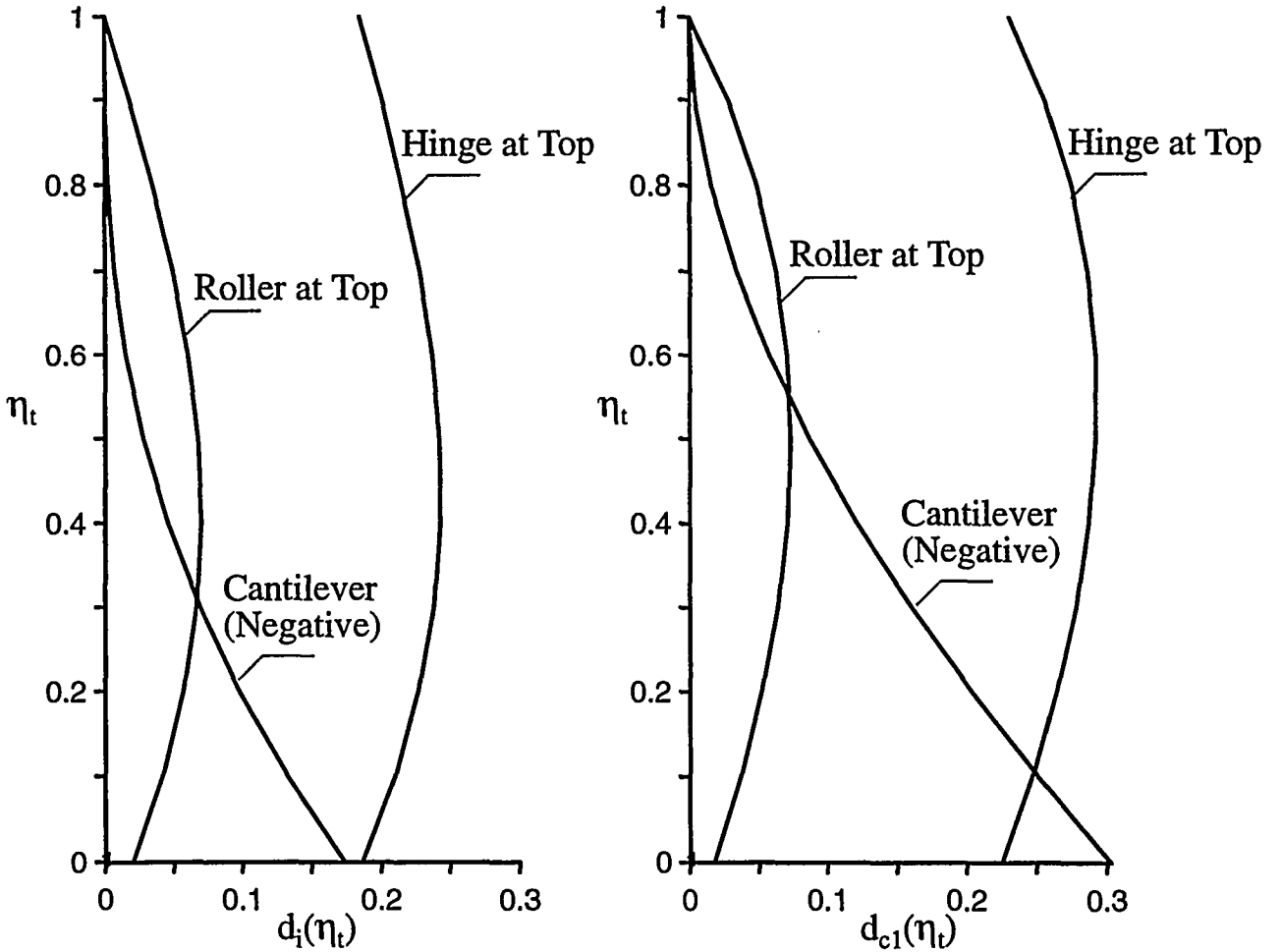

Figure 4.4 Dimensionless Functions $d_i(\eta_t)$ and $d_{c1}(\eta_t)$ in Expressions for Impulsive and Fundamental Convective Components of Bending Moment Across Normal Sections of Tanks with Different Conditions of Support at the Top; $H_t/R=0.75$

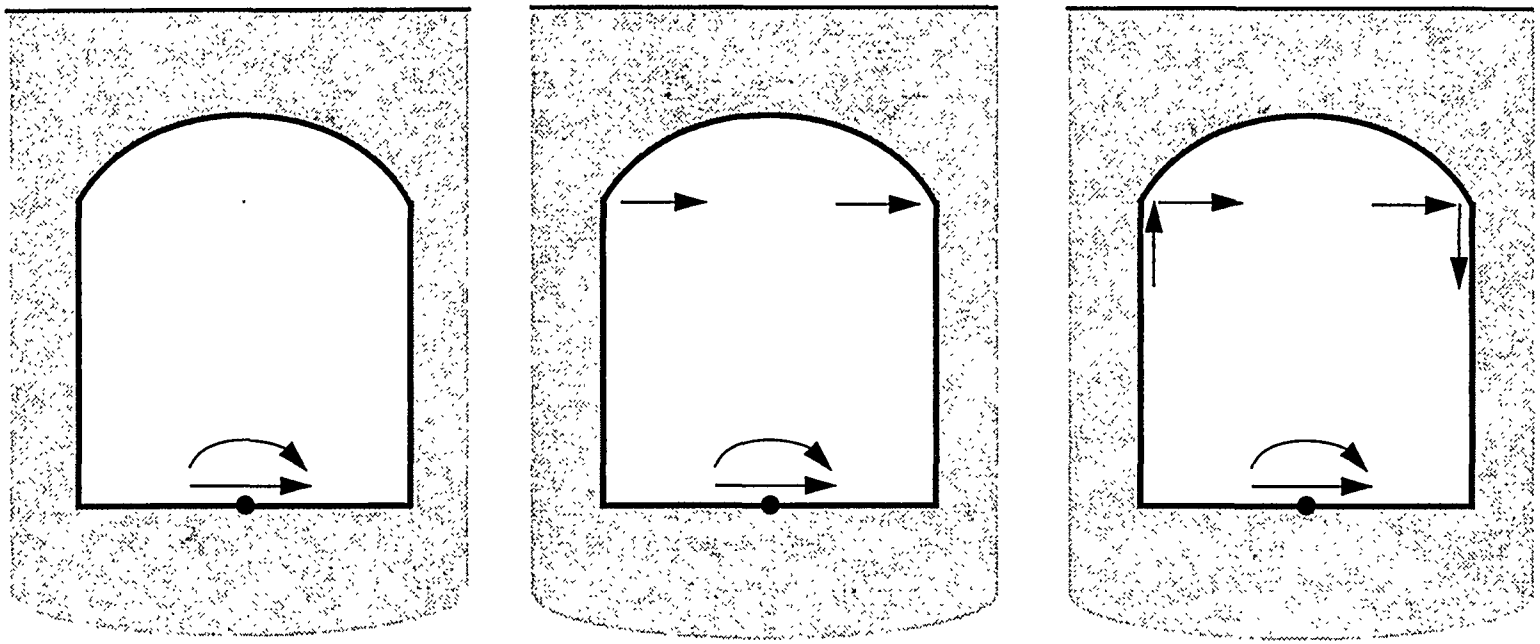

(a) For Cantilever Tank

(b) For Tank with Roller Top Support

(c) For Tank Hinged at Top

Figure 4.5 Forces Transmitted by Tank to Supporting Vault

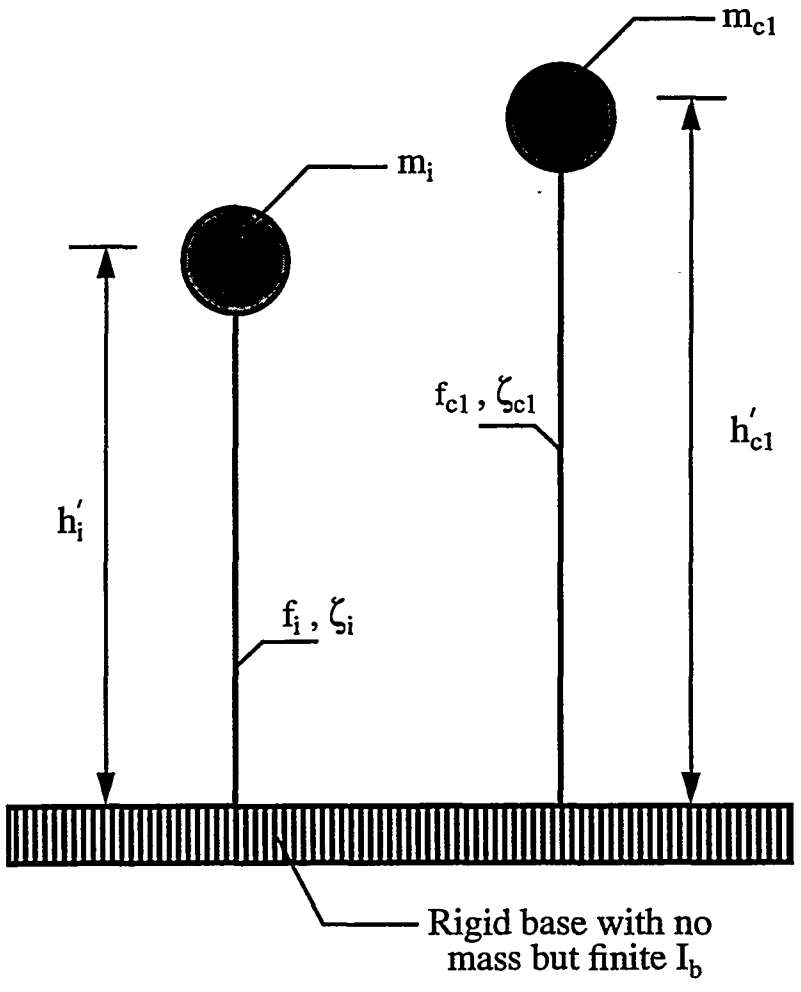

Figure 4.6 Modeling of Tank-Liquid System for Explicit Purpose of Evaluating Total Hydrodynamic Forces Transmitted to Supporting Vault

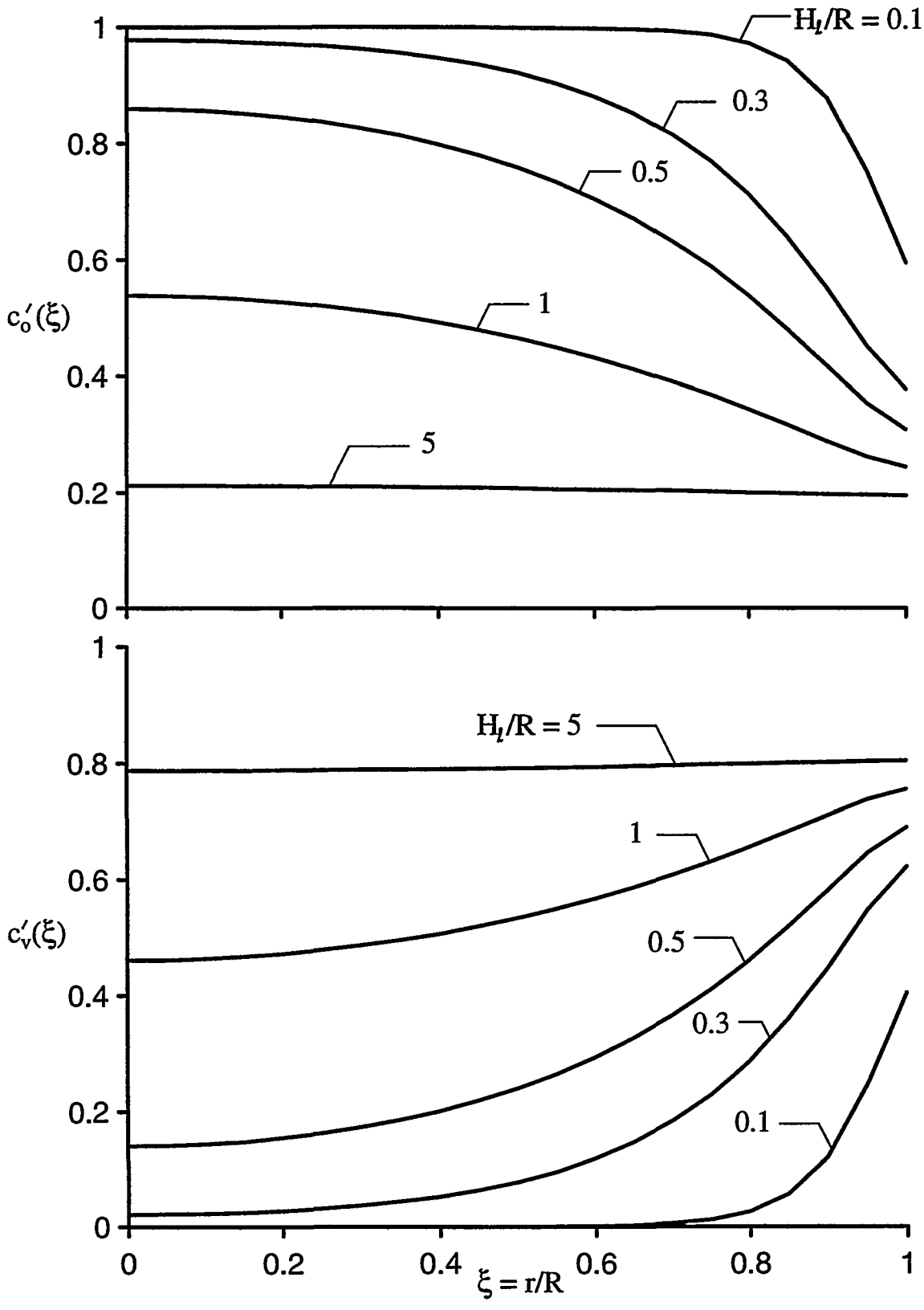

Figure 4.7 Dimensionless Functions $c_o'(\xi)$ and $c_v'(\xi)$ in Expression for Hydrodynamic Base Pressure of Vertically Excited Tanks

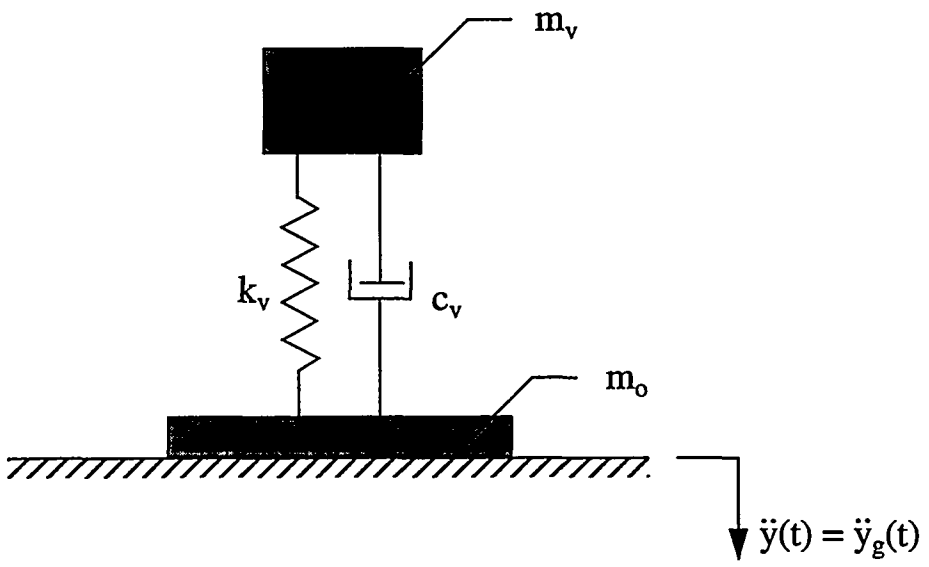

(a)

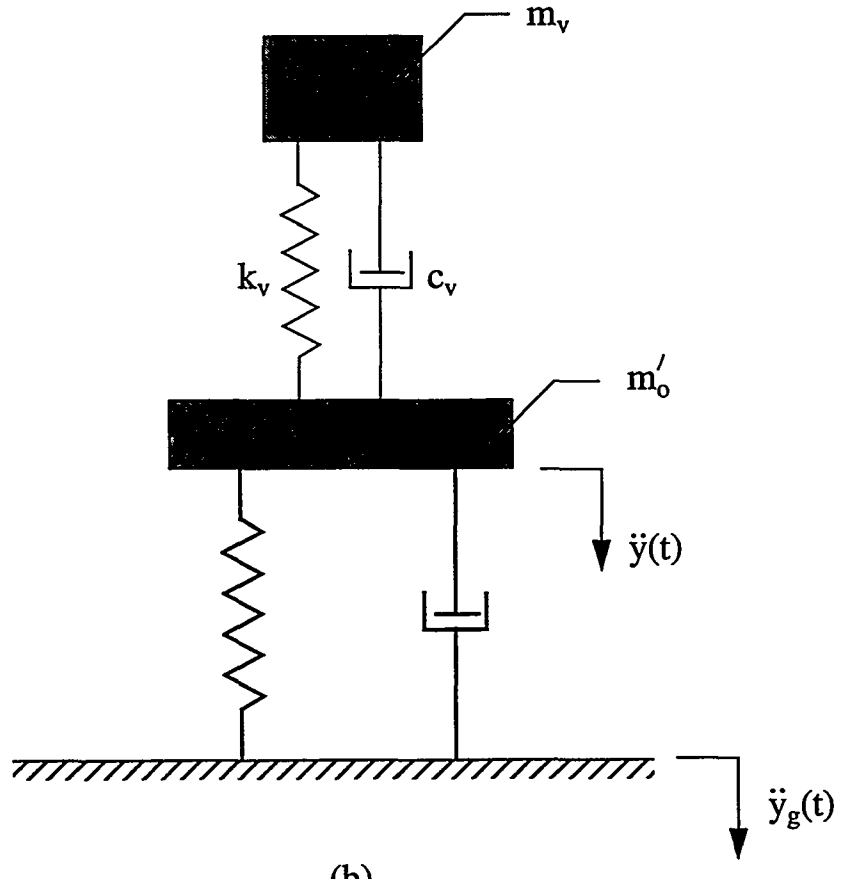

(b)

Figure 4.8 Modeling of Vertically Excited Tank-Liquid System

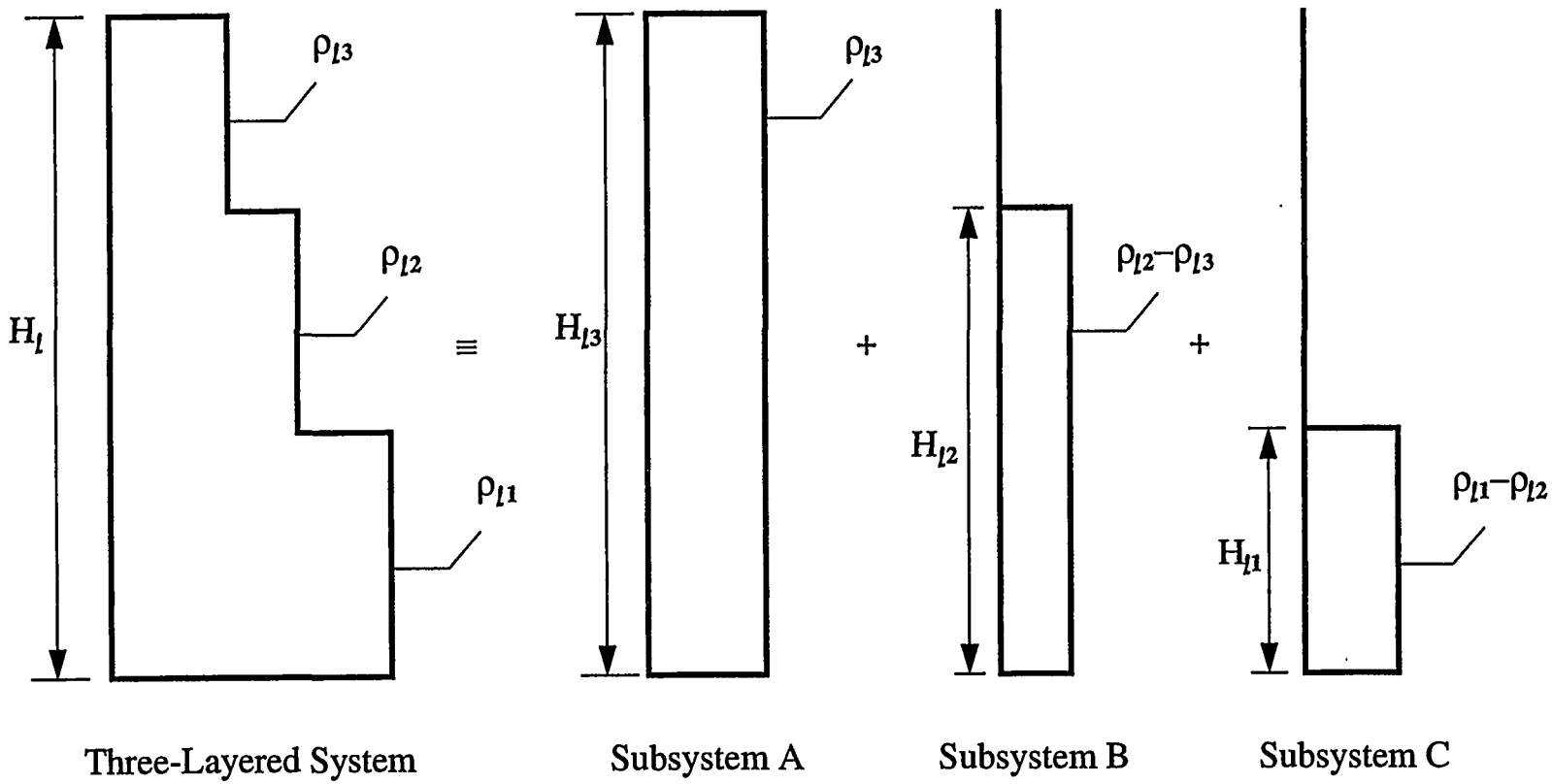

Figure 4.9 Representation of a Three-Layered System by Three Homogeneous Subsystems

CHAPTER 5

SEISMIC CAPACITY OF TANKS

5.1 INTRODUCTION

This chapter presents an approach for evaluation of seismic capacities of anchored and unanchored tanks. In this approach, a minimum capacity is determined based on the nominal ultimate strength, and then this capacity is reduced by applying a factor of safety consistent with Section 3.7. For applicability of the provisions included in this document, it is assumed that the tanks are flat-bottom and fabricated following certain standard construction procedures, examples of which are included in Appendix E. The structural capacities need to be estimated by precluding known failure modes. A general description of earthquake experience related to failure of above-ground liquid storage tanks is presented in the following section.

Internal appurtenances have not been explicitly addressed in this document. However, they must be evaluated in a manner consistent with this document. Guidance on their seismic response evaluation is given in ASCE 4-86 (Reference 5.1) and capacities should be determined in accordance with the requirements of Sections 3.6 and 3.7.

5.2 EARTHQUAKE EXPERIENCE ON FAILURE MODES

Flat-bottom vertical liquid storage tanks have sometimes failed with loss of contents during strong earthquake shaking. For tanks with radius-to-wall thickness ratios greater than about 600 or tanks with minimal or no anchorage, failure has often been associated with rupture of the tank wall near its connection to the base, due either to excessive tank wall buckling or bolt stretching and excessive base-plate uplift. Both failure modes are primarily due to dynamic overturning moment at the tank base from impulsive mode fluid pressure on

the tank wall.

Another common failure mode has been breakage of piping connected to a tank as a result of relative movement. When the pipe enters the tank below the fluid level, then breakage of a pipe between the tank wall and shutoff valve is one of the most prevalent causes of loss of fluid from a storage tank. Another common cause of tank failure has been severe distortion of the tank bottom at or near the tank wall due to a soil failure (soil liquefaction, slope instability, or excessive differential settlement). For new tanks these soil-induced failures are best prevented by proper soil compaction prior to placement of the tank and through the use of reinforced mat foundations under tanks. For existing tanks either founded on ring foundation or directly founded on the soil (i.e., no reinforced mat foundation), these soil-induced potential failure modes should also be investigated.

Other failure modes which are of much lesser importance either because of their general lack of occurrence or less severe consequences, but which deserve some attention, are tank sliding, excessive hoop tensile stresses due to hydrodynamic pressures on the tank wall, and damage to the roof and internal attachments. Sliding is a concern for unanchored smaller diameter tanks. However, sliding of an unanchored tank with greater than a 30-foot diameter and fluid height less than the diameter is extremely unlikely. Simple calculations indicate that there is sufficient friction between the tank bottom and foundation to prevent sliding for these tanks. Tensile hoop stresses due to shaking-induced pressures between the fluid and tank wall can become large and lead to splitting and leakage. This phenomenon has occurred in riveted tanks where leakage at the riveted joints has resulted from seismic pressure-induced hoop yielding. This occurrence is more common in the upper tank wall because the ratio of seismic induced pressures to

hydrostatic pressure is greater in the upper portions. There does not appear to be any case where a welded steel tank has actually ruptured due to seismically induced hoop strains. Tank ductility appears to be sufficient to accommodate these hoop strains. However, large tensile hoop stresses combined with compressive longitudinal stresses contribute to the likelihood of "elephant foot" buckling near the tank base due to overturning moment. Lastly, there have been a number of instances of roof damage when insufficient freeboard exists to accommodate fluid sloshing. In addition, lateral movement and torsional rotations of the fluid which develop during ground shaking have broken guides, ladders, and other internal appurtenances attached between the roof and bottom plate.

5.3 SEISMIC EVALUATION

Each of the potential failure modes described above should be considered in the seismic evaluation of tanks. Emphasis should be given to ensure adequate overturning moment capacity, piping flexibility, and prevention of foundation failures. The seismic evaluation consists of two parts: a seismic response evaluation, and a seismic capacity assessment. The topic of response evaluation is covered in Chapter 4. For the tank evaluation, the following responses should be obtained for comparison with the respective capacities:

1. *The overturning moment in the tank shell immediately above the base plate of the tank:* This moment should be compared with the base moment capacity which is governed by a combination of shell buckling and anchor bolt yielding or failure, and generally governs the seismic capacity of the tank.

2. *The overturning moment applied to the tank foundation through a combination of the tank shell and the base plate:* This moment is needed only for tanks founded on soil sites,

for which the potential of foundation failure should be investigated. This moment which is generally obtained as part of the SSI evaluation seldom governs the seismic design.

3. *The base shear beneath the tank base plate:* This base shear is compared to the horizontal sliding capacity of the tank. For atmospheric tanks with a radius greater than 15 feet, it seldom controls the seismic capacity.

4. *The moment in the tank shell at locations where the tank shell is thinner than at the base (such as occurs at 9 feet above the base in the Figure G.1 example tank), and at the location of maximum moment if such a location is away from the base as would be the case for a tank laterally supported at the top of the side wall as well as the base.*

5. *The hydrostatic pressure p_{st}; the seismic-induced hydrodynamic pressures due to the horizontal input component (combination of impulsive and convective modes) p_{dh}; and the hydrodynamic pressures due to the vertical input component p_{dv}:* It is common design practice to compare these combined pressures with the membrane hoop capacity of the tank wall at one-foot above the base and each location where thickness changes. In addition, the pressure at the base is needed for the base moment and shear capacity calculations. These combined pressures essentially never govern the seismic capacity of a properly designed tank.

6. *The fluid slosh height:* This slosh height is compared with the freeboard above the top of the fluid to estimate whether roof damage or an increase of the hydrodynamic pressure is likely.

For each of the computed tank responses and failure modes

described above, capacity criteria are presented in the following sections.

5.4 SLOSH HEIGHT CAPACITY

The approach given in Chapter 4 for computing the dynamic response of liquid storage tanks is conditional on the liquid surface being free to move vertically unconstrained by the tank roof. In order to provide an adequate factor of safety above the computed slosh height response h_{sr}, the slosh height capacity h_{sc} should be determined as follows:

$$h_{sc} \geq 1.6 SF\, h_{sr} \tag{5.1}$$

where SF is the appropriate seismic scale factor from Section 3.3.1. The factor 1.6 in Equation 5.1 has been made slightly larger than the factor of 1.5 in Equation 3.11 to provide for increased slosh heights due to nonlinear surface effects.

For a spherical domed roof or a domed roof that can be approximated by a combination of cylindrical and spherical segments (such as a torispherical roof), the available slosh height capacity h_{sc}, before excessive forces result on the dome, can be approximated by:

$$h_{sc} \approx h_c + \frac{h_d}{4} \tag{5.2}$$

where h_c is the cylindrical wall height above the liquid and h_d is the dome height above the cylindrical wall.

If Equation 5.2 does not satisfy Equation 5.1, then the liquid may slosh against a substantial portion of the tank roof due to inadequate freeboard between the liquid surface and the tank roof, and the following phenomena occur:

1. The hydrodynamic pressure against the tank wall increases due to the vertical constraint of the liquid surface. The

hydrodynamic pressure may be estimated in accordance with the procedure described in Appendix D.

2. The shear force and bending moment throughout the tank height also increase in a manner corresponding to the increase in the hydrodynamic pressure.

3. The liquid pressure acting against the tank roof will change the longitudinal force in the cylindrical walls of the tank and also could damage the roof. The performance of the tank at its base might be adversely influenced by the changed longitudinal force.

When h_{sc} defined by Equation 5.2 satisfies Equation 5.1, the above defined adverse consequences are considered to be negligible and do not need to be addressed.

5.5 HOOP TENSION CAPACITY

For seismic loads, the hoop membrane stress capacity, σ_c, of the tank shell should be taken as the ASME Code (Reference 5.2) Service Level D limit for a primary stress of 2.0S or the yield stress, whichever is less. For example, 2.0S = 37.5 ksi for SA240-Type 304 stainless steel for which the yield stress is 30 ksi. Thus, the pressure capacity p_c is:

$$p_c = \frac{\sigma_c t_{tw}}{R} \tag{5.3}$$

where t_{tw} is the tank wall thickness, and R is the tank radius. This capacity is then compared with the total factored inelastic demand (p_{ti}) given by:

$$p_{ti} = p_{st} + \frac{SF}{F_{\mu D}} \left(p_{dh}^2 + p_{dv}^2\right)^{1/2} \tag{5.4}$$

where hydrodynamic pressures from the horizontal earthquake ground motion component (p_{dh}) and from the vertical component (p_{dv}) are combined probabilistically by the square-root-sum-of-

squares method, $F_{\mu D} = 1.5$ from Table 3.3 and SF is the appropriate seismic scale factor from Section 3.3.1.

However, as will be discussed at the end of Section 5.6.1.2.1, when the combined hydrostatic and hydrodynamic pressure produces a hoop stress that exceeds about 85% of the yield stress σ_y, the allowable axial compressive stress capacity will drop to less than 6% of σ_y. Therefore, where axial buckling is an important consideration, it is generally undesirable to allow the hoop stress to exceed 85% of σ_y.

5.6 MAXIMUM PERMISSIBLE AXIAL COMPRESSION OF TANK SHELL

The cylindrical tank shell is subjected to an axial compression force on one side and an axial tensile force on the other side due to the seismic-induced overturning moment. At the base of the fully-anchored tank and away from the base for all tanks, the moment capacity is controlled by the maximum permissible axial compression of the tank shell. In turn, this permissible axial compression capacity must be set sufficiently low to avoid either plastic collapse ("elephant-foot" buckling) or bifurcation ("diamond") buckling of the tank shell.

The most likely way for fluid filled tank shells to buckle is in "elephant foot" buckling near the base of the tank shell. The tank shell is subjected to a biaxial stress state consisting of hoop tension and vertical (axial) compression. In addition, radial deformations under internal pressure which are prevented at the base due to membrane tension in the base plate introduce eccentricity and bending stresses in the axial plane which further induce the tendency to "elephant foot" buckle. However, the initiation of an "elephant foot" buckle does not directly correspond to a failure of a tank. Many tanks have continued to perform their function of containing liquid even after developing substantial "elephant foot" buckles. However, no simple method to predict tank performance after the development

of "elephant foot" buckling exists. Therefore, the onset of "elephant foot" buckling will be judged to represent the limit to the compressive buckling capacity of the tank shell.

5.6.1 Allowable Axial Compressive Stress

A cylindrical shell buckles when subjected to large compressive loads. This usually occurs at a stress lower than the yield strength of the shell material. The classical linear elastic buckling stress for a cylinder of perfect geometry subjected to an axial compressive load is given by

$$\sigma_{c\ell} = \frac{E_t}{3\sqrt{1-\nu_t^2)}} \left(\frac{t_{tw}}{R}\right) = \frac{0.605\ E_t}{R/t_{tw}}\ ,\ for\ \nu_t = 0.3 \qquad (5.5)$$

In reality, the shell exhibits buckling at a compressive stress even lower than $\sigma_{c\ell}$. The reduction of the compressive strength compared to $\sigma_{c\ell}$ depends on inherent geometric imperfection of the shell and nature of loading. Thus, for bifurcation buckling, the nominal ultimate axial compressive stress, σ_{au}, is given by

$$\sigma_{au} = (\sigma_{c\ell})\ (a\ reduction\ factor) \qquad (5.6)$$

where, the reduction factor includes the effect of geometric imperfection and plasticity. For plastic collapse under a large hoop stress, σ_{au} can be directly computed by considering instability under the biaxial stress state. Ultimately, a factor of safety FS is introduced for computing the allowable axial compressive stress, σ_a, as follows:

$$\sigma_a = \frac{\sigma_{au}}{FS} \qquad (5.7)$$

For the tank wall design, the allowable compressive force, C_a, per unit circumferential length may be required and is given as follows:

$$C_a = = \sigma_a \cdot x \; t_{tw} \qquad (5.8)$$

The effects of various parameters on the shell compressive strength are further discussed in the following sections.

5.6.1.1 Geometric Imperfection

Standard fabrication and construction procedures usually introduce a small amount of geometric imperfection on the shape of the shell, such as, a bulge at welds. The buckling strength is sensitive to the shape as well as magnitude of the imperfection. The larger the bulge, for example, the greater is the reduction of the buckling strength. With realistic geometric imperfections, the actual compressive strength may be as low as 20% of the classical buckling strength, when the shell is subjected to static loading.

5.6.1.2 Loading

The buckling strength is also greatly influenced by the nature of loading. Most test data available in the literature were obtained from static tests subjecting the cylinders to uniform axial compressive loads (References 5.3 and 5.4). There are examples of static tests where the specimens were subjected to static bending compressive stresses (References 5.5 and 5.6). Test data indicate that a cylinder can withstand a higher buckling stress when subjected to bending compressive stresses which vary along the circumference as opposed to uniformly distributed membrane stresses. The load combination can also influence the buckling capacity of the shell. For example, an internal radial pressure may reduce the geometric imperfection, such as, a bulge, and, in turn, increase the buckling strength. These examples are for static loading. Earthquake experience and shake table testing data, on the other hand, indicate a greater buckling strength for dynamic loading conditions. The effects of loadings and load combinations on the shell buckling

strength are further elaborated and quantified in the following sections.

5.6.1.2.1 Effect of Internal Pressure

Internal pressure reduces the effects of existing geometric imperfections and this, in turn, increases the buckling strength, as depicted by curve ABC in Figure 5.1. At a very high pressure, the effects of existing imperfections are expected to be eliminated and the elastic buckling strength approaches that of a perfect cylindrical shell, i.e., the classical buckling stress, $\sigma_{c\ell}$. Such elastic bifurcation buckling is also called "diamond buckling." On the other hand, the existence of internal pressure simultaneously with the axial load introduces a biaxiality effect. At low pressure, the effect is relatively small and the axial compressive load required for plastic collapse (also called "elephant foot" buckling) of the shell is relatively large. As the pressure increases, the hoop tensile stress plays a significant role and plastic collapse can occur at a small axial compressive stress. Curve DBE in Figure 5.1 shows the plastic collapse locus following a standard biaxiality failure criterion, e.g., the effective stress reaches the yield strength of the shell material. As can be observed from Figure 5.1, up to a certain pressure, elastic buckling occurs prior to plastic collapse, and beyond that plastic collapse occurs first. Thus, the governing compressive strength of the shell in the presence of internal pressure will be denoted by curve ABE.

There are empirical formulas available in the literature for determination of the allowable axial compressive stress as influenced by the internal pressure (References 5.7 through 5.11). Most of these references require separate computations of the elastic buckling and plastic collapse stresses. An ASME Code Case that directly provides the allowable compressive stress for any pressure is presented in this document.

ASME Code Case N-530

The allowable axial compressive stress in a cylindrical shell can be calculated by using ASME Code Case N-530 (Reference 5.12). The Code Case is based on a comparative study of the available test and analytical data (References 5.13 and 5.14), and adopts the recommendations of the European Convention for Constructional Steelwork (Reference 5.15). The effects of the internal pressure and possible geometric imperfections are included in the Code Case formulas. At low pressure, the ECCS which is the basis of the Code Case introduces an additional factor of 0.75 to the elastic buckling curve shown in Figure 5.1 to obtain σ_{au}. At high pressure, when biaxiality plays a key role, the Code Case introduces an "effective stress" and uses an empirical formula based on data fitting (Reference 5.4) to compute σ_{au}. The Code Case approach is summarized in the remainder of this section.

For uniform compression, the classical linear elastic buckling stress, σ_{cl}, given by Equation 5.5 is reduced by introducing a buckling capacity reduction factor, α_o, which is defined by

$$\alpha_o = \frac{0.7}{\sqrt{0.1 + 0.01R/t_{tw}}}, \quad for\ R/t_{tw} > 212 \tag{5.9}$$

For practical tanks, R/t_{tw} is expected to be greater than 212. The capacity reduction factor increases with the internal pressure as defined by

$$\alpha_p = \alpha + (1-\alpha)\ \frac{F_p}{F_p + 0.007} \tag{5.10}$$

$$where,\ F_p = \frac{p}{E_t}(R/t_{tw})^{1.5}$$

For uniform compression, $\alpha = \alpha_o$ given by Equation 5.9. For a combination of uniform and bending compression, α is given by Equation 5.17. By using the above capacity reduction factor and

introducing the nominal hoop stress[1]

$$\sigma_h = pR/t_{tw} \quad , \tag{5.11}$$

the axial compressive strength can be obtained by solving the following simultaneous equations

$$\sigma_{eff} = \sqrt{\sigma_{au}^2 + \sigma_h^2 + \sigma_{au}\sigma_h} \tag{5.12}$$

$$\frac{\sigma_{eff}}{\sigma_y} = \frac{0.75}{\lambda_p^2}, \quad for\ \lambda_p \geq 1.414 \tag{5.13}$$

$$\frac{\sigma_{eff}}{\sigma_y} = 1.0 - 0.4123\ \lambda_p^{1.2}, \quad for\ \lambda_p < 1.414 \tag{5.14}$$

$$\lambda_p = \sqrt{\frac{\beta_c \sigma_y}{\alpha_p \sigma_{cl}}} \tag{5.15}$$

$$and, \qquad \beta_c = \frac{\sigma_{au}}{\sigma_{eff}} \tag{5.16}$$

In the above equations, σ_{eff} denotes the effective stress considering both the axial and hoop stresses; σ_{au} is positive for a compressive axial stress; σ_h is positive for a tensile hoop stress; $\lambda_p \geq 1.414$ indicates elastic buckling; and $\lambda_p < 1.414$ indicates plastic collapse. The simultaneous equations can be solved by trial and error. For convenience of solution, Equations 5.10, 5.12 and 5.13 can be rewritten as follows:

$$\alpha_p = \frac{F_p + 0.007\alpha}{F_p + 0.007} \tag{5.10a}$$

[1]Hoop stresses due to other sources, if any, should be added to this equation.

$$\sigma_{au} = \sqrt{\sigma_{eff}^2 - 0.75\sigma_h^2} - 0.5\sigma_h \qquad (5.12a)$$

$$\sigma_{au} = 0.75\ \alpha_p\ \sigma_{cl},\ for\ \lambda_p \geq 1.414 \qquad (5.13a)$$

The following is an algorithm for the solution:

Step 1. Compute α_o, F_p, α, α_p, σ_{cl} and σ_h for the set of conditions being evaluated.

Step 2. Estimate a value of β_c; call the value β_c'.

Step 3. Compute λ_p from Equation 5.15 using β_c' for β_c.

Step 4. Compute σ_{eff} from Equation 5.13 or 5.14.

Step 5. Compute σ_{au} from Equation 5.12a. For $\lambda_p \geq 1.414$, σ_{au} can be computed directly from Equation 5.13a.

Step 6. Compute β_c from Equation 5.16.

Step 7. Compare the computed value of β_c (Step 6) with the estimated value, β_c' (Step 2). If the computed value of β_c is close to the estimated value, β_c', note the value of σ_{au} as the ultimate axial compressive stress. If not, select a revised value of β_c and return to Step 3. Repeat the process until a desired degree of accuracy is achieved.

At low pressure, elastic buckling governs, and at high pressure, plastic collapse controls the failure (References 5.13 and 5.14). Therefore, σ_{au} should be calculated for the lowest and highest possible pressure values concurrent with the axial loads at the desired location (e.g., see Equations 5.18a and 5.18b), and the lower of the two values of σ_{au} should be used for the design or evaluation.

The ASME Code Case (Reference 5.12) provides a tolerance on the bulges or flat spots in the cylindrical walls. The amplitude of

the bulge should not exceed 1% of the length over which it is measured. This is further illustrated in Appendix E. With the increase in pressure, the failure mode changes from bifurcation buckling to plastic collapse (References 5.13 and 5.14). Thus, the effect of imperfection is less pronounced at a high pressure.

An example of the ASME Code Case is presented in Figure 5.1. At low pressure, the Code Case curve is related to the elastic bifurcation buckling curve ABC by a factor of safety. At high pressure, the Code Case capacity is controlled by plastic collapse and the plot resembles curve BE described earlier. At very high pressure (e.g., $\lambda_p < 0.3$), the Code Case formula (i.e., Equation 5.11) seems to be excessively conservative (Reference 5.4).

For tank designs, it is recommended that, in general, the hoop stress be limited to 85% of the material yield strength. If this limit is exceeded, the nominal axial compression capacity σ_{au} may be computed using large displacement theory and an appropriate nonlinear stress-strain relationship, in lieu of the Code Case approach in order to avoid the excessive conservatism in this pressure range. Even so, σ_{au} is expected to be very low, e.g., less than 10% of the yield strength.

5.6.1.2.2 Effect of Bending

Code Case N-530 does not consider the beneficial effect of bending in computing the allowable axial compressive stress. The ECCS (Reference 5.15) revises the capacity reduction factor as follows when the tank is subjected to bending concurrently with the axial compressive load:

$$\alpha = \frac{\alpha_o \sigma_o + \alpha_b \sigma_b}{\sigma_o + \sigma_b} \qquad (5.17)$$

where, α_o is given by Equation (5.6)

$\alpha_b = 0.1887 + 0.8113\alpha_o$, for $R/t_{tw} \leq 1500$

σ_o = uniform compressive stress due to axial load

σ_b = maximum compressive stress due to bending

In the absence of internal pressure, σ_{eff} becomes σ_{au} and can be directly computed from Equations 5.13a and 5.14. Also, in Equation 5.15, β_c is equal to 1, and α_p should be taken as α given by Equation 5.17. Note that for pure bending α is equal to α_{bn}.

The ECCS Code (Reference 5.15) does not consider the direct effect of internal pressure in computing the capacity reduction factor for the bending case as evident from Equation 5.17. A New Zealand study shows that the shell compressive strength for bending compression increases further if the influence of internal pressure is considered (Reference 5.11). Therefore, in order to combine the effects of internal pressure and bending, it is recommended that in Equation 5.10, use the value of α given by Equation 5.17. As before, solve for σ_{au} using Equations 5.11 through 5.16 following the seven steps. Since the ASME Code Case does not include the bending effect, a tank requiring qualification according to the ASME rules may not be designed or evaluated with the higher capacity reduction factor for bending.

5.6.1.2.3 Effect of Earthquake Loading

The aforementioned formulas for shell compressive strength have been developed by use of test and analytical data for static loading. When a tank is subjected to earthquake loading, the shell compressive strength is not only influenced by the simultaneous application of internal pressure and bending as discussed earlier, it is also affected by the dynamic nature of the load. In the literature, there are examples of liquid storage tanks subjected to actual earthquakes or simulated earthquake loading on shake tables (References 5.16, 5.17 and 5.18). The buckling stresses observed for the actual or

simulated earthquake cases are significantly greater than what would have been predicted by Code Case N-530 or the ECCS formulas. For example, based on an evaluation of performance of unanchored cylindrical liquid storage tanks during major past earthquakes as well as shake table testing, an empirical capacity reduction factor of 0.75 is proposed in Reference 5.16. Reference 5.17 reports occurrence of diamond buckling on the shake table at an axial compressive stress of 60% of the classical buckling strength. The increased buckling resistance to earthquake loading has been attributed primarily to the reversing nature of the load and local initiation of buckling due to confinement of high stresses to a relatively narrow area of the tank wall for a short duration. For a more realistic estimate of the buckling strength under earthquake loading refer to Appendix F.

5.6.1.2.4 Pressure Estimates for Earthquake Loading

The pressure p to be used for calculation of the axial strength under earthquake loading should be set equal to the probable combined hydrostatic and hydrodynamic pressure p_{com} at the point of maximum compression around the tank circumference corresponding to the time of maximum seismic induced moment. For bottom supported cantilever tanks:

$$p_{com} = p_{st} + [p_{dh} \pm 0.4p_{dv}]\frac{SF}{F_{\mu D}} \qquad (5.18a)$$

where p_{st} is the hydrostatic pressure, p_{dh} is the hydrodynamic pressure from the horizontal earthquake component, and p_{dv} is the hydrodynamic pressure from the vertical earthquake component. A value of $F_{\mu D}$ between 1.0 and 1.5 should be used, and SF is the appropriate seismic scale factor from Section 3.3.1. The use of an $F_{\mu D}$ value greater than unity is appropriate when σ_h/σ_y is sufficiently high that the axial compressive capacity is controlled by the biaxial plastic collapse mode which is ductile. When σ_h/σ_y is small so that elastic bifurcation

buckling controls, $F_{\mu D}$ should be taken as unity. At the time of occurrence of the maximum moment, p_{dh} will be maximum so that 100% of p_{dh} is used in Equation 5.18a. However, to account for the random phasing between p_{dv} and the moment, only 40% of p_{dv} is included, but it must be either added or subtracted depending on which gives the lesser axial compressive capacity σ_{au}.

For tanks supported laterally at both their top and bottom, the maximum moment generally occurs near midheight and the point around the circumference at which the compressive stress is maximum corresponds to a location where p_{dh} should be subtracted rather than added. Thus for tanks supported at both top and bottom:

$$p_{com} = p_{st} - [p_{dh} \pm 0.4 p_{dv}] \frac{SF}{F_{\mu D}} \qquad (5.18b)$$

5.6.1.3 Acceptance Criteria

The axial compressive strengths under various loads and load combinations are discussed above. A set of acceptance criteria is presented in this section.

Static Uniform Axial Compression with or without Internal Pressure

Use Equations 5.9-5.16 (Code Case approach).

Static Bending Compression Combined with Uniform Axial Compression and With or Without Internal Pressure

Use Equation 5.17 and follow subsequent steps described in Section 5.6.1.2.2 (Similar to ECCS approach).

Earthquake Loading

Use conservatively the above acceptance criteria for the respective static loading. Alternatively, for more real-

istic results, refer to Appendix F. Regardless of the loading and load combination, a tank requiring qualification in accordance with the ASME rules may need to be designed or evaluated following the Code Case.

A factor of safety needs to be introduced on the computed axial compressive strength in accordance with the general acceptance criteria presented in Chapter 3 so that a high confidence of avoiding a buckling failure can be achieved. The Code Case recommends a factor of safety of 1.33 for the Service Level D loading (e.g., seismic loading).

From the static uniform compression test data (Reference 5.4), that are the basis of the ECCS (Reference 5.14) and the Code Case, it can be estimated that the buckling capacity corresponds to about the 2% failure probability level (i.e., at approximately -2β) with a logarithmic standard deviation, β, between 0.14 and 0.19. Thus, in order to achieve a factor of safety of 1.5 on the capacity corresponding to the 10% failure level as required by Equation 3.9 for a scale factor of unity, the factor of safety to be applied on the Code Case axial ultimate compressive stress, σ_{au}, should be

$$FS = 1.5\ e^{-0.718\beta}$$

where 0.718 is the number of standard deviation between 2% and 10% failure probability levels.

Thus,

$$\text{for } \beta = 0.14, \quad FS = 1.36$$
$$\text{and, for } \beta = 0.19, \quad FS = 1.31$$

These values are comparable to 1.33 recommended by the Code Case. Thus, the Code Case factor of safety satisfies the criteria of Chapter 3. It is judged that the same factor of safety is also applicable for the bending compression and earthquake loading cases.

5.6.1.4 Existing Tanks

The above approach for determination of the shell compressive strength equally applies for existing high-level waste storage tanks as well as new tanks. But, the only difficulty in applying this procedure is that the Code Case formulas are contingent upon satisfaction of geometric tolerance, i.e., the bulge amplitude should not exceed 1% of the wall length over which it is measured (see Appendix E). For existing underground radioactive tanks, the geometric tolerance cannot be verified. Because of overwhelming evidence of greater capacities of tanks in actual and simulated earthquake situations for realistic tank geometric imperfections compared to the Code Case and ECCS formulas, it is judged that no further penalty be imposed and the same formulas can be used for the existing tanks.

5.7 MOMENT CAPACITY AWAY FROM TANK BASE

At locations along the cylindrical shell away from the base, the moment capacity is given by:

$$M_C = C_a \pi R^2 - \frac{P_a R}{2} \qquad (5.19)$$

where P_a is any concurrent axial compressive force on the cylindrical shell (generally negligible).

5.8 ANCHORAGE CAPACITY AT TANK BASE

The base anchorage bolt hold-down capacity, T_{cb}, is governed by the weakest of the following elements:

1. Bolt tensile capacity

2. Anchorage of bolt into concrete foundation

3. Capacity of the top plate of bolt chairs to transfer bolt loads to the vertical chair gussets

4. Attachment of the top plate and vertical chair gussets to the tank wall

5. Capability of tank wall to withstand concentrated loads imposed on it by chairs.

Each of these capacities should be based on code minimum ultimate strength or limit state capacities with the appropriate code-imposed strength reduction factor (ϕ).

5.9 BASE MOMENT CAPACITY OF FULLY ANCHORED TANKS

A tank is considered fully anchored only when the hold-down capacity T_{cb} per bolt satisfies the following condition:

$$T_{cb} \geq 2\pi RC_a\left(\frac{\theta_b}{360^\circ}\right) \qquad (5.20)$$

where θ_b is the circumferential angle between bolts. In this case, the neutral axial remains through the centerline of the tank at maximum capacity and the base moment capacity is also given by Equation 5.19.

However, satisfying Equation 5.20 will require very closely spaced anchor bolts and is seldom practical. In most cases, Equation 5.20 is not satisfied and the tank is treated as either partially anchored or unanchored. In either case, the neutral axis will shift toward the compression side of the tank [see Figure 5.2] resulting in an increase in the peak compressive force for a given overturning moment. The base moment capacity of the partially anchored or unanchored tank will be substantially less than that given by Equation 5.19.

5.10 BASE MOMENT CAPACITY OF PARTIALLY ANCHORED OR UNANCHORED TANKS

A reasonable approximation of the loading that exists at the base of the tank shell can be estimated based upon the following approximations:

1. Compressive stresses vary linearly from zero at the neutral axis to C_m' at the outer compression side of the tank wall (i.e., at $\theta = 180°$).

2. Uplift heights δ_θ vary linearly from zero at the neutral axis to δ_o at the outer tension side of the tank wall (i.e., at $\theta = 0°$).

3. For simplicity, fluid hold-down forces are also assumed to vary linearly from T_{fn} at the neutral axis to T_{fo} at $\theta = 0$.

Figure 5.2 illustrates the loading that exists at the base of the tank wall based on the above approximation. Also shown is the uplift of the tank wall due to an assumed rigid rotation of the base. In Figure 5.2, C_m' is the maximum compressive stress in the tank wall, T_{fn} is the effective fluid hold-down force at the neutral axis, ΔT_f is the increase in fluid-hold down force at $\theta = 0$, T_{bi} are anchor bolt hold-down forces if the tank is anchored, W_t is the tank weight, and M_c is the moment capacity which results from this loading distribution.

For any given angle θ_n to the neutral axis:

$$C_m' = \left[\frac{W_t + \sum_{i=1}^{n} T_{bi}}{2R} + T_{fn}\theta_n\right]C_1 + \Delta T_f C_3 \qquad (5.21)$$

$$M_C = C_m' C_2 R^2 + \sum_{i=1}^{n} (T_{bi} R \cos\theta_i) + T_{fn} R^2 (2 \sin\theta_n) + \Delta T_f C_4 R^2 \qquad (5.22)$$

where:

$$C_1 = \frac{1 + \cos \theta_n}{\sin \theta_n + (\pi - \theta_n)\cos \theta_n}$$

$$C_2 = \frac{\sin \theta_n \cos \theta_n + \pi - \theta_n}{1 + \cos \theta_n} \qquad (5.23)$$

$$C_3 = \frac{\sin \theta_n - \theta_n \cos \theta_n}{\sin \theta_n + (\pi - \theta_n) \cos \theta_n}\left[\frac{1 + \cos \theta_n}{1 - \cos \theta_n}\right]$$

$$C_4 = \frac{\theta_n - \sin \theta_n \cos \theta_n}{1 - \cos \theta_n}$$

Numerical values for C_1, C_2, C_3, and C_4 as functions of θ_n are tabulated in Table 5.1.

The moment capacity depends upon the axial compressive buckling capacity of the tank wall (C_a) from Section 5.6, the tensile hold-down capacity of the anchor bolts including their anchorage and attachment to the tank (T_{cb}) from Section 5.8, the permissible uplift height (δ_o) from Section 5.11, and the hold-down force of fluid pressure acting on the tank base plate (T_f) from Section 5.12. Thus, each of these quantities must be estimated prior to estimating the overturning moment capacity.

The steps in solving for the moment capacity are as follows:

1. Establish the maximum permissible uplift height δ_o [see Section 5.11].

2. Compute the fluid hold-down force T_{fo} corresponding to the uplift height δ_o and the fluid hold-down force T_{fn} at the neutral axis [see Section 5.12] and then:

$$\Delta T_f = T_{fo} - T_{fn} \qquad (5.24)$$

3. Assume an initial value of the angle θ_n to the neutral axis and estimate the anchor bolt tension T_{bi} in anchor bolt "i" from:

$$T_{bi} = T_{bp} + K_b \left(\frac{\cos \theta_i - \cos \theta_n}{1 - \cos \theta_n} \right) \leq T_{cb} \qquad (5.25)$$

where

$$K_b = \frac{\delta_o A_b E_b}{h_e} \qquad (5.26)$$

and θ_i is the angle θ at bolt "i," T_{bp} is any bolt pretension (generally should be taken as zero since it is likely to be lost over time), T_{cb} is the bolt capacity [see Section 5.8], A_b is the bolt area, E_b is the bolt modulus of elasticity and h_e is the effective bolt length from its attachment to the tank to its effective anchor depth in the concrete.

4. Compute C_m' from Equation 5.21 and compare it to the shell buckling capacity C_b. Vary θ_n and repeat Steps 3 and 4 until $C_m' = C_b$.

5. Determine the moment capacity M_c from Equation 5.22.

As will be shown in the solution for capacity of the example tank in Appendix G, it is unnecessary to converge to a refined estimate of the angle θ_n to the neutral axis in Step 4 in order to estimate the moment capacity M_c. Although C_m' is sensitive to changes in the angle θ_n, M_c is not sensitive to small changes in θ_n.

Also, as will be shown in Appendix G, the base moment capacity of even a minimally anchored tank is substantially greater than that of an unanchored tank. Therefore, for new designs it is recommended that the tank should be either laterally supported near its top (thus greatly reducing the applied base moment) or should be anchored at its base.

5.11 PERMISSIBLE UPLIFT DISPLACEMENT

In order to prevent anchorage failure, the maximum uplift displacements δ_o of anchored tanks should be limited to a small value. For anchored tanks in which the bolt tensile capacity controls T_{cb}, δ_o should be limited as follows:

$$\delta_o \leq 0.01 h_e \tag{5.27}$$

where h_e is the effective bolt length. When other failure modes control, δ_o should be limited to the lesser of Equation 5.24 or 1/4 inch.

For unanchored tanks, much greater uplift heights are permissible. To avoid failure at the junction of the base plate and wall, it is suggested that uplift heights be limited to:

$$\delta_o = 0.1L \tag{5.28}$$

where L is the computed uplift length of the base plate (see Figure 5.4 and Section 5.12.2). Equation 5.28 will typically produce uplift heights of several inches. However, if piping or other components are attached to the tank wall or uplifted region of the base plate, δ_o must also be limited to tolerable displacements for such piping or other components.

5.12 FLUID HOLD-DOWN FORCE

5.12.1 Anchored Tanks

The situation in the region of axial tension in the tank wall is illustrated in Figure 5.3 for a small uplift, δ. At point "0" away from the tank wall, the tank bottom is in full contact with the foundation and the displacements, rotation, and moment in the tank bottom are zero. However, at the intersection of the tank bottom and wall at point "1," the tank bottom has uplifted δ and rotated α. The length of the uplift zone is L, and the fluid pressure, p_e, on the tank bottom and wall resists this

uplift. This uplift is accompanied by the development of tension, T_f, and moment, M_f, in the tank wall at the intersection with the tank bottom. This tension, T_f, acts as a fluid hold-down force on the tank wall. For a given uplift height, δ, the hold-down tension, T_f, that develops is both a function of the bending stiffness of the tank wall which is a function of its thickness, t_{tw}, and radius, R, and the bending stiffness of the base plate which is a function of its thickness, t_{tb}.

For a tank wall restrained against radial displacement at point "1" by the base plate, the relationship between M_f and α can be obtained from pages 276 through 278 of Flugge (Reference 5.18) for axisymmetric loading as follows:

$$M_f = K_s\alpha + M_{fx} \qquad (5.29)$$

where M_{fx} represents the fixed end moment, and

$$K_s = \frac{2K\kappa}{R}$$

$$\frac{M_{fx}}{p_e} = \frac{Rt_{tw}}{\sqrt{12\,(1-\nu_t^2)}}\left[1 - \frac{R}{H_t\kappa}\right] \qquad (5.29a)$$

$$K = \frac{E_t\, t_{tw}^3}{12\,(1-\nu_t^2)}$$

$$\kappa = \left[(R/t_{tw})\sqrt{3\,(1-\nu_t^2)}\right]^{1/2}$$

Even though the actual loading around the circumference is not axisymmetic, Equation 5.29 is considered to be reasonably appropriate for the actual loading condition.

Since L is a very small fraction of R, over the length L, the base plate may be approximated as a radial beam. Thus, from the boundary conditions at point "0":

$$\alpha = \frac{p_e L^3}{12 E_t I_{tb}} - \frac{M_f L}{2 E_t I_{tb}}$$
$$\delta = \frac{p_e L^4}{24 E_t I_{tb}} - \frac{M_f L^2}{6 E_t I_{tb}} \qquad (5.30)$$
$$T_f = \frac{p_e L}{2} + \frac{M_f}{L}$$

where

$$I_{tb} = \frac{t_{tb}^3}{12(1-\nu_t^2)}$$

Combining Equations (5.29) and (5.30), one obtains:

$$\frac{E_t I_{tb} \delta}{p_e} = \left[\frac{L^4}{24} - \left(\frac{1}{F}\right)\left(\frac{K_s L^5}{72 E_t I_{tb}} + \frac{M_{fx}}{p_e}\,\frac{L^2}{6}\right)\right] \qquad (5.31)$$

$$\frac{T_f}{p_e} = \left[\frac{L}{2} + \left(\frac{1}{F}\right)\left(\frac{K_s L^2}{12 E_t I_{tb}} + \frac{M_{fx}}{p_e L}\right)\right] \qquad (5.32)$$

$$\frac{M_f}{p_e} = \left(\frac{1}{F}\right)\left(\frac{K_s L^3}{12 E_s I_{tb}} + \frac{M_{fx}}{p_e}\right) \qquad (5.33)$$

$$\frac{M_+}{p_e} = \frac{L^2}{8} - \frac{(M_f/p_e)}{2} + \frac{(M_f/p_e)^2}{2L^2} \qquad (5.34)$$

where

$$F = \left[1 + \frac{K_s L}{2 E_t I_{tb}}\right]$$

Using Equations 5.31 through 5.34, one can determine the uplift height (δ), tank wall hold-down tension (T_f) and moment (M_f), and maximum positive moment (M_+) in the base plate as a function of the uplift length, L, and fluid pressure, p_e. From this information the relationship between δ and T_f is obtained. This solution based on small displacement theory is strictly

applicable under the following conditions:

1. $(L/R) \leq 0.15$. The solution ignores the stiffening of the base plate from hoop behavior and thus conservatively overpredicts the displacement δ corresponding to a given T_f as the ratio (L/R) becomes larger.

2. $(\delta/t_{tb}) \leq 0.6$. This solution being based upon small displacement theory conservatively ignores the beneficial effect that could be obtained by use of large displacement membrane theory together with membrane tensions in the base plate to reduce δ corresponding to a given T_f. For unanchored tanks, it has been shown (References 5.16 and 5.19) that large displacement membrane theory greatly increases the fluid hold-down forces, T_f. Thus, for unanchored tanks, ignoring large displacement membrane theory is likely to lead to excessive conservatism. For anchored tanks, the uplift heights (δ) are not expected to be so great and only moderate conservatism is expected to result from ignoring large displacement membrane effects. Unfortunately, no simple solution exists for considering such membrane effects and, therefore, currently one must either accept this source of conservatism for anchored tanks or make judgmental corrections to the computed fluid hold-down forces following guidance from References 5.16 and 5.19.

3. $(M_f/M_{pb}) \leq 0.9$; $(M_f/M_{pw}) \leq 0.9$; and $(M_+/M_{pb}) \leq 0.9$ where M_{pb} and M_{pw} are the plastic moment capacity of the base plate and tank wall, respectively. The previous solution is an elastic solution and becomes nonconservative if these conditions are not met. An alternate solution with plastic hinges at locations where these conditions are not met is easily formulated following the same approach as was used herein but is judged to be unwarranted because violation of

these conditions is highly unlikely for δ levels associated with anchored tanks.

Only violation of the third condition leads to a nonconservative estimate of the hold-down force T_f corresponding to a given uplift displacement δ. The first two conditions can be violated so long as one is willing to accept the resulting conservative underestimation of the fluid hold-down force.

For anchored tanks, it is recommended that small displacement theory be used to compute the fluid hold-down forces. It is further recommended that the following pressures be used to compute the fluid hold-down forces at locations $\theta = 0$ and $\theta = \theta_n$ as defined in Figure 5.2:

$$\begin{aligned} p_e &= p_{st} - (p_{dh} + 0.4p_{dv})\,SF \qquad at\ (\theta = 0) \\ p_e &\geq p_{st} - (0.4p_{dv})\,SF \qquad at\ (\theta = \theta_n) \end{aligned} \tag{5.35}$$

The pressure defined at $\theta = 0$ represents the probable minimum pressure at this location at the time the maximum moment occurs. The pressure defined above at $\theta = \theta_n$ represents the probable minimum pressure at $\theta = 90°$ at the time the maximum moment occurs, and is thus conservative for the location $\theta = \theta_n$ since θ_n will always exceed 90° for partially anchored or unanchored tanks.

5.12.2 Unanchored Tanks

The small displacement theory of the previous subsection is excessively conservative for unanchored tanks. An upper bound theory is considered more appropriate and is used in the following analyses.

The uplift length, L, illustrated in Figure 5.4, is assumed to be a very small fraction of R, and, therefore, over the length L, the base plate may be approximated as a radial beam. An

upper bound solution results after a full plastic hinge develops at point "2" (location of maximum positive bending moment M_{pb}) and at point "1" (base plate to wall junction and location of maximum negative moment M_{pw}). Since no shear may cross point "2", the following relations hold:

$$\frac{p_e L^2}{2} = [M_{pb} + M_{pw}] + F_h \delta \tag{5.36}$$

and

$$T_f = p_e L \tag{5.37}$$

where F_h is the horizontal component of the membrane tension in the base plate at its junction with the cylindrical shell.

Combining equations 5.36 and 5.37 one obtains:

$$T_f = [2p_e (M_{pb} + M_{pw} + F_h \delta)]^{1/2} \tag{5.38}$$

with

$$M_{pb} = \frac{\sigma_{ye} t_{tb}^2}{4} \tag{5.39}$$

In Equation 5.38, M_{pw} is the smallest of the plastic moment capacities of the following: (1) the base plate from Equation 5.39, (2) the tank wall with t_{tw} substituted for t_{tb} in Equation 5.39, and (3) the welded connection between the base plate and wall. For a material with a well defined yield point such as A36 carbon steel, σ_{ye} should correspond to this yield stress. For a tank shell material with no specific yield point, σ_{ye} should be set at the ASME Code (Reference 5.20) Service Level (D) limit for bending which is $2.4S$[1]. For example, for SA240-Type 304 stainless steel, S = 18.75 ksi and σ_{ye} = 45.0 ksi.

An upper bound on the horizontal component of the membrane

---

[1]S depends on temperature and should be determined for the expected temperature of the tank.

tension in the base plate, F_h, is governed by the maximum local hoop compression capacity of the tank wall. For an axisymmetric application of F_h and M_{pw} at the base of the wall, the maximum hoop compression in the tank wall occurs at the intersection of the wall and base plate and is given by:

$$N_{\theta m} = 2\kappa \left[F_h - \frac{M_{pw}\,\kappa}{R} \right] \qquad (5.40)$$

so long as

$$F_h \geq \left[\frac{2M_{pw}\kappa}{R} \right]$$

Conservatively $N_{\theta m}$ should be limited to $(\sigma_{ye} t_{tw})$. With this limit:

$$F_h \leq \frac{\sigma_{ye} t_{tw}}{2\kappa} + \frac{M_{pw}\kappa}{R} \qquad (5.41)$$

Local plastic hoop yielding might allow some increase in F_h but it is recommended that no credit be taken for such an increase.

For conservatism, it is recommended that the probable minimum pressure from Equation 5.35 be used for p_e. Then T_{fn} is computed from Equation 5.38 with $\delta = 0$, and T_{fo} is computed with $\delta = \delta_o$. The ΔT_f is computed from equation 5.24.

5.13 BASE SHEAR CAPACITY

For large diameter (greater than about 30 feet) flat bottom tanks with fluid heights less than the diameter, it is common and acceptable practice to rely on friction between the tank bottom and its foundation to provide the base shear capacity. Since the base shear response, V_r and the base overturning moment response, M_r are primarily due to the fluid horizontal impulsive mode of response, they both are maximum at the same time. Thus, the nominal sliding shear capacity is:

$$V_{cs} = (COF)\ [W_e + (\sum T_{bi})] \qquad (5.42)$$

where

$$W_e = W_t + p_a(\pi R^2) \qquad (5.43)$$

ΣT_{bi} is the sum of anchor bolt tensions from the overturning moment analysis, (COF) is the coefficient of friction between the tank base and its foundation, p_a is the probable average fluid pressure on the base given by $(p_{st} - 0.4\ P_{dv})$, and W_t is the tank wall and roof weight. The equivalent code capacity V_c is obtained by applying a strength reduction factor (ϕ) of 0.75 to the nominal shear capacity V_{cs}, i.e.,:

$$V_c = 0.75V_{cs} \qquad (5.44)$$

Such a low factor (ϕ) is used because of the uncertainty associated with the coefficient of friction.

For small diameter (less than about 10 feet) tanks, or tanks with fluid heights substantially greater than the tank diameter, it is unlikely that the friction-based shear capacity given by Equation 5.41 will exceed the base shear demand from the DBE. In this case, the shear capacity should be provided by anchor bolts. It is not acceptable to credit friction for a portion of the shear capacity and provide the remainder by anchor bolts. Either 100% of the reported shear capacity is to be provided by friction, or 100% must be provided by anchor bolts or other means of positive anchorage.

Some large diameter flat-bottom tanks such as the example tank (Appendix G, Figure G.1) have a slight cone to their bottom plate so that contained fluid will always drain away from the center toward the drain pipe at the edge. This cone is generally created by a variable thickness sand cushion between the tank bottom plate and its foundation. Furthermore, the tank bottom is often made up of slightly overlapped fillet welded

individual plates. Thus, the surface between the bottom plate and the sand cushion contains a series of rough steps. Under these conditions, it is reasonably conservative to estimate

$$(COF) \geq 0.7^{*} \qquad (5.42)$$

For flat-bottom steel tanks on concrete the COF is estimated as 0.55.

5.14 OTHER CAPACITY CHECKS

For tanks on soil sites, one should also check the capacity of the tank foundation and this capacity sometimes governs.

Lastly, the possibility of piping failure or the failure of nozzles/penetrations where such piping is attached to the tank should be checked. Such failure will likely lead to loss of tank contents. In fact, a significant fraction of the cases of seismic induced loss of tank contents have been due to such failures when the piping contained poor seismic details. The issues to be checked are as follows:

1. Are heavy valves or long piping runs being supported through the piping nozzles off either the tank walls or the bottom plate, or are they independently supported? If heavy valves or long piping runs are being supported off the tank, then the ability of the nozzles and the tank wall or bottom plate to withstand the imposed seismic-induced inertial forces should be checked. Methods outlined in Welding Research Bulletin 107 (Reference 5.21) may be used to compute local stresses in the tank wall, and the strength acceptance criteria for vessels contained in Chapter 3 can be used for the stress capacity.

---

*Applicable for large diameter tanks with coned and uneven base.

2. Is there sufficient piping flexibility to accommodate relative seismic anchor movements (SAM) between the locations where the piping is supported from the tank wall and where it is independently supported? Particularly for unanchored tanks, the piping nozzle and tank shell should be evaluated for their ability to withstand the expected relative SAM.

5.15 TOP SUPPORTED TANKS

Many of the DOE underground waste storage tanks are laterally supported by the surrounding concrete vault near the top of the cylindrical tank wall. As shown in Chapter 4, the presence of this top lateral support will greatly reduce the overturning moment applied at the base and will also reduce the base shear. In this case, the base moment capacity (Section 5.10) and base shear capacity (Section 5.13) are not likely to control the seismic capability of such tanks, but should still be checked. In addition, the lateral force (shear) capacity of the top anchorage must be checked in accordance with the capacity requirements of Section 3.7. Furthermore, these lateral forces must be applied to the concrete vault when checking the seismic capacity of the vault. Tanks with lateral support near the top of the cylindrical tank wall are likely to have substantially greater seismic capacity than a similar tank without this top support.

REFERENCES

5.1 American Society of Civil Engineers, Standard 4-86, "Seismic Analysis of Safety-Related Nuclear Structures and Commentary on Standard for Seismic Analysis of Safety-Related Nuclear Structures," September 1986.

5.2 American Society of Mechanical Engineers, "ASME Boiler and Pressure Vessel Code, Section III, Rules for Construction of Nuclear Power Plant Components, Division 1, Subsection NC-3800," 1992.

5.3 ASME Boiler and Pressure Vessel Code, Nuclear Code Case N-284-1, "Metal Containment Shell Buckling Design Methods," Section III, Division 1, Class MC," March 1995.

5.4 Vandepitte, D., and Rathe, J., "Buckling of Circular Cylindrical Shells under Axial Load in the Elastic-Plastic Region," Der Stahlbau, Heft 12, 1980.

5.5 National Aeronautics and Space Administration, "Buckling of Thin-Walled Circular Cylinders," NASA SP-8007, August 1968.

5.6 Weingarten, V., Moran, E., and Seide, P., "Final Report of Development of Design Criteria for Elastic Stability of Thin Shell Structures," Space Technology Laboratories, Inc., STL TR-60-0000-19425, 1960.

5.7 Rotter, J.M., "Buckling of Ground-Supported Cylindrical Steel Bins Under Vertical Compressive Wall Loads," Proceedings of The Metal Structures Conference, Institution of Engineers, Australia, Melbourne, pp. 112-127, 1985.

5.8 Rotter, J.M. and Teng, J.G., "Elastic Stability of Cylindrical Shells with Weld Depressions," Journal of Structural Engineering, Vol. 115, No. 5, ASCE, May 1989.

5.9 Rotter, J.M., "Local Inelastic Collapse of Pressurized Thin Cylindrical Steel Shells Under Axial Compression," Research Report, School of Civil and Mining Engineering, University of Sydney, Australia, 1985.

5.10 Priestly, M.J.N., et al., "Seismic Design of Storage Tanks," Bulletin of the New Zealand National Society for Earthquake Engineering, Vol. 19, No. 4, December 1986.

5.11 Priestly, M.J.N., "Seismic Design of Storage Tanks, Recommendations of a Study Group of the New Zealand National Society for Earthquake Engineering," December 1986.

5.12 ASME Boiler and Pressure Vessel Code, Nuclear Code Case N-530, "Provisions for Establishing Allowable Axial Compressive Membrane Stresses in Cylindrical Walls of 0-15 Psi Storage Tanks, Classes 2 and 3, Section III, Division 1," December 1994.

5.13 Bandyopadhyay, K., Xu, J., Shteyngart S., and Eckert, H., "Plastic Buckling of Cylindrical Shells," PVP-Vol. 271, Natural Hazard Phenomena and Mitigation, ASME, 1994.

5.14 Bandyopadhyay, K., Xu, J., Shteyngart S., and Gupta, D., "Cylindrical Shell Buckling Through Strain Hardening," 1995 ASME/JSME Pressure Vessel and Piping Conference, PVP-FSI-Vol. 6, Natural Hazards Phenomena and Mitigation, Honolulu, July 1995.

5.15 "Buckling of Steel Shells - European Recommendations," European Convention for Constructional Steelwork (ECCS), Fourth Edition, No. 56, 1988.

5.16 Manos, G.C., "Earthquake Tank-Wall Stability of Unanchored Tanks," Journal of Structural Engineering, Volume 112, No. 8, ASCE, pp. 1863-1880, August 1986.

5.17 Niwa, A., and Clough, R.W., "Buckling of Cylindrical Liquid-Storage Tanks Under Earthquake Loading," Earthquake Engineering and Structural Dynamics, Volume 10, 1982.

5.18 Flugge, W., "Stresses in Shells," Springer-Verlag, 1960.

5.19 Haroun, M.A., and Badawi, H.S., "Nonlinear Axisymmetric Uplift of Circular Plates," Dynamics of Structures, ASCE, pp. 77-89, August 1987.

5.20 American Society of Mechanical Engineers, "ASME Boiler and Pressure Vessel Code, Section III, Rules for Construction of Nuclear Power Plant Components, Division 1, Subsection NC-3900," 1992.

5.21 Wichman, K.R., Hooper, A.G., and Mershon, J.L., "Local Stresses in Spherical and Cylindrical Shells Due to External Loadings," Welding Research Council Bulletin 107, August 1965, Revised March 1979.

NOTATION

A_b	bolt area
C_a	allowable compressive force per unit of circumferential length
C_b	maximum permissible axial compressive force per unit length
C'_m	compressive force per unit length at the outer compression side of tank wall
COF	coefficient of friction between the tank base and the foundation
E_b	bolt modulus of elasticity
E_t	modulus of elasticity of tank material
F_h	horizontal component of the membrane tension in the base plate at its junction with the cylindrical shell
$F_{\mu D}$	permitted inelastic energy absorption factor from Table 3.3
FS	factor of safety
h_c	height of cylindrical tank wall above the liquid
h_d	dome height above cylindrical wall
h_e	effective length of anchor bolt
h_{sc}	slosh height capacity
h_{sr}	slosh height response
I_{tb}	moment of inertia of base plate
L	length of uplifted portion of base plate
M_+	maximum positive moment
M_c	moment capacity of tank
M_f	moment in tank due to fluid hold-down
M_{fx}	fixed end moment
M_{pb}	plastic moment capacity of base plate

M_{pw} plastic moment capacity of wall

M_r base overturning moment response

$N_{\theta m}$ maximum hoop compression

p liquid pressure

P_a probable average fluid pressure on the base

P_{com} probable combined hydrostatic and hydrodynamic pressure at the point of maximum compression around the tank circumference corrresponding to the time of maximum induced moment

p_{dh} hydrodynamic pressure due to horizontal component of seismic motion

p_{dv} hydrodynamic pressure due to vertical component of seismic motion

p_e effective pressure defined by Equation 5.35

p_c total internal pressure on tank wall at location of maximum longitudinal compressive stress

p_{st} hydrostatic pressure

p_{ti} total inelastic factored demand pressure

P_a axial compressive force on tank wall

R radius of the tank

SF appropriate seismic scale factor from Section 3.3.1

t_{tb} thickness of base plate

t_{tw} thickness of tank wall

T_{bi} tensile force on anchored bolt "i"

T_{bp} anchor bolt pretension

T_{cb} tensile capacity of anchor bolt

T_f fluid hold-down tensile force (tension)

T_{fo} fluid hold-down tensile force at the outer tension side of the tank wall

T_{fn} fluid hold-down tensile force at the neutral axis

V_c	base sliding shear capacity using code coefficient
V_{cs}	nominal base sliding shear capacity
V_r	base shear response
W_e	effective weight for determination of base shear capacity
W_t	tank weight
$\alpha_o, \alpha_p, \alpha_b$	buckling capacity reduction factor for cylindrical shell without internal pressure, with internal pressure, and with bending moment, respectively
δ_o	uplift height at outer tension side of tank wall
δ_θ	uplift height of tank wall at an angle θ
θ	circumferential angle
θ_b	circumferential angle between anchor bolts
θ_n	circumferential angle to neutral axis
ν_t	Poisson's ratio of tank material
σ_a	allowable axial compressive stress
σ_{au}	nominal ultimate axial stress
σ_b	maximum compressive stress due to bending
σ_c	hoop membrane stress capacity
σ_{cl}	classical buckling stress
σ_{eff}	effective stress considering both the axial and hoop stresses
σ_h	tensile hoop stress
σ_o	uniform compressive stress due to axial load
σ_y	code minimum yield stress
σ_{ye}	effective yield stress
ϕ	strength reduction factor

Table 5.1 Tank Parameters

Θ_n	C_1	C_2	C_3	C_4
1.60	1.017	1.558	1.034	1.583
1.65	1.048	1.534	1.095	1.602
1.70	1.081	1.508	1.159	1.619
1.75	1.117	1.480	1.228	1.634
1.80	1.155	1.450	1.302	1.647
1.85	1.197	1.417	1.380	1.658
1.90	1.242	1.383	1.465	1.667
1.95	1.291	1.346	1.555	1.674
2.00	1.345	1.307	1.654	1.679
2.05	1.403	1.266	1.760	1.683
2.10	1.468	1.223	1.876	1.685
2.15	1.539	1.179	2.003	1.686
2.20	1.618	1.132	2.142	1.684
2.25	1.706	1.083	2.296	1.682
2.30	1.804	1.033	2.467	1.679
2.35	1.915	0.981	2.658	1.674
2.40	2.042	0.927	2.874	1.668
2.45	2.187	0.872	3.119	1.661
2.50	2.354	0.815	3.400	1.654
2.55	2.551	0.757	3.727	1.646
2.60	2.783	0.698	4.112	1.638
2.65	3.064	0.637	4.573	1.630
2.70	3.408	0.576	5.134	1.621
2.75	3.840	0.513	5.834	1.612
2.80	4.400	0.449	6.735	1.604
2.85	5.151	0.385	7.939	1.596
2.90	6.215	0.320	9.633	1.589
2.95	7.834	0.254	12.20	1.583
3.00	10.60	0.188	16.57	1.578
3.05	16.38	0.122	25.68	1.574
3.10	36.07	0.055	56.63	1.571

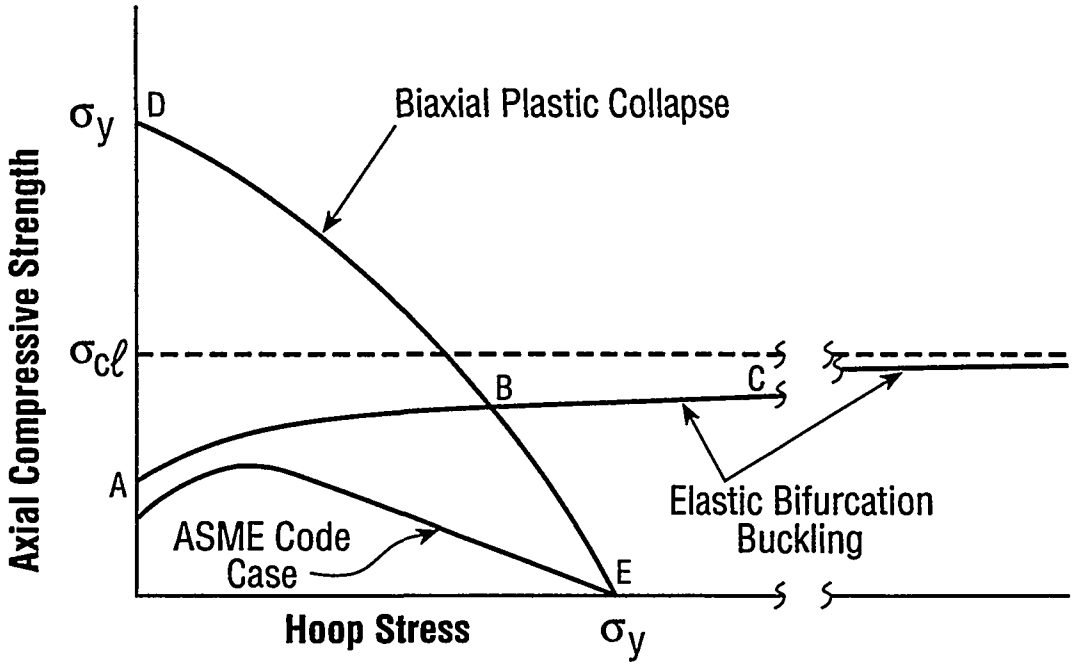

Figure 5.1 Effect of Internal Pressure on Axial Compressive Strength of a Cylindrical Shell

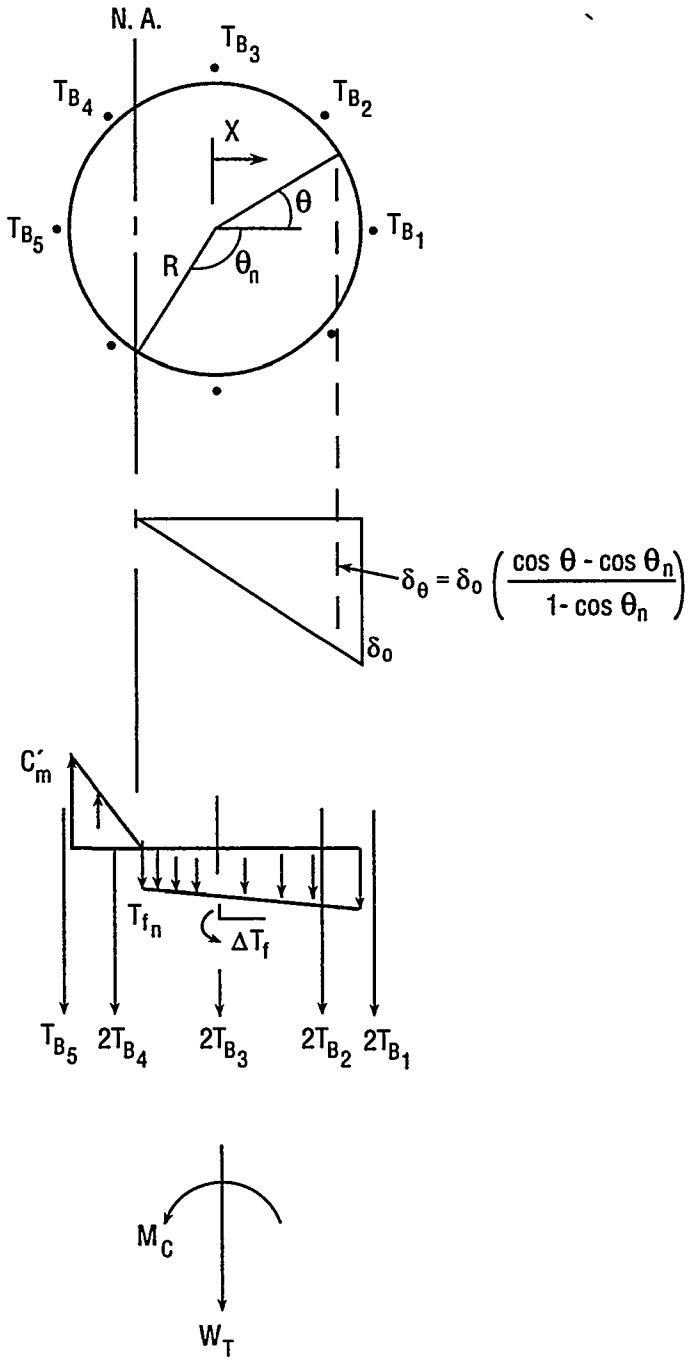

Figure 5.2 Vertical Loading on Tank Wall at Base

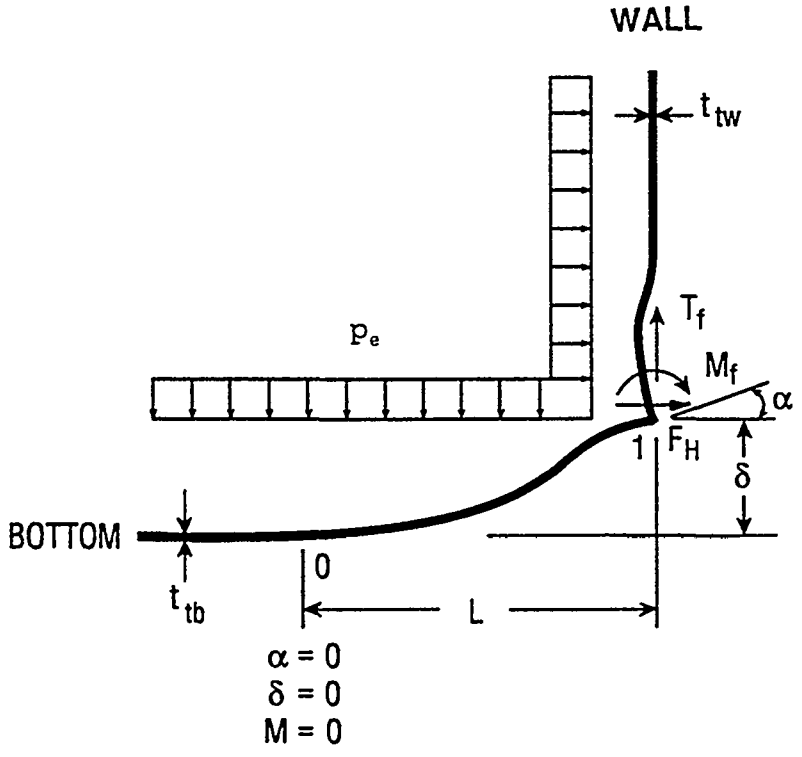

Figure 5.3 Schematic Illustration of Anchored Tank Bottom Behavior at Tensile Region of Tank Wall

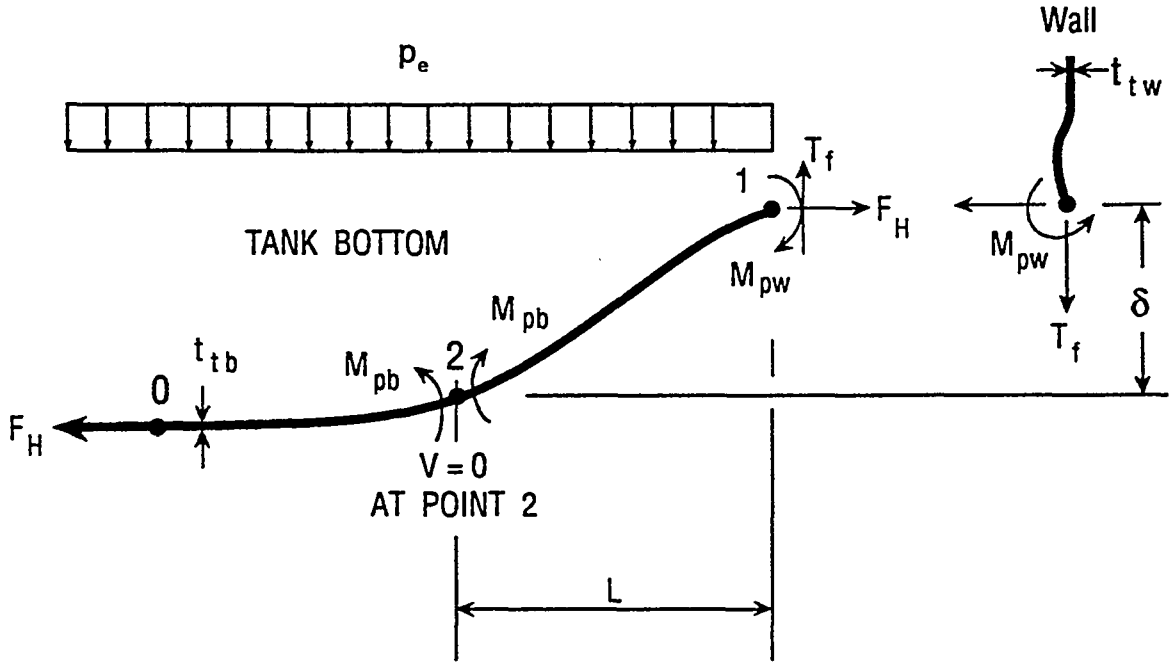

Figure 5.4 Schematic Illustration of Unanchored Tank Bottom Behavior at Tensile Region of Tank Wall

CHAPTER 6

EVALUATION OF SOIL-VAULT INTERACTION

6.1 INTRODUCTION

This chapter presents provisions for the evaluation of the seismic input motion to the support points of the tank and the seismically induced pressures on the walls of the vault. The input motion is to be used in the seismic evaluation of the tank (Chapter 4), whereas the wall pressures are to be used in the stress analysis of the vault structure. The free field design motion (DBE) (defined in terms of a response spectrum) to be used as input to this evaluation is discussed in Chapter 3. The tank model used for the combined vault/tank system is discussed in Chapter 4, and it is further amplified in this chapter.

There are two important considerations involved in the evaluation of soil-vault (soil-structure) interaction effects. The first consideration relates to the evaluation of the vertical spatial variation of the free field ground motion. A free field motion is defined at a control point, and motions compatible with the soil properties are then computed at other locations in the free field. This evaluation is performed using standard convolution methods assuming vertically propagating, horizontally polarized shear waves in the free field. The soil properties affecting the vault response at many of the HLW sites are relatively uniform over the depth of the vault. At these sites it is reasonable to assume that the free field motion is uniform with depth so that convolution studies are not required to define the vertical spatial variation of the ground motion. The actual variation of the free field motion with depth for this uniform site is discussed in Section H.2.2. It is shown that the free field motion at all depths is less than the corresponding surface motion so that use of the surface motion is conservative.

The second consideration requires an evaluation of the soil-vault interaction effects since the vault motion may differ from the free field motion. Soil pressures acting on the vault can then be determined from the results of this evaluation. There are two approaches that have been used in the literature to evaluate these effects. One approach is based on finite element models of the free field and vault with continuity conditions imposed at the soil-vault interface. A second approach utilizes spring/damper models, connecting the vault model to the free field, to represent soil-vault interaction effects. Both approaches are recommended in References 6.1 and 6.2 and they have both been used extensively and successfully in seismic analyses of nuclear power plant facilities. The first approach is theoretically rigorous and leads to excellent results provided that the numerical details (element size, frequency or time increments, and boundary conditions) are properly treated. However, this approach is difficult and costly to implement. The second approach is simpler and more cost-effective, but several assumptions (see Section 6.4.2.1 for a discussion of these assumptions) used in the method may limit its applicability to HLW storage facilities.

An evaluation of the mass and stiffness characteristics of typical vault-tank systems indicates that soil-vault interaction effects are of minor significance for many vaults. Therefore, the additional effort required to apply the first approach may not be warranted for underground concrete vaults. Conditions under which the soil-vault interaction effects can be neglected are also discussed in this chapter.

The provisions of this chapter are applicable to vaults which are circular in cross section. The results may be applied, however, to non-circular cross sections provided that the longer plan dimension is no larger than 1.5 times the shorter plan dimension. In these cases, the vault shall be assumed to be

circular in cross section with a plan area equal to the actual plan area. This chapter includes discussions of the definition of the required soil properties, free field motion, response to horizontal seismic motions, response to vertical seismic motions, and vault-vault interaction effects.

6.2 SOIL PROPERTIES

Soil properties (shear modulus, density, Poisson's ratio and damping) are required both for the free field convolution studies and the soil-structure interaction (SSI) analyses. These analyses should account for the dependence of the soil properties on strain levels in the soil during the DBE.

A soils exploration program should be implemented to evaluate the soil properties to be used in the seismic analyses. The exploration should be performed as close as practical to the location of the vault and should extend down to a depth at least equal to two vault radii below the vault foundation. Sufficient data should be obtained so that mean values and variability of the properties can be statistically defined. The statistical evaluation of soil properties should be done within layers, the vertical extent of which are defined so as to include a zone of similar material as identified from the boring logs. Information on properties of backfill should be developed to the same degree as for the in-situ soils. Details of the exploration program are also discussed in Section 7.3.

Cyclic confined compression, resonant column or torsion testing of undisturbed soil samples should be performed so that the variation of soil properties (shear modulus and damping) with strain levels may be defined.

As a minimum, SSI and convolution calculations should be performed using 15 (lower bound), 50 (best estimate), and 85 (upper bound) percentile low strain soil shear moduli. These

studies are not required if SSI effects can be neglected based on the criteria of Section 6.4. The lower bound shear moduli are equal to the best estimate moduli divided by one plus the coefficient of variation of the shear moduli data and the upper bound moduli are equal to the best estimate moduli times one plus the coefficient of variation. The minimum coefficient of variation should be taken as 0.5. If sufficient soil data are not available to evaluate the coefficient of variation of the shear modulus, the coefficient of variation should be taken as 1. The soil damping should be consistent with the strain values determined from the convolution analyses.

6.3 FREE FIELD MOTION

The objective of the calculations discussed in this section is to determine the variation of the two horizontal components of the free field ground motion over the depth of embedment of the vault. This variation should be included in the SSI calculations used to evaluate the seismically induced motion of the tank and the associated soil pressures acting on the vault. If the site is "uniform," the DBE horizontal ground motion can be conservatively assumed to be uniform over the depth of the vault. A site can be considered to be "uniform" when the shear wave velocity variation between the surface and one vault diameter below the vault basemat is less than 1.5. Justification for this conclusion is given in Section H.4. Convolution studies are still required, however, to evaluate the magnitude of the seismically induced soil strains which are needed to determine the strain-dependent soil properties to be used in the SSI analyses.

A DBE ground motion time history should be developed which leads to response spectra that envelope the free field spectra discussed in Chapter 3. Response spectra should be developed for the time history for all damping values of interest, and these spectra should be compared with the DBE spectra discussed

in Chapter 3. Criteria specified in Reference 6.1 can be used to evaluate the adequacy of these comparisons. Special care should be taken to ensure that the ground motion is baseline corrected (i.e., its final velocity is zero and the peak displacements are consistent with the magnitude and focal distance of the DBE).

The control point for the placement of the DBE horizontal ground motion should be taken as discussed in Section 3.3. The variation of horizontal free field motions occurring at elevations within the depth of the vault should be evaluated using convolution methods associated with vertically propagating, horizontally polarized shear waves. Computer codes such as FLUSH (Reference 6.3) or CARES (Reference 6.4) can be used to perform these calculations. The number and thickness of the layers to be used in the analysis should be consistent with the soil property variation with depth. The mesh size should be sufficiently fine over the depth of the vault to provide ground motion data at the top, midpoint, and bottom of the vault, and should be capable of transmitting frequencies containing most of the energy in the DBE and at least twice the primary system frequencies. The system frequencies may be taken as the tank/fluid frequency (as evaluated in Chapter 4) and the combined horizontal/rocking SSI frequencies using the lumped parameter SSI models given in Appendix H. However, the mesh does not have to transmit frequencies greater than 25 cps. Larger mesh sizes may be used if justified with a parametric study. Convolution studies should be performed using lower bound, best estimate, and upper bound soil properties. Three SSI calculations should be performed using the free field motion obtained from each of the convolution studies. Of course, the soil properties used in the SSI calculations should be the same as those used in the corresponding convolution study.

The convolution calculations should be performed accounting for

the variation of soil properties (shear modulus and hysteretic soil damping) with strain. The models used to relate the soil properties to strain should be determined from measured properties or computed using generally accepted models. Typical values of soil strain will generally result in hysteretic soil damping values of 15% or less. When higher values are obtained, the strains are likely to be sufficiently large so that the possibility of soil failure should be investigated.

The convolution studies should be performed using in-situ soil properties unless backfill has been used and the backfill extends out to an average distance of at least 3 vault radii from the vault wall. In this case, the backfill properties should be used in the convolution analysis for the upper portion of the soil column.

6.4 HORIZONTAL SSI CALCULATIONS

Methods for calculation of the combined horizontal and rocking seismic response of the vault/tank system are discussed in this section. The calculation requires modeling of the liquid/tank system, the vault, and the soil-structure interaction effect. Input to the model is the horizontal free field seismic motion as defined in the previous section, and the required outputs from this calculation are the seismic input to the liquid/tank model and the seismically induced pressures and forces acting on the vault.

In many cases, the vault will undergo the same horizontal displacement as the free field, and horizontal/rocking SSI effects may be neglected. These effects may be neglected when the site is relatively uniform (see Section 3.3 for the definition of a uniform site) and when it can be shown that the amplifications of the free field motions caused by SSI effects are small (see the following paragraph for a discussion of the vault parameters required for this to be true). When this is

the case, the vault seismic motion and the seismic input to the base of the tank (to be used for the seismic analysis of the tank) can be taken as uniform over the depth of the vault and expressed by the free field spectra as defined in Chapter 3.

The significance of SSI effects in the evaluation of the horizontal/rocking response of the vault/tank system is discussed in Section H.2.3. It is shown that, for vaults located at sites with uniform soil conditions and having a depth to radius ratio less than one and no soil cover, the errors in floor response spectra resulting from neglecting SSI effects will be less than 20%. SSI effects actually reduce the seismic loads acting on the tank/liquid system for the same conditions. Ratios of vault and liquid mass responses including SSI effects to that obtained when SSI effects are neglected are shown on Figures H.7 through H.10 for a wide range of HLW tank properties. These responses are given in terms of transfer functions relating the response of the system to that of the free field at a particular frequency. The seismically induced loads acting on the liquid are obtained by convolving the liquid mass transfer functions with the DBE response spectra and multiplying the result by the liquid mass in the model. Since the DBE spectra usually have constant accelerations in the frequency range of interest for the tank, the likely difference in tank loads between the cases where SSI effects are included and neglected is an average value taken through those shown on the figures. The data contained in Figures H.7 through H.10 should be reviewed before making a decision as to whether an SSI analysis is required. It should be noted, however, that in many cases SSI effects could significantly reduce the response.

When the SSI effects are neglected, the input to the base of the tank/liquid system can be taken equal to the free field motion, and the normal horizontal soil pressure (p_n) acting on the vault can be distributed uniformly in the vertical direction and as a

cosine function around the circumference of the vault. The magnitude of the peak pressure can be conservatively (since the shear force which is transmitted to the soil at the base of the vault is neglected) estimated based on the peak inertial force required to satisfy dynamic equilibrium when the vault follows the free field motion. The result of these assumptions is:

$$p_n = \rho_v R_v A_{max} \cos\theta \qquad (6.1)$$

where,

ρ_v = average density of vault/tank system (total mass divided by the total volume)

R_v = radius of vault

θ = circumferential angle measured from the direction of the horizontal seismic input

A_{max} = peak free field acceleration

These wall pressures are in dynamic equilibrium with the inertial loads acting on the tank/vault system. Since the major portion of the inertial loads results from the liquid mass, the earth pressures on the vault wall are in equilibrium with the inertial loads in the tank. The vault should be assumed to be supported in a manner such that the reactions resisting the soil pressure loading are located where the liquid inertial loads act on the vault. The stress analysis of the vault can, therefore, be performed by placing the earth pressures on the vault while supporting the vault in a manner that is compatible with the support conditions for the tank within the vault. The vault should be treated as a cantilever beam supported at the basemat when the tank is supported only from the base of the vault. The vault should be treated as a simple beam supported at the top and base when the tank is top-supported.

When SSI effects are considered, two alternative methods are available to evaluate the horizontal/rocking response of the liquid/tank/vault system. The first method models the soil and

vault with discrete elements (e.g., finite elements) and the SSI effects are obtained based on compatibility conditions at the soil/vault interface. The second method utilizes spring/damper lumped parameter models connecting the vault and free field models to represent SSI effects. In either of these methods, the solutions may be carried out in the frequency or time domain. The discretization parameters (e.g., time or frequency increment, element sizes, boundary locations, etc.) should be selected based on the range of frequencies that are expected to be significant. Criteria such as those contained in References 6.1 or 6.2 may be used to satisfy these requirements.

SSI solutions should be carried out for the seismic input in each of the three directions (two horizontal and vertical). The total seismic response of the vault/tank system can then be computed by either the SRSS of the responses computed in each of the three directions or by the absolute sum of the responses in each of the three directions. In the latter case 100% of the largest response should be combined with 40% of the response in each of the remaining two directions. It is recommended that these combinations be done after the stress analyses have been performed using the seismic input in each of the directions.

6.4.1 Continuum Model Using Time History Analysis

The SSI calculations may be based on a continuum model of the vault/tank/soil system. Since the computer codes (e.g., References 6.3 and 6.5) used to implement these solutions are usually quite complex, special care should be taken to ensure that the code being used has been verified and that the results of the calculations are subjected to "sanity" checks ensuring their validity. As an example, SASSI (Reference 6.5) performs the response calculations in the frequency domain. Solutions are obtained at discrete frequencies (selected by the user) and results at intermediate frequencies are obtained by interpolating between the selected frequencies. A poor

selection of the number and value of the discrete frequencies can lead to results that are seriously in error, especially results for the stresses in the vault and/or tank. These validity checks are discussed at the end of this section after the modeling characteristics are presented.

6.4.1.1 Free Field Motion

A separate free field computation is normally performed which results in the definition of the free field motion throughout the site which is consistent with the criteria motion as discussed in Section 6.3. This same analysis results in estimates of soil properties which are consistent with the seismically induced soil strains. The free field motion used for the SSI computation is usually defined at either the surface or base of the model.

6.4.1.2 Soil Model

The soil properties should be those that are determined from the free field analysis (see Section 6.2) and are consistent with the free field strains induced by the seismic input motion. Solutions should be obtained at best estimate, upper bound, and lower bound soil properties (see Section 6.2) and the system response should be taken as the envelope of the responses determined from the three soil cases.

The soil is modeled with discrete elements requiring that decisions be made regarding the extent of the half space that is to be modeled and the element sizes to be used for the model. The model should extend far enough so that reflections from artificial boundaries do not affect the results at the vault. Most of the computer codes used for these analyses contain "non reflecting" boundaries so that seismic waves reaching the artificial boundary are absorbed rather than reflected back to influence the response of the vault. The size of the discrete

elements must be selected to pass the highest frequencies of interest. This requires that the element size be no larger than the material wave velocity (shear velocity for vertically propagating shear waves) divided by five times the maximum frequency of interest. For example, the element size should be restricted to ten feet if the soil shear wave velocity is 1,000 fps and solutions having accurate components at 20 cps are needed.

6.4.1.3 Vault Model

The vault will normally be modeled with plate or shell finite elements. The details of this model should be sufficient to capture the dynamic characteristics of the vault. Since most vaults of interest are quite stiff compared to the surrounding soil, rather crude models are adequate for this purpose. If the computer code is to be used to directly evaluate stresses in the vault, however, sufficient detail must be included in the model to capture the stresses at critical locations. This detail may add significant complexity to the model and result in costly SSI solutions. As an alternate, the simpler vault model adequate to capture the vault's dynamic characteristics can be used in the SSI analysis. A more detailed static vault model can then be used to evaluate vault stresses. The soil pressures and inertial loads determined from the SSI solution at a specific time is used as input loading to the static model.

6.4.1.4 Tank and Contents Model

The cantilever model of the tank and its contents, discussed in Section 4.3.8, results in the proper total overturning moment and total horizontal load applied to the vault by the tank during the seismic response. It does not, however, distribute these loads to the tank support points on the vault for the top supported tanks. A modification is required to the model of Section 4.3.8 if this load distribution is to be used in the

solution. This modification is required for most computer codes used to implement continuum solutions since the same model of the tank is used to compute the seismic response of the vault/tank system and the stresses in the vault. The computation of stresses in the vault, of course, requires that the tank loads are properly distributed on the vault.

A general model that can be used to represent the tank in evaluating the combined horizontal and rocking seismic response of the tank/vault system is shown on Figure 6.1. The model consists of two cantilevers, one supported by the vault at the elevation of the top tank support and the other at the base of the tank. These cantilever models should be located along the centerline of the tank and connected to nodes located on the vault wall with rigid links. This model applies to all support conditions and reduces to the model of Section 4.3.8 for the cantilever support condition. A rotary inertia must be added at the base to model the moment developed by the impulsive mode hydrodynamic pressures acting on the basemat. The magnitude of this rotary inertia is given on column 6 of Table 4.2.

In general, two mass models are used: one representing the effects of the impulsive liquid mass and the other representing the response of the convective liquid mass. While the effects of the convective mass of the system response may not be significant, inclusion of this model allows one to determine the sloshing height of the liquid directly from the seismic response computation. The symbols shown on Figure 6.1 apply to either the impulsive or convective mode and the differences between the two models are introduced when the parameters are numerically defined. The parameters of the model are given for the full tank represent the most severe load case.

The distribution of liquid mass m_ℓ between the impulsive m_i and first convective mode m_{c1} are given in columns 3 and 7 of Table 4.2, respectively. The distribution of mass between the top and

base cantilevers shown in Figure 6.1 is proportioned to achieve the proper force distribution between the two supports so that:

$$m_t = (1 - m_b/m^*)\, m^* \qquad (6.2)$$

where,

m_b/m^* = 1 for either the impulsive or convective modes for cantilever tanks

= α_i (from Table 4.5) for the impulsive mode for top supported tanks

= α_{c1} (from Table 4.5) for the convective mode for top supported tanks

m^* = m_i or m_{c1} for the impulsive and convective modes, respectively

The lengths of the cantilever beams in the model are determined to match the top and base support moments. These moments consist of components due to the liquid pressure acting on the basemat and liquid pressure acting on the tank wall. The resulting cantilever heights are:

$$h'_b = [d(O) + e]\,(m_t/m^*)\, H_t/(m_b/m^*)$$
$$h'_t = d(1)\,(m_t/m^*)\, H_t/(1 - m_b/m^*) \qquad (6.3)$$

where,

d = moment coefficients to account for liquid pressure acting on the tank wall and defined in Tables 4.6 through 4.11. These coefficients depend on the tank support condition and whether the mode is impulsive or convective. Note that d(0) and d(1) define the moment coefficients at the lower and upper supports, respectively.

e = moment coefficients to account for liquid pressure acting on basemat and defined in columns 4 and 11 of Table 4.2 for the impulsive and convective modes,

respectively.

H_t = height of tank

Note that negative values of h'_t or h'_b indicate that the cantilever extends below the support rather than above.

The correct seismic acceleration imposed on the masses of the model is obtained by matching the frequencies of the cantilever beams to the tank frequency f_{c1} or f_i as given in Sections 4.3.2.1 (convective) and 4.3.2.2 (impulsive) respectively. This is done by selecting the stiffness of the cantilever beam EI as:

$$EI = 4\pi^2 f^2 L^3 m/3 \qquad (6.4)$$

where,

EI = flexural rigidity of the top or bottom cantilever for either the impulsive or convective mode

f = f_{c1} for the convective mode and f_i for the impulsive mode

L = h'_b or h'_t for the base and top cantilever models, respectively

m = top or base mass associated with the mode being considered (convective or impulsive)

If the length of the top cantilever is zero, the mass must be attached to the support with a spring stiffness k_c so that the tank frequency is matched. This spring stiffness will be:

$$k_c = 4\pi^2 f^2 L^3 m^* (1 - m_b/m^*) \qquad (6.5)$$

The accelerations (e.g., A_i) shown in Chapter 4 are used to determine bending moments in the tank and fluid slosh heights. These accelerations can be related to the accelerations of the masses in the model shown on Figure 6.1. If the computed acceleration of the top and bottom masses are A_t and A_b, respectively, then:

$$A_i = A_b + (A_t - A_b)(z^* - h'_b)/(H_t + h'_t - h'_b) \qquad (6.8)$$

where,

$$z^* = \textit{center of gravity of the two masses}$$
$$= [m_t(H_t + h'_t) + m_b h'_b]/(m_t + m_b)$$

As an alternative to this model, it is possible to include a detailed model (e.g., finite element model) of the tank and liquid in the soil/vault model. As discussed in Section 4.1, the validity of these models should be established by comparing the results obtained for limiting cases using the methods discussed in Chapter 4.

6.4.1.5 Verification of Results

As indicated above, these codes are difficult to use and the results obtained must be reviewed with care to ensure that they are accurate. Significant errors can stem from several sources: the soil boundaries may result in artificial seismic wave reflections; element sizes may be too large to pass the frequencies of interest; the element size may be too crude to model sharp stress or pressure gradients; and the number of frequencies for which solutions are obtained (solutions at intermediate frequencies are obtained by interpolation) may be too small.

Soil pressures (normal and shear) acting on the vault should be evaluated and compared with vault deformations relative to the soil to demonstrate that the soil pressure variation is similar to that of the relative deformations. The soil pressures acting on the vault should be determined and shown to be consistent with the moments and shears computed in the vault structure and to satisfy dynamic equilibrium conditions. Of course, checks such as these should be made at a single time point in the solution. It is recommended that the checks be performed at a time which is close to the time when maximum responses occur.

This time is likely to be very close to the time at which the peak free field acceleration occurs.

6.4.2 Lumped Parameter Model

Details of this method are given in Section H.2 and summarized here. It is important to note that these methods have been used extensively in performing SSI analyses for nuclear power plant structures (References 6.4 and 6.6). Experimental verification of the methods is discussed in Reference 6.7, and results obtained using the lumped parameter models are compared with those obtained from continuous solutions in Reference 6.8.

Lumped parameter models employ "impedance functions" which relate the forces acting on the foundation to the deformation of the foundation in the soil media. Three steps are required to implement this method as discussed in Section H.2: a solution to the far free field problem; a solution to the local free field problem (kinematic interaction); and a solution to the structural response problem (inertial interaction). SSI impedance functions relating the forces acting on the soil/structure interface to the deformation of the interface are the essential data required to perform the last two of these three problems. These impedance functions are first considered followed by discussions of each of the three problems.

6.4.2.1 Impedance Functions

The method is relatively simple to apply once the impedance functions are available. Descriptions of two available impedance function models are given in Section H.2.1 with specifics contained in Tables H.1 and H.2. These are based on the work presented in References H.3 and H.4. These impedance functions are restricted to rigid foundations and to structures which are not completely buried so that the method can only be applied to rigid vaults and vaults which have minimal cover.

Two criteria should be satisfied for the vault to be considered as rigid:

- The vault shear stiffness should be at least 3 times the shear stiffness of the soil it replaces. This condition is satisfied if the thickness/radius ratio of the vault is greater than $3 \times 10^{-8} V_s^2$ where V_s is the shear wave velocity in fps.

- The methodology requires that the free field motion be represented by its rigid body components. This is done reasonably well for nondimensional frequencies $\omega R_v/V_s < 4.5$ R_v/H_v (see Section H.2.2), where R_v and H_v are, respectively, the radius and height of the vault.

It is also recommended that the method be restricted to those cases where the soil cover over the vault is less than one half the vault radius.

The impedance functions presented in Reference H.3 are only applicable to sites having uniform soil properties while the solutions contained in Reference H.4 are applicable to sites where the soil properties vary over the depth of the vault and are constant beneath the vault. The functions contained in Reference H.4 are more generally applicable but as discussed in Appendix H the derivation of these functions is based on assumptions which may not be valid when large differences in soil properties occur between the soil underlying the vault basemat and the soil to the side of the vault. The method neglects shear stresses which transmit side wall interaction forces vertically down to the underlying soil. The resulting SSI stiffness coefficients are therefore likely to be softer than actual, especially for those cases where the underlying soil is much stiffer than the soil to the side of the vault. Recent studies (References 6.9 and 6.10) have shown that the differences are significant when the underlying soil is rigid

(such as might be the case for a vault founded on rock with backfill placed against the vault walls). This work is continuing and hopefully will lead to an improved SSI model. It is recommended that "continuum model" solutions be used unless the difference in shear wave velocity between the foundation and side soils is less than a factor of 3 to 4.

6.4.2.2 Free Field Solution

The objective of the first step in the calculations is to evaluate the vertical spatial variation of the free field motion over the depth of the vault that is consistent with both the free field motion as discussed in Section 6.3 and the soil properties (which usually depend on soil strain). This computation is usually performed with a free field computer code (e.g., References 6.3 and 6.4) starting with a time history generated to fit the DBE spectra. The sloshing motion of fluid and the relative displacement component of the seismically induced pressure acting on the vault depend on the low frequency content of the free field motion. The time history generated to fit the DBE spectra will often contain excessive low frequency energy content unless care is taken in fitting the spectra with the generated time history. This could result in over-conservative predictions for sloshing motion and vault pressure.

After the variation of the free field motion is obtained over the depth of the vault, an equivalent rigid body free field deflection is defined describing the soil/structure interface motion. This is defined with a free field horizontal deflection at the elevation of the base of the vault and a rotation of the free field about the elevation of the vault base. These deflection components are determined so as to fit (in a least squared error sense - see Equation H.6) the actual free field deflection variation with depth.

6.4.2.3 Kinematic Interaction

The objective of the second step in the solution is to obtain the near free field solution considering the space to be occupied by the vault as a void. This entails evaluating the stresses from the free field solution of the first step which act on the block of soil that is located in the void. The impedance functions are then used to determine interface deflections required to generate the negative of the free field stresses. The solution to this kinematic interaction problem is obtained by using Equations H.7 and H.8. The sum of this solution and the first solution then represents the near free field deflections which result in zero tractions acting on the foundation void.

This problem is evaluated in Appendix H, and a simple approximation is shown to be adequate for geometries typical of the HLW vaults of interest. Rather than solving the kinematic interaction problem, it is possible to define the near field motion with two components: the free field deformation at the elevation of the base of the vault plus a rotational component equal to the difference between the free field deformation at the elevations of the top and base of the vault divided by the height of the vault.

6.4.2.4 Inertial Interaction

The objective of the third problem is to evaluate the response of the vault/tank system using the near free field displacement as input. The impedance functions are used to generate interaction loads so that compatible deflections occur in the structure and the soil when the loads are applied to both the structure (to equilibrate inertial loads) and to the free field. Of course, the free field deflections are the sum of the near field deflections found from solutions to the first two problems and the additional deflections resulting from the SSI loads.

The model used for this problem is shown on Figure H.6 and the equations of motion are given as Equation H.11. These equations may be either numerically integrated in the time domain or solved in the frequency domain.

The liquid/tank model to be used in the SSI analyses should properly account for the liquid impulsive vibration mode and may include the first convective mode of the liquid. The model characteristics may be taken directly from the results given in Chapter 4. The model is shown on Figure 4.6 and discussed in Section 4.3.8. The accelerations ($A_i(t)$ and $A_{c1}(t)$ of Equations 4.34 and 4.35) of Chapter 4 are used to find tank loads (moments and shears) and slosh heights. These are the accelerations of the masses of the tank model shown on Figure 4.6.

The vault is modeled as a rigid body and should include the mass of the vault and the soil overburden. The equations of motion (H.11) of the vault are written with reference to the center of gravity of the vault.

6.4.2.5 Calculation of Wall Pressures

Once the three solutions have been found, the pressures acting on the vault wall may be determined from the side soil forces computed from the relative motion of the vault and free field. For vaults with a circular cross section it may be assumed that the wall shear pressures contribute 40% of the total load. The normal pressures then contribute 60% of the force and are distributed as a cosine function around the circumference of the vault. The resulting normal and shear pressure distributions are:

$$p_n = 0.6F\cos\theta/(\pi R_v)$$
$$p_s = 0.4F\sin\theta/(\pi R_v) \qquad (6.9)$$

where,

p_n = normal pressure

p_s = shear pressure
F = sidewall force at elevation of interest
θ = circumferential angle defining location on tank

Wall pressures for vaults of other shapes should be determined in a manner consistent with the spring/damper models used for these geometries.

The pressures acting on the wall are primarily reacted by the inertial effects in the tank/fluid system. It is, therefore, recommended that the stress analysis of the vault be performed by assuming the vault walls to be cantilevered from the basemat for the base supported tank, and simply supported at the top and bottom for the top supported tank. Of course, it is essential that the pressures applied to the vault walls are those pressures that occur at the same time in the SSI analysis. It is recommended that the total force acting on the vault walls be monitored during the SSI analysis and that the pressures which occur when this force is a maximum be used for the vault stress analysis.

A more rigorous stress analysis of the vault may be performed by saving all forces (sidewall SSI forces and moments, and the inertial loads) acting on the vault at the time that the force acting on the vault wall is a maximum. These forces and moments are in dynamic equilibrium and may be used to calculate stresses at any location in the vault.

The response solutions may be conservatively developed based on the assumption that nonlinear effects are unimportant. The wall pressures developed from these solutions may, however, be limited by Coulomb-Mohr soil strength parameters to be:

$$p_{sc} = \sigma_{sv}[\tan^2(45 + \phi/2) - 1/2] + 2C\tan(45 + \phi/2)$$
$$p_{st} = \sigma_{sv}[1/2 - \tan^2(45 - \phi/2)] + 2C\tan(45 - \phi/2) \qquad (6.10)$$

where,

C = cohesive strength of the soil

p_{sc} = peak compressive pressure in excess of at rest static pressure

p_{st} = peak tensile pressure below static pressure

σ_{sv} = vertical normal stress in the soil at depth of interest

ϕ = angle of internal friction in the backfill soil

When this is done the ductility factors used for the stress analysis of the vault (see Chapter 3) should be limited to unity.

6.5 VERTICAL SSI CALCULATIONS

Vertical SSI effects are not significant for most HLW tanks. This is discussed in Section H.3 where it is demonstrated that any amplifications to the free field vertical motion are likely to be small because of the high damping in the vertical SSI models, and that it is unlikely that the seismic load will be controlling for the tank as compared to the static load case. The seismic load may be significant for the roof of the vault if the soil cover is significant. In this case, the seismically induced loading may be evaluated by multiplying the mass of the vault roof and soil cover by an acceleration taken from the vertical DBE response spectrum defined in Chapter 3. The acceleration should be evaluated at the vertical frequency of the vault including vault wall and roof flexibilities, and the masses of the vault and overburden soil.

The assessment of vertical SSI effects in Appendix H is based on the assumption that the vault basemat is rigid. In many cases the basemat behaves as a rigid plate (i.e., seismically induced deformations are uniform across the mat) because the loads acting on the mat (inertial loads of the fluid and vertical SSI soil pressures) are uniform. However, inertial loads resulting

from the mass of the vault wall, dome, and overburden soil cause edge loads acting on the mat which may result in nonuniform mat deformation. This effect can result in vertical liquid accelerations which are not uniform and larger than the vertical free field accelerations at the center of the mat. This effect results in increased liquid hydrodynamic fluid pressures as compared with the result when the rigid basemat assumption is made. This effect should be considered when the mass of the vault wall, dome, and overburden soil is greater than 15% of the liquid mass. Computer codes such as SASSI (Reference 6.5) can be used to perform this evaluation.

Vertical SSI calculations can be performed, if deemed necessary, using either finite element or lumped parameter methods. Details of the lumped parameter method are discussed in Section H.3. These include the vertical SSI model parameters and a suggested model for the vault and tank/liquid system. Of course, the free field input motion should be the vertical DBE as defined in Chapter 3. The finite element methodology can be implemented with a computer code such as SASSI (Reference 6.5) or FLUSH (Reference 6.3). The "stick" model described in Section H.3 can be used for these calculations or more detailed finite element models of the vault and tank may be used.

6.6 VAULT-VAULT INTERACTION

There is evidence indicating that vault-vault interaction effects are not significant unless the spacing between vaults is less than one half of the vault radii. Additional studies are underway to confirm these conclusions and to develop definitive guidance in this area. Until such data become available, vault-vault interaction effects should be evaluated for spacings closer than one half of the vault radius.

REFERENCES

6.1 American Society of Civil Engineers, Standard 4-86 "Seismic Analysis of Safety-Related Nuclear Structures and Commentary on Standard for Seismic Analysis of Safety-Related Nuclear Structures," September 1986.

6.2 U.S. Nuclear Regulatory Commission, "Standard Review Plan, NUREG-0800," Sections 3.7.1 through 3.7.3, Rev. 2, August 1989.

6.3 Lysmer, J., Udaka, T., Tsai, C., and Seed, H., "FLUSH, A Computer Program for Approximate 3-D Analysis of Soil-Structure Interaction Problems," EERC 75-30, University of California, Berkeley, 1975.

6.4 "Computer Analysis for Rapid Evaluation of Structures - CARES," Brookhaven National Laboratory, NUREG/CR-5588, 1989.

6.5 Lysmer, J., Tabatabaie, M., Tajirian, F., Vahdani, S., and Ostadan, F., "SASSI, A System for Analysis of Soil-Structure Interaction," UCB/GT/81-02, University of California, Berkeley, 1981.

6.6 Hadjian, A.H., "Bechtel Topical Report, Seismic Analysis of Structures and Equipment for Nuclear Power Plants," BC-TOP-4, August 1980.

6.7 Hadjian, A.H., Howard, G.E., and Smith, C.B., "A Comparison of Experimental and Theoretical Investigations of Embedment Effects on Seismic Response," 3rd SMiRT, September 1975.

6.8 Tseng, W.J., and Hadjian, A.H., "Guidelines for Soil-Structure Interaction Analysis," prepared for Electric Power Research Institute," Project 2225-9, June 1991.

6.9 Veletsos, A.S., and Younan, A.H., "Dynamic Modeling and Response of Soil-Wall Systems," American Society of Civil Engineers, Journal of Geotechnical Engineering, Vol. 120, No. 12, December 1994.

6.10 Veletsos, A.S., and Younan, A.H., "Dynamic Soil Pressures on Rigid Vertical Walls," Earthquake Engineering and Structural Dynamics, Vol. 23, 1994.

NOTATION

A_{max}	peak free-field acceleration
C	cohesive strength of soil
DBE	design basis earthquake
$(EI)_b$	stiffness of the base cantilever model of tank and contents
$(EI)_t$	stiffness of the top cantilever model of tank and contents
F	total force acting on vault wall
g	acceleration due to gravity
h'_b	length of the base cantilever model of tank and contents
h'_t	length of the top cantilever model of tank and contents
H_v	height of vault
m_b	mass of the base cantilever model of tank and contents
m_t	mass of the top cantilever model of tank and contents
p_n	normal horizontal soil pressure acting on the vault wall
p_{sc}	peak compressive soil pressure acting on the vault wall
p_{st}	peak tensile soil pressure acting on the vault wall
SSI	soil structure interaction
R_v	radius of the vault
V_s	soil shear wave velocity
θ	circumferential angle defining location on the vault
ω	circular frequency
σ_{sv}	vertical component of the intergranular stress in the soil
ϕ	angle of internal friction in the backfill soil

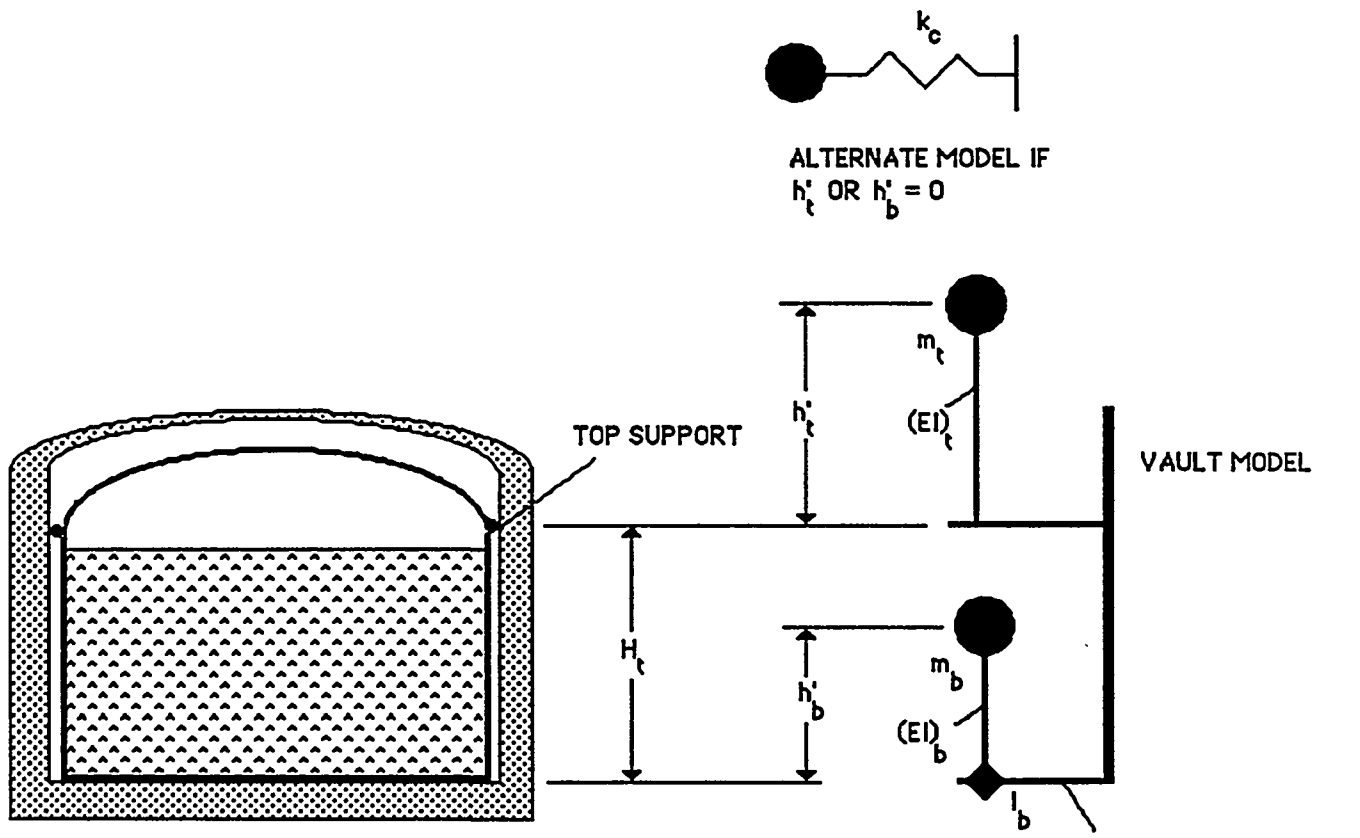

Figure 6.1 Model for Tank-Fluid System

CHAPTER 7

UNDERGROUND PIPING AND CONDUITS

7.1 INTRODUCTION

The design of underground piping systems (process piping and encasing) and conduits must demonstrate the ability of the piping system to withstand strains and stresses caused by potential seismic movement of foundation soils in conjunction with stresses induced by other normal or accidental loadings applied to the piping and conduits. Stress resultants (forces and moments) computed from these various load conditions must be suitably combined to obtain stresses and strains which can be shown to be less than the appropriate allowables. Current Codes typically used for piping systems do not specifically address design requirements for underground piping systems. As a result, design criteria and evaluation guidelines are provided herein to facilitate the assessment of DOE HLW underground piping systems and conduits. The references listed at the end of this document can be used to address specific analysis issues. A numerical example is provided in Appendix I to demonstrate the application of the recommended procedures and guidelines.

Most, if not all, of the underground waste process piping systems are encased (or double containment) piping systems. In double containment piping, the inner pipe (or core) serves to transport the wastes and maintain the pressure boundary, if required, while the outer pipe provides secondary containment in case of leakage from the inner pipe. The outer or encasement pipe is not normally subjected to internal pressure. Hence, maintaining pressure boundary integrity is of secondary concern. Rather, it is essential that the structural integrity of the outer pipe be maintained during extreme design loadings, such as seismic loadings. The inner piping is typically supported by guides, saddles, support keys, spiders (or bars), deadweight

supports and/or anchors within the outer pipe. The outer pipe may be buried directly in soil or could itself be placed within a ceramic tile or concrete containment which is then buried within the soil. Appropriate corrosion protection should be provided.

For the case of soil supported piping, the outer piping is in direct contact with the surrounding soil and will therefore be subjected to potential soil loading from wave passage effects (anchor point loads, soil friction and normal pressures) due to the relative transient movement between the piping system and the surrounding soil as well as potential long term effects due to permanent ground and support point displacements. The inner pipe, through its support within the outer pipe, will not only be affected by the movements of the outer pipe, but will also respond to its own inertia during the seismic wave passage. In this case, the inner pipe responds much like above ground piping, with the added concern that the interaction between the inner and outer pipes could be significant and must be assessed. For the case where the outer pipe is contained within a tile or concrete containment which is below grade, the containment will be subjected to the soil loads. In this case, if the space between the outer pipe and the containment is sufficiently large, both the inner and outer piping could be analyzed as aboveground piping.

Potential seismic effects on underground piping and conduits are in general caused by different aspects of ground movements, namely, (1) abrupt relative displacements of the ground caused by dislocation at the ground surface from fault dislocations, (2) ground failure of relatively large areas caused by liquefaction, landslides, gross surface settlements, or collapse of voids at depth, (3) transient deformation of the ground during the seismic event due to wave passage effects, (4) inertial response of the inner piping system in response to

induced movements of the outer piping, and (5) transient movements of anchor points or buildings connected to the buried facilities.

For construction of new facilities, zones susceptible to abrupt ground movements or ground failure should be avoided. However, for evaluation of existing facilities, the effects of these potential seismically induced movements must be suitably accounted for and incorporated into the evaluation. As described in Reference 7.1, rigorous analytic treatment of the response of buried facilities to these seismic movements is in general not practical, particularly for piping in direct contact with the soil. However, in view of the use of the double-walled piping design, the potential for increased rigidity of the outer piping at the elbow due to the effect of the inner piping is present. Therefore, suitable procedures must be adopted to ensure that stresses and strains remain within the recommended design allowables.

In addition to seismic loads, other design loads must also be considered. They include thermal expansion, selfweight of the piping system, internal pressure, overburden soil loads and loads developed by at-grade live loads. Forces and moments from all loading conditions must be suitably determined, combined and assessed for their adequacy.

7.2 DESIGN FEATURES AND GENERAL CONSIDERATIONS

In order to accommodate potential thermal and seismic displacements (excluding SAM) between the outer pipe and the soil, some older designs used bubble wrap around the outer pipe. Vermiculite concrete was poured over the wrapper so that no portion of the length was directly exposed to the soil except at or near anchor block locations. Later designs used polyurethane foam material around the outer pipe whose thickness depended on the magnitude of displacements anticipated. If current designs allow

use of such wrapping materials, the adequacy of such interface materials (as defined by its stiffness, yield strength, lock-up strain and thickness) must be justified to demonstrate their ability to absorb potential seismic and thermal displacements as well as sustain all other appropriate loading conditions. If the designs do not use such compliant materials around the outer piping, analysis can then be used to demonstrate compliance of the design to the requirements as described herein.

For outer piping in direct contact with the soil, soil displacement and wave passage effects have more significant effects on forces and moments developed in the outer piping than do its own inertial effects. However, the inner pipe is supported and/or restrained by the outer pipe. Thus the stiffness of the inner pipe could make an important contribution to the overall stiffness of the outer pipe. In contrast with the outer pipe, the inner pipe is not in contact with the soil but is only supported at regular spacings by the outer pipe. Hence, the inertial response of the inner pipe due to seismic loads could be significant. Yet, since the inner pipe is confined by the outer pipe, the lateral displacements of the inner pipe with respect to the outer pipe are limited to the annular gap size.

7.3 REQUIRED SEISMIC AND SOIL DATA

Appropriate seismic and soils data must be assembled to allow for evaluation of the loadings and maximum responses of the buried facilities. The seismic environment must include estimates of peak ground acceleration (PGA), peak ground velocity (PGV) and peak ground displacement (PGD) defined at the ground surface appropriate for the hazard specification. Details on recommended procedures to be used to define the seismic environment at a particular site are presented in Chapter 3. If site specific evaluations are not available but broad banded ground response spectra anchored to PGA are used,

estimates of the PGV and PGD must be determined from other appropriate approximations. For a particular site, the approach used to estimate these parameters must be justified.

Sufficient data should be gathered to suitably categorize the foundation soils surrounding the buried piping and conduits, and to determine their appropriate parameters. These can be gathered using standard methods of foundation investigation, namely, standard borings to take SPT drive samples, cone penetrometer testing, seismic reflection surveys, crosshole, uphole and/or downhole geophysical testing, etc. Of specific interest for the program is to ascertain soils susceptible to liquefaction, densification leading to ground settlement, ground collapse at depth, near surface landslides and lateral spreading. Recommendations for appropriate geophysical and geotechnical field investigations as well as laboratory testing are presented in References 7.2 and 7.3. Such investigations must also suitably define changes of soil properties along the route of the buried facilities. If piping was or is placed in trenches, properties of backfill materials must also be included in the evaluation.

Soil properties of specific interest may include:

- grain size distribution description
- plasticity characteristics and Atterberg limits
- density and relative density
- equivalent SPT blow count information
- effective coefficient of subgrade reaction in both the horizontal and vertical directions
- liquefaction potential
- equivalent cyclic properties obtained from either site specific laboratory testing or generic data for appropriate soil types

Sufficient data must be available to allow for evaluation of the

loads induced on the buried system from relative movements between the ground and the piping caused by anticipated motions at the ground surface, as well as the potential for deep seated ground movements caused by seismically induced pore pressures and/or other ground failure or collapse conditions.

7.4 ANALYSIS LOADS AND CONDITIONS

When either analyzing or designing buried piping to withstand seismic effects, only those loadings which can normally be expected to occur during and immediately following the event need be considered. The following load conditions should be considered where appropriate.

1. Internal pressures: design pressure of the inner and annulus fluids, if any, including outer pipe pressure from postulated inner pipe leakage, and pressures induced during pressure testing.

2. External sustained loadings: deadweight of inner pipe; soil and surface loads for outer pipe. The type of buried pipe, method of installation and bedding characteristics should all be accounted for when determining the effects of these external loads (Reference 7.4).

3. Thermal expansion: thermal expansion effects of inner pipe treated as above ground piping; thermal expansion of the outer pipe accounting for the stiffness effects of the surrounding soil. Thermal movements of equipment connections must considered.

4. Natural soil settlements: vertical movement of tanks due to construction methods and normal filling and emptying processes.

5. Wave passage: effect of soil strains from seismic wave passage on outer pipe and transfer to inner pipe through

anchors and spacers.

6. Inertia: vibratory response of inner pipe subjected to motions compatible with the 5% damped ground response spectra. The vibratory response of pipe in direct contact with soil is not considered significant and need not be analyzed.

7. Oscillatory Seismic Anchor Motion (SAM): during wave passage, transient differential movements of buildings and other attachment points.

8. Permanent Seismic Anchor Motion (SAM): permanent vertical settlements due to densification of dry or partially saturated soil caused by ground shaking; dissipation of pore pressures developed in saturated soils; settlements due to consolidation or collapse of soft zones or voids at depth. Development of liquefaction conditions in soils immediately surrounding or below the buried pipe can lead to permanent vertical and horizontal movements of anchor points, or of pipe with respect to anchor points. The possibility of flotation of buried facilities with average densities less than that of the surrounding soils must also be considered.

9. Other Loadings: the analysis shall consider any other site specific loading not defined above. For example, the buried piping may extend through or adjacent to areas where slopes exist. The stability of these slopes must be assured for both normal operating conditions as well as the design seismic event including the potential effects of pore pressure development. Potential disruption of buried piping from ground failure due to slope instability and lateral spreading effects must be considered.

If unacceptable conditions are found to develop from any of the

conditions listed above, for example, from transient wave passage effects, permanent ground settlement and/or ground failure phenomena, alternate solutions must be developed to preclude failure of the buried piping, particularly for safety class piping. This approach must be followed for both new and existing facilities. Such procedures can include rerouting the piping, removal and replacement of poor soil surrounding the buried piping, application of soil stabilization procedures (e. g., grouting, densification, slope stabilization, permanent dewatering of affected areas), or supporting the buried piping on alternate supports such as pile supported cradles.

7.5 ANALYTIC METHODS AND PROCEDURES

Due to the complexity of the seismic problem as well as difficulty in assessing controlling properties of foundation soils, it is recommended that conservative methods of analysis be used to estimate stresses and strains developed by each load component and condition. Suitable variation in soil properties must be included in these evaluations to account for the normal variability in soil properties that can be expected at any site. The use of generic soil descriptions to define appropriate soil parameters in such analyses generally leads to consideration of broad variations in these controlling parameters. Therefore, site specific information, when available, which properly defines effective soil stiffness and strength as well as the character and density of bedding and trench soils surrounding the piping system can be used to minimize the degree of variability that must be considered in the analyses.

7.5.1 Design Internal Pressure Loads

For inner pipe, stresses due to design internal pressure can be calculated as in the case of aboveground piping. Internal pressure effects on outer piping is considered negligible. In older piping systems which consist of single-walled buried

piping, stresses due to internal pressure can be determined conservatively by neglecting the restraint provided by the surrounding soil. The internal pressure that may develop from leakage testing (e.g., pressure tests) must be considered in defining the design pressure.

7.5.2 External Soil Loadings

Standard methods of soil mechanics, such as those presented in References 7.4 and 7.5, can be used to assess external loadings developed on buried piping due to deadweight of surface soils as well as any design surface live loadings. The analyst should consider the combined behavior of both the foundation soils and the buried piping, suitably accounting for soil arching and the effects of potential hard spots, to arrive at estimates of stress and strain.

7.5.3 Inertial Response Analyses

For the case of piping not supported directly by the surrounding soil, the pipe is typically supported intermittently within other piping or support boxes and is free to move transversely within the outer pipe. Friction between the inner pipe and its supports will provide some restraining effects in the longitudinal direction. Otherwise, the response of the inner pipe can be expected to behave as conventional aboveground piping during a seismic event. Dynamic or equivalent static load methods of analysis are applicable to treat such inertial response modes of the pipe (References 7.10 and 7.25). A damping value of 5% is considered appropriate for these pipes. The design response spectra (defined typically as the free-field ground surface spectra) for the three directions of input should be applied and the results combined on a square-root-sum-of-squares (SRSS) basis. In view of the fact that the inner piping is anchored and supported by the outer piping, interaction effects between the two must be addressed.

7.5.4 Transient Differential Movements

For estimating stress resultants (forces and moments) due to transient seismic loadings, the recommendations presented in Reference 7.6 shall be utilized as supported by the analytic techniques and descriptions presented in References 7.1 and 7.8 through 7.16. Such stress resultants induced in both long straight sections of pipe as well as at critical locations such as at bends must be evaluated. For estimating transient ground displacements from wave passage effects, current procedures permit estimates due to assumed plane wave motion either across or parallel to the axis of the pipe.

Assuming a sinusoidal wave of a single wave type (compression or shear) traversing long straight sections of pipe, the maximum axial ground strain is found to be

$$(\epsilon_a)_{max} = \pm \frac{PGV}{\alpha_\epsilon C} \qquad (7.1)$$

where α_ϵ is either 1 or 2 depending upon whether the traversing wave type is a shear, compression or Rayleigh wave (Reference 7.6). Values of this coefficient for each wave type are presented in Table 7.1. The parameter C is the apparent wave velocity traversing the site and PGV is the peak ground velocity appropriate for the particular site and earthquake characteristics.

The specific value of the wave velocity and wave type to be used in any particular situation is in general not obvious and must be selected with care. If the buried pipe is located at a depth of 20 feet or more in ordinary soils, the effect of the Rayleigh wave at these depths can be considered negligible. For shallow buried systems located at large distances from a potential fault (beyond about 200 km), the effects of Rayleigh waves may predominate. For closer distances to a potential seismic source, body waves are generally the largest contributors to the

seismic hazard. In this case, the apparent horizontal wave velocity is often controlled by the deeper and higher velocity material at depth and not by the wave speeds of the soil immediately surrounding the piping system. For vertical motions, however, the local soil wave velocity may predominate.

For a uniform soil site overlying stiffer materials, the free-field ground motion tends to be dominated by shear waves propagating nearly vertically. In this case, the propagation velocity of the seismic wave at the ground surface is strongly influenced by the wave speed in the bedrock below (Reference 7.17). Based upon limited empirical observations (e.g., Reference 7.15), the use of shear wave velocities in Equation 7.1 less than about 2,000 fps (Reference 7.6) leads to overly conservative strain estimates. For vertical runs of pipe, it is recommended that PGV for vertical motions be used in Equation 7.1 together with the local P-wave velocity to treat wave passage effects.

7.5.4.1 Axial Differential Ground Movements

The maximum axial force that may be induced in long straight sections of buried pipes by the axial ground strain is controlled by the ability of the surrounding soil to transmit loads to the pipe through friction. Considering the ground wave to vary sinusoidally as it traverses the site, the maximum ground strain that can be developed will occur over a quarter wave length of the predominant seismic wave associated with the peak ground velocity. Thus, the maximum axial strain that can be transmitted to the buried pipe through shear is limited to

$$(\epsilon_a)_{max} \leq (\epsilon_a)_{sh} \qquad (7.2)$$

where

$$(\epsilon_a)_{sh} = \left[\frac{F_{max} L_w}{4 E_{sct} A_p}\right] \qquad (7.3)$$

where L_w is the dominant wave length of the passing seismic wave, E_{sct} is the secant modulus of elasticity of the buried pipe, A_p is the net cross-sectional area of the pipe, and F_{max} is the maximum force that can be developed in the pipe defined below. The dominant wave length L_w can be estimated from the site response spectrum using the relation $L_w = C/f_d$ where C is the apparent wave velocity and f_d is the cyclic frequency at which the peak spectral velocity occurs (typically of the order of 1 hz). For straight sections of a pipe whose length is less than $L_w/4$, the peak axial strain in the pipe will be proportionally less than $(\epsilon_a)_{sh}$ from Equation 7.3.

The maximum force per unit length F_{max} that can be transmitted through friction to the pipe is related to the characteristics of both the pipe (pipe material, surface condition) and the soil (soil density and gradation, soil confining pressure, etc.). For the general case of a soil possessing both frictional and cohesive strength components, the shear force per unit length of pipe can be estimated from:

$$F_{max} = (\pi D)\ [C_a + \sigma_n \tan(\phi_a)] \qquad (7.4)$$

where

$$\sigma_n = [\gamma H\ (1 + K_o)/2] + [W_p/\pi D]$$

σ_n = average normal pressure between the soil and pipe due to soil weight as well as surcharge loadings and weight of pipe itself and its contents
D = pipe diameter
C_a = soil adhesion (units of stress)
ϕ_a = apparent angle of pipe wall friction (degrees)
K_o = coefficient of soil pressure at rest
γ = soil unit weight
W_p = weight of pipe and its contents per foot of pipe

Soil properties to use in these evaluations can be estimated

from laboratory test data for site specific soils or from generic data for particular soil types. Suitable variation in soil properties should be considered in the analyses to account for variability in soil properties typically encountered at the site. In general, when evaluating transient loadings, the shear strength parameters should be obtained from consolidated-undrained test results while consolidated-drained results can be used to assess permanent effects of relative displacement. For typical soil types, estimates of the adhesion and apparent friction angle between the pipe wall and the soil are provided in Tables 7.2 and 7.3 for the case of soils bearing against either concrete or steel buried piping or conduits.

7.5.4.2 Transverse Differential Ground Movements

Again assuming passage of sinusoidal waves of a single type traversing long straight runs of pipes, the maximum curvature of the ground can be estimated from (Reference 7.6) as

$$(\kappa)_{max} = \pm \frac{(PGA)}{(\alpha_\kappa C)^2} \qquad ((7.5)$$

where C is the apparent wave speed of the seismic motion discussed previously, PGA is the maximum ground acceleration of the seismic wave and α_κ is a wave coefficient dependent on the wave type and listed in Table 7.1. For pipes of diameter less than about 48 inches, bending strains computed from Equation 7.5 for straight sections of pipe are usually found to be negligible. However, sufficient rotational capacity should be provided at the pipe joints to accommodate the computed curvature.

7.5.5 Pseudostatic Beam-On-Elastic-Foundation Analyses

Since the outer pipe is buried within the soil, it is directly exposed to seismic motion effects, both transient and long-term, and can therefore be treated by pseudostatic

beam-on-elastic-foundation models. This pseudostatic approach is appropriate for piping directly buried in soil since inertial effects between the piping and the soil during wave passage transients can be considered negligible. For designs with both inner and outer pipes housed within concrete or tile boxes or caissons, both the inner and outer piping can be analyzed as aboveground piping, with the box enclosure then treated by the pseudostatic beam-on-elastic-foundation methods.

The recommendations presented herein are based on the methods of analysis summarized in References 7.1, 7.6 and 7.8 through 7.16 which are in general use and which have been keyed to available empirical data. These methods are based on representation of the piping system, including both straight and curved sections, with relatively simple beams supported on elastic foundations modeled as simple linear Winkler springs. One aspect that needs to be considered in the pipe stress analysis using the beam-on-elastic-foundation approach is the potential increase in outer pipe stiffness due to the presence of the inner pipe. More rigid pipe generally leads to higher pipe strains and stresses, particularly at elbows, due to the applied soil displacement profiles. The effect of this added stiffness should be assessed.

7.5.5.1 Normal Operating Thermal Loads

In the simplified beam-on-elastic-foundation approach, pipe stresses due to thermal loads can be calculated similarly as in the case of seismic loads. The maximum axial strain due to thermal expansion along the straight pipe run is first determined. This strain is then used to compute pipe stresses at elbows, bends and tees using the appropriate beam-on-elastic-foundation formulae established for these configurations (Reference 7.18).

7.5.5.2 Selection of Coefficients of Subgrade Reaction

As mentioned above, the maximum forces and moments developed in long straight sections of pipe typically do not lead to the maximum stress conditions in the pipe or conduit. Rather, the controlling condition usually occurs at pipe bends and elbows as a result of differential motions developed from the wave passage effect. The effects of changes in direction, size and material of the buried structure must be considered for a complete evaluation of critical conditions. From the maximum ground strain estimates obtained from the analyses of long straight sections of pipe, the forces and moments developed at these critical locations can be determined by following the procedures as outlined in References 7.1 and 7.8 through 7.15 for typical pipe elements and particular configurations. Typically, the buried piping system is analyzed as a series of beam elements on an elastic foundation, requiring the assumption of coefficients of subgrade reaction for the soil/pipe system. Sufficient variability must be incorporated in this calculation since the parameters of the usual coefficients of subgrade reaction are not well founded by either theory or experiment.

The coefficient of subgrade reaction is a simplified concept that has often been used to assess pseudo-static interaction between buried structures (foundations, buried piping, piles, etc.) and the surrounding soil (References 7.4 and 7.5). Unfortunately, the simple one-parameter coefficient of subgrade reaction (Winkler spring coefficient), even for the ideal case of linear soil stress-strain behavior, does not properly account for shear transfer between adjacent points in the soil. Therefore, approximate comparisons with elastic solutions lead to a stiffness parameter which is a function of both the structural and soil properties. For real soils, the stiffness parameter is found to be also related to soil type, depth of burial, direction of loading (horizontal or vertical), strain

level developed, etc. The representation of this complex interaction with a single parameter has given rise to the many recommendations presented in the open literature (Reference 7.5).

For long straight sections of piping, induced moments and stresses are found to be relatively insensitive to the specific value of the stiffness parameter, except for the relatively unusual case of piping traversing areas of significantly different soil properties. Unfortunately, induced loads computed at or near pipe bends and structural intersection points can be strongly dependent on the specific value of the coefficient. It is, therefore, important that conservative estimates of this coefficient be selected for any analysis. This is typically accomplished by incorporating the effects of variability in this parameter on the computed stress resultants. It should be noted that, for buried piping analyses, conservative estimates of the subgrade modulus, which maximize computed pipe stresses, tend to lie on the stiffer side of the range of potential variability. This is different from the normal assumptions of foundation analyses which typically are made to underestimate the stiffness parameter so as to overestimate settlement values.

Due to the greater uncertainty associated with the selection of the subgrade modulus, the analyses performed should incorporate a wider variation in the modulus than is typically used in standard soil-structure interaction analyses so as to lead to bounding estimates of induced loading. It should be noted that the use of site specific measurements can be used to reduce the variability in parameters that must be incorporated into the evaluations since the recommendations for generic soils incorporate such wide variations in the appropriate coefficients.

The form of the reaction-displacement relations required to perform the analysis of buried piping is as shown in Figure 7.1. In each case, the soil reaction to the specified displacement can be approximated by means of a linearly varying relationship to a maximum value defined by the soil strength as well as the piping configuration (pipe diameter, trench width, depth, etc.). The slope of the straight line segment (with dimension of pressure per unit displacement such as pci) is defined as the coefficient of subgrade reaction. For application to simple beam models, the Winkler spring coefficient is then defined as the product of the coefficient of subgrade modulus and the pipe diameter (with units of pounds per inch of beam length per inch of deflection, such as psi).

For the case of piping placed near the surface in uniform soils, with a soil cover of several diameters, the effective subgrade modulus in the horizontal direction, k_h, can normally be expected to be larger than the vertical modulus, k_v, since the resistance of the soil cover above the piping is less effective for resisting displacement. For example, some test data on piping placed in uniform clays indicates that the subgrade modulus in the horizontal direction is approximately 1.6 times the vertical modulus. The relation between horizontal and vertical moduli in any particular case depends upon several factors, such as the thickness of soil cover over the piping, and compaction characteristics of the bedding soil as well as the soil to the sides of and above the piping. If the pipe is buried at least three pipe diameters, it is recommended that the horizontal stiffness be selected at least equal to the vertical stiffness, unless special conditions indicate such is not the case.

7.5.5.2.1 Transverse Stiffness from Plate Load Testing

Estimates of in-situ stiffness can be obtained from simple field tests using plate loads, although such test results tend to underestimate the stiffness of fully confined soils. In

addition, the results quoted from such tests are typically associated with shear strains in the range of 0.1% to 1%, higher than the strains associated with the initial slope of the load-displacement curve. The stiffness from these tests can be increased by a factor of about 2 to arrive at results appropriate or the lower strain levels associated with the vibratory problem.

In addition, if the plate load test is conducted using a 1-foot diameter rigid plate, the slope of the pressure-displacement curve must be suitably modified to account for the difference between the pipe and plate diameter; that is:

$$k_s = k_{s1} f(D) \tag{7.6}$$

where k_{s1} is the coefficient of subgrade reaction for the 1-foot diameter plate and f(D) is a function of the pipe diameter, D, as well as the soil type. For plate tests conducted on the surface of sandy soils, the experimentally determined relationship is found to be

$$k_s = k_{s1}\left[\frac{D + 1}{2D}\right]^2 \tag{7.7}$$

while for typical cohesive soils, the relationship is

$$k_s = k_{s1}\left[\frac{1}{D}\right] \tag{7.8}$$

Typical values of the coefficient of subgrade reaction from plate load tests are listed in Tables 7.4 and 7.5.

7.5.5.2.2 Analytical Estimates of Transverse Stiffness

Based upon the results of comparisons of Winkler solutions with uniform halfspace solutions for infinitely long beams on the surface of the halfspace and subjected to vertical point loads, Vesic (Reference 7.19) found an effective Winkler spring coefficient in terms of parameters of both the halfspace

material and the beam in the following form:

$$k_o = \frac{0.65 E_s}{1 - \nu^2}\left[\frac{E_e D^4}{E_b I_b}\right]^{1/12} \qquad (7.9)$$

where

k_o = Winkler spring coefficient in units of force per unit beam length per unit beam deflection
E_s = elastic modulus of the halfspace soil
ν = Poisson's ratio of the halfspace material
D = effective width of the beam, or pipe diameter in this case
E_b = elastic modulus of the beam
I_b = moment of inertia of the beam

In application, the effective modulus of the soil E_e to use in Equation 7.9 must be selected with care, since it is a function of depth for most soils although the analytic solution assumes uniform properties with depth. The coefficient of subgrade modulus is then related to Vesic's solution by

$$k_s = k_o/D \qquad (7.10)$$

An alternative formulation was developed (Reference 7.18) by comparing analytic solutions with some limited test data on buried piping. The result for the horizontal direction, which is appropriate for pipes buried in trenches with backfill soils compacted to a medium dense condition, can be written as

$$k_s = \frac{1}{(0.15B)}\left[\frac{\gamma H D N_{qh}}{0.04\left(H + \frac{D}{2}\right)}\right] \qquad (7.11)$$

where

H = depth to the top of the pipe
D = pipe diameter
γ = backfill density
N_{qh} = bearing capacity factor for horizontal displacements

The bearing capacity factor, N_{qh}, is itself a function of depth of burial of the pipe. For the case of a pipe buried about 3 pipe diameters, the value of N_{qh} is approximately 8. The value of k_s found from either Equation 7.10 or 7.11 (References 7.18 or 7.19) leads to similar estimates which correspond to the generic values indicated in Tables 7.4 and 7.5.

Considering the wide range of potential variability in these parameters for typical soils, either approach (i.e., Equation 7.9 or 7.10) can be used to obtain appropriate estimates of the coefficient of subgrade reaction. Again, if generic soil properties are used to select Winkler spring coefficients, sufficient variability in these properties must be considered to compute appropriate stress resultants. Site specific data, if available, can be used to limit the amount of variability that can be justified.

7.5.5.2.3 Axial Stiffness Estimates

The effective axial stiffness used in the elastic foundation model for the soil surrounding the pipe is based upon studies of pile behavior subjected to axial loads (Reference 7.18). For example, the displacement required to develop the full adhesion force on a pile which is 12 inches in diameter is estimated to be 0.2 to 0.5 inch. A knowledge of the maximum frictional force, as specified in Equation 7.4, together with the displacement estimate for full mobilization leads to an estimate of axial stiffness of

$$\frac{25\ F_{max}}{D} \leq k_{oa} \leq \frac{60\ F_{max}}{D} \qquad (7.12)$$

where F_{max} is the shear force per unit length as defined in Equation 7.4, and D is the pipe diameter. The Winkler spring coefficient in the axial direction, k_{oa}, has units of force per length of pipe per unit displacement (such as psi) and is directly used in the beam-on-elastic-foundation analysis.

7.5.5.2.4 Limiting Values of Lateral Load

The upper bound values of reaction or yield values of the pressure-displacement curves of Figure 7.1 for each displacement mode of interest can be estimated from bearing capacity relations available in the literature, a summary of which is provided in Reference 7.18. For vertical displacements, the limit on pressure due to upward pipe displacement is controlled by the breakout capacity of the trench material above the pipe. These limiting loads in both the horizontal and vertical directions typically tend to reduce the computed maximum moments from linear analyses.

7.5.5.2.5 Discretization Recommendations

When using analytic solutions for beam-on-elastic-foundation models, stresses, displacements, etc., are written directly in terms of the system characteristic parameter defined by

$$\beta = \left[\frac{k_o}{4\ E_b\ I_b}\right]^{1/4} \qquad (7.13)$$

where k_o is the Winkler lateral stiffness coefficient and E_bI_b is the beam stiffness of the pipe. This parameter relates soil and beam stiffnesses, and controls the magnitude of responses. Unfortunately, analytic solutions are available for only the simplest of pipe problems. For the vast majority of problems, with pipes of differing diameters, intersection of pipe segments, and/or possibly differing stiffness parameters, the finite element procedure is typically utilized. In this method, short beam elements are modeled along the straight and curved sections of the pipe route and are connected to each other at their ends. Special elements can be added to represent specific sections (e.g., elbows and tees) and also springs representing soil connections placed at the ends of each finite element. In such a model, the accuracy of the computed stresses in regions

of significant bending is directly related to the discretization selected.

In regions of high bending (near concentrated loads or at pipe bends), the pipe displacements generally decrease relatively rapidly with distance from the discontinuity. The length of this zone is sometimes called the "bearing span" and is estimated to be

$$L_b = \frac{3\ \pi}{4\ \beta} \qquad (7.14)$$

Within this distance from the discontinuity, spacing of the Winkler springs should be limited to about 1.5 to 2 times the pipe diameter to obtain reasonable accuracy in the computed stresses. For zones away from these points of discontinuity, discretization of soil springs could be relaxed since changes in bending moment per element decrease. Additional discussions of these considerations are presented in the sample problem presented in Appendix I.

7.5.5.3 Support Anchor Movements (SAM)

In addition to the stresses developed in the buried piping system from the wave passage effects discussed previously, stresses induced in the piping system from relative movement at anchor points and other building attachment points must also be considered. These support anchor movements (SAMs) can be caused by both time dependent wave passage effects as well as long term or permanent ground displacements associated with ground settlements and/or horizontal movements as described in Section 7.5.5.4 following.

It is usual when considering the effects of SAMs on the piping system to perform static analyses, using the analytic procedures associated with the beam-on-an-elastic-foundation model (Winkler spring method). The assumed static displacement profile placed

on the system must be selected with care so as to arrive at conservative estimates of peak stresses. In some cases, it is reasonable to assume full out-of-phase displacements leading to maximum stress estimates. In other cases, the anchor point displacements may not reach their maxima at the same time, so that assuming full out-of-phase conditions may be overly conservative. In addition, for systems with more than two support points, the selection of worst case conditions may not be obvious. One approach which has been used in such situations is to place the peak SAM on the system, one support point at a time, and to use SRSS combination of the peak stresses computed from each case to obtain conservative estimates of the combined stress. Finally, as recommended in Reference 7.6, the stress resultants computed for anchor point movements can be combined with those computed for wave passage effects using the SRSS method.

7.5.5.4 Permanent Differential Ground Movements

Both horizontal and vertical long term total and differential ground displacements must be estimated to account for gross settlement or consolidation of foundation soils as well as potential movements of building attachment points. Stress resultants (forces and moments) induced by these movements can then be estimated by considering the buried piping to be supported on an elastic foundation. The stiffness coefficients selected for the analysis of long term response should take into account any differences in soil behavior associated with the effects of long term loading as opposed to the effective stiffness associated with the short durations associated with wave passage effects. Again, sufficient variability in soil stiffness properties must be included in the analysis to assess worst case conditions.

A summary of approaches to evaluate the potential of inducing permanent settlements from a variety of sources is presented in

Reference 7.20. For example, earthquakes have caused settlements of dry cohesionless sandy deposits which are related to their densification due to the seismic environment. Standard procedures are available (References 7.21 and 7.22) to estimate induced vertical strain levels from the maximum cyclic shear strains developed in the soil layer during the seismic loading. The cyclic shear strains are typically computed from the equivalent linear analysis for upward propagation of shear waves.

For the case of saturated soils, the decrease in soil volume that can occur with dissipation of the excess pore pressures can also lead to ground settlements. Similar one-dimensional analysis procedures can be used to estimate effective shear stresses and strains in the saturated soil column. Induced pore pressures developed in the soil column by this cyclic loading can, in turn, be estimated from either empirical data or from laboratory cyclic loading tests from which vertical strains and settlements can be estimated (References 7.23 and 7.24). When pore pressure ratios (ratio of pore pressure to effective soil pressure) are less than unity, full liquefaction of the soil does not occur. When induced pore pressure ratios reach levels approaching unity, the potential for full liquefaction must be considered. If driving shear stresses are available which equal or exceed the available shear strength of the soil, a complete loss of strength can develop which may lead to flow slides and settlement of heavy structures.

The induced inertial loads developed during such an event can lead to cracking and movements of embankments and earth slopes, both with and without pore pressure effects. Simplified procedures available to treat these slope stability problems are based on static methods of analysis by incorporating horizontal and/or vertical inertial loading components into traditional slide analyses and computing gross safety factors. Such

procedures should be used with extreme caution since large errors are possible. Unless stability numbers or safety factors are sufficiently high, dynamic methods of analysis are recommended to assess slope stability. As mentioned above, rigorous analytic treatment of the response of buried facilities to these potential movements is in general not practical. Therefore, conservative procedures must be adopted to ensure that ground failure does not occur. Standard procedures to estimate liquefaction potential (such as are summarized in Reference 7.20) of a particular site are available to assess the importance of this phenomena.

7.6 DESIGN CONSIDERATIONS

It is intended that the criteria presented herein be consistent with the operational and functional requirements of the facility. Basic design guidelines for all mechanical and fluid systems, both hazardous and nonhazardous, are provided in DOE Order 6430.1 "General Design Criteria Manual."

7.6.1 General Considerations

The following general considerations are presented for guidance in the design of new facilities or for evaluation of existing buried piping systems.

(a) System Requirements:

Safety class buried piping systems must satisfy the non-seismic requirements described in 40 CRF 264 and 265. The selection of specific pipe sizes must consider flow and viscosity requirements, soil and fluid pressures, thermal and seismic effects as well as the potential degradation of material properties (such as by radiation and corrosion). In general, the effects of seismic loadings on nonsafety class systems need not be considered. However, the impact of their failure on safety class equipment must be considered.

(b) Bedding and Backfill Soils:

Bedding and backfill soils placed against safety class buried piping shall be free of any rocks, cobbles or boulders or other extraneous materials which may damage the piping by creating hard points on the piping surface. For new construction, the bedding and backfill soils shall be composed of clean sands with maximum grain sizes passing the No. 4 sieve and no more than 12% by weight passing the No. 200 sieve. A minimum of six inches of the clean sand shall be placed around the entire piping.

For new construction, bedding sands shall be compacted to 95% Standard Proctor dry density. Backfill sands shall be compacted using procedures that will not damage the pipe, and in a manner so as to provide complete coverage. Flooding methods can be used to ensure compaction and coverage if no other safety considerations are violated.

7.6.2 Design Criteria for Steel Piping and Components

New safety class buried steel piping is considered in this section to be double-walled welded steel pipe which meets the requirements of the ASME Boiler and Pressure Vessel Code, Section III, Division I, Class 2 or ANSI/ASME B31.3. For purposes of use with the criteria equations discussed below, the resultant moment at any pipe section may be calculated by SRSS of the moments computed in the three orthogonal directions, or:

$$M_j = \left[M_{xj}^2 + M_{yj}^2 + M_{zj}^2\right]^{1/2} \qquad (7.15)$$

where M_{xj}, M_{yj}, M_{zj} = moments at a given section in the three principal directions

M_j = resultant moment due to loading j

(a) Loading Conditions:

The analysis of the buried piping system must address the

loading conditions specified in Section 7.4 and the stress and strain combinations of this section.

(b) Inner Piping:

The stress criteria specified herein are intended to ensure the structural integrity and to maintain the pressure boundary integrity of the inner piping. For the purposes of these analyses, the stress equations are written in the nomenclature of the ANSI/ASME B31.1 Code (Reference 7.25).

(i) The effect of seismically induced inertial loads on underground piping shall meet the following equation when the inner piping is not in direct contact with the soil:

$$\left[\frac{P\ D_o}{4\ t_n}\right] + 0.75\ i\ \frac{M_{DW} + M_I}{Z} \leq 3\ S_h \qquad (7.16)$$

but not greater than $2S_y$, where

i = stress intensity factor
P = internal design pressure
D_o = outside pipe diameter
t_n = nominal pipe wall thickness
M_{DW} = resultant moment from deadweight and other sustained loads
M_I = resultant moment from piping seismic inertia response;
Z = section modulus of pipe
S_h = allowable stress value given in Table I-7.1 or I-7.2 of Reference 7.26
S_y = minimum yield stress from Table I-7.1 or I-7.2 of Reference 7.26

(ii) In addition to meeting the requirements for inertial loads, the combined effect of thermal expansion and seismic anchor motions (non-inertial, soil

displacement controlled) loads, which include the effect of wave passage and building anchor movements, shall meet the following equation:

$$\frac{F_C + F_{DISP}}{A} + 0.75\, i \frac{(M_C + M_{DISP})}{Z} \leq 3\, S_h \qquad (7.17)$$

but be not greater than $2S_y$, where

F_C = axial force from thermal expansion
F_{DISP} = axial force from seismic loads due to both anchor movement as well as wave passage
A = pipe cross-sectional area
M_C = range of resultant moments due to thermal expansion of piping system and attached equipment
M_{DISP} = resultant moment from seismic loads due to both anchor movements as well as wave passage; use half the range

Other notations have been defined for Equation 7.16.

For purposes of Equation 7.17, the resultant moment (and forces) from seismic anchor motions shall include the maximum of short term and long term effects. For short term effects, the resultant moment M_{DISP} can be found from:

$$M_{DISP} = \left[M_{WP}^2 + M_{O\text{-}SAM}^2\right]^{0.5} \qquad (7.18)$$

where M_{WP} is the moment induced in the pipe by distortion during wave passage, while $M_{O\text{-}SAM}$ is the moment induced by anchor movement caused by motions of the tank or building attachment points. For long term effects, the resultant M_{DISP} is the moment induced by long term settlement of the ground.

(iii) If Equations 7.16 and 7.17 cannot be met, the piping design is still considered acceptable if the maximum piping strain amplitude due to axial plus bending loads is less than 2% for stainless steel and less

than 1% for carbon steel (Reference 7.27), that is,:

$$\epsilon_t \leq 2\% \text{ for stainless steel} \quad \leq 1\% \text{ for carbon steel} \tag{7.19}$$

In addition, the axial compressive strain in Equation 7.17 should be limited to

$$\epsilon_{axial} \leq \frac{0.2}{(R/t_n)} \tag{7.20}$$

to avoid compressive wrinkling. In Equation (7.20), R is the nominal pipe radius and t_n is the nominal pipe wall thickness.

To evaluate the piping system to higher strains would generally require inelastic or nonlinear analyses. However, in lieu of conducting such an analysis, a stress-strain correlation technique may be used (Reference 7.27). For pipe diameter/thickness ratios less than 50, the maximum strain can be calculated as:

$$\epsilon_t = K_s \frac{\sigma_e}{E} \tag{7.21}$$

where

ϵ_t = maximum piping membrane-plus-bending strain

K_s = strain correlation factor, set to 5 for carbon steel, 6.66 for stainless steel (including the effect of strain hardening exponent)

σ_e = elastically calculated stress due to pressure and bending loads (left hand side of Equation 7.17)

E = Young's modulus at operating temperature.

(c) Outer or Containment Piping:

The following stress criteria specified are intended to ensure that the structural integrity of the outer piping will be maintained.

(i) Meet Equations 7.16 and 7.17 if the outer pipe is not in direct contact with the soil. If the pipe is in contact, the effects of inertial response are considered negligible.

(ii) Meet Equations 7.17, 7.18 and 7.21 for the combined effect of thermal, expansion anchor motion and seismic (non-inertial, soil displacement controlled) loads, which include the effects of wave passage and building anchor movements.

(iii) If Equation 7.17 cannot be met for seismic anchor movements due to ground settlement, the piping design is still considered acceptable if the total strain due to axial plus bending loads does not exceed 4% for piping sections other than at branch connections or 2% for piping sections containing branch connections. To minimize the potential effects of compressive wrinkling, the maximum axial compressive strain should be limited by Equation 7.20. The simplified stress-strain correlation technique of Equation 7.21 may be applied.

(d) Inner Piping Supports:

The inner piping support stresses shall not exceed 1.2 S_y, where S_y is the material yield stress at the temperature, when elastic analysis is performed.

(e) Material Condition:

The design criteria in this section are based on nominal material properties. Degradation in material condition may result in failures at lower stress and strain levels. Material degradation must be avoided by design (corrosion protection, material selection, corrosion allowances, etc.), by periodic inspections or by properly accounting for the effects of

degradation mechanisms on pipe stress and strain.

7.6.3 Design Criteria for Concrete Conduits

Concrete components of any piping system, which may be used to provide added strength to the steel piping, shall be designed and fabricated to meet the general requirements of the applicable version of the ACI Code 349-85 (Reference 28). Compressive strains developed in the concrete shall be limited to no more than 0.3%. Tensile requirements shall be controlled by the amount of reinforcing steel added to the concrete as specified in the ACI Code. If it is required to prevent any cracking from developing in the concrete, tensile strains should be limited to

$$\epsilon_t = 7.5\frac{[f_c']^{0.5}}{E_c} \qquad (7.22)$$

where f_c' is the strength and E_c is the elastic modulus of the concrete, both in psi units.

REFERENCES

7.1 "Seismic Response of Buried Pipes and Structural Components," ASCE Structural Division Committee on Nuclear Structures and Materials, ASCE, New York, 1983.

7.2 U.S. Nuclear Regulatory Commission, Regulatory Guide 1.132, "Site Investigations for Foundations of Nuclear Power Plants," Rev. 1, March 1979.

7.3 U.S. Nuclear Regulatory Commission, Regulatory Guide 1.138, "Laboratory Investigations of Soils for Engineering Analysis and Design of Nuclear Power Plants," April 1978.

7.4 Spangler, M.G., and Handy, R.L., "Soil Engineering," Fourth Edition, Harper & Row, New York, 1982.

7.5 Winterkorn, H.F., Fang, H.Y., "Foundation Engineering Handbook," Van Nostrand and Reinhold, 1975.

7.6 American Society of Civil Engineers, Standard 4-86, "Seismic Analysis of Safety-Related Nuclear Structures and Commentary on Standard for Seismic Analysis of Safety Related Nuclear Structures," September 1986.

7.7 U.S. Nuclear Regulatory Commission, "Standard Review Plan, NUREG 0800," Sections 3.7.1 through 3.7.3, Rev. 2, August 1989.

7.8 Newmark, N.M., "Problems in Wave Propagation in Soil and Rock," Proceedings of the International Symposium on Wave Propagation and Dynamic Properties of Earth Materials, Albuquerque, NM, August 1968.

7.9 Newmark, N.M., "Earthquake Response Analysis of Reactor Structures," Nuclear Engineering & Design, Volume 20, 1972.

7.10 Shah, H.H., and Chu, S.L., "Seismic Analysis of Underground Structural Elements," ASCE, Journal of the Power Division, Vol. 100, No. P01, July 1974.

7.11 Yeh, G.C.K., "Seismic Analysis of Slender Buried Beams," Bulletin of the Seismological Society of America, Volume 64, No. 5, October 1974.

7.12 Iqbal, M.A., and Goodling, E.C., "Seismic Design of Buried Piping," Second ASCE Specialty Conference on Structural Design of Nuclear Plant Facilities, New Orleans, LA, 1975.

7.13 Goodling, E.C., "Flexibility Analysis of Buried Piping," Joint ASME/CSME Pressure Vessels and Piping Conference, Montreal, Canada, June 1978.

7.14 Goodling, E.C., "Seismic Stresses in Buried Elbows," ASCE National Convention, Boston, MA, 1979.

7.15 Goodling, E.C., "Buried Piping - An Analysis Procedure Update," International Symposium on Lifeline Earthquake Engineering, Fourth U.S. National Conference on Pressure Vessels and Piping Technology, ASME, Portland, OR, 1983.

7.16 Lin, C.W., "Seismic Analysis of Buried Piping," Transactions SMIRT 11, Volume K, pp. 429, Tokyo, Japan, August 1991.

7.17 Newmark, N.M., and Hall, W.J., "Development of Criteria for Seismic Review of Selected Nuclear Power Plants," NUREG/CR-0098, May 1978.

7.18 "Guidelines for the Seismic Design of Oil and Gas Pipeline Systems," American Society of Civil Engineers, 1984.

7.19 Vesic, A., "Bending of Beams Resting on Isotropic Elastic Solids," Proceedings, American Society of Civil Engineers, Engineering Mechanics Division, EM2, Volume 87, pp. 35-51, April 1961.

7.20 Ferritto, J.M., "Evaluation of Earthquake Induced Ground Failure," Technical Report of Subcommittee 7, Interagency Committee on Seismic Safety in Construction, U.S. Department of Interior, Geological Survey, 1982.

7.21 Seed, H.B., and Silver, M.L., "Settlements of Dry Sands During Earthquakes," Journal Geotechnical Division, ASCE, April 1972.

7.22 Silver, M.L., and Seed, H.B., "Volume Changes in Sand During Cyclic Loading," Journal SMFE Div., ASCE, September 1971.

7.23 Castro, G., "On The Behavior of Soils During Earthquakes - Liquefaction," Soil Dynamics and Liquefaction, A.S. Cakmak, Editor, Elsevier, 1987.

7.24 Seed, H.B., Tokimatsu, K., Harden, L.F., and Chung, R.M., "Influence of SPT Procedures in Soil Liquefaction Resistance Evaluations," Journal Geotechnical Division, ASCE, December 1985.

7.25 ANSI/ASME B31.1-1992, Power Piping.

7.26 ANSI/ASME B31.3-1993, Chemical Plant and Petroleum Refinery Piping.

7.27 Stawniczy, G., Bak, W.R., and Hau, G., "Piping Stress-Strain Correlation for Seismic Loading," Journal Pressure Vessel Technology, Volume 110, November 1988.

7.28 American Concrete Institute, "Code Requirements for Nuclear Safety-Related Concrete Structures (ACI 349-85) and Commentary - ACI 349R-85," 1985.

7.29 ASME Boiler and Pressure Vessel Code, Nuclear Code Case N-411-1, "Alternative Damping Values for Response Spectra Analysis of Class 1, 2 and 3 Piping, Section III, Division 1," February 1986.

7.30 Lin, C.W., "Criteria for Seismic Analysis of Buried Piping," ASME PVP Vol. 237-1, pp. 171-174, 1992.

7.31 American Society of Mechanical Engineers, "ASME Boiler and Pressure Vessel Code, Section III, Rules for Construction of Nuclear Power Plant Components, Division 1, Subsection NC," 1986 Edition.

NOTATION

A pipe cross sectional area

A_p net cross sectional area of the pipe

C apparent wave velocity traversing the site

C_a soil adhesion

D pipe diameter

D_o outside pipe diameter

E_b elastic modulus of the beam (pipe)

E_c elastic modulus of the concrete

E_s elastic modulus of the halfspace soil

E_{sct} secant modulus of elasticity of the buried pipe

f'_c strength of the concrete

f_d cyclic frequency at which the peak spectral velocity occurs

F_c axial force from thermal expansion

F_{disp} axial force from seismic loads due to anchor movement and wave passage

F_{max} maximum force that can be developed in the pipe

H depth to top of the pipe

i stress intensity factor

I_b moment of inertia of the pipe

k_o Winkler spring coefficient

k_{oa} Winkler spring coeeficient in the axial direction

k_s coefficient of subgrade modulus

k_{s1} coefficient of subgrade reaction for the 1-foot diameter plate

K_o coefficient of soil pressure at rest

K_s strain correlation factor

L_b length of the "bearing span"

L_w dominant wave length of the passing seismic wave

M_c range of resultant moments due to thermal expansion of piping system and attached equipment

M_{disp} resultant moment from seismic loads due to both anchor movements as well as wave passage; use half the range

M_{DW} resultant moment from deadweight and other sustained loads

M_I resultant moment from piping seismic inertia response

M_j resultant moment due to M_{xj}, M_{yj}, and M_{zj}

M_{O-SAM} moment induced by anchor movement caused by motions of the tank or building attachment points

M_{WP} moment induced in the pipe by distortion during wave passage

M_{xj} moment at a given section in the pipe about the X-axis

M_{yj} moment at a given section in the pipe about the Y-axis

M_{zj} moment at a given section in the pipe about the Z-axis

N_{qh} bearing capacity factor for horizontal displacements

P internal design pressure

PGA peak ground acceleration

PGD peak ground displacement

PGV peak ground velocity

R nominal pipe radius

S_h allowable stress value given in Table I-7.1 or I-7.2 of Reference 7.26

S_y minimum yield stress from Table I-7.1 or I-7.2 of Reference 7.26

SAM seismic anchor motion

SPT standard penetration test

SRSS square-root-sum-of-squares

t_n nominal pipe wall thickness

W_p weight of pipe and its contents per foot of pipe

Z section modulus of pipe

α_ϵ coefficient equal to either 1 or 2 depending on whether the traversing wave type is a shear, compression or Rayleigh wave

β system characteristic parameter

γ soil unit weight
backfill density

$(\epsilon_a)_{max}$ maximum axial ground strain

$(\epsilon_a)_{Sh}$ maximum axial strain transmitted through shear

ϵ_{axial} axial compressive strain to avoid compressive wrinkling

ϵ_t maximum piping membrane-plus-bending strain
tensile strain in the concrete

$(\kappa)_{max}$ estimate of the maximum curvature of the ground

ν Poisson's ratio of the halfspace material

σ_e elastically calculated stress due to pressure and bending loads

σ_n average normal pressure between the soil and the pipe

ϕ_a apparent angle of pipe wall friction (degrees)

Table 7.1 Seismic Coefficients for Estimating Ground Strain (Reference 7.6)

Coefficient	Compression Wave	Shear Wave	Rayleigh Wave
α_ϵ	1.0	2.0	1.0
α_κ	1.6	1.0	1.0

Table 7.2 Effective Friction Angle (ϕ_a) in Degrees

Soil Type	Concrete		Steel Pipe	
	Against Soil	Formed	New	Rustled
Sand & gravel mixtures	29-31	22-26	22	29
Fm Sands, silty cm sands	24-29	17-22	17	24
f Sands, silty fm sands	19-24	17	14	20
Nonplastic silts, sandy silts	17-19	14	11	16
Very stiff clays	22-26	18	15	15
m stiff to stiff clays	17-19	13	10	15

f = fine, m = medium, c = coarse grain size descriptor

Table 7.3 Effective Adhesion (C_a) For Cohesive Soils (in psf)

Soil Consistency	Cohesive Strength C	Effective Adhesion C_a
Very soft	0-250	0-250
Soft	250-500	250-500
Medium stiff	500-1000	500-750
Stiff	1000-2000	750-950
Very stiff	2000-4000	950-1300

Table 7.4 Typical Plate Load Test Results For Sandy Soils

Soil Density	SPT Blow Counts	k_{s1} (tsf)
Loose	3-6	20-60
Medium	7-15	60-300
Dense	16-30	300-1000

Table 7.5 Typical Plate Load Test Results For Clayey Soils

Soil Consistency	Unconfined Compressive Strength (tsf)	k_{s1} (tsf)
Stiff	1-2	50-100
Very stiff	2-4	100-200
Hard	> 4	> 200

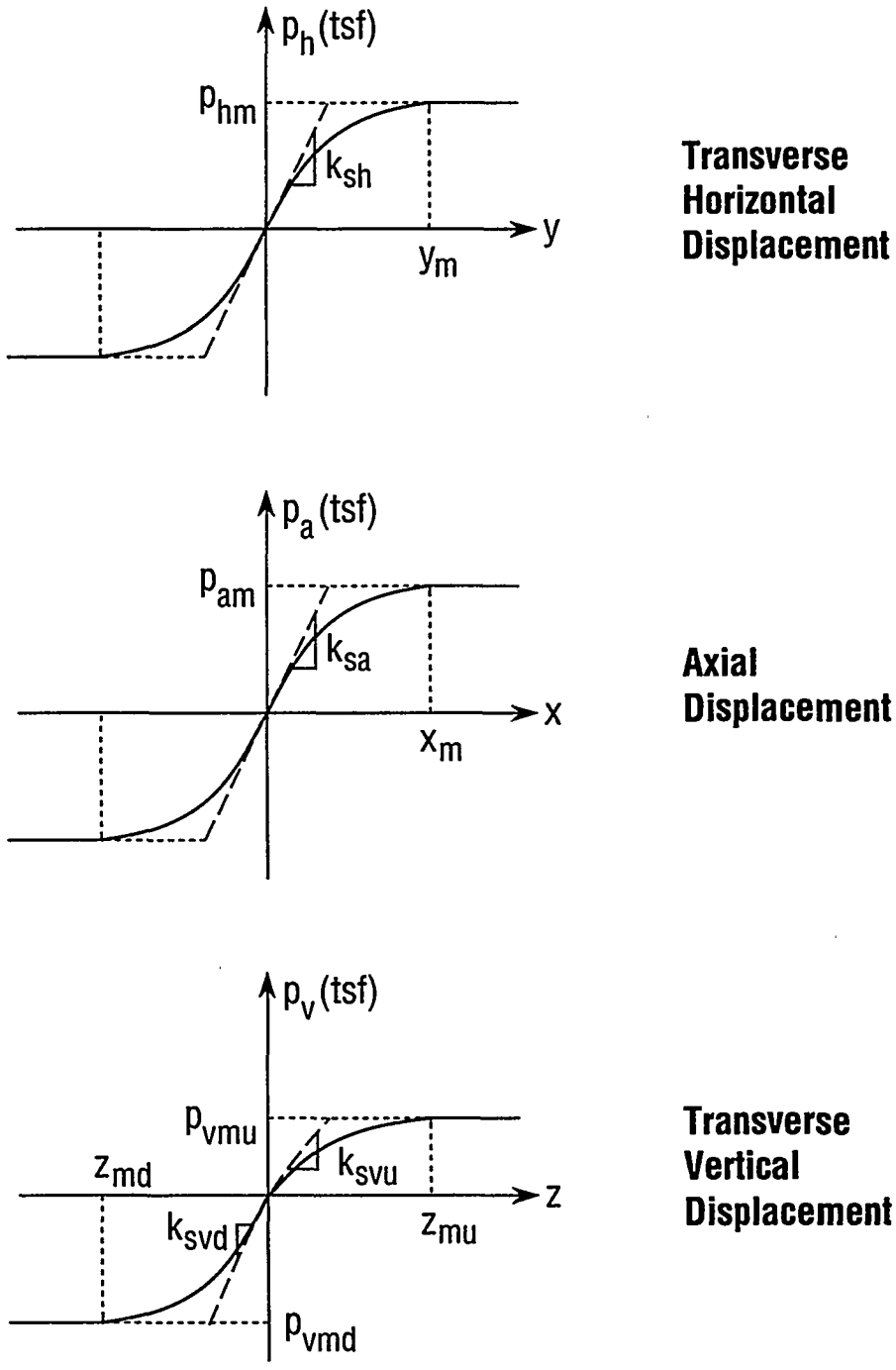

Figure 7.1 Soil Reaction to Specific Ground Displacements

CHAPTER 8

SEISMIC QUALIFICATION OF EQUIPMENT

8.1 GENERAL APPROACH

The equipment required for safe operation and maintenance of the tank farms must perform its intended function at a ground motion level sufficiently above the DBE level to achieve the desired risk reduction factor (see Section 3.10). Not all equipment items used for normal operation are required for safety. Therefore, a list should be prepared identifying the safety-related equipment, and a seismic qualification is required for these items. Some equipment pieces may not be required to perform a function during the earthquake event but they may need to remain functional after the event; whereas, some other equipment items may be required to function during as well as after the earthquake. Such distinction of the functional requirements helps selection of the appropriate qualification approach and, therefore, should be made along with the equipment listing.

Seismic qualification of equipment can be demonstrated employing one or more of the following approaches:

- Dynamic or Equivalent Static Analysis
- Testing
- Similarity Analysis

The selection of the appropriate method depends on the functional requirements and availability of data. A structural analysis may be adequate for equipment if demonstration of the structural integrity alone ensures its functional operability. Otherwise, shake table testing may be required to verify functionality especially for electrical equipment. Static testing may provide functional data for some (although very few) equipment classes, such as valves. In a similarity analysis,

the qualification equipment item and level are compared with similar information available in an existing data base. The dynamic similarity of the two equipment items shall be demonstrated (e.g., identical models) and the required vibration level must be enveloped by the level to which the equipment may have been qualified by a structural analysis, testing or a combination of analysis and testing, or may have successfully withstood a real earthquake for which sufficient reliable data exist.

8.2 EXISTING STANDARDS

The equipment qualification methods discussed above are described in detail in existing literature, for example, in IEEE Standard 344 (Reference 8.1). Both the NRC Regulatory Guide (Reference 8.2) and the Standard Review Plan (Reference 8.3) endorse the IEEE Standard with certain additions and clarifications, especially for mechanical equipment. Recently, the nuclear power industry has established a data bank based on shake table testing and earthquake experience, and intends to use it generically for verification of equipment in operating power plants under a program called "Unresolved Safety Issue A-46" (Reference 8.4).

The NRC has accepted the industry approach for seismic verification of equipment in older operating power plants (Reference 8.5) but does not endorse use of the A-46 approach for qualification of equipment in new plants (Reference 8.6). Although the basic data of Reference 8.4 were derived from testing and earthquake experience and may be treated as the required data base for qualification by the method of similarity analysis, the industry criteria do not require demonstration of one-to-one similarity (between the equipment to be qualified and the equipment in the data base) as required by the IEEE Standard (Reference 8.1).

Since the early 70's, a large number of equipment items have been shake table tested by the manufacturers or users. Although the information constitutes a valid data base for qualification by the method of similarity analysis, this may not be available to a new user. Generic interpretations of the industry data are available in the existing literature (References 8.7 and 8.8). However, these documents do not provide as much information as is necessary to demonstrate similarity as required by the IEEE Standard (Reference 8.1). One important observation that has been made in the generic interpretation documents (References 8.7, 8.8 and 8.9) is that certain equipment classes by design are relatively strong and can withstand a high earthquake level provided they are adequately anchored (e.g., horizontal pumps). Therefore, if the information developed in these references is properly used, the demonstration of the similarity analysis as required by IEEE std 344 can easily be made without much rigor and expense. On the other hand, as pointed out in the generic documents, certain other equipment (e.g., electrical panels) would require a much more detailed comparison for an effective use of the similarity method.

8.3 QUALIFICATION LEVEL

Regardless of which one of the above three approaches (i.e., structural analysis, testing or similarity analysis) is used for qualification, the equipment shall withstand the required vibration level. For convenience, response spectra are used as a measure of the qualification level. The qualification or the capacity response spectra should be compared with the required response spectra at the location of the structure where the equipment is installed. For qualification by either testing or similarity analysis (e.g., use of experience data) if the required response spectra are computed as discussed in chapter 3, the qualification or capacity response spectra shall envelop the required response spectra amplified by a factor as explained

below in Section 8.3.1. Exceptions in enveloping at certain frequencies may be justified following the procedures of IEEE std 344 (Reference 8.1).

8.3.1 Justification for RRS Amplification Factor

When equipment is qualified by shake table testing and the DBE input to the equipment is defined by a required response spectrum (RRS) obtained by enveloping and smoothing (i.e., filling in valleys) the in-structure spectra computed at the support of the equipment by a linear elastic analysis then in order to obtain the seismic margin defined by Equation 3.9, the equipment must be shake table tested to a test response spectrum (TRS) defined by:

$$TRS \geq \left(\frac{TRS}{RRS}\right)_R RRS \qquad (8.1)$$

where the required ratio of the TRS to RRS corresponding to the desired scale factor SF is:

$$\left(\frac{TRS}{RRS}\right)_R = 1.4\,SF \qquad (8.1a)$$

from which:

R_R	Constant SF*	$(TRS/RRS)_R$*
20	1.6	2.25
10	1.25	1.75
5	1.0	1.4

The basis for Equations 8.1 and 8.1a are summarized in Section 4.3 of Reference 8.10. For qualification by similarity analysis

---

*Improved estimates of SF as a function of A_R can be obtained from Figure 3.2, and these improved SF estimates will change the required $(TRS/RRS)_R$ value.

when experience data are used, it is recommended that the above factors be used unless the user chooses to justify for alternate factors.

REFERENCES

8.1 Institute of Electronic and Electrical Engineers, IEEE Std. 344-1987, "Recommended Practices for Seismic Qualification of Class 1E Equipment for Nuclear Power Generating Stations," 1987.

8.2 U.S. Nuclear Regulatory Commission, Regulatory Guide 1.100, "Seismic Qualification of Electric Equipment for Nuclear Power Plants," Rev. 1, August 1977.

8.3 U.S. Nuclear Regulatory Commission, "Standard Review Plan, NUREG-800," Section 3.10, Rev. 2, July 1981.

8.4 Seismic Qualification Utility Group, "Generic Implementation Procedure (GIP) for Seismic Verification of Nuclear Plant Equipment," Rev. 2, February 1992.

8.5 U.S. Nuclear Regulatory Commission, NUREG-1211, "Regulatory Analysis for Resolution of Unresolved Safety Issue A-46, Seismic Qualification of Equipment in Operating Plants," February 1987.

8.6 "Supplemental Safety Evaluation Report No. 2 on Seismic Qualification Utility Group's Generic Implementation Procedure, Revision 2, corrected February 22, 1992," attached to U.S. NRC letter, "Supplement No. 1 to Generic Letter (GL) 87-02," May 22, 1992.

8.7 Bandyopadhyay, K.K., et al., "Seismic Fragility of Nuclear Power Plant Components," NUREG/CR-4659, Vol. 4, June 1991.

8.8 EPRI Report NP-5223, Rev. 1, "Generic Seismic Ruggedness of Power Plant Equipment in Nuclear Power Plants," February 1991.

8.9 Kennedy, R.P., et al., "Use of Seismic Experience and Test Data to Show Ruggedness of Equipment in Nuclear Power Plants," 1991.

8.10 Kennedy, R.P., and Short, S.A., "Basis for Seismic Provisions of DOE Standard 1020-94," UCRL-CR-111478 and BNL-52418, Lawrence Livermore National Laboratory and Brookhaven National Laboratory, 1994.

NOTATION

R_R risk reduction factor defined in chapter 3

RRS required response spectrum

TRS test response spectrum

APPENDIX A

GUIDANCE ON ESTIMATING THE INELASTIC ENERGY ABSORPTION FACTOR F_μ

A.1 INTRODUCTION

It is recognized that the inherent seismic resistance of a well-designed and constructed structure is usually much greater than that expected based on an elastic analysis. This occurs largely because the nonlinear behavior is mobilized to limit the imposed forces.

Two general methods currently exist for treating the nonlinear behavior of a structure. One approach is to perform a time history nonlinear analysis and compare the maximum element demand ductility to a conservative estimate of its ductility capacity. An alternate means of accounting for the inelastic energy dissipation of civil structures and equipment at response levels above yield is the use of an inelastic energy absorption factor F_μ, based on a ductility modified inelastic response spectrum approach (References A.1 through A.4).

In general, the analyst would first make an estimate of a permissible inelastic distortion corresponding to about a 5% failure probability level. For example, for a low-rise concrete shear wall or concentric braced frame structure, a permissible total story distortion of 0.4% of the story height for in-plane drift would provide an adequately low probability of severe structural distress, and thus would result in an adequately conservative distortion criterion for overall structural failure (Reference A.5). However, such a distortion would result in severe cracking of a low rise concrete shear wall structure such that if there were safety related equipment mounted off the wall, the anchorage on this equipment might fail. To protect such anchorage, permissible total story distortions would more

appropriately be limited to the range of 0.2% to 0.25% of the story height for low rise concrete shear walls. Once a permissible distortion has been selected, the inelastic energy absorption factor F_μ may be determined from nonlinear analysis of an appropriate model of the structure using multiple realistic input time histories. First, the input time history is scaled to a level at which the elastic-computed demand is equal to the limit state (yield or ultimate) capacity, C_c'. Then, the input is further scaled until the distortion resulting from a time history nonlinear analysis reaches the selected permissible value. The in-elastic energy absorption factor F_μ is equal to this second or beyond limit state scaling factor.

Alternatively, a simplified nonlinear analysis procedure may be used at least for cantilever type structures. First, the analyst must estimate the nonlinear deformed shape of the structure corresponding to the maximum permissible distortion being reached in the story with the highest value of the ratio of the demand to the capacity. Then the system ductility μ is estimated from:

$$\mu = \frac{\sum W_i \delta_{T_i}}{\sum W_i \delta_{e_i}} \qquad \text{(A.1)}$$

where W_i is the inertial weight applied at each story of the structure, δ_{Ti} is the total displacement of story "i" (relative to the base) when the total distortion in the critical story reaches a permissible level, and δ_{ei} is the elastic displacement of story "i" (relative to the base) corresponding to a unit value of the ratio of the elastic demand to the capacity for the critical story. For a single story, Equation A.1 simplifies down to a story ductility, μ_s, of:

$$\mu_s = \frac{\delta_T}{\delta_y} \qquad (A.2)$$

where δ_T is the total permissible story displacement and δ_y is the yield displacement (demand/capacity equals unity). However, for multi-story structures, μ from Equation A.1 is always less than μ_s from Equation A.2 except when the nonlinear distortions are spread throughout the structure which is very unlikely. The following equation can be used to relate μ to μ_s:

$$\mu = 1 + F_k\ (\mu_s - 1) \qquad (A.3)$$

where F_k is a reduction factor to convert a story ductility estimate to a system ductility estimate. For a well designed structure in which the ratio of the demand to the capacity does not differ by more than a factor of about 1.3 over the structure height, F_k will typically range from 0.5 to 0.75. In these cases, Equation A.3 may be used with a conservatively estimated F_k of 0.5 in lieu of Equation A.1 or nonlinear time history analyses.

Once the permissible system ductility μ has been established, many approaches can be used for estimating F_μ. For broad, smooth input spectra and moment-frame structures with essentially full elasto-plastic nonlinear hysteretic loops, either the Newmark-Hall (Reference A.6) or Riddell-Newmark (Reference A.3) approach is commonly used. However, for concrete shear wall structures or braced frames which have severely pinched hysteretic loops, Kennedy, et al. (Reference A.4) have shown that these approaches are likely to be slightly nonconservative. For such structures, the approach of Reference A.4 is preferred.

A.2 ILLUSTRATION OF COMPUTATION OF SYSTEM DUCTILITY

The following provides an example application of this simplified nonlinear analysis procedure for estimating F_μ for a concrete

shear wall structure.

For purposes of this illustration, a three-story structure with the properties shown in Figure A.1 will be used. This figure shows the weights, W, at each story, the elastic stiffnesses, K, and ultimate capacities, V_u, for the walls between story levels. This structure has a fundamental frequency f of 8.25 Hz.

Assuming a damping parameter ζ of 7%, for a reference 1.0 g NUREG/CR-0098 median spectrum (Reference A.6), at f equal to 8.25 Hz the elastic spectral acceleration is:

$$S_A(f,\zeta) = 1.86g \qquad \text{(A.4)}$$

and the elastic response of this structure is given in Table A.1. For this reference spectrum response, the ratio of the elastic demand to the capacity ranges from 1.02 for the first story wall to 1.32 for the second story. Thus yielding will initially occur in the first story wall, and the elastic displaced shape at the onset of yielding is given by δ_e in Table A.1. Note in Table A.1 that the minimum value of V_u/V_r (i.e., 1.02) is used to calculate δ_e since this corresponds to the first element which reaches yield (i.e., level 1).

In accordance with the recommendations given above, a permissible total story distortion of 0.4% of the total story height will be selected for the critical first story. Thus:

$$\delta_{T_1} = 0.004\,(22\ ft)\,(12\ inch/ft) = 1.06\ inch \qquad \text{(A.5)}$$

and the story ductility μ_s from Equation A.2 is:

$$\mu_s = \frac{1.06}{0.147} = 7.2 \qquad \text{(A.6)}$$

From Equation A.3, the system ductility μ is expected to lie within the range of:

$$\mu = 4.1\ to\ 5.6 \qquad \text{(A.7)}$$

However, a more accurate estimate of μ may be obtained from Equation A.1 after estimating the inelastic deformed shape. A slightly conservative estimate of the inelastic deformed shape may be obtained by assuming that all of the nonlinear drift occurs in the story with the lowest ratio of the capability to the demand (the first story for this example). The other stories retain the same differential drifts as given by δ_e in Table A.1. Thus:

δ_{T_1} = 1.06 inch
δ_{T_2} = 1.12 inch
δ_{T_3} = 1.22 inch

and from Equation A.1:

$$\mu = \frac{6300(1.22) + 2100(1.12) + 2500(1.06)}{6300(0.310) + 2100(0.212) + 2500(0.147)} = 4.6 \quad \text{(A.8)}$$

A.3 ILLUSTRATION OF COMPUTATION OF INELASTIC ENERGY ABSORPTION FACTOR

For concrete shear wall structures, it is recommended that the inelastic energy absorption factor F_μ be computed by the effective frequency/effective damping approach of Reference A.4, as summarized herein. For this example, it will be assumed that the force-deflection relationship on initial loading is elastic-perfectly-plastic with an ultimate capacity V_u. Thus, the ratio of secant to elastic frequency is given by:

$$(f_s/f) = \sqrt{1/\mu} = \sqrt{1/4.6} = 0.466 \quad \text{(A.9)}$$

Then, the effective frequency is given by:

$$(f_e/f) = (1 - A) + A\,(f_s/f) \quad \text{(A.10)}$$

where,

$$A = C_f[1 - (f_s/f)] \leq 0.85 \quad \text{(A.11)}$$

For ground motions with strong durations greater than one second,

C_f may be approximated as 2.3. Thus, for (f_s/f) less than or equal to 0.63 one may take A equal to 0.85. For this example:

$$(f_e/f) = 0.15 + 0.85(0.466) = 0.546$$
$$f_e = 0.546(8.25\ Hz) = 4.5\ Hz \qquad \text{(A.11)}$$

The effective damping ζ_e may be estimated from:

$$\zeta_e = (f_s/f_e)^2[\zeta + \zeta_h] \qquad \text{(A.12)}$$

where ζ is the elastic damping (7% in this case) and ζ_h is the pinched hysteretic damping which can be approximated by:

$$\zeta_h = 11\%\ [1 - (f_s/f)] = 11\%\ (.534) = 5.9\% \qquad \text{(A.13)}$$

for strong durations greater than one second. Thus, for this example:

$$\zeta_e = \left(\frac{.466}{.546}\right)^2[12.9\%] = 9.4\% \qquad \text{(A.14)}$$

For the reference 1.0 g NUREG/CR-0098 spectrum, at f_e = 4.5 Hz and ζ_e = 9.4%, the spectral acceleration is given by:

$$S_A(f_e, \zeta_e) = 1.68g \qquad \text{(A.15)}$$

and the inelastic energy absorption factor is estimated (Reference A.4) by:

$$F_\mu = \left[\frac{f_e}{f_s}\right]^2 \frac{S_A(f, \zeta)}{S_A(f_e, \zeta_e)} = \left[\frac{.546}{.466}\right]^2 \left[\frac{1.86}{1.68}\right] = 1.52 \qquad \text{(A.16)}$$

REFERENCES

A.1 Villaneuva, A.S., "Ductility Reduction Factors for Earthquake Design," Reprint 3209, ASCE Spring Convention, Pittsburgh, Pennsylvania, 1978.

A.2 Newmark, N.M., "A Response Spectrum Approach for Inelastic Seismic Design of Nuclear Reactor Facilities," Proceedings from 3rd International Conference on Structural Mechanics in Reactor Technology, SMiRT, Berlin, September 1975.

A.3 Riddell, R., and Newmark, N.M., "Statistical Analysis of the Response of Non-linear Systems Subjected to Earthquakes", Department of Civil Engineering, Report UILU 79-2016, Urbana, Illinois, August 1979.

A.4 Kennedy, R.P., et al., Engineering Characterization of Ground Motion - Task 1, Effects of Characteristics of Free-Field Motion on Structural Response, NUREG/CR-3805, Nuclear Regulatory Commission, May 1984.

A.5 Kennedy, R.P., et al., "Probabilistic Evaluation of the Diablo Canyon Turbine Building, Seismic Capacity Using Nonlinear Time History Analyses", Pacific Gas and Electric Company, December 1988, Report No. 1643.01.

A.6 Newmark, N.M., and Hall, W.J., "Development of Criteria for Seismic Review of Selected Nuclear Power Plants," NUREG/CR-0098, Nuclear Regulatory Commission, May 1978.

NOTATION

f	elastic frequency
f_e	effective frequency
f_s	secant frequency
F_K	a reduction factor relating μ and μ_s
F_μ	inelastic energy absorption factor
K_i	elastic stiffness of component "i"
$S_A( )$	elastic spectral acceleration
V_u	ultimate shear capacity
V_r	elastic demand (i.e., response) shear
W_i	inertial weight of story "i"
δ_{ei}	elastic displacement of story "i"
δ_r	demand (i.e., response) displacement
δ_{Ti}	total displacement of story "i" allowing distortion
ζ	elastic damping
ζ_e	effective damping
ζ_h	pinched hysteretic damping
μ	system ductility
μ_s	ductility for a single story

Table A.1 Elastic Response to Reference 1.0 g NUREG/CR-0098 Spectrum (7% Damping)

Level	Demand		Capacity/ Demand V_u/V_r	Yield Displacement (inch) $\delta_e = \delta_r\ (V_u/V_r)_{min}$
	Displacement δ_r (inch)	Shear V_r (kips)		
3	0.304	13,400	1.24	0.310
2	0.208	16,400	1.32	0.212
1	0.145	18,900	1.02	0.147

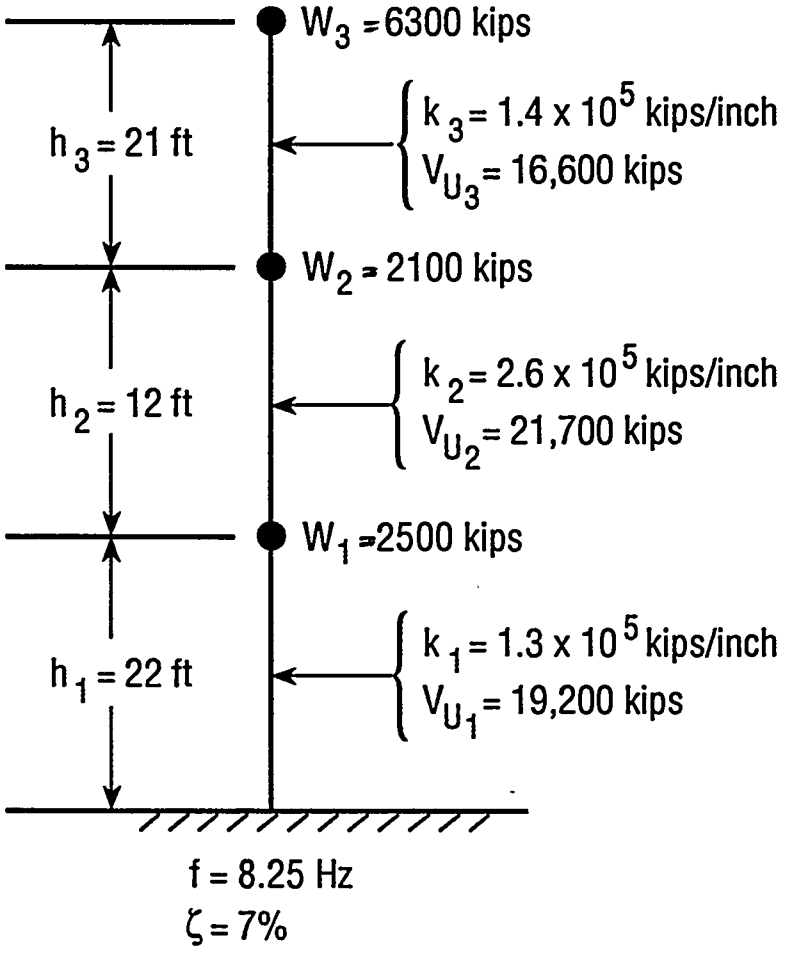

Figure A.1 Three Story Shear Wall Structure

APPENDIX B

INFLUENCE OF LIQUID VISCOSITY ON HYDRODYNAMIC EFFECTS

B.1 GENERAL

The viscosity of the liquid in tanks increases the liquid's damping capacity in sloshing, and this increase, in turn, decreases the sloshing or convective component of the liquid mass and increases the corresponding impulsive component. The reduced convective mass decreases the convective components of the wall pressures and of the associated forces, but the increased impulsive mass does not necessarily have the opposite effect, as a fraction of the inertia forces for the viscous liquid is transferred by horizontal shearing action to the base.

While the net effect of these changes cannot be defined precisely without detailed and generally complex analyses, the influence on the effective damping in sloshing can be determined from the results of previous theoretical and experimental studies, valuable summaries of which are given in References B.1 and B.2. The purpose of this Appendix is to provide, based on existing information, an order-of-magnitude estimate of the effect of liquid viscosity on the response of the class of upright, circular cylindrical tanks examined in Chapter 4.

B.2 APPROACH TO ANALYSIS

The approach used consists in evaluating first the effective damping of the liquid in its fundamental antisymmetric sloshing mode. If it can be demonstrated that, for the tank dimensions and viscosity levels that are of practical interest, this damping is not affected significantly by liquid viscosity, it can then be concluded that its effect on the impulsive components of response is also insignificant, and that the solutions for the inviscid liquid presented in Chapter 4 may be used with reasonable accuracy for viscous liquids as well.

When defined by the ratio ζ of the equivalent viscous damping to its critical value, the effective damping of the liquid in its fundamental antisymmetric sloshing mode may be expressed as

$$\zeta = C\zeta_\infty \qquad \text{(B.1)}$$

where ζ_∞ is the damping ratio for a slender, tall system, and C is a dimensionless shape factor that depends on the ratio of liquid height to tank radius, H_ℓ/R. The factor ζ_∞ is given by

$$\zeta_\infty = \frac{\alpha}{2\pi}\frac{\nu^{1/2}}{g^{1/4}R^{3/4}} \qquad \text{(B.2)}$$

where α is a dimensionless coefficient identified in the following; g is the acceleration due to gravity; and ν is the kinematic viscosity of the liquid, which is the ratio of the absolute viscosity μ and the liquid density ρ. The absolute viscosity is normally expressed in units of centipoise (cP). It may be recalled that

$$1\ cP = 10^{-2}\ Poise = 10^{-3}\ Newton\text{-sec}/m^2 = 20.89 \times 10^{-6}\ lb\text{-sec}/ft^2$$

and that for water at about 25° C, μ = 1 cP, whereas for SAE 30 oil and glycerine at the same temperature, μ is approximately equal to 100 cP and 500 cP, respectively. As would be expected, ζ_∞ increases with increasing liquid viscosity, but the increase is not very rapid, as ν appears to the 1/2 power in Equation B.2. Note further that ζ_∞ decreases with increasing tank radius.

The form of Equation B.2 follows from theory and dimensionless analysis, and its validity has been confirmed by experiments. Two independent theoretical studies (References B.3 and B.4; see also References B.1 and B.2) led to a value of 3.52 for the factor α, while two experimental studies (References B.5 and B.2) led to values of 4.98 and 5.23, respectively. The available data are limited to values of $\nu^{1/2}g^{-1/4}R^{-3/4}$ less than about 3 percent which, on taking α = 5.23, correspond to values of ζ_∞ less than about 2.5 percent.

The following two expressions have been proposed for the shape factor C (References B.5 and B.2). The first, denoted by C_1, is given by

$$C_1 = 1 + \frac{0.318}{\sinh(1.84\, H_\ell/R)} \left[1 + \frac{1 - H_\ell/R}{\cosh(1.84\, H_\ell/R)}\right] \qquad \text{(B.3)}$$

and the second, C_2, is given by

$$C_2 = \left[1 + \frac{2(1 - H_\ell/R)}{\sinh(3.68\, H_\ell/R)}\right] \tanh^{-1/4}(1.84\, H_\ell/R) \qquad \text{(B.4)}$$

These factors are compared in Figure B.1, from which it is clear that they both decrease with increasing H_ℓ/R, and that they reach their limiting value of unity for values of H_ℓ/R of about one. The larger factors for the lower values of H_ℓ/R are attributed to the viscosity effects of the liquid moving along the tank base.

As an indication of the values of ζ that may be encountered in practice, this factor is evaluated for the tank-liquid system examined in Appendix G, for which H_ℓ = 20.4 ft, R = 25 ft, and the unit weight of the liquid is 1.15 times that of water, or 71.76 lb/ft^3. The gravitational acceleration is taken as g = 32.17 ft/sec^2. Listed below are the values of ζ_∞ and ζ, in percent of critical, determined from Equations B.1 and B.2 by taking α = 5.23 and C = C_1. Inasmuch as the factor C_1 for the system being examined is larger than the factor C_2, its use leads to upper bound estimates for the desired damping. Three values of μ in the range between 100 cP and 10,000 cP are considered.

Absolute Viscosity cP	ζ_∞ in percent	ζ in percent
100	0.096	0.11
1,000	0.303	0.35
10,000	0.957	1.11

It is observed that even for viscosity levels as high as 10,000 cP, the effective damping of the liquid in its fundamental sloshing mode is only slightly greater than 1 percent. Furthermore, as may be appreciated from Equation B.2, this value would be even lower for tanks of larger radii and liquids of higher specific gravities than those considered. It follows that, for the tank proportions and liquid viscosity levels examined in this document, the effect of liquid viscosity on the maximum values of the earthquake-induced wall pressures and associated tank forces are insignificant, and that the solutions for the inviscid liquid presented in Chapter 4 may be used as reasonable approximations for viscous liquids as well. This conclusion is consistent with the results of finite element solutions reported for selected systems in References B.6 and B.7.

The reported damping values for the lower viscosity levels used in the illustrative example are clearly lower than the 0.5 percent value recommended in Chapter 3 for the evaluation of the convective components of response. The latter value is deemed to be appropriate for design use, as the presence in the tank of such appurtenances as pipes, cooling coils and instrumentation tubes will increase the effective damping of the liquid in sloshing. Additionally, the peak values of the response components associated with the relatively low-frequency sloshing action of the liquid are generally not as sensitive to variations in damping as are those of the impulsive components which are associated with much higher-frequency oscillations.

B.2.1 Limitations

It is important to note that for wastes with viscosity levels of the order of 10,000 cP or more, the representation of the waste as a liquid may not be appropriate, and that it may be necessary to consider other idealizations for the tank contents. Fundamental studies are currently in progress of the response to

earthquakes of tanks containing a viscoelastic solid. Some preliminary results from these studies have been reported in Reference B.8 and additional results will be reported in the near future.

B.2.2 Width of Boundary Layer

A high proportion of the damping of liquids sloshing in tanks is contributed by the viscosity of the liquid in a narrow region adjacent to the tank wall, referred to as the boundary layer region. For a liquid undergoing simple harmonic motion with a cyclic frequency f, the width of this layer, ℓ, is given by (Reference B.4)

$$\ell = \sqrt{\frac{\nu}{2\pi f}} \tag{B.5}$$

As a measure of the practical range of ℓ, a listing is presented of the results obtained for the tank referred to earlier in this Appendix, considering the liquid to vibrate freely in its fundamental sloshing mode with a frequency $f = f_{c1} = 0.233$ cps.

Absolute Viscosity cP	Width ℓ in inches
100	0.3
1,000	0.96
10,000	3.03

It is observed that, even for the highest viscosity level considered, the width of the boundary layer is extremely small. It follows that, in analyses of such problems by numerical techniques, the mesh sizes for the liquid near the tank wall should be sufficiently small so as to adequately represent the localized nature of this source of energy loss.

REFERENCES

B.1 Silverman, S., and Abramson, H.N., "Damping of Liquid Motions and Lateral Sloshing," Chapter 4 of The Dynamic Behavior of Liquids in Moving Containers, Edited by H. Norman Abramson, NASA SP-106, National Aeronautics and Space Administration, Washington, D.C., pp. 105-143, 1966.

B.2 Stephens, D.G., Leonard, H.W., and Perry, T.W., "Investigation of the Damping of Liquids in Right-Circular Cylindrical Tanks, Including the Effects of a Time-Variant Liquid Depth," NASA TN D-1367, National Aeronautics and Space Administration, Washington, D.C., pp. 30, July 1962.

B.3 Miles, J.W., "On the Sloshing of Liquid in a Cylindrical Tank," Report No. AM6-5, GM-TR-18, Guided Missile Research Div., The Ramo-Wooldridge Corp, April 1956.

B.4 Case, K.M., and Parkinson, W.C., "Damping of Surface Waves in an Incompressible Liquid," Journal Fluid Mechanics, Vol. 2, Part 2, pp. 172-184, March 1957.

B.5 Mikishev, G.N., and Dorozhkin, N.Y., "An Experimental Investigation of Free Oscillations of a Liquid in Containers," (in Russian), Izv. Akad, Nauk SSSR, Otd. Tekh, Nauk, Mekh. i Mashinostr, No. 4, pp. 48-83, July/August 1961. (For brief review, see Reference B.1)

B.6 Tang, Y., Uras, R.A., and Chang, Y.W., "Effect of Viscosity on Seismic Response of Waste Storage Tanks," ANL/RE 92/2, Argonne National Laboratory, Argonne, Illinois, June 1992.

B.7 Tang, Y., Uras, R.A., and Chang, Y.W., "Effect of Viscosity on Dynamic Response of a Liquid Storage Tank," Proceedings, ASME 1993, Pressure Vessel and Piping Conference, Denver, Colorado, PVP-Vol. 258, pp. 135-142, 1993.

B.8 Veletsos, A.S., Parikh, V.H., Younan, A.H., and Bandyopadhyay, K., "Dynamic Response of a Pair of Walls Retaining a Viscoelastic Solid," Report BNL-52454, Brookhaven National Laboratory, Upton, New York, 1995.

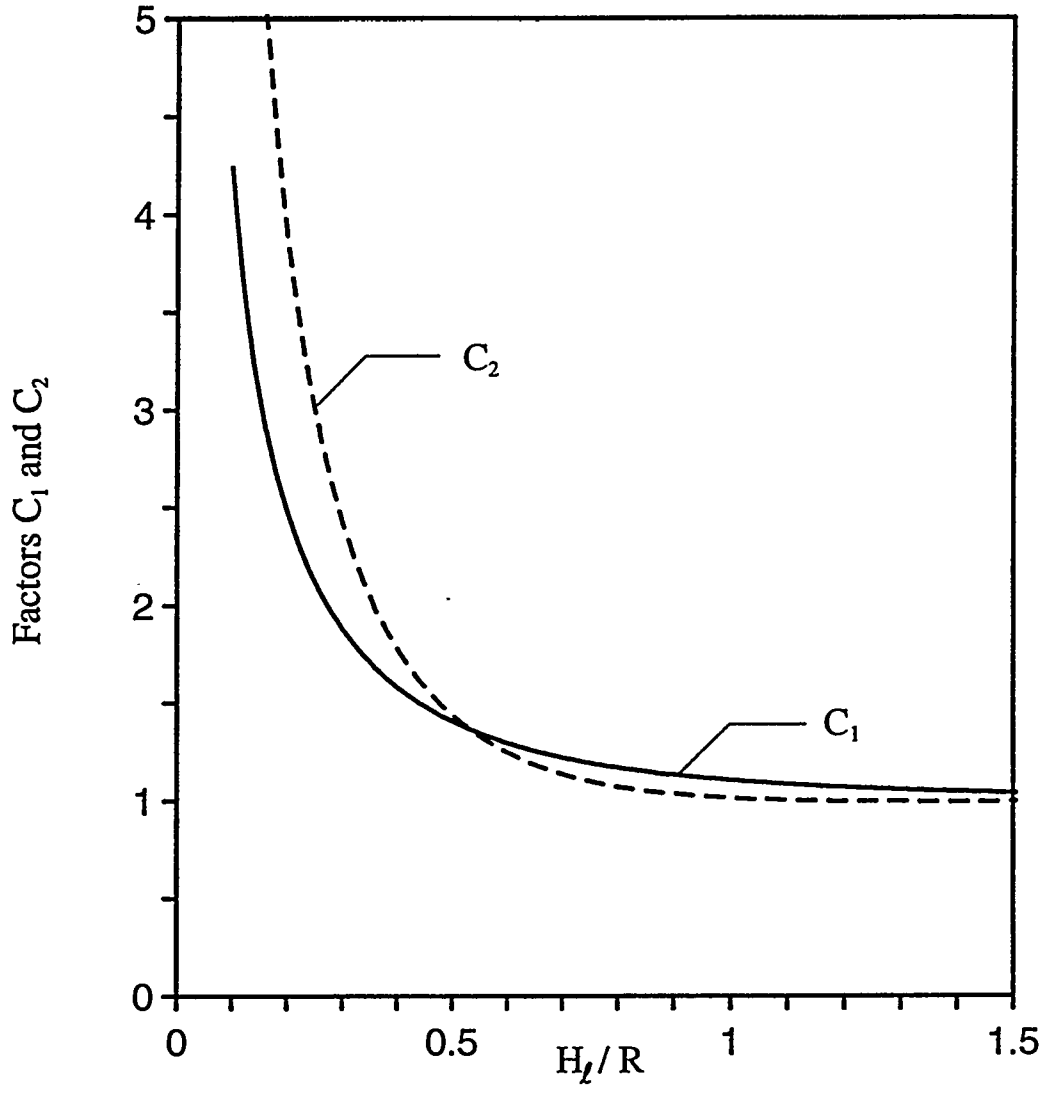

Figure B.1 Dimensionless Shape Factors C_1 and C_2 in Expression for Damping of Sloshing Liquid in Tanks

APPENDIX C

MEMBRANE SOLUTIONS FOR TOP-CONSTRAINED TANKS

The solutions in this Appendix are for the in-plane membrane forces induced in fully filled circular cylindrical tanks subjected to static radial pressures of the form

$$p(\eta,\theta) = a_o \rho_\ell R S_A \cos\theta \qquad \text{(C.1)}$$

and

$$p(\eta,\theta) = a_n \left[\cos\frac{n\pi}{2}\eta\right] \rho_\ell R S_A \cos\theta \qquad \text{(C.2)}$$

where a_o and a_n are arbitrary constants; n is an odd integer; η, which is equivalent to the symbols η_ℓ and η_t used in Chapter 4, represents the vertical distance from the base to an arbitrary point of the tank wall normalized with respect to the liquid or tank height, $H_\ell = H_t$; S_A is a spectral acceleration value; and the remaining symbols in these and the following equations are the same as those used in Chapter 4. The tanks are presumed to be of uniform wall thickness and supported at the base such that both their circumferential and radial displacement components vanish. The following support conditions are considered for the top boundary:

- A roller support, for which no axial forces can develop and the circumferential displacements vanish; and
- A hinged support, for which both the axial and circumferential displacements vanish.

With the membrane theory being employed, the conditions of vanishing radial displacement for a rigid support cannot be satisfied.

The forces evaluated are the transverse shear across normal sections, $V(\eta)$, and the corresponding bending moment, $M(\eta)$.

These forces are related to the circumferential shear per unit of length of the tank wall, $N_{z\theta}$, and the corresponding axial force per unit of length, N_z, by

$$N_{z\theta}(\eta,\theta) = \frac{V(\eta)}{\pi R}\sin\theta \qquad (C.3)$$

and

$$N_z(\eta,\theta) = \frac{M(\eta)}{\pi R^2}\cos\theta \qquad (C.4)$$

For the uniform axial distribution of the pressure defined by Equation C.1, the results are as follows. For the **roller** support,

$$V(\eta) = (\eta-\Gamma_r)\, a_o m_\ell S_A \qquad (C.5)$$

and

$$M(\eta) = (1-\eta)\left[\frac{1}{2}(1+\eta) - \Gamma_r\right] a_o m_\ell H_\ell S_A \qquad (C.6)$$

in which

$$\Gamma_r = \frac{1.5\,(2+\nu_t) + \frac{5}{8}(H_\ell/R)^2}{6\,(1+\nu_t)+(H_\ell/R)^2} \qquad (C.7)$$

For the **hinged** support,

$$V(\eta) = (\eta-0.5)\, a_o m_\ell S_A \qquad (C.8)$$

and

$$M(\eta) = \left[-\frac{\eta^2}{2} + \frac{\eta}{2} - \frac{1}{12} + \nu_t\left(\frac{R}{H_\ell}\right)^2\right] a_o m_\ell H_\ell S_A \qquad (C.9)$$

For the cosine distribution of loading represented by Equation C.2, the corresponding results are: For the **roller** support,

$$V(\eta) = \frac{2}{n\pi}\left[\sin\frac{n\pi}{2}\eta - \frac{2}{n\pi}\Gamma_r\right] a_n m_\ell S_A \qquad (C.10)$$

and

$$M(\eta) = \frac{4}{n^2\pi^2}\left[\cos\frac{n\pi}{2}\eta - (1-\eta)\Gamma_r\right] a_n m_\ell H_\ell S_A \qquad (C.11)$$

in which

$$\Gamma_r = 3\frac{(2+\nu_t) + \frac{4}{n^2\pi^2}(H_\ell/R)^2}{6(1+\nu_t) + (H_\ell/R)^2} \qquad (C.12)$$

For the **hinged** support,

$$V(\eta) = \frac{2}{n\pi}\left[\sin\frac{n\pi}{2}\eta - \frac{2}{n\pi}\Gamma_h\right] a_n m_\ell S_A \qquad (C.13)$$

and

$$M(\eta) = \frac{4}{n^2\pi^2}\left\{\cos\frac{n\pi}{2}\eta - \Gamma_h(\eta-0.5) - \frac{2}{n\pi}\left[\frac{4}{n^2\pi^2} - \nu_t\left(\frac{R}{H_\ell}\right)^2\right]\right\} a_n m_\ell H_\ell S_A \qquad (C.14)$$

in which

$$\Gamma_h = 3\frac{8 + (4+n\pi)\nu_t + \frac{4}{n^2\pi^2}(4-n\pi)(H_\ell/R)^2}{24(1+\nu_t) + (H_\ell/R)^2} \qquad (C.15)$$

APPENDIX D

EFFECTS OF SLOSHING LIQUID IMPACTING ROOF

D.1 GENERAL

The precise evaluation of the dynamic pressures induced by sloshing liquid in tanks impacting the roof is a highly complex problem in fluid-structure interaction requiring computationally intensive methods of analysis. In particular, the response of the system must be evaluated as a function of time, making due provision for the varying state of the liquid after each impact.

Of special interest in practice are the magnitudes and distributions of the maximum pressures exerted on the tank roof and wall. It is believed that reasonable approximations to these pressures may be obtained by application of the impulse-momentum relation and the concept of a time-dependent participating liquid mass considering only the impact effect of the wave with the maximum slosh height. The details of this approach will be described in a future report. The purpose of this Appendix is to describe a simplistic, design-oriented procedure which may be used in the interim.

In the proposed procedure, when the slosh height of the liquid exceeds the available freeboard, the liquid column between the maximum impacted area and the tank base is considered to act impulsively, experiencing the same motion as the tank wall. This approach represents an improvement over currently employed procedures in which the entire mass of the liquid is presumed to act impulsively for tanks with inadequate freeboard. Furthermore, based on preliminary comparisons with results obtained by a more rigorous analysis, the proposed procedure is still believed to be conservative.

D.2 SYSTEM CONSIDERED AND IMPACTED AREA

The system examined is shown in Figure D.1. It is a horizontally excited, vertical, circular cylindrical tank of radius R and height H_t, which is filled with a liquid of density ρ_ℓ to a height H_ℓ. The tank roof is presumed to be horizontal and rigid. The effect of a curved roof is examined separately at the end. Points on the liquid surface are defined by the polar coordinates r and θ, with θ=0 taken parallel to the direction of the ground shaking. The freeboard, representing the difference between the roof elevation and the elevation of the upper liquid surface at rest, is denoted by h_o.

If h_s represents the absolute maximum vertical displacement or slosh height of the liquid in the absence of a roof, and the liquid is considered to respond in its fundamental sloshing mode as shown by the dashed curve in the upper part of Figure D.1, then the maximum displacement of an arbitrary point, $h(r,\theta)$, may be expressed as

$$h(r,\theta) = h_s \sin\frac{\pi r}{2R}\cos\theta \qquad \text{(D.1)}$$

in which the sine function is used for simplicity in lieu of the exact, normalized Bessel function $J_1(\lambda_1 r/R)/J_1(\lambda_1)$ with $\lambda_1 = 1.841$.

For freeboards $h_o<h_s$, the sloshing liquid will impact the roof over an area such as that shown shaded in the upper part of Figure D.1. The maximum impacted area is defined by the central half-angle, θ_o, given by

$$\theta_o = \cos^{-1}\left(\frac{h_o}{h_s}\right) \qquad \text{(D.2)}$$

and by the radial distances to the inner boundary of the area, $r_o(\theta)$, given by

$$r_o(\theta) = \frac{2}{\pi} R \sin^{-1}\left(\frac{h_o}{h_s \cos\theta}\right) \qquad \text{(D.3)}$$

The impacted areas for several freeboard-to-slosh-height ratios h_o/h_s are shown in Figure D.2.

D.3 PROCEDURE

For the purpose of estimating the maximum values of the impact-induced forces on the tank roof and wall, the liquid column beneath the maximum impacted roof area is considered to be fully constrained and to respond impulsively, i.e., to move in synchronism with the tank wall. Accordingly, the resulting wall pressures are uniformly distributed over the full tank height $H_t = H_\ell + h_o$ and vary circumferentially as $\cos\theta$ from $\theta=-\theta_o$ to $\theta=\theta_o$. Additionally, the peak values of the roof pressures, $p_r(r,\theta)$, are presumed to increase linearly in the radial direction. The latter variation is consistent with that obtained for the limiting case of a system for which the upper liquid surface is fully constrained vertically.

D.3.1 Roof and Wall Pressures

For the conditions considered, the maximum roof pressures are defined by

$$p_r(r,\theta) = \rho_\ell r (S_A)_i \cos\theta \quad for\ |\theta| \le |\theta_o| \qquad \text{(D.4)}$$

where $(S_A)_i$ is the spectral value of the pseudoacceleration for the impulsive component of response of the roofless tank-liquid system. Similarly, the corresponding wall pressures, referred to as the impulsive component of the pressures due to the constrained portion of the liquid and designated by p_i^c, are given by

$$p_i^c(z,\theta) = \rho_\ell R (S_A)_i \cos\theta \quad for\ |\theta| \le |\theta_o| \qquad \text{(D.5)}$$

The wall pressures induced by the unconstrained portion of the liquid beneath the non-impacted part of the roof are considered to

be the same as those for the corresponding roofless tank. They include the impulsive component, defined by Equation 4.2 of Chapter 4, and the convective component, defined by the first term of the series in Equation 4.3. Their maximum values, identified by the symbols p_i^u and p_c^u, respectively, are given by

$$p_i^u(z,\theta) = c_i(z)\rho_\ell R(S_A)_i \cos\theta \quad for\ |\theta| > |\theta_o| \tag{D.6}$$

and

$$p_c^u(z,\theta) = c_{c1}(z)\rho_\ell R(S_A)_{c1} \cos\theta \quad for\ |\theta| > |\theta_o| \tag{D.7}$$

where $c_i(z)$ and $c_{c1}(z)$ are dimensionless functions defined in Section 4.3.2 of Chapter 4, and $(S_A)_{c1}$ is the spectral value of the pseudoacceleration for the fundamental sloshing mode of vibration of the liquid in the roofless tank. The superscripts 'c' and 'u' in Equations D.5 through D.7 stand for the constrained and unconstrained portions of the liquid, respectively. The total impulsive component of the wall pressure, $p_i(z,\theta)$, is given by the sum of Equations D.5 and D.6, whereas the convective component is defined completely by Equation D.7.

D.3.2 Wall Forces

With the maximum wall pressures established, the corresponding forces in the tank wall may be computed, as for a tank with ample freeboard, by a static analysis, making use of an appropriate shell theory and any one of a number of available computer programs. It is desirable, however, to compute also the maximum value of the total hydrodynamic wall force and to compare it with that which would be obtained in the absence of a roof.

The maximum value of the wall force per unit of tank height due to the constrained portion of the liquid, F_i^c, is obtained by integrating the pressure p_i^c over the circumferential distance over which it acts. This yields

$$F_i^c(z) = \rho_\ell R(S_A)_i \int_{-\theta_0}^{\theta_0} R\cos^2\theta d\theta = \epsilon\pi\rho_\ell R^2(S_A)_i \qquad (D.8)$$

where ϵ is a dimensionless factor given by

$$\epsilon = \frac{2\theta_0 + \sin 2\theta_0}{2\pi} \qquad (D.9)$$

with θ_o expressed in radians. As before, the subscript i identifies the impulsive nature of this force. Proceeding similarly with the unconstrained portion of the liquid, one obtains the force

$$F_i^u(z) = (1-\epsilon)\, c_i(z)\, \pi\rho_\ell R^2(S_A)_i \qquad (D.10)$$

for the impulsive component of response, and the force

$$F_c^u(z) = (1-\epsilon)\, c_{c1}(z)\, \pi\rho_\ell R^2(S_A)_{c1} \qquad (D.11)$$

for the convective component.

The maximum value of the total wall force, P, is finally obtained by integrating the forces F_i^c, F_i^u, and F_c^u over the heights over which they act. The impulsive component of the force induced by the constrained portion of the liquid, P_i^c, is given by

$$P_i^c = \int_0^{H_t} F_i^c(z)\, dz = \epsilon \frac{H_t}{H_\ell} m_\ell (S_A)_i \qquad (D.12)$$

where $m_\ell = \pi R^2 H_\ell \rho_\ell$ is the total liquid mass. Similarly, the impulsive and convective components due to the unconstrained portion, P_i^u and P_c^u, are given by

$$P_i^u = (1-\epsilon)\, m_i (S_A)_i \qquad (D.13)$$

and

$$P_c^u = (1-\epsilon)\, m_{c1} (S_A)_{c1} \qquad (D.14)$$

where m_i and m_{c1} are the impulsive and the fundamental convective components of the liquid mass for the roofless system. The total

impulsive wall force, P_i, is then given by the sum of P_i^c and P_i^u, whereas the total convective force $P_c = P_c^u$. For a free-standing cantilever tank, the forces referred to above also represent the relevant components of the horizontal base shear.

D.3.3 Base Moment

For a free-standing cantilever tank, the components of the overturning moment at a section immediately above the tank base are obtained by multiplying the components of the total wall force by the appropriate centroidal distances. In particular, the impulsive component of the moment due to the constrained portion of the liquid, M_i^c, is given by

$$M_i^c = P_i^c \frac{H_t}{2} \tag{D.15}$$

and the components due to the unconstrained portion, M_i^u and M_c^u, are given by

$$M_i^u = 0.40 P_i^u H_t \tag{D.16}$$

and

$$M_c^u = P_c^u h_{c1} \tag{D.17}$$

where $0.4H_t$ represents the effective height or centroidal distance for the impulsive component of the wall pressures induced in the roofless system, and h_{c1} represents the corresponding height for the fundamental convective component.

D.3.4 Combination for the Component Effects

The impulsive effects due to the unconstrained and constrained portions of the liquid should be combined by taking the sum of their absolute values, whereas the convective component should be combined with the total impulsive component by the square-root-of-the-sum-of-squares rule. For most practical cases, the convective components are likely to be negligibly small, particularly when the roof impact effects are substantial.

D.3.5 Application to Curved Roofs

For tanks with curved roofs and with the freeboard h_o interpreted as the height from the free liquid surface at rest to the junction of the wall with the roof, the analysis must be implemented for a modified or effective freeboard, $(h_o)_e$, which is greater than h_o. Pending the results of additional studies that are currently in progress, it is recommended that $(h_o)_e$ be taken in a form analogous to Equation 5.2 of Chapter 5 as

$$(h_o)_e = h_o + \frac{h_d}{4} \qquad \text{(D.18)}$$

where h_d is the height of the top of the roof or dome from its junction with the cylindrical wall. For values of $(h_o)_e$ greater than the liquid slosh height, h_s, the impact effects will be negligible.

D.4 ILLUSTRATIVE EXAMPLE

As an illustration of the method of analysis and of the sensitivity of critical responses to variations in the available freeboard, the maximum base shear and base moment induced in the free-standing cantilever tank examined in Appendix G are evaluated considering the roof to be horizontal. The system parameters and response values needed in the analysis are as follows:

$$H_\ell = 20.4\ ft, \quad R = 25\ ft, \quad h_s = 3.85\ ft, \quad (S_A)_{c1} = 0.175(S_A)_i \qquad \text{(D.19)}$$

Additionally, the impulsive and fundamental convective components of the liquid mass for the roofless tank are $m_i=0.471m_\ell$ and $m_{c1} = 0.504m_\ell$, and the corresponding centroidal height for the fundamental convective component of response is $h_{c1}=0.577H_\ell$.

Table D.1 lists the components of the total tank wall force or base shear computed for several values of the freeboard-to-slosh-height ratio h_o/h_s. They include the impulsive components for the constrained and unconstrained portions of the liquid mass, P_i^c and

P_i^u, the total impulsive component, P_i, and the convective component associated with the unconstrained portion of the liquid. The impulsive components are normalized with respect to $m_\ell (S_A)_i$, whereas the convective component is normalized with respect to $m_\ell (S_A)_{c1}$. The corresponding base moments are listed in Table D.2, with the impulsive components normalized with respect to $m_\ell H_\ell (S_A)_i$, and the convective component normalized with respect to $m_\ell H_\ell (S_A)_{c1}$. Also listed in these tables are the central half-angles of the maximum impacted roof areas, θ_o, expressed in degrees.

It is worth observing in Table D.1 that, even when the available freeboard is 95 percent of the maximum slosh height for the roofless tank, the total impulsive component of the base shear exceeds by about 30 percent the corresponding value obtained for the roofless system. It should further be noted that with decreasing h_o/h_s, the total impulsive component of the wall force approaches rapidly the limiting value of

$$P = \frac{1}{2} [m_\ell + m_i] (S_A)_i \qquad (D.20)$$

For the particular example considered, for which $m_i=0.471m_\ell$, the latter value is $P=0.736m_\ell (S_A)_i$. Incidentally, this value is lower than that obtained for the total liquid mass because, even with minimal freeboard, the portion of the liquid below the non-impacted roof area will experience some sloshing action. Only when the upper surface of the liquid is fully constrained would the entire liquid mass act impulsively.

Table D.1 Components of Total Wall Force for Illustrative Example

h_o/h_s	θ_o (degrees)	Component of Wall Force			
		Impulsive			Convective
		$\frac{P_i^c}{m_\ell (S_A)_i}$	$\frac{P_i^u}{m_\ell (S_A)_i}$	$\frac{P_i}{m_\ell (S_A)_i}$	$\frac{P_c^u}{m_\ell (S_A)_{c1}}$
0	90	0.500	0.236	0.736	0.252
0.10	84.3	0.509	0.236	0.745	0.252
0.25	75.5	0.520	0.237	0.757	0.254
0.50	60.0	0.516	0.249	0.765	0.267
0.75	41.4	0.443	0.288	0.731	0.309
0.90	25.8	0.314	0.345	0.659	0.369
0.95	18.2	0.231	0.379	0.610	0.406
1	0	0	0.471	0.471	0.504

Table D.2 Components of Overturning Moment Immediately Above Tank Base for Illustrative Example

h_o/h_s	θ_o (degrees)	Component of Overturning Base Moment			
		Impulsive			Convective
		$\frac{M_i^c}{m_t H_\ell (S_A)_i}$	$\frac{M_i^u}{m_t H_\ell (S_A)_i}$	$\frac{M_i}{m_t H_\ell (S_A)_i}$	$\frac{M_c^u}{m_t H_\ell (S_A)_{c1}}$
0	90	0.250	0.095	0.345	0.146
0.10	84.3	0.259	0.095	0.354	0.146
0.25	75.5	0.272	0.095	0.367	0.147
0.50	60.0	0.282	0.100	0.382	0.154
0.75	41.4	0.253	0.116	0.369	0.178
0.90	25.8	0.184	0.138	0.322	0.213
0.95	18.2	0.136	0.152	0.288	0.234
1	0	0	0.189	0.189	0.291

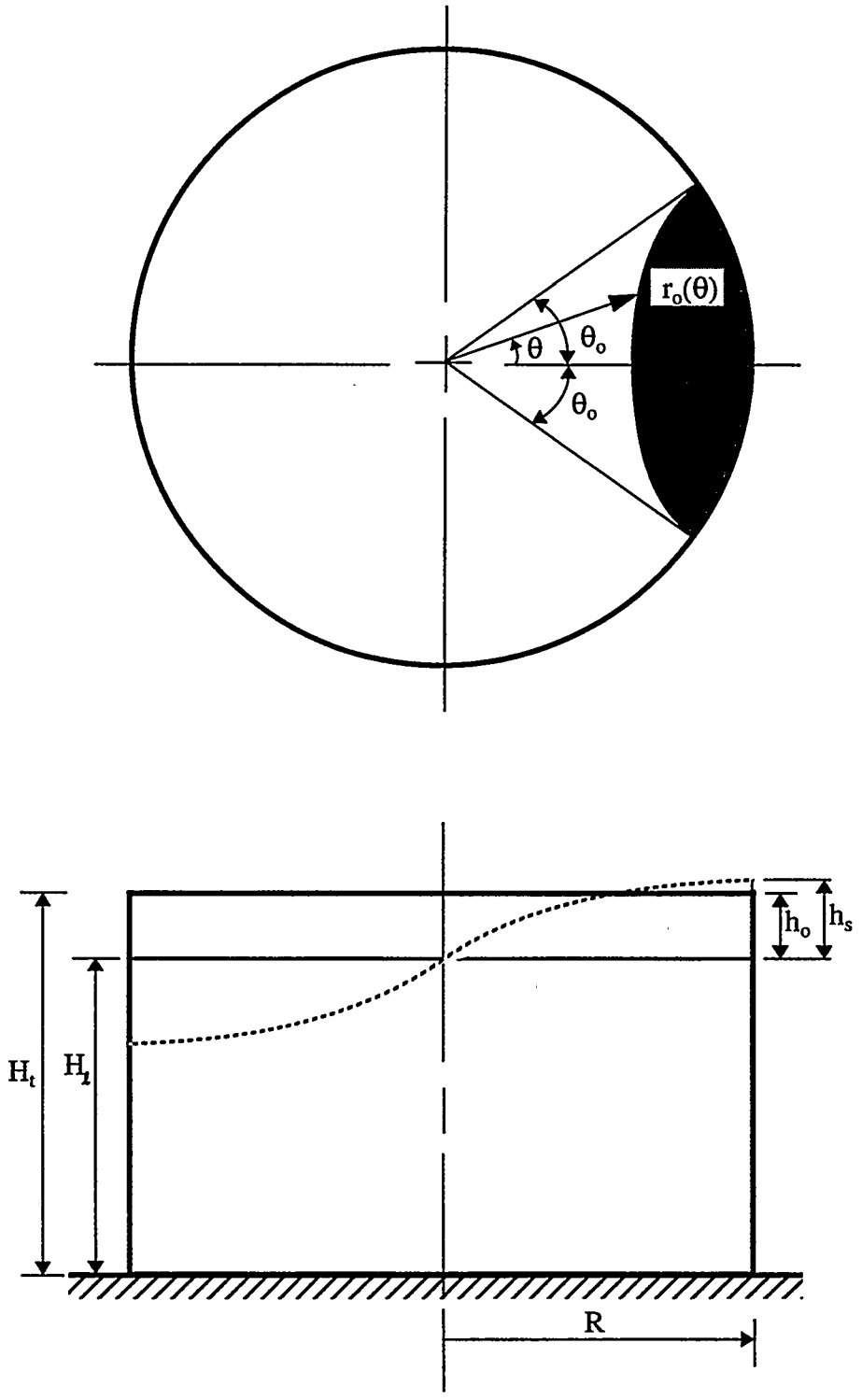

Figure D.1 System Considered and Geometry of Impacted Area

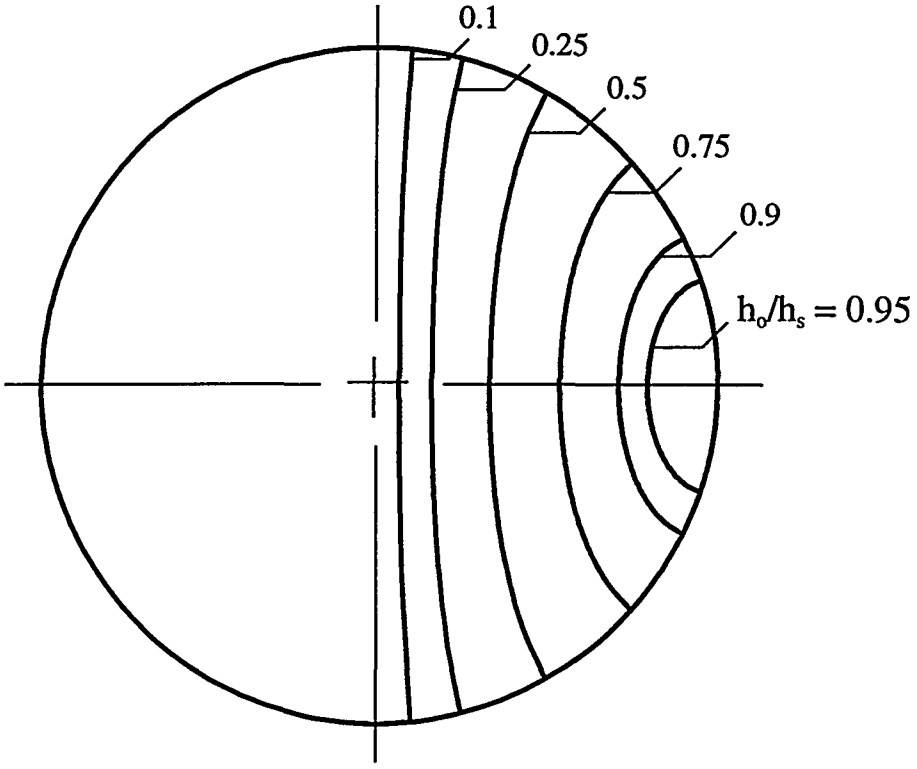

Figure D.2 Impacted Roof Areas for Different Values of h_o/h_s

APPENDIX E

DIMENSIONAL TOLERANCES AND FABRICATION DETAILS

E.1 INTRODUCTION

Tanks similar to those considered herein are designed, fabricated, constructed, examined, and tested to various design specifications and industry codes or standards. The same is true for new tanks that will be designed and constructed in the future. The topics that influence a wide range of design requirements for such tanks have been, and will continue to be, dealt with on site-specific specifications. It is recognized that each site, and even each group of tanks at a particular site, may have unique requirements. Those unique requirements have been or will be established by individual specifications that in turn refer to specific industry codes or standards. It is not the purpose of these guidelines to either mandate or preclude the use of specific industry codes or standards. Rather, these guidelines focus attention on construction details that may influence the ability of a tank to accommodate earthquake loading.

Some aspects of the responses of tanks to earthquake loading suggest a need for certain design or construction details that might not otherwise be required for such tanks. One such issue is the allowable compressive stress in the tank wall and a concern for buckling of the walls. The acceptable compressive stress is influenced by the dimensional tolerances imposed on the as-constructed tank geometry. This topic is addressed in Section E.2.

Another unique consideration related to the design of the underground HLW tanks is that usually it will not be possible to conduct an inspection of the structural details after a seismic event. Seismic loading may induce some large cyclic stresses and strains. This suggests that consideration be given to the design

details where large stress concentration factors are otherwise tolerated. This topic is addressed in Section E.3.

E.2 DIMENSIONAL TOLERANCES

Both the horizontal and vertical components of seismic loads produce meridional compressive stresses in the walls of cylindrical storage tanks. Suggested bases for establishing allowable values of those compressive stresses are provided in Chapter 5. In order to ensure that the compressive stress criteria are appropriate, deviations in the as-constructed tank geometry from that of a perfect right circular cylinder must be limited. Two types of dimensional checks are therefore suggested by these guidelines. While it may be possible in particular cases to justify larger deviations than suggested herein, it should be required that such application-unique justifications demonstrate margins of safety comparable to those provided by these guidelines.

E.2.1 Differences in Cross-Sectional Diameters

The difference in inches between the maximum and minimum diameters at any cross-section [see Figure E.1(a)] should not exceed the smaller of (D + 50)/200 and D/100. In the above expressions, D is the nominal inside diameter of the tank, expressed in inches, at the cross-section under consideration. If the cross-section passes through one or more openings, the permissible difference in diameters may be increased by 0.02 times the diameter of the largest opening, again expressed in inches. These dimensional tolerances are the same as those established by ASME Section III for Class 2 and Class 3 vessels and storage tanks (Reference E.1).

E.2.2 Shell Straightness Tolerances

A tolerance is suggested in Code Case N-530 (Reference E.2) on bulges or flat spots in the cylindrical walls that result from vertical or horizontal elements of the cylinder being other than straight lines. This tolerance is expressed in terms of the

quantities illustrated in Figure E.1. A straight rod is to be positioned either inside or outside the tank, as appropriate, for the deviation being evaluated. The length of the rod, L_x, should be $4\sqrt{Rt}$ plus or minus 10%. The amplitude of the deviation, Δ_x, should not exceed 1% of L_x. This tolerance requirement applies only to regions of the cylindrical walls where allowable compressive stresses are established through application of the Code Case. The reduction of the allowable stress for a larger geometric deviation is discussed in Chapter 5.

E.3 FABRICATION DETAILS

While primary load carrying capability evaluations may indicate the acceptability of a wide range of design details, other considerations may suggest the need to minimize the use of some types of details. The use of single sided and partial penetration welds is an example. Of particular concern is the performance of such welds in regions where large magnitude, reversing stresses (or strains) occur as a result of the seismic loading. In those regions, it is desireable to reduce large stress (strain) concentration factors at the roots and fusion boundaries of the welds, whenever practical. This section makes some suggestions relative to those issues.

All of the details shown in this section are permitted by ASME Section III for Class 2 and Class 3 construction. They are also permitted by API Standard 650. It is not the purpose of these guidelines to preclude any of the details. Rather, the purpose is to identify the desirability of certain details, especially if the seismic capacity of the tank is determined following the guidelines presented in Chapter 5.

E.3.1 Tank Bottom Details

Most codes and standards applicable to the construction of flat bottom tanks allow the bottom plates to be lap welded as shown in

Figure E.2. This is true (up to a certain plate thickness) even for the region where the tank wall is joined to the bottom. Yet, it has been reported that seismic loading may be such as to actually lift the bottom plate off the foundation of the tank by a small amount. As a minimum, for those regions of the bottom, it is recommended that weld details such a those shown in Figure E.3 be specified. In any case, the bottom course of shell plate should be welded to the bottom plate with a full penetration weld as shown in Figure E.4(a). It may even be advisable to specify a bottom shell plate to tank bottom detail as shown in Figure E.4(b).

E.3.2 Nozzle Penetration Details

Industry codes and standards permit a wide range of details for penetration through the walls of storage tanks. Many of them involve partial penetration and single sided welds as illustrated in Figure E.5 for small diameter fittings and as illustrated in Figure E.6 for larger nozzles, with or without reinforcements. For those cases where the penetrations are in regions of the tank that are highly stressed by seismic loadings, it is recommended that better design details be specified. Examples of such details for small fittings are shown in Figure E.7. For larger nozzles, some acceptable details are illustrated in Figures E.8.

E.4 ROOF PLATE AND OTHER DETAILS

The issues relative to strain concentrations at the roots of single sided welds in tank roofs, their supporting structures (if any) and their attachments to the tank wall may not be of such concern as elsewhere in the tank. However, certain design considerations may be applicable and important for specific tanks. For example, sloshing loading on the tank wall to tank roof juncture could have a major influence on the acceptability of that weld design detail.

REFERENCES

E.1 American Society of Mechanical Engineers, "ASME Boiler and Pressure Vessel Code, Section III, Rules for Construction of Nuclear Power Plant Components, Division 1, Subsection NC-3900," 1992.

E.2 ASME Boiler and Pressure Vessel Code, Nuclear Code Case N-530, "Provisions for Establishing Allowable Axial Compressive Membrane Stresses in Cylindrical Walls of 0-15 Psi Storage Tanks, Classes 2 and 3, Section III, Division 1," December 1994.

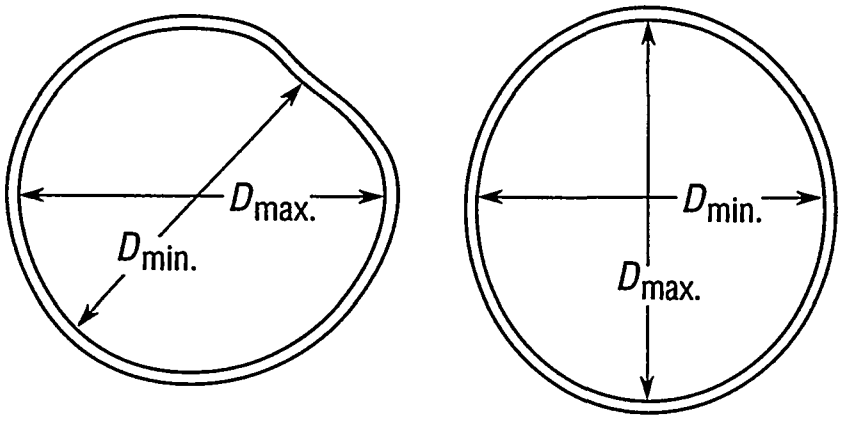

(a) Differences in Diameters

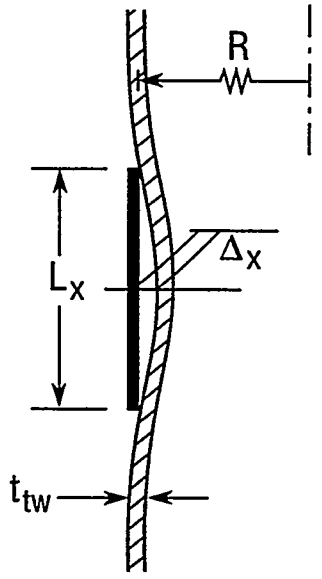

(b) Meridional-Straightness Tolerance

Figure E.1 Dimensional Tolerance Measurements

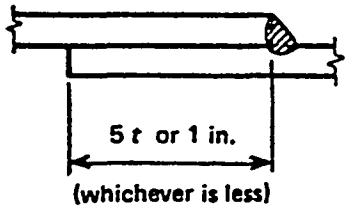

(a) Single Welded Tank Bottom Lap Joint

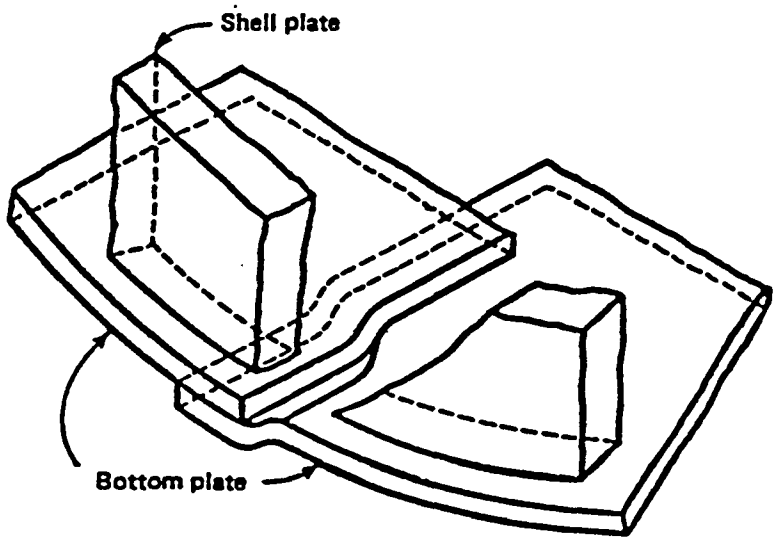

(b) Lap Welded Bottom Plates Under Tank Shell

Figure E.2 Less Desirable Tank Bottom Details

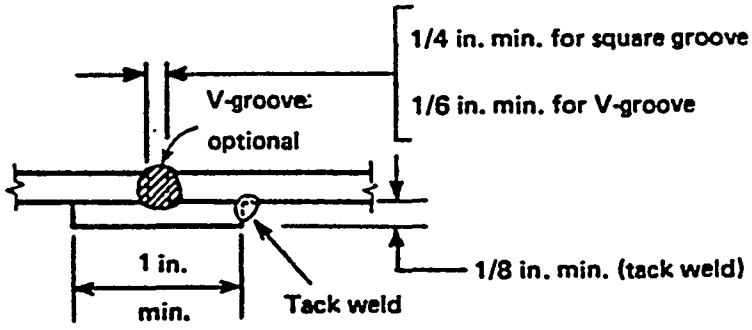

(a) Single Welded Butt Joint With Backing Strip

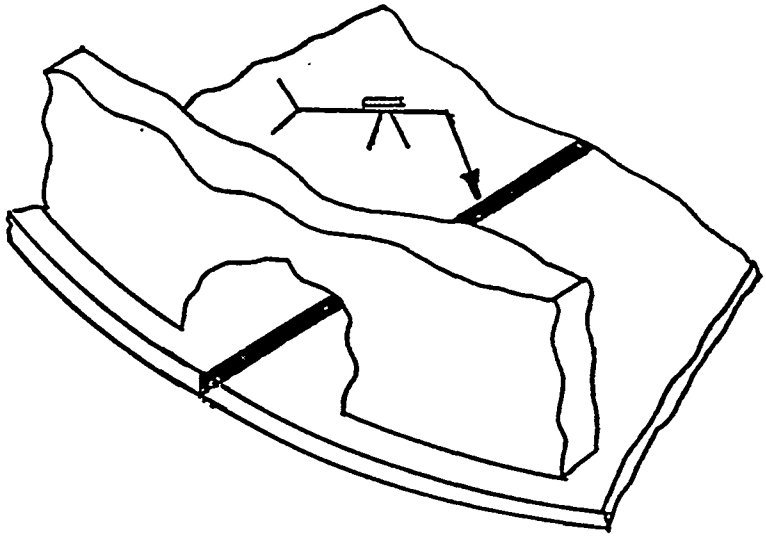

(b) Butt Welded Sketch Plate Under Tank Shell

Figure E.3 Acceptable Tank Bottom Details

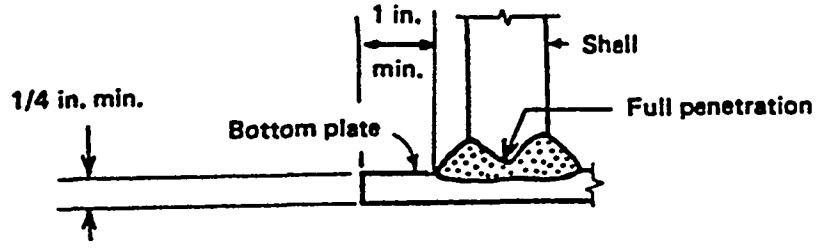

(a) Full Penetration Weld of Bottom To Tank Wall

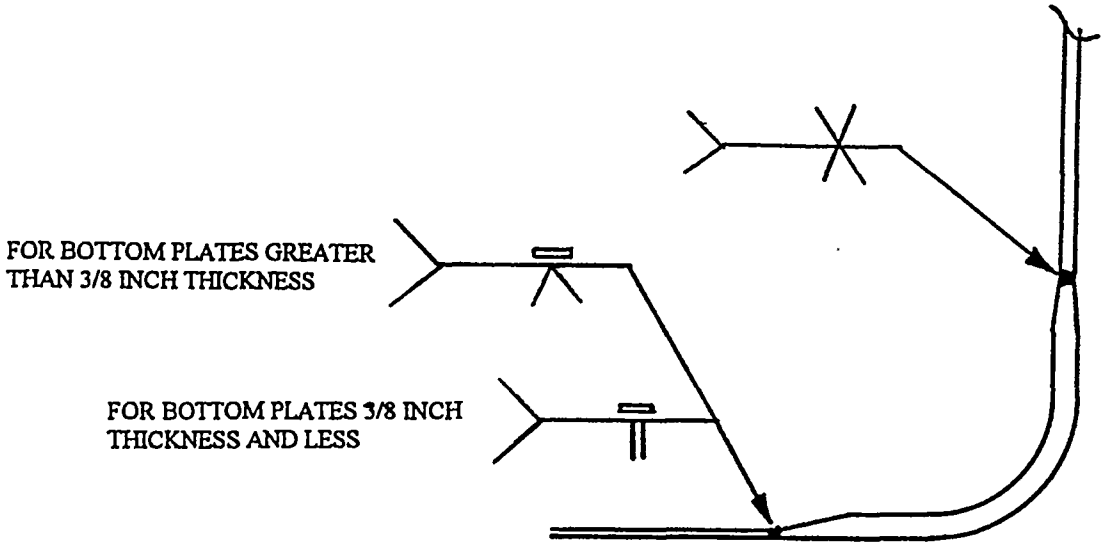

(b) Alternate Bottom to Tank Wall Design Detail

Figure E.4 Desirable Tank Wall to Bottom Plate Details

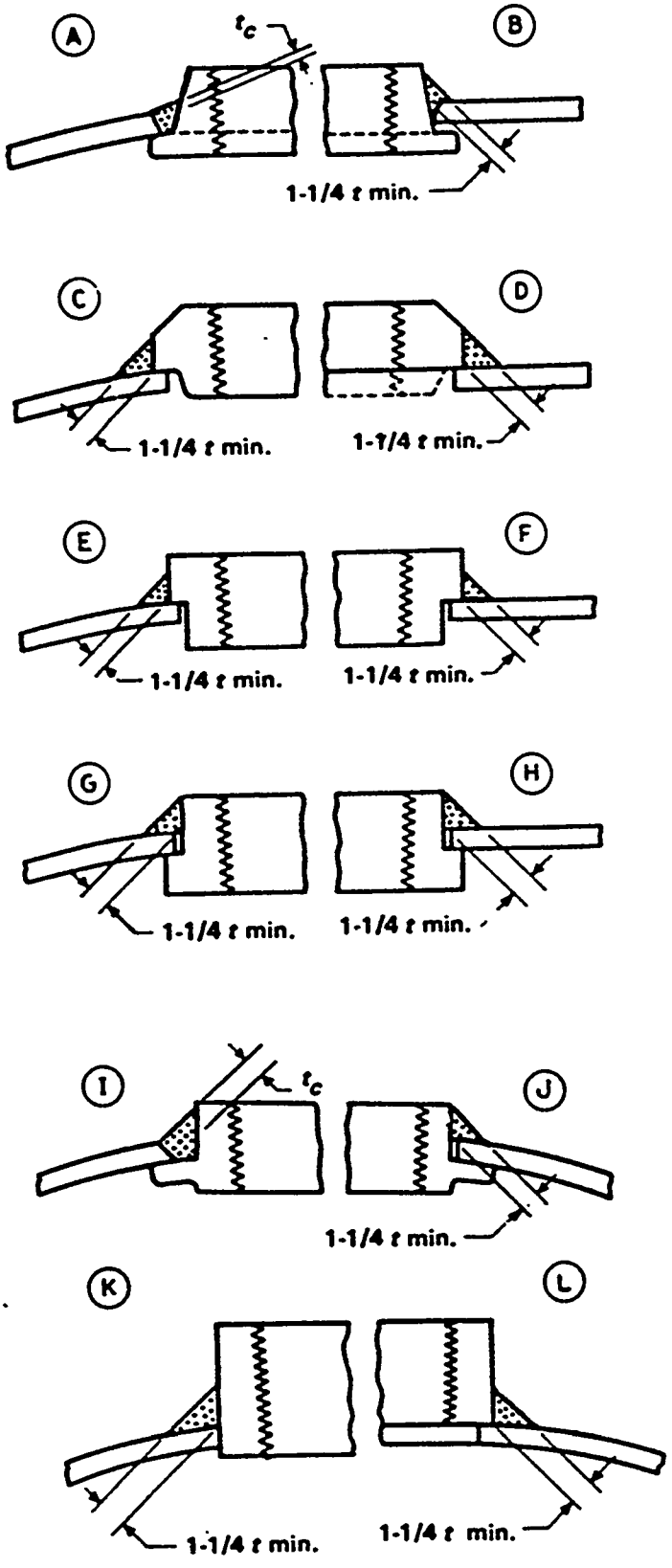

Figure E.5 Fittings with Single Sided Welds

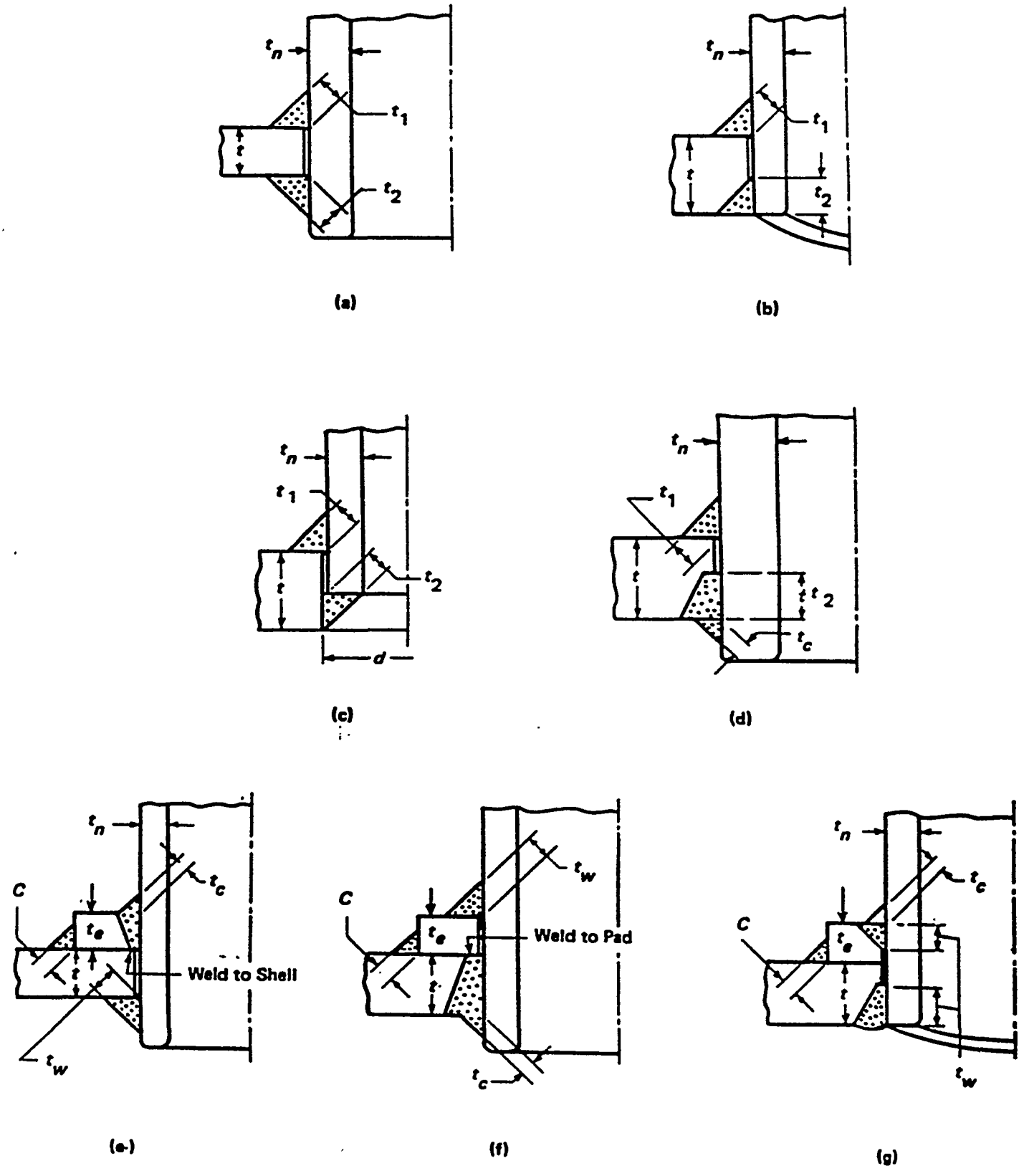

Figure E.6 Nozzles with Partial Penetration Welds

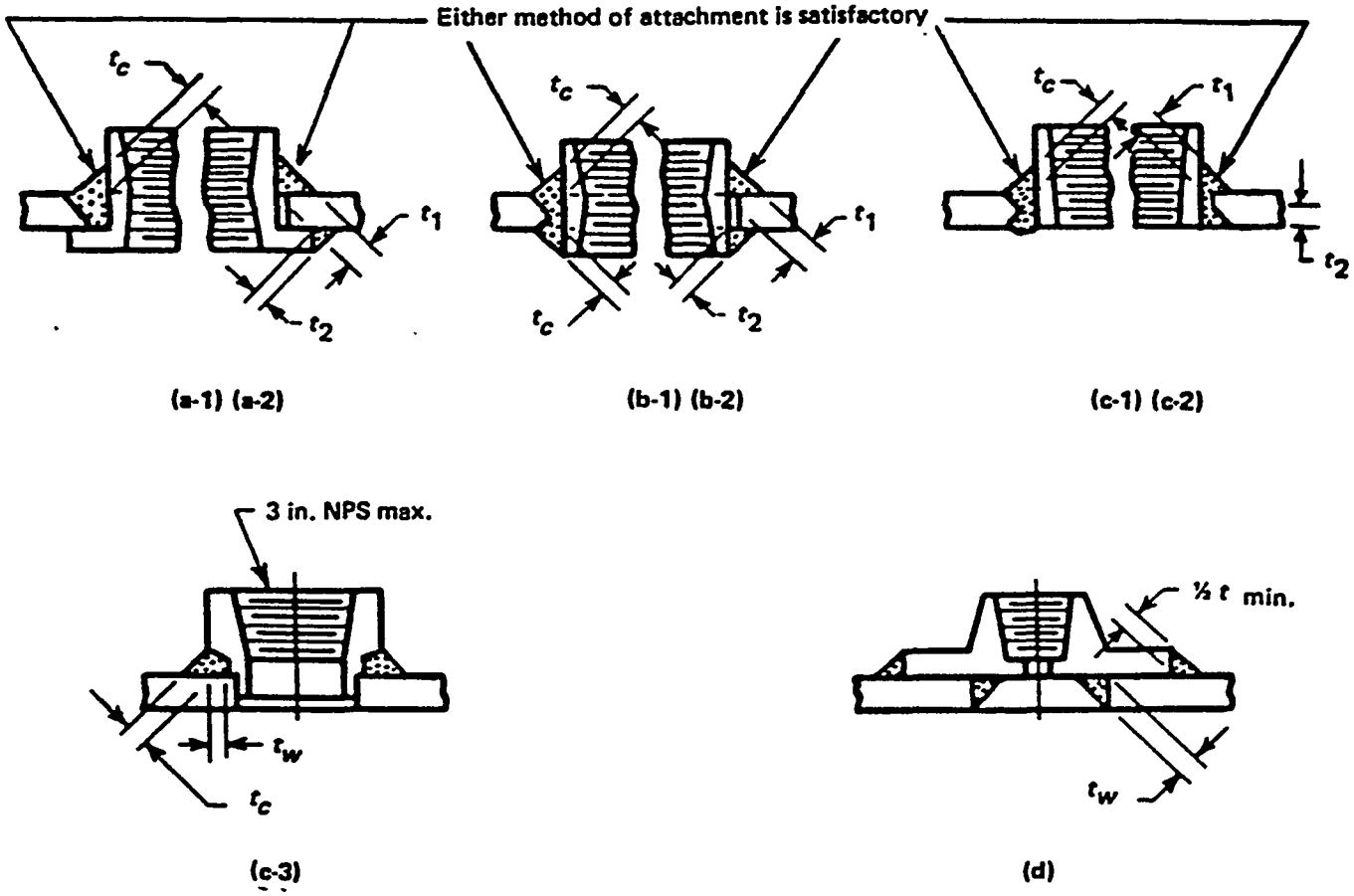

Figure E.7 Fittings Welded from Both Sides

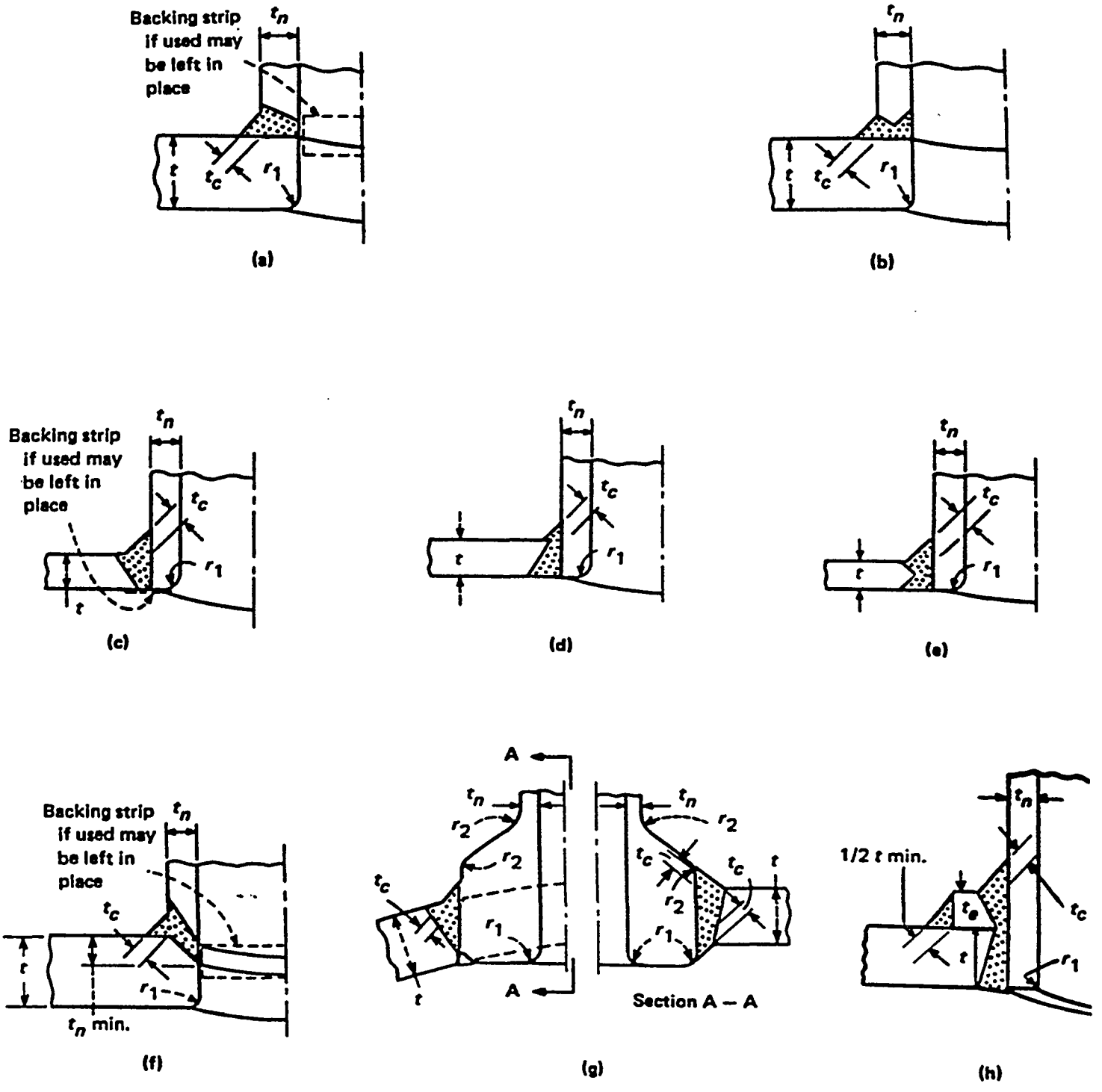

Figure E.8 Nozzles with Full Penetration Welds

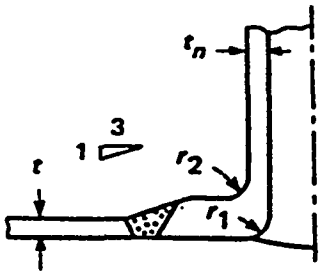

(a)

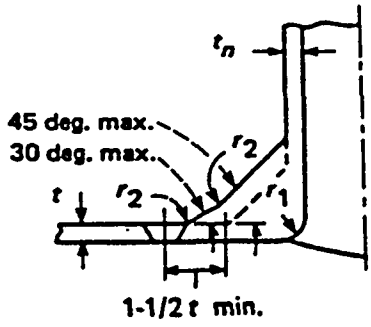

(b)

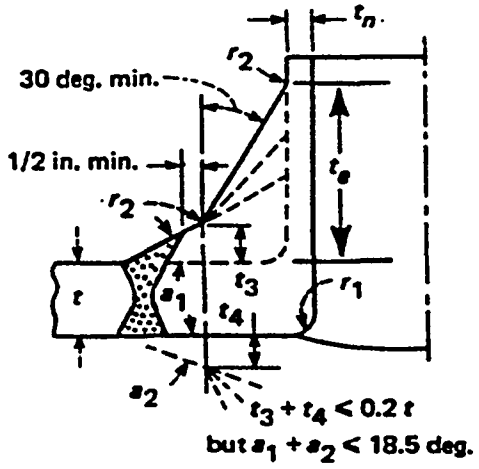

(c)

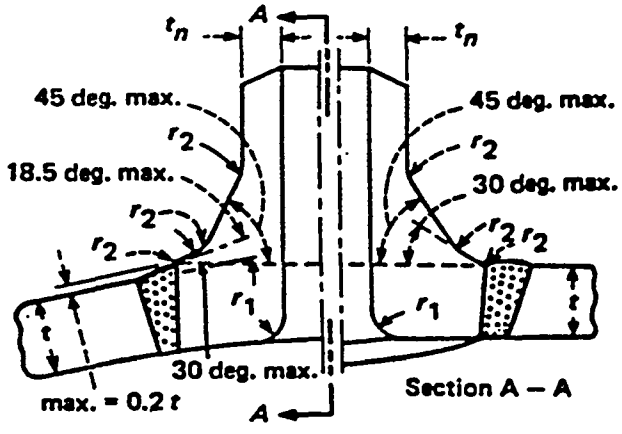

Sections Perpendicular and Parallel to the Cylindrical Vessel's Axis

(d)

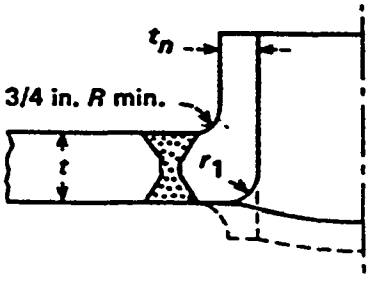

(e)

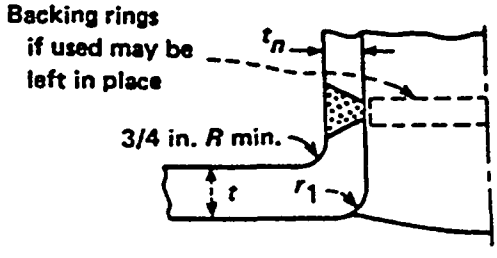

(f)

Figure E.8 Nozzles with Full Penetration Welds (Concluded)

APPENDIX F

BUCKLING OF CYLINDRICAL TANKS WITH INTERNAL PRESSURE SUBJECTED TO VIBRATORY MOMENT LOADING

F.1 INTRODUCTION

For tanks which are to be designed in accordance with ASME code requirements, it is recommended in Chapter 5 that the nominal axial buckling capacity σ_{au} be estimated based on the ASME Code Case N-530 (Reference F.1) which has adopted the provisions of the European Convention for Constructional Steelwork Code (Reference F.2). Herein, this approach will be called the ECCS Code approach. The ECCS Code provisions are presented in Chapter 5.

It is also noted in Chapter 5 that the ECCS Code provisions appear to be excessively conservative when compared with shake table test data for buckling of cylindrical tanks with internal pressure subjected to vibratory moment loading. Therefore, it is recommended that the ECCS Code provisions not be used for the purpose of estimating realistic buckling capacities of existing tanks subjected to vibratory moment loading. This appendix provides an alternative approach aimed at obtaining a more realistic, yet conservative, buckling capacity for tanks.

Experimental shake table performance data are presented in References F.3 through F.5 that demonstrate that the buckling capacity under vibratory, non-uniform, bending moment as is experienced in an earthquake greatly exceeds that predicted by the ECCS approach. Based on data reported in References F.3 and F.4, Manos (Reference F.3) has suggested limiting the maximum seismic-induced axial stress to 75% of the classical buckling stress, σ_{cl}. Such a value is substantially above the ratio of σ_{au} to σ_{cl} of 0.40 to 0.55 obtained following the ECCS provisions for

uniform compression in typical tanks with ratios of hoop to yield stresses (σ_h/σ_y) between 0.2 and 0.55.

In addition, Reference F.6 has compared the value of σ_{au}/σ_{cl} for uniform membrane compression as predicted by the ECCS Code provisions with σ_{au}/σ_{cl} predicted by the New Zealand Code (References F.7 and F.8) provisions and by Brookhaven National Laboratory (BNL) BOSOR5 (Reference F.9) analyses. Figures F.1 through F.5 show these comparisons[1] of σ_{au}/σ_{cl} versus σ_h/σ_y for tanks with various radius-to-thickness ratios (R/t_{tw}). When $\sigma_h/\sigma_y < 0.25$, results obtained from the ECCS Code provisions, the New Zealand Code provisions, and the BNL BOSOR5 analyses are very similar. However, as σ_h/σ_y is increased beyond about 0.25, the ECCS Code provisions begin to result in substantially lower predicted σ_{au}/σ_{cl} than do either the New Zealand Code Provisions or the BNL BOSOR5.

In this Appendix, the experimental shake table data from References F.3 through F.5 will be compared with the nominal axial capacity, σ_{au}, predicted following both the ECCS Code and the New Zealand Code provisions. It will be shown that the New Zealand Code provisions provide a substantially better, yet conservative, prediction of the experimental results than does the ECCS code provisions over the stress range $0.2 < \sigma_h/\sigma_y < 0.55$. Therefore, the New Zealand Code provisions are described in the next section.

F.2 NEW ZEALAND CODE PROVISIONS

By the New Zealand Code (References F.7 and F.8), the nominal axial capacity, σ_{au}, is taken as the lesser of the "diamond" (membrane compression) buckling capacity σ_{ad}, and the plastic ("elephant-foot") collapse capacity σ_{ap}. When σ_h/σ_y exceeds about

[1]Data from Reference F.6 are replotted with smooth curves. Also, additional data are provided.

0.2, the plastic collapse capacity σ_{ap} generally controls, and will be discussed first.

F.2.1 Plastic Collapse Capacity

The plastic collapse capacity, σ_{ap}, is based on the work of Rotter (Reference F.10) and is given by:

$$\sigma_{ap} = F_1 \, F_2 \, F_3 \, \sigma_{cl} \leq \sigma_y \qquad \text{(F.1)}$$

where $\sigma_{cl} = \dfrac{0.605 \, E_t}{R/t_{tw}}$

$$F_1 = \left[1 - (\sigma_h/\sigma_y)^2\right]$$

$$F_2 = 1 - \left[\frac{1}{1.12 + S_1^{1.5}}\right]$$

$$F_3 = \left[\frac{S_1 + (\sigma_y/36 \; ksi)}{S_1 + 1}\right]$$

$$\sigma_h = p_{mx}\left(\frac{R}{t_{tw}}\right)$$

where $S_1 = R/(400t_{tw})$, R is the tank radius, E_t is the modulus of elasticity of the tank material, t_{tw} is the tank wall thickness near the shell base, p_{mx} is the maximum tank internal pressure, and σ_y is the yield stress of the tank material. For situations where additional hoop stress results from other loadings, the total σ_h should be substituted for $p_{mx}(R/t_{tw})$ in the equation for F_1. F_1 is a correction factor related to σ_h/σ_y. F_2 is a correction factor related to (R/t_{tw}). F_3 is an additional correction factor related to the yield stress, σ_y, and (R/t_{tw}). However, since Rotter developed Equation F.1 based on BOSOR5 analyses conducted using σ_y = 36 ksi and σ_y = 50 ksi only, it is questionable whether F_3 should be used outside of the range of

30 ksi $\leq \sigma_y \leq$ 60 ksi. Because of a lack of evidence to the contrary, it is conservatively recommended that F_3 be used even when $\sigma_y <$ 30 ksi.

In accordance with Chapters 3 and 5, it is recommended that p_{mx} be taken as the total inelastic factored pressure p_{ti} as given by:

$$p_{mx} = p_{ti} = p_{st} + \left(\frac{SF}{F_{\mu D}}\right) p_d \qquad \text{(F.2)}$$

where p_{st} is the hydrostatic pressure, p_d is the probable hydrodynamic pressure occurring at the time of maximum axial compression, SF is the appropriate scale factor from Chapter 3, and $F_{\mu D}$ is between 1.0 and 1.5 in accordance with the hoop capacity provisions of Table 3.3. In the comparisons made in this Appendix, SF = 1.0 and $F_{\mu D}$ = 1.5. From Equation 5.18a, for cantilevered tanks:

$$p_d = p_{dh} \pm 0.4\ p_{dv} \qquad \text{(F.3)}$$

where p_{dh} is the maximum hydrodynamic pressure from the horizontal earthquake component, and p_{dv} is the maximum hydrodynamic pressure from the vertical earthquake component. The 0.4 factor is to obtain a probable combination and the positive or negative sign should be chosen so as to give the minimum axial capacity (a positive sign will always give the minimum for plastic collapse, and a negative sign will always give the minimum for "diamond" buckling).

F.2.2 <u>"Diamond" (Membrane Compression) Buckling Capacity</u>

From the New Zealand Code, the "diamond" axial buckling capacity σ_{ad} under bending loads with internal pressure is given by:

$$\sigma_{ad} = 0.19\sigma_{cl} + 0.81\ \sigma_p \qquad \text{(F.4)}$$

where

$$\sigma_p = \sigma_{cl}\left[1 - f_p\left(1 - (\sigma_o/\sigma_{cl})^2\right)\right]^{1/2} \leq \sigma_{cl}$$

$$f_p = \left(1 - \frac{p_{mx}\, R}{5\sigma_{cl}\, t_{tw}}\right)^2 \geq 0$$

in which σ_o is the "diamond" buckling capacity under uniform compression without internal pressure computed from:

$$\alpha = 1 - \left(1.24\frac{\delta}{t_{tw}}\right)\left[\left(1 + \frac{2}{(1.24\delta/t_{tw})}\right)^{1/2} - 1\right]$$

$$\lambda_o^2 = \frac{\sigma_y}{\alpha\sigma_{cl}}$$

$$\sigma_o = \alpha\sigma_{cl} \quad \text{when } \lambda_o^2 \geq 2$$

$$\sigma_o = \sigma_y\left(1 - \frac{\lambda_o^2}{4}\right) \quad \text{when } \lambda_o^2 < 2$$

and (δ/t_{tw}) is the ratio of the maximum imperfection amplitude to wall thickness. For tanks which meet the tolerance limits of Appendix E:

$$(\delta/t_{tw}) \leq 0.04\,(R/t_{tw})^{1/2} \qquad \text{(F.5)}$$

F.3 SHAKE TABLE TEST DATA

Table F.1 presents the available shake table test data. For the tests reported by Manos (Reference F.3), neither the yield stress, σ_y, nor the hydrodynamic pressure, p_d, was reported. Therefore, σ_y and p_{mx} need to be estimated. Lower, best, and upper bound estimates were made for each of these quantities. Therefore, a range is given on $(\sigma_h/\sigma_y) = \left(\frac{p_{mx}\, R}{\sigma_y\, t_{tw}}\right)$.

However, Manos reported an observed resisting overturning moment, M_R, and recommends the following equation for predicting M_R:

$$M_R = 1.29\gamma_\ell H_\ell^2 R^2 \left(\frac{S_{ah}}{g}\right)\left(\frac{m_i}{m_\ell}\right)\left(\frac{H_\ell}{R}\right)^{0.15} \qquad \text{(F.6)}$$

where (m_i/m_ℓ) is the Housner estimate of the ratio of the impulsive mass to the total liquid mass (see Equation 3500-3 of Reference F.11) and γ_ℓ is the specific weight of the liquid. Thus, for water, the horizontal spectral acceleration S_{ah} can be computed from:

$$\frac{S_{ah}}{g} = \frac{M_R}{1.29\,(\gamma_\ell)\,H_\ell^2 R^2 \left(\frac{m_i}{m_\ell}\right)\left(\frac{H_\ell}{R}\right)^{0.15}} \qquad \text{(F.6a)}$$

Then, the vertical spectral acceleration S_{av} can be approximated by:

$$S_{av} = (2/3)\, S_{ah} \qquad \text{(F.7)}$$

and the hydrodynamic pressure from the vertical component p_{dv} can be estimated from:

$$p_{dv} = 0.8\,(p_{st})\,(S_{av}) \qquad \text{(F.8)}$$

The hydrodynamic pressure from the horizontal component p_{dh} can be directly estimated from M_R using Equation 3500-6 of Reference F.11, i.e.,

$$p_{dh} = \frac{M_R}{1.36 R H_\ell^2} \qquad \text{(F.9)}$$

Given p_{dv} and p_{dh}, p_{mx} can be obtained from Equations F.2 and F.3. Table F.2 presents the estimated values of p_{dh}, p_{dv}, and p_{mx} for each of the Reference F.3 tanks.

Figure 5c of Reference F.4 provides a plot of the measured

hydrodynamic pressure time history for Tank W1. At the time when buckling is initiated (13.8 sec), the hydrodynamic pressure p_d was 1.7 psi which is in close agreement with the 1.5 psi value estimated in Table F.2 following the above approach. This measured p_d of 1.7 psi is used to estimate p_{mx} for both tanks W1 and W2 in Table F.1.

The hoop stress σ_h used in Table F.1 is the nominal hoop stress computed from $\sigma_h = \left(\frac{p_{mx} R}{t_{tw}}\right)$ since this is the hoop stress to be used in both the ECCS and the New Zealand Code capacities. The actual measured hoop stress may be higher because of local curvature effects, particularly after a bulge is initiated.

It should also be noted that Reference F.5 provides shake table test data for two tanks. Only the results for Tank No. 2 are reported in Table F.1. Tank No. 1 was essentially identical to Tank No. 2. Tank No. 1 was initially subjected to a high-frequency long duration sinusoidal input. Reference F.5 reports that this input resulted in violent vibration around the middle part of the tank shell. This vibration had multiple lobes around the circumference. A slight bulge was reported to have been found after this test. The reported maximum axial strain corresponded to an axial stress of only 36% of the classical buckling capacity. This result is being ignored for two reasons:

1. The input motion and reported response were not similar to what would be expected on a thicker walled tank subjected to seismic input. Furthermore, because of the multiple circumferential lobes and axial variation of response, it is questionable as to whether the maximum strain was measured.

2. After developing this slight bulge, the tank was subjected

. to various amplitudes of simulated El Centro input motion. The slight bulge did not appear to affect the tank response or capacity when subjected to the simulated seismic shaking. Despite the presence of this bulge, the reported behavior and capacity for Tank No. 1 under simulated seismic shaking was similar to that of Tank No. 2.

The buckling capacity reported in Table F.1 for Tank No. 2 is that at which no damage was visible but the strain gage record showed that a small amount of permanent strain had been accumulated. This tank severely buckled at an input 1.2 times greater. Therefore, the exact buckling capacity of Tank No. 2 is slightly greater than what is reported in Table F.1. The hydrostatic pressure was 1.3 psi and for the test in which the slight bulge developed, the hydrodynamic pressure was 1.1 psi leading to a p_{mx} of 2.0 psi from Equation F.2.

F.4 COMPARISON OF SHAKE TABLE TEST DATA TO CODE CAPACITIES

Table F.3 compares the axial compressive stress, σ_{at}, obtained from the test with the nominal axial capacity, σ_{au}, predicted by the ECCS and New Zealand Codes for each of the tanks reported in Table F.1. Both stresses are nondimensionalized with respect to the classical buckling stress, $\sigma_{c\ell}$. The results for tanks W2 and T-T are not of much interest. The axial stress was below nominal code capacities and no damage was observed. The results for the remaining tanks are plotted in Figure F.6. The influence of uncertainty on σ_y and p_{mx} is shown by uncertainty bands on this figure. These uncertainty bands make the figure difficult to read. Even so, it is clear that the ECCS Code σ_{au} is excessively conservative when compared to the test results, σ_{at}, and this conservatism increases with increasing σ_h/σ_y. The New Zealand Code σ_{au} provides a more uniform conservatism in the range $0.2 < \sigma_h < 0.55$. At $\sigma_h = 0.2$, the ECCS and New Zealand Code capacities are very similar and thus have roughly the same conservatism. However, as σ_h/σ_y increases, the New Zealand Code

capacity retains about this same level of conservatism whereas the ECCS Code capacities become increasingly more conservative. These points are clearer in Figure F.7 which compares σ_{at}/σ_{au} for both the ECCS Code and New Zealand Code capacities using only the "best" estimate σ_y and p_{mx} results. Over the range of $0.2 \leq \sigma_h/\sigma_y \leq 0.55$, the value of σ_{at}/σ_{au} has the following statistics:

	ECCS Code	New Zealand Code
σ_{at}/σ_{au} Mean	1.62	1.27
Coef. of Variation	0.15	0.07

F.5 RECOMMENDATIONS FOR A MORE REALISTIC BUCKLING CAPACITY ESTIMATE

When σ_h/σ_y exceeds about 0.2, it is recommended that the nominal code buckling capacity, σ_{au}, be estimated using the New Zealand Code provisions as summarized in Section F.2 of this Appendix as opposed to the ECCS Code provisions summarized in Chapter 5, for a more realistic, yet conservative, buckling capacity estimate.

When σ_h/σ_y exceeds about 0.55, Figure F.1 indicates that even the New Zealand Code provisions might become excessively conservative. However, because of the lack of experimental data, further relaxation beyond the New Zealand Code provisions is not recommended at this time.

The question remains as to what factor of safety, FS, should be applied to the nominal code capacity, σ_{au}, when it is predicted following the New Zealand Code provisions. The New Zealand Code does not provide an additional factor of safety to the nominal capacity σ_{au}, whereas Chapter 5 recommends an FS = 1.33 to be applied to σ_{au} in order to obtain the allowable axial compressive stress. It is recommended that the same FS (i.e., FS = 1.33) be applied to the σ_{au} capacity predicted by the New Zealand Code provisions.

REFERENCES

F.1 ASME Boiler and Pressure Vessel Code, Nuclear Code Case N-530, "Provisions for Establishing Allowable Axial Compressive Membrane Stresses in Cylindrical Walls of 0-15 Psi Storage Tanks, Classes 2 and 3, Section III, Division 1," December 1994.

F.2 "Buckling of Steel Shells - European Recommendations," European Convention of Constructional Steelwork (ECCS), Fourth Edition, No. 56, 1988.

F.3 Manos, G.C., "Earthquake Tank-Wall Stability of Unanchored Tanks," Journal of Structural Engineering, Vol. 112, No. 8, ASCE, pp. 1863-1880, August 1986.

F.4 Niwa, A., and Clough, R.W., "Buckling of Cylindrical Liquid-Storage Tanks Under Earthquake Loading," Earthquake Engineering and Structural Dynamics, Vol. 10, John Wiley & Sons, pp. 107-22, 1982.

F.5 Jia, Z.H., and Ketter, R.L., "Experimental Study of 'Elephant Foot Bulge' Instability of Thin-Walled Metal Tanks," Technical Report NCEER-89-0004, National Center for Earthquake Engineering Research, February 1989.

F.6 Bandyopadhyay, K., Xu, J., Shteyngart, S. and Gupta, D., "Cylindrical Shell Buckling through Strain Hardening," American Society of Mechanical Engineers, PVP-Volume 308, 1995.

F.7 Priestly, M.J.N., et al., "Seismic Design of Storage Tanks," Bulletin of the New Zealand National Society for Earthquake Engineering, Vol. 19, No. 4, December 1986.

F.8 Priestly, M.J.N., et al., "Seismic Design of Storage Tanks Recommendations of a Study Group of the New Zealand National Society for Earthquake Engineering," December 1986.

F.9 Bushnell, D., "BOSOR5: A Computer Program for Buckling of Elastic-Plastic Complex Shells of Revolution including Large Deflection and Creep," Lockheed Missiles & Space Co., December 1974.

F.10 Rotter, J.M., "Local Inelastic Collapse of Pressurized Thin Cylindrical Steel Shells Under Axial Compression," Research Report, School of Civil and Mining Engineering, University of Sydney, Australia, 1985.

F.11 American Society of Civil Engineers, Standard 4-86, "Seismic Analysis of Safety-Related Nuclear Structures and Commentary on Standard for Seismic Analysis of Safety-Related Nuclear Structures," September 1986.

NOTATION

E_t	modulus of elasticity of tank material
F_1	correction factor related to σ_h/σ_y
F_2	correction factor related to (R/t_w)
F_3	additional correction factor related to the yield stress σ_y and (R/t_w)
$F_{\mu D}$	permitted inelastic energy absorption factor from Table 3.3
FS	factor of safety
H_ℓ	height of liquid
m_i	impulsive mass
m_ℓ	total liquid mass
M_r	base resisting overturning moment
p_d	probable hydrodynamic pressure occurring at the time of maximum axial compression
p_{dh}	maximum hydrodynamic pressure due to horizontal component of seismic motion
p_{dv}	maximum hydrodynamic pressure due to vertical component of seismic motion
p_{mx}	maximum tank internal pressure
p_{st}	hydrostatic pressure
p_{ti}	total inelastic factored demand pressure
R	radius of the tank

S_{ah}	horizontal spectral acceleration
S_{av}	vertical spectral acceleration
SF	appropriate seismic scale factor from Chapter 3
t_{tw}	thickness of tank wall
γ_ℓ	specific weight of the liquid
δ	maximum imperfection amplitude
σ_{at}	axial compressive stress obtained from tests
σ_{ad}	"diamond" (membrane compression) buckling capacity
σ_{ap}	plastic ("elephant-foot") collapse capacity
σ_{au}	nominal axial buckling capacity
$\sigma_{c\ell}$	classical buckling stress of cylindrical shell
σ_h	tensile hoop stress
σ_o	"diamond" buckling capacity under uniform compression without internal pressure
σ_y	code minimum yield stress

Table F.1 Shake Table Test Data

Source Ref.	Tank	Material	Fluid Ht H_ℓ (ft)	Radius R (ft)	Wall Thick. t_{tw} (in)	R/t_{tw}	σ_{cl} (ksi)	σ_y (ksi)	p_{mx} (psi)	$\frac{\sigma_h}{\sigma_y}$	Measured Axial Comp. σ_{at} (ksi)	Status
F.3	W1	Stainless Steel	20.0	4.75	0.078	731	24.3	30.0 36.0 43.0	9.8	0.24 0.20 0.17	14.8	Buckled
	S1	Steel	22.6	16.4	0.126	1562	11.4	36.0 43.0 52.0	≥ 12.1 ≥ 11.8 ≥ 11.5	≥ 0.52 ≥ 0.43 ≥ 0.35	9.7	Buckled
	C1	Steel	18.0	19.5	0.180	1300	13.8	36.0 43.0 52.0	19.4 17.9 16.4	0.70 0.54 0.41	12.0	Buckled
	W2	Stainless Steel	20.0	4.75	0.141	404	43.9	30.0 36.0 43.0	>9.8	>0.13 >0.11 >0.09	14.8	No Damage
	T-BR	Aluminum	5.0	6.0	0.080	900	6.8	13.0 15.5 18.5	4.5 4.2 3.9	0.31 0.24 0.19	5.2	No Damage
	T-T	Aluminum	13.0	3.875	0.090	517	11.8	13.0 15.5 18.5	6.0 5.9 5.9	0.24 0.20 0.16	2.5	No Damage
F.5	No. 2	Aluminum	3.0	1.5	0.010	1800	3.0	7.2	2.0	0.50	2.3	Slight Bulge

Table F.2 Estimated Hydrodynamic and Inelastic Factored Maximum Pressure for Reference F.3 Tanks

Tank	p_{st}	M_R (10^6lb-ft)	S_{ah} (g)	p_{dh} (psi)	p_{dv} (psi)	p_d (psi)	p_{mx} (psi)
W1	8.7	0.305	0.38	0.8	1.8	1.5	9.7
S1	9.8	$\geq$3.49(1)	$\geq$0.45	$\geq$2.1	$\geq$2.3	$\geq$3.0	$\geq$11.8
C1	7.8	13.2	2.65	10.7	11.0	15.1	17.9
W2	8.7	>0.305	>0.38	>0.8	>1.8	>1.5	>9.7
T-BR	2.2	0.062	1.89	2.1	2.2	3.0	4.2
T-T	5.6	0.033	0.15	0.3	0.5	0.5	5.9

(1) An observed M_r value is not reported in Reference F.3 for this tank. The value shown is the M_r predicted in Reference F.3. The observed M_r is likely to be higher for this buckled tank.

Table F.3 Comparison of Shake Table Measured Axial Compressions to Code Capacities

Tank	Status	σ_{cl} (ksi)	σ_y (ksi)	p_{mx} (psi)	$\frac{\sigma_h}{\sigma_y}$	Measured (σ_{at}/σ_{cl})	Code Capacities $\left(\frac{\sigma_{au}}{\sigma_{cl}}\right)$	
							ECCS Code	New Zealand Code
W1	Buckled	24.3	30.0 36.0 43.0	9.8	0.24 0.20 0.17	0.61	0.42 0.45 0.46	0.51 0.51 0.51
S1	Buckled	11.4	36.0 43.0 52.0	12.1 11.8 11.5	0.52 0.43 0.35	0.85	0.46 0.55 0.60	0.64 0.75 0.79
C1	Buckled	13.8	36.0 43.0 52.0	19.4 17.9 16.4	0.70 0.54 0.41	0.87	0.27 0.45 0.57	0.44 0.63 0.78
W2	No Damage	43.9	30.0 36.0 43.0	9.8	0.13 0.11 0.09	0.34	0.33 0.36 0.38	0.45 0.45 0.45
T-BR	No Damage	6.8	13.0 15.5 18.5	4.5 4.2 3.9	0.31 0.24 0.19	0.76	0.50 0.52 0.52	0.56 0.59 0.58
T-T	No Damage	11.8	13.0 15.5 18.5	6.0 5.9 5.9	0.24 0.20 0.16	0.21	0.43 0.46 0.48	0.42 0.44 0.47
No. 2	Slight Bulge	3.0	7.2	2.0	0.50	0.77	0.42	0.58

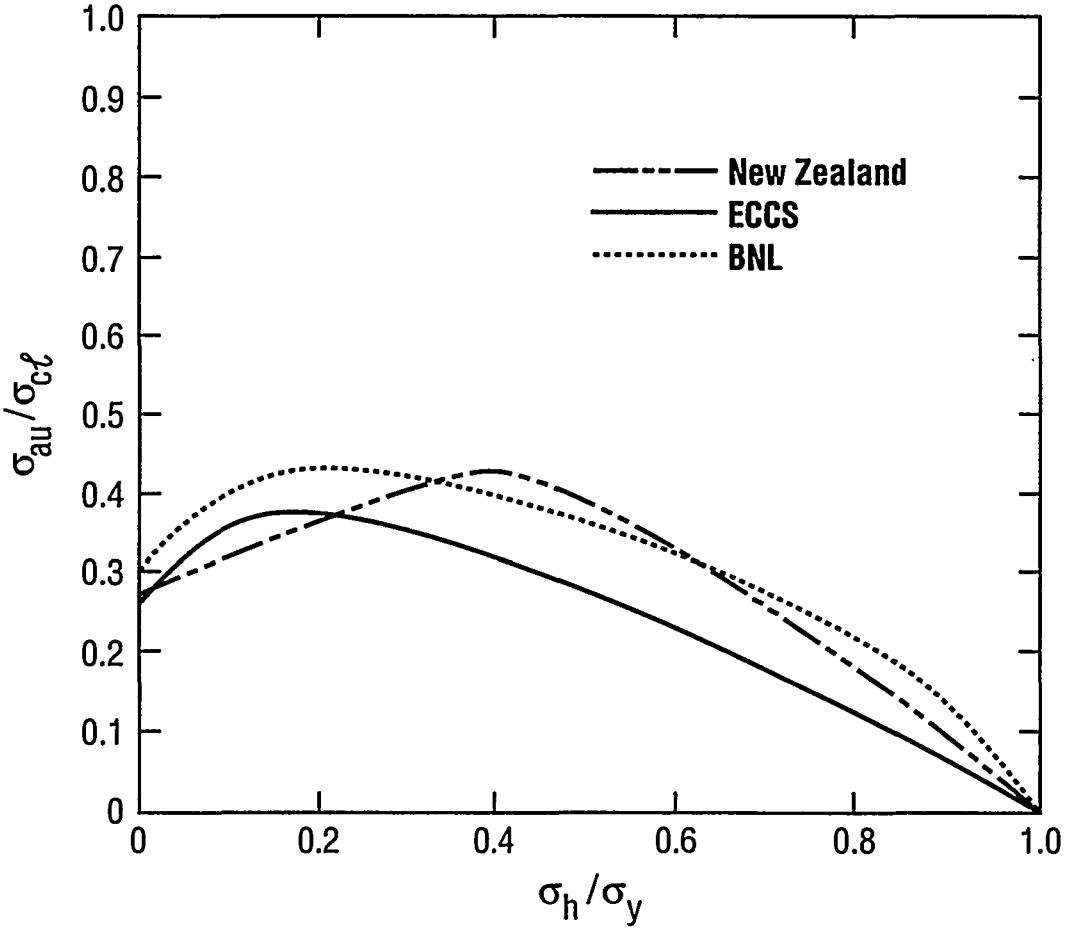

Figure F.1 Comparison of Results for $R/t_w = 400$

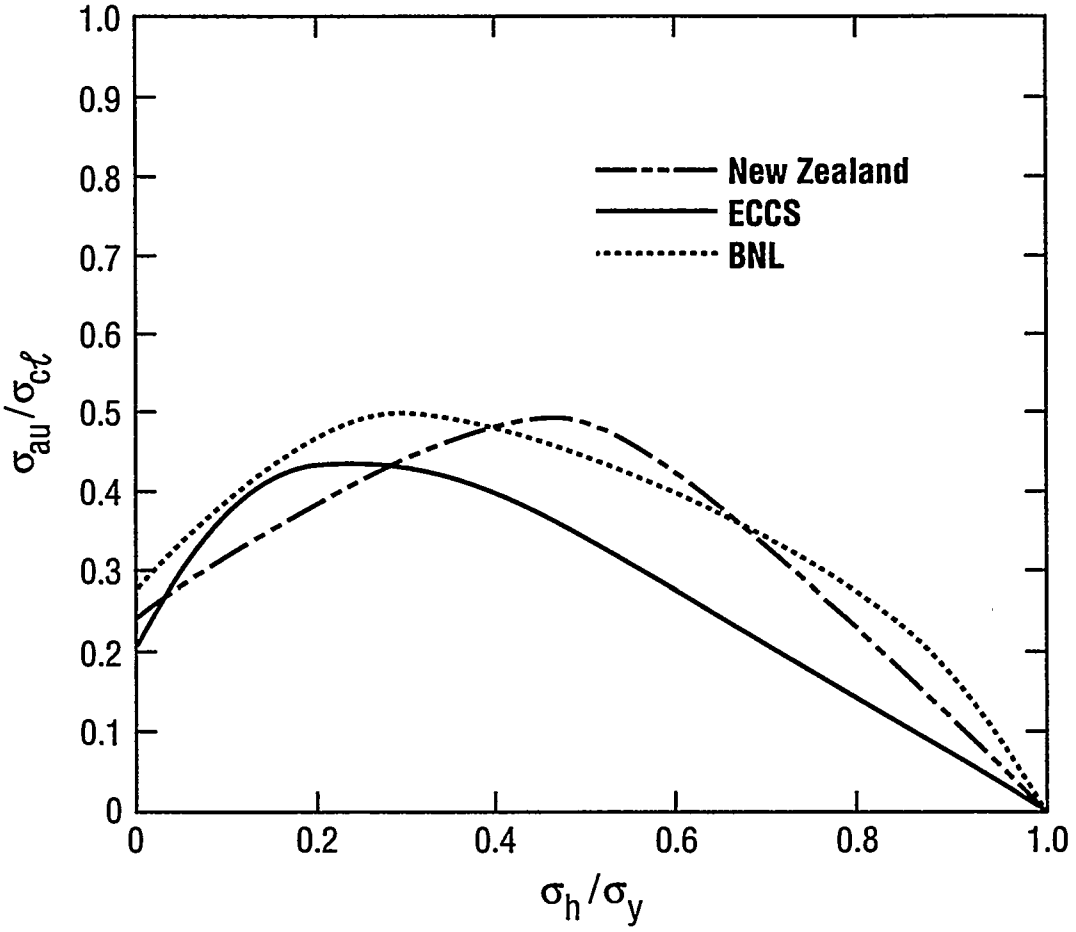

Figure F.2 Comparison of Results for $R/t_w = 600$

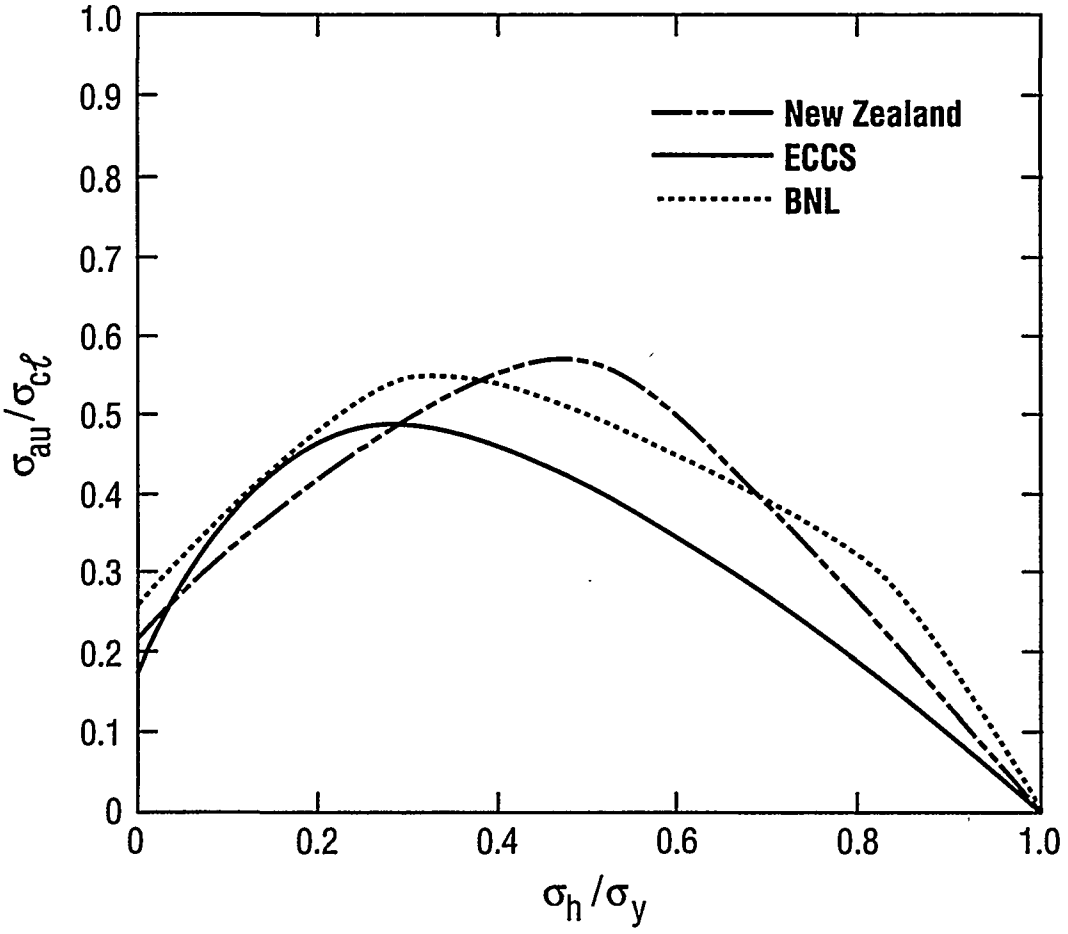

Figure F.3 Comparison of Results for R/t_w = 900

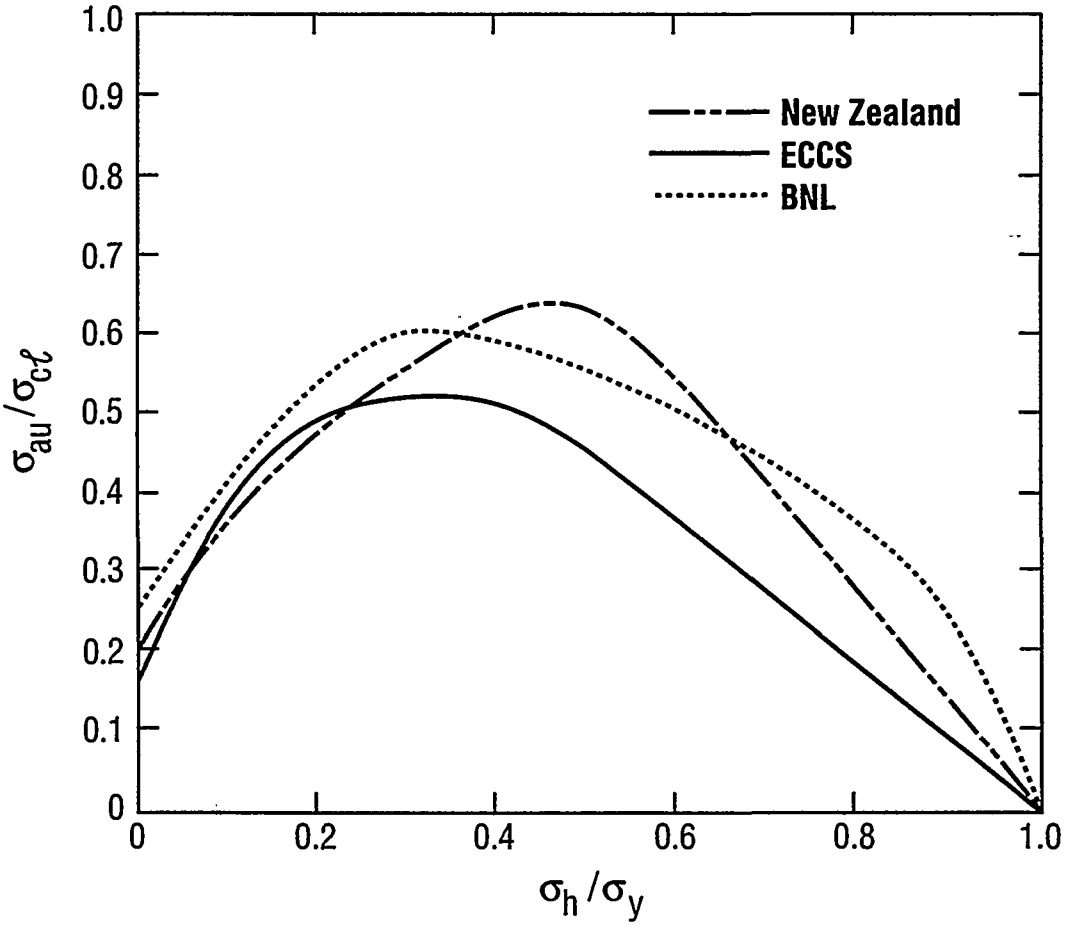

Figure F.4 Comparison of Results for $R/t_w = 1200$

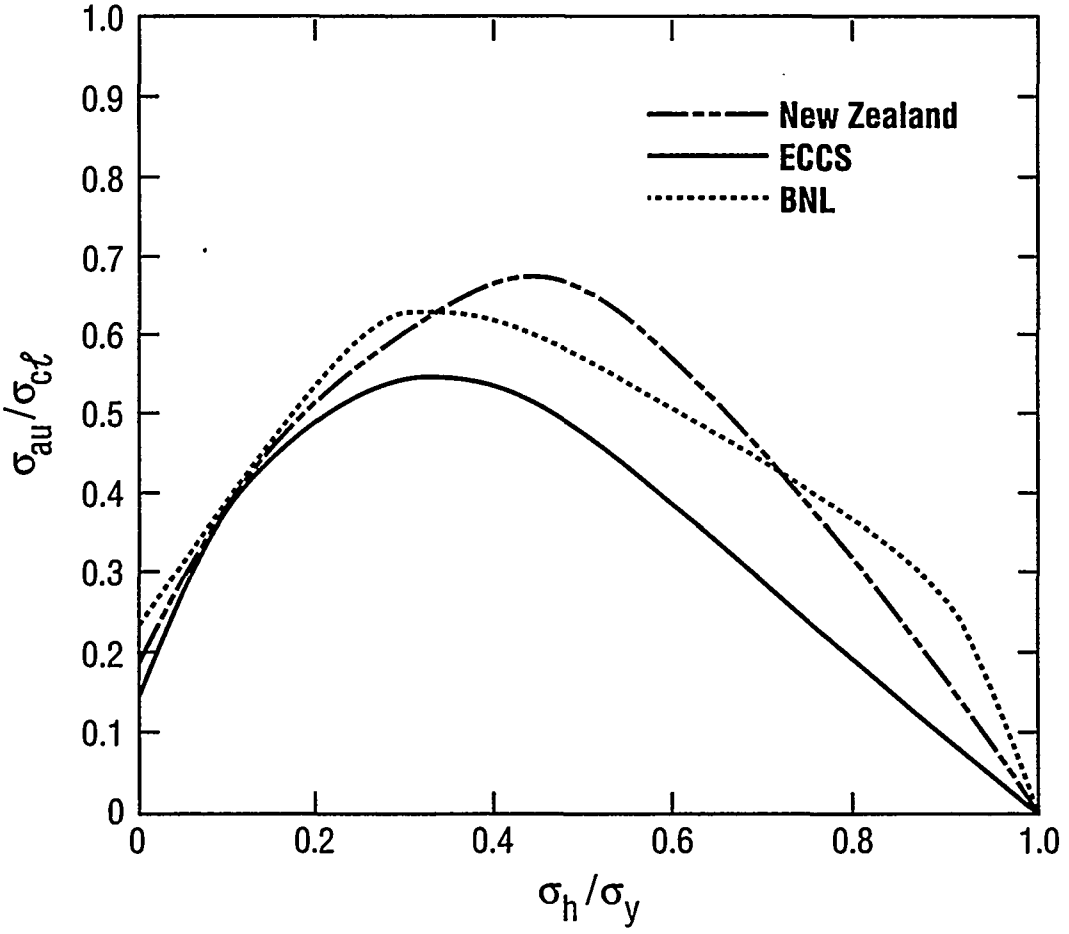

Figure F.5 Comparison of Results for R/t_w = 1500

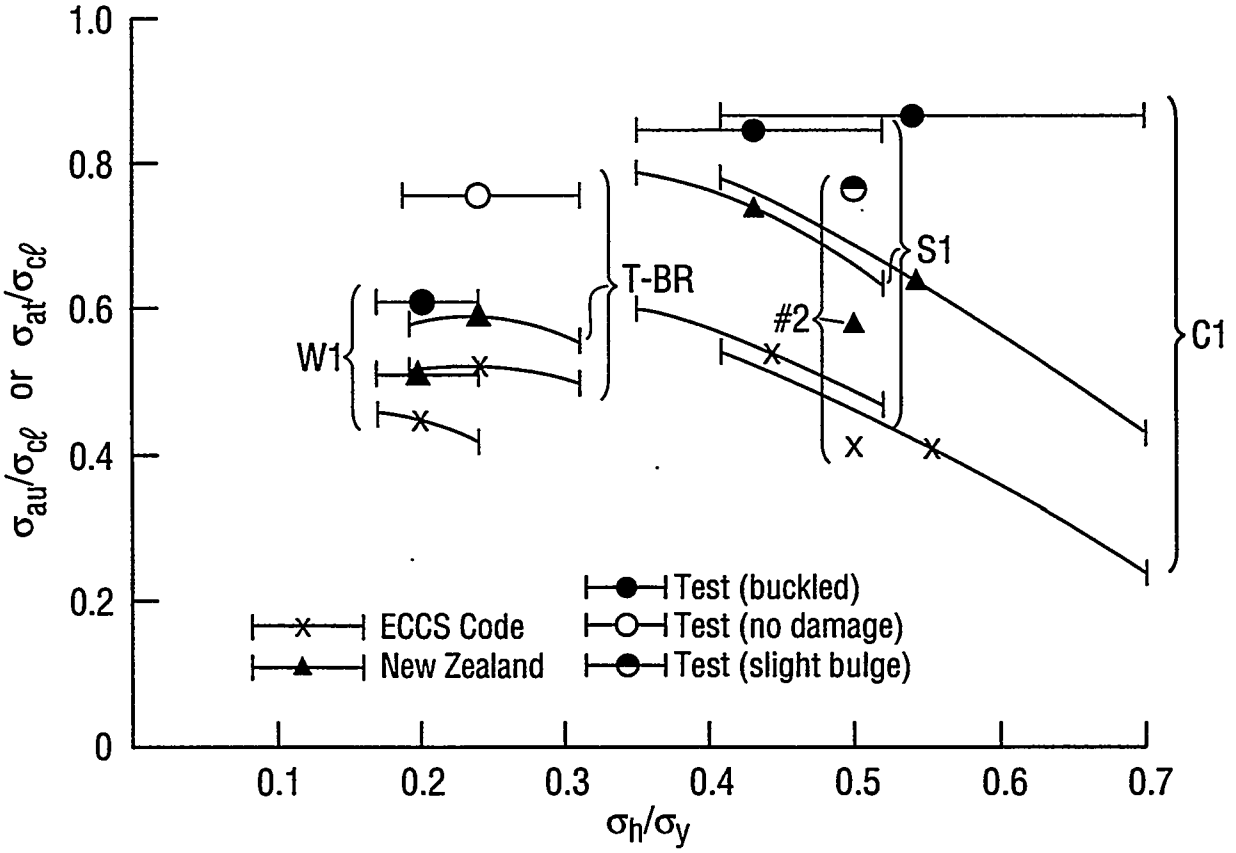

Figure F.6 Comparison of Test Versus Code-Predicted Axial Compression Capacities

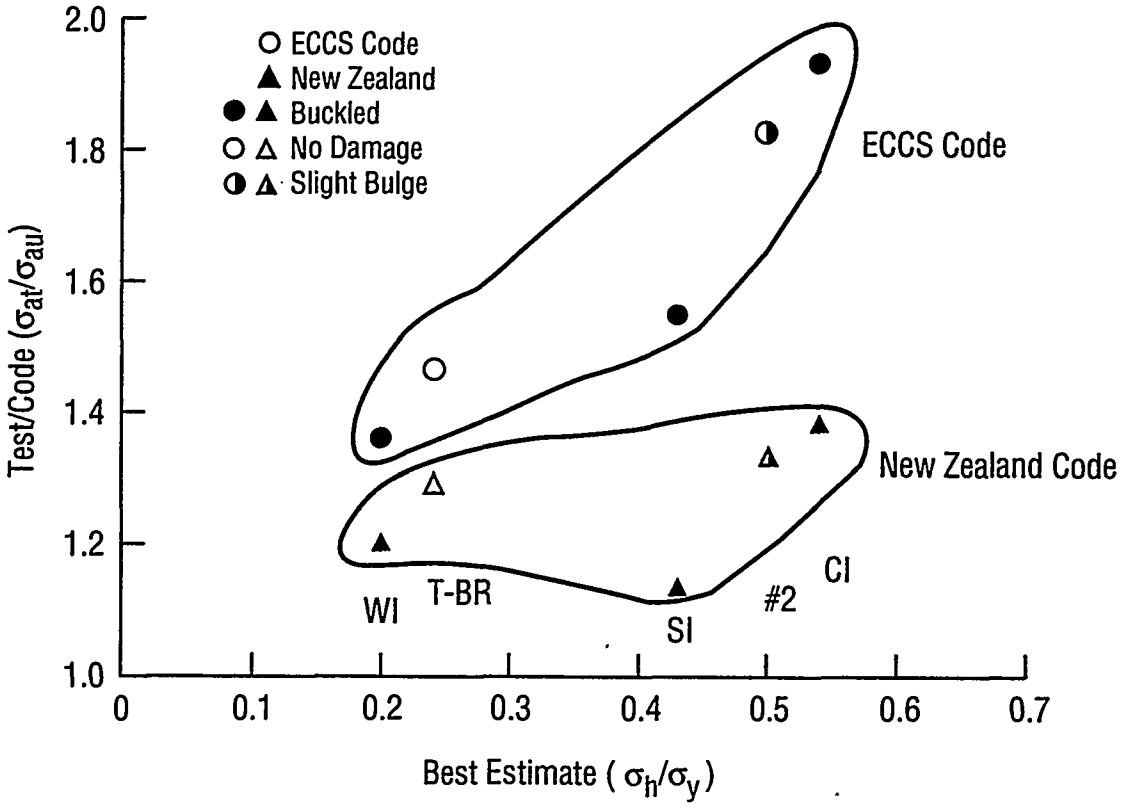

Figure F.7 Comparison of Test Results σ_{at} and Code Capacities σ_{au} for "Best" Estimate σ_h/σ_y Values

APPENDIX G

AN EXAMPLE FOR DETERMINATION OF SEISMIC RESPONSE AND CAPACITY OF A FLAT BOTTOM VERTICAL LIQUID STORAGE TANK

G.1 INTRODUCTION

The steps required for computation of the seismic response and capacity of flat-bottom vertical storage tanks are illustrated in this Appendix considering an example tank as shown in Figure G.1. The tank radius R is 25 feet, while the liquid height H_ℓ is 20.4 feet, with the overall tank height to the top of the dome roof being 31.5 feet. The tank sits on a concrete mat foundation. Initially the tank will be assumed to be un-anchored. However, for capacity comparison purposes, the tank will subsequently be assumed to be anchored by eight 2-inch diameter A307 bolts spaced at 45 degrees. The tank shell is SA240-Type 304 stainless steel. Since this is an atmospheric storage tank (no internal pressure), the tank head, side wall, and base plate thicknesses are thin which is typical for these tanks. The fluid contained in this tank has a specific gravity of 1.15 and weighs 2,880 kips while the combined tank side wall and roof weight is:

$$W_t = 57.3 \; kips \qquad \text{(G.1)}$$

acting at the center of gravity at a height h_t = 15.8 feet. Therefore the tank weight is negligible compared to the fluid weight. The static pressures p_{st} at various distances z above the tank base are listed in Table G.2.

It will be assumed that the Design Basis Earthquake (DBE) horizontal ground motion response spectrum at the base of the tank is given by a 0.25g NUREG/CR-0098 (Reference G.1) median amplification soil-site response spectrum shown in Figure G.2. The amplification factors as a function of damping are shown in Table G.1. It will also be assumed that the vertical spectrum is

2/3 of the horizontal. The peak horizontal ground velocity and displacement at the base of the tank will be taken as 12 inches/second and 9 inches, respectively. A seismic scale factor SF = 1.15 will be used. This scale factor should be determined based on Section 3.3.1.

G.2 SEISMIC RESPONSE

The response quantities that must be evaluated in the analysis of the tank-liquid system are identified in Section 5.3 and not repeated here.

In estimating each of these response quantities at least two horizontal modes of combined fluid-tank vibration and one vertical mode of fluid vibration should be considered. The two horizontal response modes should include the fundamental impulsive mode for which the response of the tank wall and roof are coupled together with the portion of the fluid contents which move in unison with the wall, and at least the fundamental sloshing (convective) mode of the fluid.

G.2.1 Horizontal Impulsive Response

The horizontal impulsive mode natural frequency f_i may be estimated from Equation 4.16 of Chapter 4. For a stainless steel tank, E_t = 27,700 ksi and $\gamma_t = \rho_t g$ = 490 lb/ft^3 from which $\sqrt{E_t/\rho_t}$ = 16,200 ft/sec. The ratio of the liquid height to tank radius, (H_ℓ/R) = 20.4/25 = 0.816. The average wall thickness t_a over the lower two-thirds of the liquid height (recommended for use in Chapter 4) is estimated to be about 0.291 inch from which the t_a/R = 0.00097. For a fluid with a specific gravity of 1.15, the ratio of liquid to tank material mass densities ρ_ℓ/ρ_t = 1.15 (0.127) = 0.146. From Table 4.4 of Chapter 4 for a "free" top support condition and H_ℓ/R = 0.816, $(C_i)_r$ = 0.0833. Correcting for t_a/R = 0.00097 and ρ_ℓ/ρ_t = 0.146 by using Equation 4.18 of Chapter 4 leads to:

$$C_i = 0.0833\,[127\,(0.00097)/(0.146)]^{1/2} = 0.077$$

Thus, from Equation 4.16 of Chapter 4, the natural frequency can be calculated as follows:

$$\overline{f}_{i_{fa}} = \frac{0.077\,(16,200 ft/sec)}{2\pi\,(20.4 ft)} = 9.7\ Hz$$

This natural frequency is the "best-estimate" natural frequency for a fully-anchored tank and is accordingly defined by appropriate notations.

In order to account for the frequency uncertainty in accordance with the requirement of Section 3.4, the following natural frequency bands are recommended for three anchorage conditions:

$$\begin{aligned} f_{i_{fa}} &= (0.85\ to\ 1.15)\,\overline{f}_{i_{fa}},\ for\ a\ fully\ anchored\ tank \\ f_{i_{pa}} &= (0.8\ to\ 1.1)\,\overline{f}_{i_{fa}},\ for\ a\ partially\ anchored\ tank \\ f_{i_u} &= (0.75\ to\ 1.05)\,\overline{f}_{i_{fa}},\ for\ an\ unanchored\ tank \end{aligned} \qquad (G.3)$$

Thus, for this unanchored tank, the horizontal impulsive natural frequency is expected to lie in the range of:

$$f_i = 7.3Hz\ to\ 10.2Hz \qquad (G.4)$$

and the highest spectral acceleration from this range should be used to define the horizontal impulsive response. In order to define the impulsive mode spectral acceleration $(S_A)_i$ in addition to the frequency f_i, a damping value is needed. In accordance with the guidance provided in Table 3.2, a 4% damping value is chosen for this impulsive mode. Thus, from Figure G.2 and Table G.1:

$$(S_A)_{i(\le 8.0Hz,4\%)} = 2.28\,(0.25g) = 0.57g \qquad (G.5)$$

At a distance z above the base, the maximum horizontal impulsive pressure p_i is defined from Equation 4.24 of Chapter 4 to be:

$$p_i(\eta) = c_i(\eta)\,\rho_\ell R(S_A)_i \qquad \text{(G.6)}$$

or

$$p_i(\eta) = c_i(\eta)\,(0.57)\,(1.15)\,(62.4 lbs/ft^3/144 inch^2/ft^2)\,(25 ft)$$
$$= c_i(\eta)\,(7.10\ psi)$$

where $c_i(\eta)$ is a function of $\eta = \eta_\ell = z/H_\ell$ and H_ℓ/R as given by Table 4.1 of Chapter 4. For $H_\ell/R = 0.816$:

z (ft)	η	$c_i(\eta)$
0	0	0.64
1	0.049	0.64
10	0.49	0.53

The resulting horizontal impulsive mode pressures p_i are given in Table G.2.

The maximum overturning moment occurs at the tank base. The horizontal impulsive mode base moment $M_{i\ell}$ due to the liquid can be obtained from Equations 4.37 and 4.39 of Chapter 4 as follows:

$$M_{i\ell} = 0.4\left(\frac{m_i}{m_\ell}\right) m_\ell\,(S_A)_i H_\ell \qquad \text{(G.7)}$$

or

$$M_\ell = 0.4\left(\frac{m_i}{m_\ell}\right)(2,880\ kips)\,(0.57)\,(20.4\ ft) = \left(\frac{m_i}{m_\ell}\right)(13,400\ kip\text{-}ft)$$

where 2,880 kips is the total liquid weight, and (m_i/m_ℓ) may be obtained from Table 4.2 of Chapter 4. For $H_\ell/R = 0.816$, $(m_i/m_\ell) = 0.471$. Thus:

$$M_{i\ell} = 0.471(13,400\ kip\text{-}ft) = 6,310\ kip\text{-}ft$$

The additional horizontal impulsive moment due to the tank shell weight is:

$$M_{it} = m_t (S_A)_i h_t = 57.3\ kip(0.57)(15.8ft) = 520\ kip\text{-}ft \quad \text{(G.8)}$$

where m_t is the tank mass and h_t is its center of gravity height. Thus:

$$M_i = M_{i\ell} + M_{it} = 6{,}830\ kip\text{-}ft \quad \text{(G.9)}$$

Similarly the impulsive mode base shear is given by:

$$V_i = \left[\left(\frac{m_i}{m_\ell}\right) m_\ell + m_t\right](S_A)_i \quad \text{(G.10)}$$

which leads to:

$$V_i = 806\ kips \quad \text{(G.11)}$$

G.2.2 Horizontal Convective (Sloshing) Mode Response

The fundamental convective mode natural frequency f_{c1} is given by Equation 4.14 of Chapter 4 with n = 1 where λ_1 is defined by Equation 4.5. Thus:

$$f_{c1} = \sqrt{\frac{1.50 ft/sec^2}{R} \tanh(1.841 H_\ell/R)} \quad \text{(G.12)}$$

or for R = 25 feet and $(H_\ell/R) = 0.816$:

$$f_{c1} = 0.233 Hz$$

In accordance with Table 3.2, the convective mode is damped 0.5% of critical damping. Thus, from the 0.5% damping spectrum shown in Figure G.2 based on the amplification factors in Table G.1:

$$(S_A)_{c1(0.233Hz,0.5\%)} = 0.100g \quad \text{(G.13)}$$

From Equation 4.24 of Chapter 4, the maximum fundamental convective mode pressures are:

$$p_{c1}(\eta) = c_{c1}(\eta)\, \rho_\ell R (S_A)_{c1} \quad \text{(G.14)}$$

or

$$p_{c1}(\eta) = c_{c1}(\eta)\,(0.100)\,(1.15)\,(62.4\ lbs/ft^3/144\ inch^2/ft^2)\,(25\ ft)$$
$$= c_{c1}(\eta)\,(1.25\ psi)$$

where $c_{c1}(\eta)$ can be obtained from Equation 4.4 of Chapter 4. For n = 1 and $H_\ell/R = 0.816$:

z(ft)	η	$c_{c1}(\eta)$
0	0	0.355
1	0.049	0.356
10	0.49	0.456

The resulting fundamental convective mode pressures p_{c1} are given in Table G.2.

The maximum values of the second convective mode pressures are less than 20% of the first convective mode pressures which in themselves are small. Thus, all higher convective modes may be ignored. In fact, from a practical standpoint, even the first convective mode pressures are negligible.

The fundamental convective mode base moment M_{c1} can be obtained from Equations 4.38 and 4.40 of Chapter 4 to be:

$$M_{c1} = \left(\frac{m_{c1}}{m_\ell}\right)\left(\frac{h_{c1}}{H_\ell}\right) m_\ell H_\ell (S_A)_{c1} \qquad \text{(G.15)}$$

or

$$M_{c1} = \left(\frac{m_{c1}}{m_\ell}\right)\left(\frac{h_{c1}}{H_\ell}\right)(2{,}880\ kips)\,(0.100)\,(20.4 ft) = \left(\frac{m_{c1}}{m_\ell}\right)\left(\frac{h_{c1}}{H_\ell}\right)(5{,}880\ kip\text{-}ft)$$

where both (m_{c1}/m_ℓ) and (h_{c1}/H_ℓ) are given in Table 4.2 of Chapter 4. For $H_\ell/R = 0.816$, $(m_{c1}/m_\ell) = 0.504$ and $(h_{c1}/H_\ell) = 0.577$. Thus:

$$M_{c1} = 0.504\,(0.577)\,(5{,}880\ kip\text{-}ft) = 1{,}710\ kip\text{-}ft \qquad \text{(G.16)}$$

Similarly:

$$V_{c1} = \left(\frac{m_{c1}}{m_\ell}\right) m_\ell (S_A)_{c1} = 145 \; kips \qquad \text{(G.17)}$$

Lastly, from Equation 4.60 of Chapter 4, the fundamental convective mode slosh height h_{s1} is:

$$h_{s1} = 0.837 R \left[\frac{(S_A)_{c1}}{g}\right] = 2.09 \; ft \qquad \text{(G.18)}$$

G.2.3 Vertical Liquid Mode Response

Hydrodynamic pressures due to the fundamental vertical liquid mode should be estimated at critical locations on the tank wall. This vertical mode natural frequency f_v may be estimated from Equation 4.53 and Table 4.17 of Chapter 4 in a manner analogous to that shown in Section G.2.1 for the horizontal impulsive mode. Thus, the "best-estimate" vertical mode natural frequency $\overline{f}_{v_{fa}}$ for a fully-anchored tank is given by:

$$\overline{f}_{v_{fa}} = 9.9 \; Hz \qquad \text{(G.19)}$$

Correcting for frequency uncertainty for an unanchored tank using the factors of Equation G.3, the vertical mode natural frequency is expected to lie in the range of:

$$f_v = 7.4 \; Hz \; to \; 10.4 \; Hz \qquad \text{(G.20)}$$

Again, 4% damping is used for this mode and the highest vertical spectral acceleration in this frequency range is:

$$(S_A)_{v(\leq 8.0Hz, 4\%)} = (2/3)(2.28)(0.25g) = 0.38g \qquad \text{(G.21)}$$

At any distance z above the base, the vertical mode pressure p_v is given by Equation 4.52 of Chapter 4 to be:

$$p_v(\eta) = 0.8\left[\cos\frac{\pi}{2}\eta\right]\rho_\ell H_\ell (S_A)_v \qquad \text{(G.22)}$$

or

$$p_v(\eta) = 0.8\left[\cos\frac{\pi}{2}\eta\right](0.38)\,(1.15)\,(62.4 lbs/ft^3/144\ in.^2/ft^2)\,(20.4 ft)$$
$$= \left[\cos\frac{\pi}{2}\eta\right](3.09\ psi)$$

The resulting vertical mode pressures p_v are given in Table G.2.

The effective tank weight W_{te} is obtained by adjusting the actual tank weight by the probable effect (40%) of the vertical earthquake component at the time of maximum moment and shear based on the Newmark 100%-40%-40% Rule (Reference G.1). Thus:

$$W_{te} = W_t\left[1 \pm 0.4\frac{A_v}{g}\right] \qquad \text{(G.23)}$$

where A_v is the peak vertical ground acceleration (A_v = 0.167g for this example). Thus, for this example:

$$W_{te} = 57.3\ kips[1\pm0.067] = 53.5\ kips\ to\ 61.1\ kips \qquad \text{(G.24)}$$

G.2.4 Combined Demand (Response)

For the hydrodynamic pressure loadings, the probable combined horizontal input hydrodynamic pressures p_{dh} are obtained by the SRSS combination of p_i and p_{c1}; the combined vertical input hydrodynamic pressures p_{dv} are just p_v; and the combined total hydrodynamic pressures p_d are obtained by the SRSS combination of p_{dh} and p_{dv}. The total inelastic factored demand pressures p_{ti} are then given by Equation 5.4 of Chapter 5 which is:

$$p_{ti} = p_{st} + \frac{SF\ p_d}{F_{\mu D}} \qquad \text{(G.25)}$$

where for this example, SF = 1.15, and $F_{\mu D}$ = 1.5 for the hoop capacity failure mode from Table 3.3. Each of these combined pressures are shown in Table G.2.

The probable combined base moment M_d and base shear V_d demands are given by the SRSS combination of the impulsive and convective mode demands. Thus:

$$M_d = [M_i^2 + M_{c1}^2]^{1/2} = 7{,}040 \; kip\text{-}ft$$
$$V_d = [V_i^2 + V_{c1}^2]^{1/2} = 819 \; kips \qquad \text{(G.26)}$$

These values are less than 3% greater than from the impulsive mode alone which illustrates the relative unimportance of the convective mode.

To obtain the total inelastic demand base moment M_{ti} and base shear V_{ti}, the combined demands (M_d and V_d, respectively) can be divided by $F_{\mu D}$ = 1.25 from Table 3.3 and must be multiplied by the appropriate SF from Section 3.3.1 (i.e., SF = 1.15 for this example). Thus ($SF/F_{\mu D}$) = 0.92 and:

$$M_{ti} = \left[\frac{SF \; M_d}{F_{\mu D}}\right] = 6{,}480 \; kip\text{-}ft$$
$$V_{ti} = \left[\frac{SF \; V_d}{F_{\mu D}}\right] = 753 \; kips \qquad \text{(G.27)}$$

Lastly, the combined slosh height response h_{sr} can be taken as equal to the fundamental convective mode slosh height h_{s1}:

$$h_{sr} = h_{S1} = 2.09 \; feet \qquad \text{(G.28)}$$

G.3 CAPACITY ASSESSMENTS

This example capacity assessment is performed in accordance with the guidance of Chapter 5.

G.3.1 Slosh Height Capacity

As noted in Section 5.4, the slosh height response, h_{sr} should be compared with the slosh height capacity, h_{sc}. From Equation 5.1, the required slosh height capacity h_{sc} for SF = 1.15 is given by:

$$h_{SC} \geq 1.6\, SF\, h_{sr} = 1.6\,(1.15)\,(2.09\ ft) = 3.85\ feet \quad \text{(G.29)}$$

whereas, the available slosh height capacity from Equation 5.2 is:

$$h_{SC} = h_C + \frac{h_d}{4} = 2.6 + \frac{8.5}{4} = 4.72\ feet \quad \text{(G.30)}$$

Therefore, this tank has a sufficient freeboard margin of safety to accommodate a SF of 1.15.

However, if h_c were reduced from 2.6 feet to 1.6 feet, then h_{sc} = 3.72 feet and the freeboard would be insufficient to satisfy Equation 5.1. In this case either (1) a response analysis such as in Appendix D which accounts for the partial roof confinement of the free liquid surface for an earthquake amplified by a factor of 1.6 SF = 1.84 must be performed, or (2) the maximum liquid height must be reduced to 20.2 feet (a 0.2 foot reduction) to enable h_{sc} to pass Equation G.29. In most cases, this last option is preferable. If it is not practical to reduce the maximum liquid height, then Appendix D provides a simplistic, yet believed to be conservative, approach to estimating the increased hydrodynamic pressures and forces resulting from inadequate freeboard.

For h_c = 1.6 feet, from Equation (D.18) the effective freeboard to slosh height ratio:

$$(h_o)_e/h_s = \frac{3.72}{3.85} = 0.966$$

is estimated. Correspondingly, the impacted perimeter half angle θ_o from Equation D.2 is 14.9 degrees. Then the impact factor ϵ from Equation (D.9) is 0.162 and:

$$\frac{H_t}{H_\ell} = 1 + \frac{(h_o)_e}{H_\ell} = 1 + \frac{3.72}{20.4} = 1.182$$

Then the total wall force from the constrained portion of the liquid P_i^c is given by Equation (D.12) to be:

$$P_i^c = (0.162)(1.182) m_\ell (S_A)_i = 0.192 m_\ell (S_A)_i$$

The impulsive and convective total force components due to the unconstrained portion, P_i^u and P_c^u, are given by Equations (D.13) and (D.14) to be:

$$P_i^u = 0.838 \left(\frac{m_i}{m_\ell}\right) m_\ell (S_A)_i$$

$$P_c^u = 0.838 \left(\frac{m_{c1}}{m_\ell}\right) m_\ell (S_A)_{c1}$$

where $(m_i/m_\ell) = 0.471$ and $(m_{c1}/m_\ell) = 0.504$ have been previously estimated for this tank. Thus, the total impulsive force is:

$$P_i = P_i^c + P_i^u = [0.192 + 0.394](2{,}880\ kips)(0.57) = 963\ kips$$

and the total convective force is:

$$P_c = 0.422(2{,}880\ kips)(0.100) = 122\ kips$$

The impulsive, convective, and total combined base shears are:

$$V_i = P_i + m_t (S_A)_i = 963\ kips + 33\ kips = 996\ kips$$

$$V_c = P_c = 122\ kips$$

$$V_d = \left[V_i^2 + V_c^2\right]^{1/2} = 1{,}003\ kips$$

Similarly, from Equations (D.15) through (D.17) the constrained and unconstrained liquid induced base moments are:

$$M_i^c = 0.192\,(2{,}880\ kips)\,(1.182)\left(\frac{20.4\ ft}{2}\right)(0.57) = 3{,}800\ kip\text{-}ft$$

$$M_i^u = 0.40\,(0.838)\,(0.471)\,(2{,}880\ kips)\,(20.4\ ft)\,(0.57) = 5{,}287\ k\text{-}ft$$

$$M_c^u = (122\ kips)\,(0.577)\,(20.4\ ft) = 1{,}430\ kip\text{-}ft$$

The total impulsive, convective, and combined base moments are:

$$M_i = M_i^c + M_i^u + M_{it} = 3{,}800 + 5{,}287 + 520 = 9{,}607\ kip\text{-}ft$$

$$M_c = M_c^u = 1{,}430\ kip\text{-}ft$$

$$M_d = [M_i^2 + M_c^2]^{1/2} = 9{,}713\ kip\text{-}ft$$

With freeboard that is inadequate by less than 0.2 feet, the total base shear and total base moment are increased by factors of 22% and 38%, respectively, over the base shears and base moments given by Equation (G.26) for the case where adequate freeboard exists. This comparison indicates the level of increased hydrodynamic loads which are predicted by the procedure of Appendix D when inadequate freeboard exists. For the conditions where the slosh height slightly exceeds the freeboard, the load increase is believed to be conservative.

G.3.2 Hoop Tension Capacity

The pressure capacity p_c based on the hoop tension is given by Equation 5.3. For SA240-Type 304 stainless steel, σ_c = 30.0 ksi, and the resulting pressure capacities p_c are listed in Table G.2 for t_{tw} = 5/16 inch (z = 1.0 foot), and t_{tw} = 1/4 inch (z = 10 feet). These pressure capacities p_c exceed the total inelastic factored demand pressures p_{ti} by a very substantial margin as shown in Table G.2. Therefore, the hoop tension capacity is easily adequate.

G.3.3 Maximum Permissible Axial Compression in Tank Wall

The allowable axial compressive stress σ_a of the tank shell should be computed at locations of maximum seismic induced

compression stresses for each shell thickness, except that by common practice such checks do not need to be made within one-foot of the locations where shell thicknesses are increased. Thus, the allowable compressive stress σ_a should be computed at z = 1.0 and 10.0 feet above the base for the example tank.

The compression stress capacity will be computed following the approach recommended in Section 5.6 assuming the tank meets the tolerance limits of Appendix E. For SA240-type 304 stainless steel, σ_y = 30 ksi and E_t = 27,700 ksi.

The compression stress capacity σ_a computation at z = 1.0 foot will be summarized. At this location t_{tw} = 5/16 inch and (R/t_{tw}) = 960. Thus, from Equations 5.5, 5.9 and 5.17:

$$\sigma_{cl} = 17.46 \; ksi$$

$$\alpha_o = 0.225$$

$$\alpha_b = 0.371$$

Following the ASME Code Case N-530 requirement to use the uniform compression factor α_o for α:

$$\alpha = 0.225$$

At the location around the circumference of maximum axial compression corresponding to the time of maximum moment, the probable combined hydrostatic and hydrodynamic pressure p_c is given by Equation 5.18a where p_{st}, p_{dh}, and p_{dv} are the values listed in Table G.2 for z = 1.0 foot. Thus:

$$p_{com} = 9.67 + [4.56 \pm 0.4(3.08)] \frac{1.15}{1.50} = \begin{cases} 14.11 \; psi \\ 12.22 \; psi \end{cases}$$

Thus:

p_{com}(psi)	σ_h/σ_y	α_p	β_c	λ_p^2	σ_{eff}/σ_y	σ_{au}/σ_y	σ_a(ksi)
14.11	0.452	0.755	0.398	0.906	0.611	0.244	5.50
12.22	0.391	0.730	0.459	1.080	0.586	0.261	5.89

and from Equation 5.8 at Z = 1.0 foot:

$$C_a = 5.50\ ksi\ (5/16\ inch) = 1.72\ kips/inch \qquad \text{(G.31a)}$$

However, in Chapter 5 it is recommended that the provisions of Appendix F be used in order to obtain a more realistic buckling capacity estimate for existing tanks subjected to vibratory moment loading. In accordance with Section F.2.1, the plastic collapse capacity is given by Equation F.1 with:

p_{com}(psi)	σ_h/σ_y	F_1	F_2	F_3	σ_{ap}(ksi)	σ_a(ksi)
14.11	0.452	0.796	0.793	0.951	10.48	7.88

The "diamond" buckling capacity of Section F.2.2, σ_{ad} = 11.27 ksi and thus does not control. Therefore, a more realistic compression capacity C_a for existing tanks is:

$$C_a = 7.88\ ksi\ (5/16\ inch) = 2.46\ kips/inch \qquad \text{(G.31b)}$$

which is a factor of 1.43 greater than that given by Equation (G.31a) based on the ASME Code Case N-530 requirements. For the remainder of this example, the ASME Code Case N-530 capacity from Equation (G.31a) will be used.

Similarly at z = 10 feet, t_{tw} = 1/4 inch, R/t_{tw} = 1,200 and:

$$\sigma_{cl} = 13.97\ ksi$$

$$\alpha_o = 0.201$$

$$\alpha_b = 0.352$$

$$\alpha = 0.201$$

$$p_{com} = \begin{cases} 8.77\ psi \\ 7.41\ psi \end{cases}$$

Thus:

p_{com} (psi)	σ_h/σ_y	α_p	β_c	λ_p^2	$\frac{\sigma_{eff}}{\sigma_y}$	$\frac{\sigma_{au}}{\sigma_y}$	σ_a (ksi)
8.77	0.351	0.723	0.454	1.348	0.507	0.230	5.19
7.41	0.296	0.691	0.507	1.576	0.458	0.232	5.23

and at z = 10 feet:

$$C_a = 1.30\ kips/inch \qquad \text{(G.31c)}$$

The value of C_a at z = 1.0 foot should also be used at the tank base (z = 0).

G.3.4 Moment Capacity Away From Tank Base

At a location along the cylindrical wall away from the base, the moment capacity is given by Equation 5.19 where P_a is equal to the upper bound estimate of the effective tank weight W_{te} from Equation G.24 corrected for the distance z above the base. Thus:

(G.32)

z (feet)	P_a (kips)	$C_a\pi R^2$ (kip-ft)	$P_aR/2$ (kip-ft)	M_c (kip-ft)
1.0	59.0	40,530	740	39,790
10.0	39.8	30,630	500	30,130

These moment capacities greatly exceed the maximum inelastic factored moment demand at the base M_{ti} = 6460 kip-ft from Equation G.27. Therefore, it is unnecessary to find moment

demands at other locations in the cylindrical wall since such demands will be less than M_{ti}. The cylindrical wall has more than adequate moment capacity.

If the tank were fully anchored, M_c = 39,790 kip-ft would also represent the moment capacity at the base. However, it will be shown in Section G.3.6 that to develop this fully anchored condition at the base requires an unreasonably large number of anchor bolts.

G.3.5 Anchorage Capacity At Tank Base

For this unanchored tank, there is no anchorage capacity at the tank base. However, for illustration purposes, it will also be assumed that this tank is anchored by eight 2-inch diameter A307 bolts spaced at 45 degrees. The capacity of such anchors must be checked for each of the five potential failure modes listed in Section 5.8. However, for this alternate example it will be assumed that the anchor-bolt tensile capacity is the weakest failure mode.

The AISC-LRFD (Reference G.2) code limit state capacity for an A307 anchor bolt is:

$$T_{cb} = 0.75(45\ ksi)A_b \qquad \text{(G.33)}$$

where A_b is the nominal cross-sectional area of the bolt. For a 2-inch diameter bolt, A_b = 3.14 square inches and:

$$T_{cb} = 106\ kips \qquad \text{(G.34)}$$

G.3.6 Anchorage Requirement for Fully Anchored Tank

If the example tank were anchored by 2-inch diameter A307 bolts with T_{cb} = 106 kips, the maximum angular spacing θ_b for these bolts to provide a fully-anchored tank is given by Equation 5.20. Thus:

$$\theta_b \leq (360°)\frac{T_{cb}}{2\pi RC_a} = (360°)\frac{106\ kips}{2\pi(300 inches)\left(1.72\frac{kips}{inch}\right)} = 11.8° \qquad (G.35)$$

which would result in at least 31 of these bolts around the circumference of the tank. This number of bolts is both unrealistic and unnecessary. Instead, a lesser number of bolts or even no bolts can be used if a lesser base moment capacity defined in Section 5.10 for partially anchored or unanchored tanks is acceptable.

G.3.7 Base Moment Capacity of Unanchored Tank

In order to estimate the base moment capacity of an unanchored tank, it is first necessary to estimate the fluid hold-down forces (Section 5.12.2) and the maximum permissible uplift displacement (Section 5.11). Section 5.12.2 recommends that the fluid hold-down capacity be estimated from Equation 5.38. Since both the tank wall and tank base have the same thickness of 5/16 inch and for SA240-type 304 stainless steel σ_{ye} = 2.4S = 45.0 ksi, the plastic moment capacities from Equation 5.39 are:

$$M_{pb} = M_{pw} = \frac{45.0\ ksi(5/16 inch)^2}{4} = 1.10\ kip\text{-}inch/inch \qquad (G.36)$$

The shell parameter κ is given by:

$$\kappa = \left[(R/t_{tw})\sqrt{3(1-\nu_t^2)}\right]^{1/2} = 39.8 \qquad (G.37)$$

Therefore, from Equation 5.41 the horizontal component of the membrane tension in the base plate is:

$$F_h = \frac{45.0 ksi(5/16 inch)}{2(39.8)} + \frac{1.10 kips(39.8)}{300 inch} = 0.323\ kip/inch \qquad (G.38)$$

The fluid pressure p should conservatively be taken as the probable minimum pressure computed from Equation 5.35 using the demand pressure at the base (z=0) from Table G.2. Thus at θ=0:

$$p_{\theta=0} = 10.17\ psi - [4.56\ psi + 0.4(3.09\ psi)]1.15 = 3.50\ psi \quad \text{(G.39)}$$

With these values for M_{pb}, M_{pw}, F_h, and p, from Equation 5.38 and after combining terms the fluid hold-down force at $\delta = \delta_o$ (i.e., $\theta = 0$) is:

$$T_{fo} = 0.124 \frac{kip}{inch}\left[1 + \left(\frac{\delta_o}{6.81\ inch}\right)\right]^{1/2} \quad \text{(G.40)}$$

Equation 5.28 limits δ_o to (0.1L) where L is the uplifted length computed from Equation 5.37. Thus, for various δ_o values:

δ_o (inch)	T_{fo} (kip/inch)	L (inch)	Upper Limit δ_o (inch)
2.0	0.141	40.3	4.03
3.0	0.149	42.6	4.26
4.0	0.156	44.6	4.46
4.6	0.161	46.0	4.60

In many cases, δ_o is limited by tolerable displacements for piping or other components attached to the tank wall. Great precision is unnecessary in establishing the permissible uplift displacement δ_o because T_{fo} is only mildly influenced by δ_o. For this example, it will be assumed that:

$$\begin{aligned} \delta &= 4.6\ inches \\ T_{fo} &= 0.161\ kip/inch \end{aligned} \quad \text{(G.41)}$$

At the neutral axis $\theta=\theta_n$, $\delta_o=0$ and from Equation 5.35:

$$p_{\theta=\theta_n} \geq 10.17\ psi - [0.4(3.09\ psi)]1.15 = 8.75\ psi \quad \text{(G.42)}$$

Therefore, from Equation 5.38:

$$T_{fn} = 0.196\ kip/inch \quad \text{(G.43)}$$

It is conservative to assume that the fluid hold-down force varies linearly from T_{fn} at $\theta=\theta_n$ to T_{fo} at $\theta=0$. Thus, from Equation 5.24:

$$\Delta T_f = 0.161 \frac{kip}{inch} - 0.196 \frac{kip}{inch} = -0.035 \frac{kip}{inch}$$

Now the maximum axial compressive stress C'_m and the base moment capacity are computed from Equations 5.21 and 5.22 for any given neutral axis angle θ_n, with W_t = 52.0 kips which, for conservatism, is taken as the minimum W_{te} from Equation G.24. The axial compressive stress must be limited to not exceed C_a = 1.72 kips/inch from Equation G.31a.

Table G.3 presents the computed base moment capacity M_c as a function of the neutral axis angle θ_n. Note that M_c is relatively insensitive to θ_n so that great precision is unnecessary in finding θ_n. The unanchored tank base moment capacity is:

$$M_c = 9{,}100 \; kip\text{-}ft \qquad (G.44)$$

This base moment capacity is only a small fraction of the fully anchored base moment capacity of 39,790 kip-ft given by Equation G.32. However, this unanchored moment capacity exceeds the inelastic factored base moment demand M_{ti} = 6,480 kip-ft given in Equation G.27. Thus, this unanchored tank has an adequate base moment capacity.

If the more realistic compression capacity from Equation (G.31b) of 2.46 kips/inch had been used, the unanchored tank base moment capacity would only have increased to 9,210 kip-ft. This increase is only 1.2% which shows that for this example tank a 43% increase in C_a results in only a 1.2% increase in M_c. The moment capacity of an unanchored tank is insensitive to the compressive capacity of the tank wall.

G.3.8 Base Moment Capacity of Partially Anchored Tank

For the alternate partially anchored tank with eight 2-inch diameter A307 anchor bolts at 45° spacing around the tank, it is

recommended that the fluid hold-down forces be computed in accordance with Section 5.12.1.

With E_s = 27,700 ksi, R = 300 inches, $t_{tw} = t_{tb}$ = 5/16 inch, and H_f/R = 0.816, from Equations 5.29 and 5.29a:

$$K = 77.41 \; kip\text{-}inch$$

$$\kappa = 39.83$$

$$K_S = 20.56 \; kips$$

$$\frac{M_{fx}}{p_e} = 27.50 \; inch^2$$

With these values, for various uplift lengths L:

(G.45)

L (inch)	T_f/p_e (inch)	δ/p_e (inch/psi)	M_f/p_e ($inch^2$)	M_+/p_e ($inch^2$)
8.885	6.66	0	19.7	2.5
12.0	8.11	0.0033	25.4	7.6
15.0	9.78	0.0107	34.2	13.6
18.0	11.57	0.0243	46.2	20.7
21.0	13.42	0.0464	61.4	28.7
24.0	15.32	0.0798	79.6	37.7
25.0	15.96	0.0940	86.4	40.9
26.0	16.60	0.1098	93.5	44.2

At θ=0, δ_o is limited by Equation 5.27. For the example anchored tank, it will be assumed that the effective bolt length (h_e) = 36 inches. Therefore:

$$\delta_o \leq 0.01 \; (36 \; inches) = 0.36 \; inch \qquad (G.46)$$

Also, at θ=0, $p_{\theta=0}$ = 3.50 psi as was computed in Equation G.39. For this value of $p_{\theta=0}$ and δ_o:

$$\delta_o/p_e = \frac{0.36 \; inch}{3.50 \; psi} = 0.1029 \qquad (G.47)$$

which from Equation G.45 corresponds to an uplift length L = 25.6 inches for which:

$$T_{fo} = 16.3\ inch\ (.00350\ ksi) = 0.057\ \frac{kip}{inch}$$
$$M_f = 90.4\ in^2(.00350\ ksi) = 0.316\ \frac{kip\text{-}inch}{inch} \qquad (G.48)$$

This M_f is well below $M_{pb} = 1.10\ \frac{\text{kip-inch}}{\text{inch}}$ from Equation G.36.

At $\theta=\theta_n$, $\delta_{\theta n}=0$ and $p_{\theta=\theta n} = 8.75$ psi as was computed in Equation G.42. For these values, from Equation G.45 the uplift length L = 8.885 inches for which:

$$T_{fn} = 6.66\ inch\ (.00875\ ksi) = 0.058\ \frac{kip}{inch} \qquad (G.49)$$

Again, it is conservative to assume that the fluid hold-down force varies linearly from T_{fn} at $\theta=\theta_n$ to T_{fm} at $\theta=0$. Thus from Equation 5.15:

$$\Delta T_f = 0.057\ \frac{kip}{inch} - 0.058\ \frac{kip}{inch} = -\ 0.001\ \frac{kip}{inch} \qquad (G.50)$$

The anchor bolt tension T_{ti} for anchor bolt "i" can be estimated from Equation 5.25 with K_b from Equation 5.26 of:

$$K_b = \frac{\delta_o A_b E_b}{h_e} = \frac{0.36in(3.14in^2)\,(29{,}000\ ksi)}{36\ inches} = 911\ kips \qquad (G.51)$$

In most situations, the bolt pretension T_{bp} should be taken as zero since even when an initial pretension is installed, it is likely to be lost after a few years.

Again, W_t = 52.0 kips which is the minimum W_{te} from Equation G.24 and the axial compressive stress C'_m must be limited to C_b = 1.72 kips/inch from Equation G.31a.

Table G.4 presents the computed base moment capacity M_c from Equations 5.21 and 5.22 as a function of θ_n. Again note that M_c is relatively insensitive to θ_n so that great precision is

unnecessary in finding θ_n. The base moment capacity for the partially anchored tank is:

$$M_c = 22{,}000\ kip\text{-}ft \qquad (G.52)$$

This base moment capacity is 2.4 times the base moment capacity of 9,100 kip-ft for the unanchored tank given by Equation G.44, but is only 55% of the base moment capacity of 39,790 kip-ft for the fully anchored tank given by Equation G.32. These examples illustrate the influence of anchorage on the base moment capacity.

If the more realistic compression capacity from Equation (G.31b) of 2.46 kips/inch had been used, the anchored tank base moment capacity would only have increased to 22,950 kip-ft. Thus, a 43% increase in C_a results in only a 4.3% increase in M_c.

G.3.9 Base Shear Capacity

The base shear capacity V_c is given by Equations 5.42, 5.43, and 5.44. Conservatively set W_t = 53.5 kips which is the minimum W_{te} from Equation G.24. ΣT_{bi}=0 for an unanchored tank, and:

$$p_a = p_{st} - (0.4\ p_{dv})\,SF = 10.17 - [0.4\ (3.09)]1.15 = 8.75\ psi$$

from the z=0 case in Table G.2. Then, from Equation 5.43:

$$W_e = 53.5\ kips + .00875\ ksi\ \pi\ (300\ inch)^2 = 2{,}528\ kips$$

Assuming a coefficient of friction (COF) of 0.70, from Equation 5.42:

$$V_{cs} = 0.70\ (2{,}528\ kips] = 1{,}769\ kips$$

Then, from Equation 5.44:

$$V_c = 0.75\ [1{,}769\ kips] = 1{,}327\ kips \qquad (G.53)$$

This base shear capacity is greater than the inelastic factored base shear demand V_{ti} = 753 kips given in Equation G.27.

Therefore, this unanchored tank has an adequate base shear capacity.

REFERENCES

G.1 Newmark, N.M., and Hall, W.J., "Development of Criteria for Seismic Review of Selected Nuclear Power Plants," NUREG/CR-0098, Nuclear Regulatory Commission, May 1978.

G.2 American Institute of Steel Construction, "Manual of Steel Construction, Load & Resistance Factor Design," 2nd Ed., 1994.

NOTATION

A_b	nominal cross sectional area of anchor bolt
A_v	peak vertical ground acceleration
$c_{c1}(\eta)$	function defining axial variation of convective component of wall pressure associated with fundamental sloshing mode
C_b	maximum permissible axial compressive force per unit length
C_i	coefficient associated with impulsive mode
$c_i(\eta)$	function defining axial variation of impulsive pressure
C_m'	compressive force per unit length at outer compression side of tank wall
E_t	modulus of elasticity of tank material
f_{c1}	natural frequency of liquid in fundamental convective mode
f_i	fundamental frequency of tank-liquid system in impulsive mode
$f_{i\ fa}$	impulsive mode fundamental frequency of a fully anchored tank
$\overline{f}_{i\ fa}$	best estimate impulsive mode fundamental frequency of a fully anchored tank
$f_{i\ pa}$	impulsive mode fundamental frequency of a partially anchored tank
$\overline{f}_{i\ pa}$	best estimate impulsive mode fundamental frequency of a partially anchored tank
$f_{i\ u}$	impulsive natural frequency of an unanchored tank
$\overline{f}_{iu}$	best estimate impulsive mode fundamental frequency of an unanchored tank
f_v	vertical mode fundamental frequency
$\overline{f}_{v\ fa}$	best estimate vertical mode fundamental frequency for a fully anchored tank

F_h	horizontal component of membrane tension
$F_{\mu D}$	inelastic energy absorption factor
h_{ci}	height associated with m_{ci}
h_d	dome height above cylindrical wall
h_e	effective length of anchor bolt
h_{sc}	slosh height capacity
h_{si}	slosh height corresponding to fundamental convective mode
h_{sr}	slosh height response
h_t	height to center of gravity of tank
H_ℓ	height of liquid
L	length of uplifted portion of base plate
L_s	seismic load factor
m_{ci}	liquid mass participating in fundamental convective mode
m_i	liquid mass participating in impulsive mode
m_ℓ	total liquid mass
m_t	tank mass
M_C	moment capacity of tank
M_{ci}	fundamental connective mode base moment
M_d	hydrodynamic base moment
M_f	moment in tank due to fluid hold-down
M_i	total horizontal base moment due to impulsive mode
$M_{i\ell}$	horizontal impulsive mode base moment due to liquid mass
M_{it}	horizontal impulsive mode base moment due to tank mass
M_{pb}	plastic moment capacity of base plate
M_{pw}	plastic moment capacity of wall

M_{ti}	total inelastic base moment
M_+	maximum positive moment
p	liquid pressure
p_c	pressure capacity
p_{ci}	fundamental convective mode pressure
P_d	total hydrodynamic pressure
p_{dh}	hydrodynamic pressure due to horizontal component of seismic motion
p_{dv}, p_v	hydrodynamic pressure due to vertical component of seismic motion
p_i	impulsive component of hydrodynamic pressure
p_m	total internal pressure on tank wall at location of maximum longitudinal compressive stress
p_{st}	hydrostatic pressure
p_{ti}	total inelastic factored pressure
P_a	axial compressive force on tank wall
R	radius of tank
R_R	risk reduction factor
$(S_A)_{ci}$	spectral acceleration for fundamental convective mode
$(S_A)_i$	spectral acceleration for impulsive mode
$(S_A)_v$	spectral acceleration for fundamental vertical mode
S_F	scale factor
t_a	average thickness of tank wall
t_{tb}	thickness of tank base plate
t_{tw}	thickness of tank wall
T_{cb}	tensile capacity of anchor bolt
T_{bi}	tensile force on anchor bolt "i"
T_{bp}	anchor bolt pretension

T_{fo}	fluid hold-down tensile force at outer tension side of tank wall
T_{fn}	fluid hold-down force at neutral axis
V_c	base sliding shear capacity using code coefficient
V_{ci}	base shear corresponding to fundamental convective mode
V_d	total hydrodynamic base shear
V_i	base shear corresponding to impulsive mode
V_{cs}	nominal base sliding shear capacity
V_{ti}	total inelastic base shear
W_t	weight of tank
W_{te}	effective weight of tank
z	vertical distance above the base
γ_t	specific weight of tank material
δ_o	uplift height at outer tension side of tank wall
θ	circumferential angle
θ_b	circumferential angle between anchor bolts
θ_n	circumferential angle to neutral axis
κ	shell parameter
λ_1	first root of first derivative of Bessel function of first kind and first order
ρ_ℓ	mass density of liquid
ρ_t	mass density of tank material
σ_a	allowable axial compressive stress
σ_c	hoop membrane stress capacity
σ_y	code minimum yield stress
σ_{ye}	effective yield stress

Table G.1 Spectral Amplification Factors for Horizontal Elastic Response

Damping, % Critical	Median (50%) Acceleration	Velocity	Displacement
0.5	3.68	2.59	2.01
1	3.21	2.31	1.82
2	2.74	2.03	1.63
3	2.46	1.86	1.52
5	2.12	1.65	1.39
7	1.89	1.51	1.29
10	1.64	1.37	1.20
20	1.17	1.08	1.01

Table G.2 Hydrostatic and Hydrodynamic Pressures at Various Locations Above Base

Height above base z (ft.)	η=z/H_t	Demand (Response) (psi)								Capacity (psi) p_c
		p_{st}	p_i	p_{c1}	p_v	p_{dh}	p_{dv}	p_d	p_{ti}	
0	0	10.17	4.54	0.44	3.09	4.56	3.09	5.51	14.39	
1	.049	9.67	4.54	0.44	3.08	4.56	3.08	5.50	13.89	31.25
10	.490	5.18	3.76	0.57	2.22	3.80	2.22	4.40	8.55	25.0

$$p_{dh} = [p_i^2 + p_{c1}^2]^{1/2}$$

$$p_{dv} = p_v$$

$$p_d = [p_i^2 + p_{c1}^2 + p_v^2]^{1/2}$$

$$p_{ti} = \frac{SF\, p_d}{F_{\mu D}} + p_{st}$$

$$SF = 1.15$$

$$F_{\mu D} = 1.5$$

Table G.3 Base Moment Capacity for The Unanchored Tank

C_b = 1.72 kips/inch W_t = 53.5 kips T_{fn} = 0.196 kip/inch
ΔT_f = -0.035 kip/inch R = 25 feet = 300 inches ΣT_{bi} = 0

Trial θ_n	C_1	C_2	C_3	C_4	C_m' (kips/inch)	M_c (kip-feet)
2.80	4.40	.449	6.74	1.60	2.57	9,220
2.70	3.41	.576	5.13	1.62	1.93	9,160
2.60	2.78	.698	4.11	1.64	1.52	9,050

M_c = 9,100 kip-ft

Table G.4 Base Moment Capacity for the Partially Anchored Tank

C_b = 1.72 kips/inch W_t = 53.5 kips T_{fn} = 0.058 kip/inch ΔT_f = -0.001 kip/inch
8 bolts @ 45° T_{cb} = 106 kips δ_o = 0.36 inch K_b = 911 kips R = 25 feet = 300 inches

Trial θ_n	$1 + \cos \theta_n$	C_1	C_2	C_3	C_4	T_{b1} (kips)	2 T_{b2} (kips)	2 T_{b3} (kips)	2 T_{b4} (kips)	ΣT_{bi} (kips)	C_m' (kips/inch)	M_C (kip-feet)
2.50	.1989	2.35	.815	3.40	1.65	106.0	212.0	212.0	95.1	625.1	3.00	23,530
2.25	.3718	1.71	1.08	2.30	1.68	106.0	212.0	212.0	0	530.0	1.88	22,320
2.00	.5839	1.34	1.31	1.65	1.68	106.0	212.0	212.0	0	530.0	1.46	21,490

M_C = 22,000 kip-ft

ΣT_{bi} = 530.0 kips

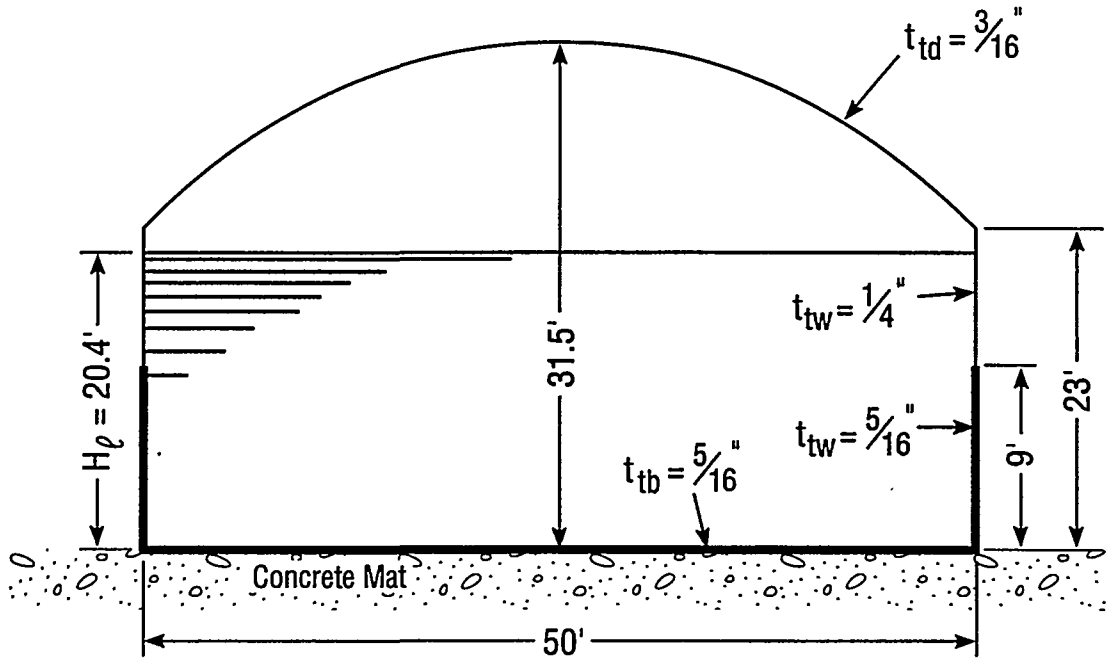

Figure G.1 Example Tank

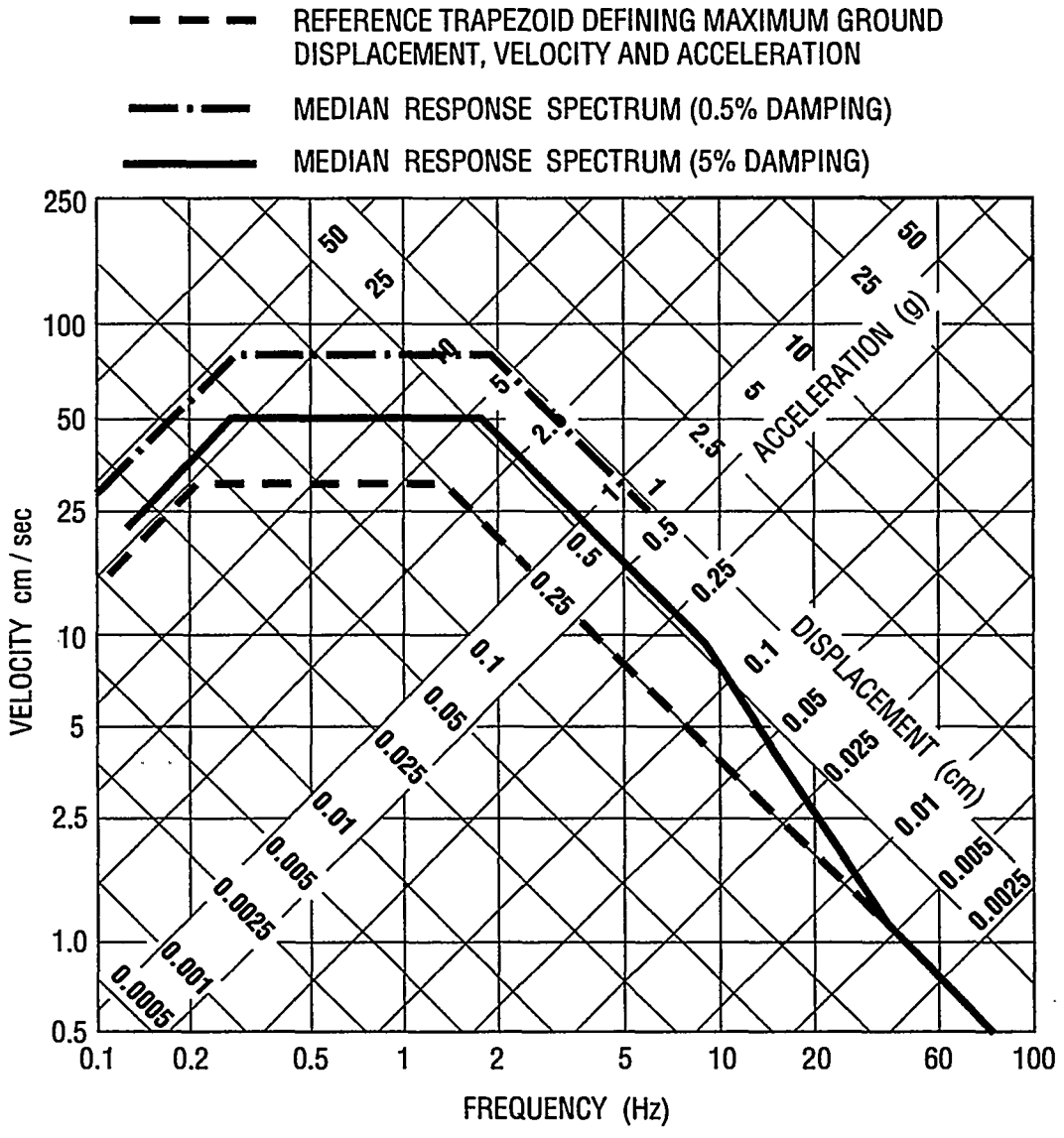

Figure G.2 Response Spectra for Systems with 0.5% and 5% of Critical Damping

APPENDIX H

LUMPED PARAMETER SOIL/STRUCTURE INTERACTION ANALYSIS

H.1 INTRODUCTION

Background material for the Lumped Parameter Soil/Structure Interaction (SSI) analysis discussed in Chapter 6 is presented in this Appendix. Data required to perform the analysis, and material supporting some of the recommendations given in Chapter 6 are included. The topics considered are: horizontal/rocking SSI analysis, vertical SSI analysis, and the conditions for which a site may be considered to have uniform properties.

H.2 HORIZONTAL/ROCKING SSI ANALYSIS

The horizontal/rocking responses of the vault/tank system to horizontal seismic motions are discussed in detail. The geometry of the soil/vault interface for the problem under consideration is shown on Figure H.1a. The vault is of radius R_v and height H_v, and the soil cover over the vault is of depth D. Rigid body horizontal and rocking displacements U and Φ, referenced to the center of the vault basemat, are used to represent the free field seismic motions as defined in Figure H.1b. The SSI analyses are based on the following assumptions:

a. The soil is modeled as a viscoelastic solid with the following properties: shear modulus G, mass density ρ, Poisson's ratio μ, and hysteretic damping ratio β. Nonlinear soil properties (degradation of shear modulus and increase in soil damping with increasing strain) may be handled in an iterative manner. The subscript s is added to differentiate the properties of the soil to the side of the vault from those of the underlying soil. When the side soil has the same properties as the underlying soil the subscript is not used. Variability of the soil properties with depth can only be considered to the extent that SSI

models are available. Limitations of available SSI models are discussed in Section H.2.1.

b. The free field motions are treated as vertically propagating, horizontally polarized shear waves.

c. The vault is considered to be rigid. This assumption is required because lumped parameter SSI models are only available for rigid foundations. This assumption is found to be valid (see below) when the dimensionless frequency parameter $\omega R_v/V_s < 4.5R_v/H_v$ and the thickness to radius ratio of the vault wall t/R_v is greater than $3x10^{-8}\ V_s^2$. The first criterion limits the frequency range of interest to less than 18 cps for typical values of V_s =1000 fps and vault radius and height equal to 40'. The second criterion requires $t/R_v > 0.03$ if V_s = 1000 fps. Most HLW tanks satisfy these criteria.

d. SSI lumped parameter models are only available for rigid foundations which come to the surface. (Models are available for deeply buried foundations but that case is not applicable to the HLW tanks of interest.) The method is therefore restricted to those cases where the depth of the soil cover D over the vault is small. It is assumed that the method can be applied when $D < R_v/2$. The mass characteristics of the soil cover are added to the vault. The free field motions effecting the vault response are determined for the actual depth of burial of the vault (from D to D + H_v below the surface). SSI stiffness and damping coefficients are evaluated neglecting the effects of the soil cover.

e. A single-degree-of-freedom system is used to model the impulsive action of the fluid/tank system as discussed in Chapter 4. The convective mass is not included in these analyses.

The combined horizontal/rocking SSI problem is approached by solving the following series of problems and superimposing the results:

a. The free field solution is obtained from the basic wave equations. Specifically, the free field displacements and stresses are evaluated over the interface surface between the vault and free field (see Figure H.1). The analyses are carried out in the frequency domain so that the free field motions are represented in terms of their Fourier components.

b. Stresses having the opposite sense of those evaluated in (a) are imposed on the interface and the resulting displacements of the interface are determined. This is the "kinematic interaction" problem. The sum of problems (a) and (b) give the free field solution for the free field with a stress free void where the vault will be placed.

c. Interaction tractions are determined which result in compatible displacements of the vault and free field when applied to both the vault (resisting the vault inertial effects) and the interface surface. This is the "inertial interaction" problem.

The solution of these problems requires that impedance functions (SSI models) be available relating the stresses (or tractions) acting on the vault/soil interface to the displacements of the interface. The extent to which the SSI models are available determines the extent to which this methodology can be applied. SSI models are available for cylindrical, rigid foundations embedded in an elastic or viscoelastic medium. The use of this methodology is therefore restricted to those foundations which can be considered to be rigid, and to those vaults where the depth of cover is small.

The SSI models are first discussed followed with derivations and typical results for the kinematic and inertial interaction problems. The application of this methodology to problems of interest require the development of a computer code. The solutions discussed in the following sections were obtained from a code running on a Macintosh PC with typical running times for complete solutions on the order of a few minutes. The short running times for these solutions are the major attraction of this methodology in that rather extensive sensitivity studies are possible.

H.2.1 SSI Models

SSI models are derived by imposing a harmonic force to a rigid foundation, calculating the resulting steady state displacements of the free field, and evaluating the foundation displacement. The impedance function (SSI model) is then defined as the ratio of the imposed forcing function to the resulting displacement. The resulting complex-valued forces F acting on the soil/structure interface are then related to the complex-valued displacements U through the SSI model as follows:

$$F = (K + iaC)(1 + 2i\beta)U \qquad \text{(H.1)}$$

where,

K, C = SSI parameters to be determined

a = dimensionless frequency parameter = $\omega R_v/V_s$

ω = circular frequency of vibration

Three components of the model described by Equation H.1 are required for the problem under consideration: horizontal force associated with the horizontal displacement, moment associated with the rotation, and the coupling term (horizontal force associated with the rotation). Subscripts (hh, pp, and hp) are applied to the parameters K and C to differentiate the three models in the subsequent discussions. It should be noted that

each of the three SSI models can be physically interpreted as a parallel spring/damper model. The spring constant of the model is $K-2a\beta C$ and the damper constant is $\{aC+2\beta K\}/\omega$. The subsequent analyses in this Appendix use numerical values of the parameters that are developed assuming that the SSI models are attached to the bottom of the vault basemat.

While difficult to obtain, several solutions are available to generate these coefficients for cases of interest. Examples of rigorous solutions to these problems include those obtained by Day (Reference H.1) and Apsel (Reference H.2). Significant work is required to deduce numerical SSI coefficients from these theoretical results however. Pais and Kausel (Reference H.3) have supplemented these theoretical results with solutions obtained with static finite element models to obtain generalized results that are applicable to a relatively wide range of problems. Expressions for the coefficients developed in Reference H.3 are given in Table H.1. There are two limitations to the application of these data to the HLW vaults. First, the solutions are based on uniform soil properties so that the soil underlying the vault foundation must have the same properties as those of the soil to the side of the vault and no variability in the side soil may be considered. Second, the SSI forces resulting from interaction along the sidewall are not separated from the SSI forces acting on the base so that the soil pressures acting on the vault walls cannot be evaluated.

Beredugo and Novak (Reference H.4) have also developed SSI models. This solution is obtained by breaking the problems into two parts. The first part treats the interaction along the base of the structure by neglecting the side soil. This approximation is not considered to be serious. The second part treats the side soil by assuming that it behaves in a state of plane strain so that the SSI forces acting on the wall are transmitted laterally through the soil layer but not vertically

down to the underlying soil. This assumption may be appropriate for uniform soil sites but could be questionable for those sites where the soil beneath the vault is considerably stiffer than the side soil. Studies are being conducted to evaluate the significance of these effects and the results will be published when available. The SSI parameters developed in this reference are also given in Table H.1. The Beredugo-Novak model is divided into the contributions of the base and sidewall interaction and the results shown in Table H.1 give the contributions from each. The base and sidewall soil properties can therefore be different. In fact, the sidewall model can be divided into several layers so that variations of the side soil properties over the depth of the vault could be considered. Uniform soil properties beneath the foundation are required. A comparison of the results obtained by the two models is discussed below.

The constants that appear in Table H.1 are defined in Table H.2. Beredugo-Novak give both frequency dependent and approximate, frequency independent definitions for these constants; both are shown in Table H.2. The constants are given for specific values of Poisson's ratio and it is recommended that interpolation be used to obtain the values of the constants for intermediate values of Poisson's ratio. Values for C_{p1} and C_{p2} are only provided for Poisson's ratio equal to 0. These constants effect the rocking stiffness and damping of the soil acting on the basemat. A comparison of the two sets of SSI parameters (References H.3 and H.4) indicate that the rocking stiffness and damping parameters compare reasonably well for Poisson ratio equal to 0 and that the Beredugo-Novak results are too low as Poisson's ratio increases. The rocking parameters depend on dilatational rather than shear wave velocity so that it is reasonable to use the factor α, defined in Table H.1, as the basis for modifying the Beredugo-Novak parameters to account for Poisson's ratio. The following correction is found to result in

coefficients which agree reasonably well with the Pais-Kausel results:

$$C_{p1}(\mu) = C_{p1}(0)\,[1 + 3\mu(\alpha-1)]$$
$$C_{p2}(\mu) = C_{p2}(0)\,[1 + 3\mu(\alpha-1)] \qquad \text{(H.2)}$$

The parameters shown in Table H.2 with an (*) have been extrapolated for dimensionless frequencies, "a", greater than that contained in Reference H.4. Essentially, the stiffness terms (with the 1 subscript) have been extrapolated to higher values of "a" by maintaining a constant value equal to the value specified at the high end of the range in Reference H.4. The damping terms (with the subscript 2) have been extrapolated with a linear extension of the specified values. These extrapolations were developed by comparisons with the Pais-Kausel results.

Both of the SSI models are restricted to foundations which may be considered rigid. The vault may be considered to be rigid when its stiffness is significantly larger than the stiffness of the soil it replaces. The stiffness of the displaced soil is $\pi R_v^2 G_s/H_v$ and the "shear beam" stiffness of the vault is $2\pi G_c R_v t/H_v$ where G_c is the shear modulus of the concrete and t is the vault wall thickness. The vault is assumed to be rigid if its stiffness is at least 3 times the SSI stiffness so that these data lead to the criterion $t/R_v > 3\times10^{-8}V_s^2$.

H.2.2 Kinematic Interaction

The objective of the kinematic interaction problem (problems a and b above) is to determine the displacements in the free field with a cavity replacing the vault. Since this approach is restricted to those cases where the vault may be considered to be rigid, the displacements at the vault/soil interface are restricted to rigid body components. These are expressed as a displacement at the base of the vault and a rotation about the

base as shown on Figure H.1b. The free field solution is first considered and followed with the modification required to account for the void.

Solutions are carried out in the frequency domain and a free field motion at a depth z is defined as:

$$U(z)\,e^{i\omega t} = [U_R(z) + iU_I(z)]\,e^{i\omega t} \qquad \text{(H.3)}$$

The subscripts R and I refer to the real and imaginary parts. The DBE is usually defined at the surface with [$U_R(0)$ and $U_I(0)$]. Solution of the wave equation assuming vertically propagating horizontally polarized shear waves gives the following relationship between the displacements at depth to those at the surface:

$$u_R(\zeta) = u_R(0)\cos a\zeta \cosh a\beta\zeta - u_I(0)\sin a\zeta \sinh a\beta\zeta$$

$$u_I(z) = u_R(0)\sin a\zeta \sinh a\beta\zeta + u_i(0)\cos a\zeta \cosh a\beta\zeta \qquad \text{(H.4)}$$

$$\textit{where, } \zeta = z/R_v$$

$$u_R = U_R/R_v;\; u_I = U_I/R_v$$

The shear stresses v are equal to the shear modulus times the first derivative of the free field displacement with respect to the depth, so that:

$$v_R/G = u_R(0)\,[-a \sin a\zeta \cosh a\beta\zeta + a\beta \cos a\zeta \sinh a\beta\zeta]$$

$$-u_I(0)\,[a \cos a\zeta \sinh a\beta\zeta + a\beta \sin a\zeta \cosh a\beta\zeta] \qquad \text{(H.5)}$$

$$v_I/G = u_R(0)\,[a\cos a\zeta \sinh a\beta\zeta + a\beta \sin a\zeta \cosh a\beta\zeta]$$

$$+ u_I(0)\,[-a\sin a\zeta \cosh a\beta\zeta + a\beta\cos a\zeta \sinh a\beta\zeta]$$

Of course, the same free field displacements and stresses may be evaluated at the points of interest using computer codes such as FLUSH (Reference H.5) or CARES (Reference H.6).

The next step in the process is to compute rigid body displacements of the void that are equivalent to those defined by Equation (H.4). The rigid body displacements of interest (see Figure H.1b) are the real and imaginary parts of the base displacement Δ_{fR} and Δ_{fI}, and the real and imaginary parts of the rotation about the base Φ_{fR} and Φ_{fI}. The f subscript indicates that the deformation represents the rigid body equivalent of the free field displacement. These displacements are normalized with respect to R_v for convenience. The rigid body displacements are determined such that the squared difference between the actual and rigid body displacements, integrated over the surface of the vault/soil interface are minimized. This is done by solving the following equations for each of the real and imaginary parts of the rigid body displacements:

$$4\,(H_v/R_v)\,\Delta_{fq} + 2\,(H_v/R_v)^2\,\Phi_{fq} = 4I_{1q} + 2u_q^* \qquad (H.6)$$

$$2\,(H_v/R_v)^2\Delta_{fq} + 4\,[H'^2H_v - H'\,(H'^2 - D^2) + (H'^3 - D^3/3]\,/R_v^3\Phi_{fq} = 4I_{2q}$$

where, q = R or I indicating real or imaginary parts

I_{1q} = integral of u_q from the top ($\zeta = D/R_v$) to bottom ($\zeta = \{D+H_v\}/R_v$) of the vault

u_q^* = nondimensional displacement at bottom of vault

$H' = H_v + D$

I_{2q} = integral of (ζu_q) from the top to bottom of the vault

The above integrals are evaluated numerically using a standard quadrature method (i.e., Simpson's rule). The free field displacements are needed at several points over the depth $D/R_v < \zeta < \{D+H_v\}/R_v$. These can be determined from either Equations H.4 or from a computer solution of the free field problem. Results of these computations are discussed below. The

variation of the free field motion with depth follows that of a lightly damped cosine curve (see Equation H.4). Large errors arise in this rigid body fit of the data when the parameter a in $\zeta = aH_v/R_v$ becomes larger than about 4.5. It is therefore recommended that this methodology which is based on a linear depth variation of the free field motion, be restricted to those cases where the nondimensional frequencies of interest are less than $4.5\ R_v/H_v$.

The forces (horizontal force F_f and moment M_f) acting on the interface are obtained by integrating the shear stresses over the surface of the interface. The results are:

$$F_{fq} = -\pi\ R_v^2 v_q^* \qquad (H.7)$$

$$M_{fq} = -4\ R_v^3\ I_{3q}$$

where, v_q^* = real or imaginary part of the shear stress at base of vault

I_{3q} = integral of real or imaginary part of the shear stress from the top to bottom of the vault

Deflections must then occur to eliminate these forces and moments. The SSI model, discussed in Section H.2.1, can be used to calculate the rigid body deflections that occur as the forces are developed to negate the above forces at the interface. The subscript k is applied to these deflections to indicate that they result from kinematic interaction effects. The total deflections in the free field including the void are the sum of the free field and kinematic interaction parts, $\Delta_{fq} + \Delta_{kq}$ and $\Phi_{fq} + \Phi_{fq}$. The equations used to solve for the kinematic interaction deflections are:

$$\begin{bmatrix} K_1 & -C_1 & K_3 & -C_3 \\ -C_1 & -K_1 & -C_3 & -K_3 \\ K_3 & -C_3 & K_2 & -C_2 \\ -C_3 & -K_3 & -C_2 & -K_2 \end{bmatrix} \begin{Bmatrix} u_{kR} \\ u_{kI} \\ f_{kR} \\ f_{kI} \end{Bmatrix} = \begin{Bmatrix} -F_{fR} \\ F_{fI} \\ -M_{fR} \\ M_{fI} \end{Bmatrix} \qquad \text{(H.8)}$$

where,

$$K_1 = (K_{hh} - 2\ a\ \beta\ C_{hh})/GR_v$$
$$K_2 = (K_{pp} - 2\ a\ \beta\ C_{pp})/GR_v^3$$
$$K_3 = (K_{hp} - 2\ a\ \beta\ C_{hp})/GR_v^2$$
$$C_1 = (a\ C_{hh} + 2\ \beta\ K_{hh})/GR_v$$
$$C_2 = (a\ C_{pp} + 2\ \beta\ K_{pp})/GR_v^3$$
$$C_3 = (a\ C_{hp} + 2\ \beta\ K_{hp})/GR_v^2$$

K_{hh}, K_{hp}, K_{pp}, C_{hh}, C_{hp}, and C_{pp} are obtained from Table H.1.

Solutions are obtained for this kinematic interaction problem for all combinations of H_v/R_v = 0.5 and 1, D/R_v = 0 and 0.5, and β = 0 and 5%. Poisson's ratio is taken as 1/3, the Beredugo-Novak SSI model is used, and the criteria input motion is specified at the surface with a magnitude of $U_R(o)$ = 1 and $U_I(o)$ = 0. Typical results of the real and imaginary parts of the free field (subscript f) and total (subscript t) rigid body displacements (U_f, U_t) and rotations (Φ_f, Φ_t) are shown as a function of the nondimensional frequency on Figures H.2 through H.5. As may be seen the total deflections U_t and Φ_t are very close to the free field deflections U_f and Φ_f indicating that the kinematic interaction effects are relatively unimportant and may be neglected. The significance of the rotational component of the free field motion can also be seen from these data. For example the results on Figure H.2 indicate that the free field motion is essentially translation at low frequencies but that at nondimensional frequencies from $\pi/2$ to about 5 the free field displacement at the elevation of the base of the vault moves in the opposite direction from the surface motion resulting in a significant rocking component to the free field motion. It may also be concluded from these results that the total translation

at any depth is less than or equal to the magnitude of the surface displacement.

The input motion to the inertial interaction problem should be the values of U_t, Φ_t shown on these figures. It should be noted, however, that a good approximation to these input motions may be obtained by setting U_t equal to the free field displacement at the elevation of the base of the vault and Φ_t equal to the difference in the free field displacement between the top and bottom of the vault divided by the height of the vault. These results can be used to determine some important characteristics of the soil column. The real displacements are zero (this should occur at the soil column frequency) at nondimensional frequencies of about $\pi/2$ for $H_v/R_v = 1$ and π for $H_v/R_v = 0.5$. This corresponds to a soil column frequency equal to the shear wave velocity divided by 4 times the column height.

H.2.3 Inertial Interaction

The response of the vault/tank system to the U_t, Φ_t free field motion is discussed next. Interaction forces are developed so that the deflection of the vault equals the sum of the free field deflection U_t, Φ_t plus that resulting from the interaction forces. The system considered is shown on Figure H.6. The vault is modeled as a rigid body with mass M and rotary inertia J with its center of gravity located Z_o above the basemat. The mass of the soil cover is included with that of the vault. The impulsive fluid of mass m_i is modeled with a cantilever beam of length h' and frequency f_t. The tank fluid model also requires a rotary inertia I_b attached to the basemat. These fluid/tank parameters are defined in Chapter 4. The complex stiffness parameters of the cantilever model of the tank $K_t + iC_t$ are:

$$K_t = 4\,\pi^2 f_t^2 m_i$$

$$C_t = 2\,\omega\,\eta\,[K_t m_i]^{1/2} \qquad \text{(H.9)}$$

where, η = *damping of tank* (4%)

The deflections considered in the problem are also defined in Figure H.6. Note that each of the deflections include a real and imaginary part designated with subscripts (R) and (I) respectively. The following relative deformations and nondimensional parameters are defined:

$$\begin{aligned} u_s &= (U^* - \Phi^* Z_o - U_t)/R_v \\ \Phi_s &= \Phi^* - \Phi_t \\ v_s &= [V^* - U^* - \Phi^* (h' - Z_o)]/R_v \\ M &= \omega^2 M/GR_v \\ J &= \omega^2 (J + I_b)/GR_v^3 \\ m_i &= \omega^2 m_i/GR_v \end{aligned} \qquad \text{(H.10)}$$

The equations of motion controlling the response of the system are:

$$\begin{aligned} &-M[(u_{sR}+iu_{sI}) + (\Phi_{sR}+i\Phi_{sI})\,Z_o/R_v] + (K_1+iC_1)\,(u_{sR}+iu_{sI}) + (K_3+iC_3)\,(\Phi_{sR}+i\Phi_{sI}) \\ &\quad - (K_t+iC_t)\,(v_{sR}+iv_{sI}) = M\,[(u_{tR}+iu_{tI}) + (\Phi_{tR}+i\Phi_{tI})\,Z_o/R_v] \end{aligned}$$

$$\begin{aligned} &-J(\Phi_{sR}+i\Phi_{sI}) + (K_2+iC_2)\,(\Phi_{sR}+i\Phi_{sI}) + (K_3+iC_3)\,(u_{sR}+iu_{sI}) - [(K_1+iC_1) \\ &\quad (u_{sR}+iu_{sI})\,Z_o/R_v - (K_3+iC_3)\,(\Phi_{sR}+i\Phi_{sI})]\,Z_o/R_v - (K_t+iC_t) \\ &\quad (v_{sR}+iv_{sI})\,(h'-Z_o)/R_v = J(\Phi_{tR}+i\Phi_{tI}) \end{aligned} \qquad \text{(H.11)}$$

$$\begin{aligned} &-m_i[(v_{sR}+iv_{sI}) + (u_{sR}+iu_{sI}) + (\Phi_{sR}+i\Phi_{sI})\,h'/R_v] + (K_t+iC_t)\,(v_{sR}+iv_{sI}) \\ &\quad = m_i[(u_{tR}+iu_{tI}) + (\Phi_{tR}+i\Phi_{tI})\,h'/R_v] \end{aligned}$$

where the K, and C SSI constants are as defined with Equation H.8.

These three equations are separated into the real and imaginary parts and the resulting six equations solved for the unknown SSI deformations. This completes the solution using this

methodology. The Fourier components of the displacements are then transformed into time histories.

Solutions are obtained for typical HLW tanks so that the significance of SSI effects may be deduced. The solutions are carried out in the frequency domain with the input at each frequency defined with unit real and zero imaginary horizontal free field displacement components at the surface. The following restrictions are placed on the system characteristics for these solutions:

- The radius of the tank is assumed to be 4′ less than the vault radius and the tank height is assumed to be 8′ less than the vault height.

- The ratio of impulsive fluid mass to total fluid mass and the length of the impulsive mass cantilever model is taken from Chapter 4 based on the H_v/R_v ratio for the vault.

- Solutions are found for fluid to soil density ratios γ_f/γ_s equal to 0.6 and 1.

- The ratio of concrete volume to total vault volume is assumed to be 0.2, 0.3, or 0.4.

- The ratio of tank frequency times vault radius to shear velocity $f_t R_v/V_s$ is taken to be 0.2 or 0.4. For a typical HLW tank with R_v = 40′ and V_s = 1000 fps the lower value corresponds to a tank frequency of 5 cps.

The results of these analyses are presented in Figures H.7 through H.10. The Fourier components of the displacements at the top of the vault, base of the vault, and the fluid mass are shown as a function of dimensionless frequency on the figures. The displacements are plotted as the ratio of the magnitude predicted with SSI effects included to that predicted when SSI effects are neglected. The range of dimensionless frequencies

of interest for typical HLW tanks (R_v = 40'; V_s = 1000 fps) is a <4. The following discussion is limited to that range.

A general review of the four figures indicates that the curves labeled 1 and 2 vary in a similar manner with dimensionless frequency as do the curves labeled 3 and 4. This indicates that the ratio of fluid to soil density is not a significant parameter. On the other hand, the 1-2 curves usually are significantly different from the 3-4 curves indicating that the tank frequency parameter f_tR_v/V_s does have a significant effect on the results. Note that the forcing function frequency $\omega/2\pi$ equals the tank frequency at values of dimensionless frequencies equal to 1.25 and 2.5 for values of f_tR_v/V_s equal to 0.2 (the 1-2 curves) and 0.4 (3-4 curves) respectively. The fluid response data on the four figures generally indicate that SSI effects increase the response of the tank for the lower tank frequency parameter (f_tR_v/V_s = 0.2) and that this increase occurs at dimensionless frequencies of about a = 1. For example, the fluid displacement ratio for the 1-2 curves on Figure H.7 is about 1.45 at a dimensionless frequency = 1. This indicates that one of the SSI frequencies is at about a = 1 (f = 4 cps for the 40' radius vault in a soil with a shear velocity equal to 1000 fps) causing an interaction between the tank and vault/soil system. The fluid response data does not show a similar characteristic for the higher frequency tanks (f_tR_v/V_s = 0.4). Similar amplifications are found for both the 1-2 and 3-4 curves at frequencies where the 3-4 curves are amplified. This implies that the input to the tank is increased by SSI effects but that no dynamic interaction occurs between the tank and the vault/soil system.

A comparison of sets of figures leads to an evaluation of the more significant parameters of the problem. The only difference in the problems represented on Figures H.7 and H.8 is that the data on Figure H.7 represents a vault with no cover while the

data on Figure H.8 represents a vault with a soil cover equal to 1/2 of the radius. Significant differences are found for these two cases indicating that the soil cover has a significant effect on the extent to which SSI influences the response. Figures H.8 and H.9 are very similar indicating that the ratio of concrete volume to vault volume has little impact on the results. Finally a comparison of Figures H.8 and H.10 indicates that the height to radius ratio of the vault has a large impact on the results with the effects of SSI becoming more significant for the shallower vaults.

These data may also be used to decide whether a SSI analysis is required. The top two plots on the figures give an indication of the extent to which the floor response spectra may be increased by consideration of SSI. As may be seen amplifications of 10% to 20% of the floor response spectra at the top of the vault would be expected unless the height to radius ratio of the vault is less than 1. Amplifications of the base floor response spectra are limited to the same range unless the height to radius ratio of the vault is less than 1 or unless there is no soil cover over the vault. In either case, amplifications of 40% may occur. The load on the tank is determined by convolving the transfer functions shown on the four figures with the input response spectra. The significant portion of the input response spectra is usually in the 2-10 cps range, corresponding to $0.5 < a < 2.5$ for a typical HLW vault. This is done assuming that the input spectral acceleration is constant within the range. The load on the tank is found to be less when SSI effects are included except for the case shown on Figure H.7 where $f_t R_v/V_s = 0.2$ (the tank load is increased by about 20% when SSI effects are included), and for the case shown on Figure H.10 where $f_t R_v/V_s = 0.2$ (the tank load is increased by about 10%). It should, however, be noted that SSI effects are important for those sites where the soil to the side of the

vault is significantly softer than the soil beneath the foundation of the vault (Reference H.8).

A comparison of the results obtained using the Beredugo-Novak and Kausel SSI models is shown on Figure H.11. A comparison of the top and base vault responses on Figure H.11 indicates reasonably good agreement until the nondimensional frequency exceeds 3.5. This corresponds to a frequency of 14 cps for a tank radius of 40′ and a soil shear wave velocity of 1000 fps. This frequency range is adequate for most HLW tanks. The comparison of the fluid response is quite good. These data indicate that both SSI models given similar results for frequencies less than about 15 cps.

H.3 VERTICAL SSI ANALYSIS

The model of the vault/tank/fluid system that can be used to determine the vertical response of the system to a vertical seismic input motion is shown on Figure H.12. The lower spring/dashpot model shown on Figure H.12 represents SSI effects with the spring (K_v) and damper (C_v) coefficients taken from Reference H.7 as:

$$K_v = 4GR_v/(1-\mu)$$

$$C_v = 0.85\ K_vR_v/V_s \qquad \text{(H.12)}$$

where,

G = foundation soil shear modulus

μ = soil Poisson's ratio

V_s = soil shear wave velocity

The fluid mass is divided into two parts as discussed in Section 4.5.4. One part m_o vibrates with the foundation and the second part m_1 vibrates with the tank wall. The frequency of the tank wall ω is related to the breathing mode of the tank as discussed in Section 4.5.4. The mass M_4 shown on Figure H.12 equals m_1 and

this mass is attached to the basemat with a spring so that the frequency of the single degree of freedom system equals ω.

The mass (M_3) shown in Figure H.12 includes the mass of: the vault mat, the lower half of the vault wall, and the fluid mass (m_o). The vault wall stiffness and structural damping are represented with the middle spring/damper model shown on Figure H.12. In many instances, the vault may be considered to be rigid and mass (M_2) lumped with mass (M_3).

The upper spring/damper model represents the stiffness and damping of the vault roof. This spring/damper model supports a portion of the vault roof mass and the overburden soil (M_1). The remaining roof and soil mass together with the mass of the upper half of the vault walls comprise mass (M_2). The total soil overburden may be assumed to be that mass of soil contained within the vertical cylinder over the vault unless ($D>R_v$) in which case the soil mass may be taken as that contained within a cone inclined inward from the vault outer radius at an angle of 30°. The following procedure may be used to determine the mass (M_1) and the stiffness of the vault roof:

a. Compute an approximate vertical deflection shape of the vault roof resulting from the roof and soil overburden weight.

b. Estimate the roof frequency as equal to the square root of the ratio of the kinetic to potential energies resulting from the dynamic deflection assuming that the shape is equal to that found in step (a).

c. Compute (M_1) so that the kinetic energies of the single degree of freedom system representing the roof response and the actual roof are equal.

d. The stiffness of the roof model is then computed from the frequency found in step (b) and the mass found in step (c).

In many cases the vertical SSI effects are relatively unimportant. The conditions under which this is true are discussed in Reference H.8 with the ratio of the vault response including SSI to that without SSI tabulated. The ratios are found to be equal to 1.28 and 1.32 for vaults with a H_v/R_v ratio equal to 0.5 for D/H_v ratios of 0.25 and 0.5 respectively. These same ratios increase to 1.48 and 1.54 when the H_v/R_v ratio increases to unity. It is unlikely that even these values are significant when one considers the magnitude of the vertical seismic acceleration (even amplified by the 1.54 factor) as compared with the dead load acceleration of 1 G. For example, the demand for the dead load case is based on an acceleration equal to 1 G times a load factor of 1.4. The demand for the dead plus seismic load cases is based on a load factor of unity applied to 1 G plus the seismic vertical acceleration. A vertical free field acceleration of 0.4/1.54 = .26 G is required for the seismic load case to equal the dead load case even with the highest amplification of 1.54.

As a conservative alternative to performing the vertical seismic response calculation the amplification factor for the vault geometry of interest may be found from Table 2 in Reference H.8. This factor may then be applied to the vertical free field motion at the basemat level and used as input to the vault and tank/fluid model.

H.4 UNIFORM SITE CRITERIA

When the soil properties at the site are "uniform" over the depth of the vault simplifications are possible in the description of the free field motion, and indeed it may be possible to eliminate the necessity to perform SSI calculations. The site is defined as uniform in Chapter 6 when the soil shear wave velocity does not vary by a factor or more than 1.5 from the surface to a depth of one vault diameter below the vault basemat. The objective of this material is to demonstrate that

free field response spectra are less than the surface spectra when this restriction is satisfied.

Deconvolution studies are performed for several soil columns satisfying the 1.5 criteria and the spectra of the motion at 100′ is compared with the surface spectra. The CARES (Reference H.6) code is used to perform the analyses. The surface input motion is an artificial time history of 20 seconds duration and fitting the RG 1.60 spectrum anchored at 0.2 G. The following columns are considered in the analysis:

1. A uniform soil column with a shear wave velocity of 1000 fps.

2. A 20′ upper layer having a shear wave velocity of 1500 fps underlaid by soil with a shear wave velocity of 1000 fps.

2A. A 20′ upper layer having a shear wave velocity of 1200 fps underlaid by soil with a shear wave velocity of 1000 fps.

3A. 1000 fps shear wave velocity for the first 50′ underlaid by a 1200 fps layer.

3B. 1000 fps shear wave velocity for the first 50′ underlaid by a 1500 fps layer.

3C. 1000 fps shear wave velocity for the first 50′ underlaid by a 2000 fps layer.

4. A stiff sand with shear wave velocity that increases from 1000 fps at the surface to 1500 fps at a depth of 50′.

The deconvolution studies are performed and response spectra (5%) generated for the motion at a depth of 100′. These spectra are divided by the input spectra and the results for the stiff upper soils, stiff lower soils, and sand columns shown on Figures H.13 through H.15 respectively. The surface spectra envelopes the foundation spectra when the data on these figures

are less than unity. The foundation/surface spectral ratios for the stiff lower soil and sand cases are always less than unity. The ratios for the stiff upper soil cases are less than unity except for frequencies exceeding 10 cps. It is concluded that it is reasonably conservative to replace the foundation free field motion with the surface motion for these cases.

REFERENCES

H.1 Day, S.M., "Finite Element Analysis of Seismic Scattering Problems," Ph.D Thesis, University of California, 1977.

H.2 Apsel, R.J., "Dynamic Green's Functions for Layered Media and Applications to Boundary Value Problems," Ph.D Thesis, University of California, 1979.

H.3 Pais, A., and Kausel, E., "Stochastic Response of Foundations," Dept. of Civil Engineering, Massachusetts Institute of Technology, Report No. R85-6, February 1985.

H.4 Beredugo, Y.O., and Novak, M., "Coupled Horizontal and Rocking Vibration of Embedded Footings," Canadian Geotechnical Journal, Vol. 9, 1972.

H.5 Lysmer, J., Udaka, T., Tsai, C., and Seed, H., "FLUSH - A Computer Program for Approximate 3-D Analysis of Soil-Structure Interaction Problems," Report EERC 75-30, College of Engineering, University of California, November 1975.

H.6 "Computer Analysis for Rapid Evaluation of Structures - CARES," Brookhaven National Laboratory, NUREG/CR-5588, 1989.

H.7 American Society of Civil Engineers, Standard 4-86, "Seismic Analysis of Safety-Related Nuclear Structures and Commentary on Standard for Seismic Analysis of Safety-Related Nuclear Structures," September 1986.

H.8 Miller, C.A., and Costantino, C.J., "Conditions for Which SSI Effects in HLW Tanks are Small," Proceedings of the DOE Natural Hazards Conference, 1993.

NOTATION

a	dimensionless frequency = $\omega R_v/V_s$
C_{hh}	imaginary part of SSI horizontal stiffness due to relative horizontal deformation
C_{hp}	imaginary part of SSI coupling stiffness
C_{pp}	imaginary part of SSI rocking stiffness due to relatine rotation
C_v	imaginary part of vertical SSI coefficient
D	depth of soil cover over vault roof
f_t	tank/fluid impulsive frequency
G	soil shear modulus - add subcript (s) to indicate side soil if different from base soil
h'	length of cantilever beam used to model tank/fluid system
H_v	height of vault
I_b	rotary interia attached to basemat to model fluid effects
J	rotary inertia of vault about its center of gravity
K_{hh}	real part of SSI horizontal stiffness due to relative horizontal deformation
K_{hp}	real part of SSI coupling stiffness
K_{pp}	real part of SSI rocking stiffness due to relative rotation
K_t	stiffness of tank/fluid impulsive model
K_v	real part of vertical SSI coefficient
M	mass of vault
m_i	impulsive mass of fluid
R_v	radius of vault
t	vault wall thickness
U	rigid body displacement of free field referenced to vault center of basemat
u	U/R_v
u_k	displacement component due to kinematic interaction
u_t	$u+u_k$
v	shear stresses acting on vault/soil interface
V_s	soil shear wave velocity - add second subcript (s) to indicate side soil if different from base soil

z	vertical coordinate measured from ground surface down
Z_o	distance of vault center of gravity above basemat
$( )_I$	imaginary part of parameter ( )
$( )_R$	real part of parameter ( )
β	hysteretic soil damping - add subcript (s) to indicate side soil if different from base soil
Δ_f	rigid body displacement component of free field deformation distribution over vault depth
Φ	rigid body rotation of free field referenced to vault center of basemat
Φ_f	rigid body rocking component of free field deformation distribution over vault dept
Φ_k	rotation component due to kinematic interaction
Φ_t	$\Phi_k + \Phi$
γ_f	fluid density
γ_s	soil density
μ	soil Poisson's ratio - add subcript (s) to indicate side soil if different from base soil
ρ	mass density of soil - add subcript (s) to indicate side soil if different from base soil
ω	circular frequency
ζ	z/R_v

Table H.1

SSI Coefficients

Parameter	Pais-Kausel Model (Ref. 3)	Beredugo-Novak Model (Ref. 4) Base	Sidewall
STIFFNESS TERMS (K)			
K_{hh}/GR	$8(1+H/R)/(2-\mu)$	$C_{u1}+(G_s/G)(H/R)S_{u1}$	
K_{pp}/GR^3	$8[1+2.3\ H/R+0.58(H/R)^3][1-0.35a^2/(1+a^2)]/3(1-\mu)$	$C_{p1}+(G_s/G)[(H/R)S_{p1}+(H/R)^3S_{u1}/3$	
K_{hp}/GR^2	$8(H/R)[0.4(H/R)-0.03]/(2-\mu)$	$0+0.5(G_s/G)(H/R)^2S_{u1}$	
DAMPING TERMS (C)			
C_{hh}/GR	$\pi[1+(1+\alpha)H/R]$	$C_{u2}/a+(G_s/G)(H/R)S_{u2}/a$	
C_{pp}/GR^3	$[\pi a^2\{\alpha/4+H/R+(1+\alpha)(H/R)^3/3\}+0.84b(1+\alpha)(H/R)^{2.5}]/(b+a^2)$	$C_{p2}/a+(G_s/G)[H/R)S_{p2}+(H/R)^3S_{u2}/3]/a$	
C_{hp}/GR^2	$\pi[1+(1+\alpha)H/R](0.4\ H/R-0.03)$	$0+0.5(G_s/G)(H/R)^2S_{u2}/a$	

G = Soil shear modulus; if side soil different than base soil G_s = sidesoil shear modulus

μ = soil Poisson's ratio; V_s = soil shear wave velocity

a = nondimensional frequency = $\omega V_s/R$

R = vault radius; H = vault height

α = ratio compression to shear wave velocity = $[2(1-\mu))/(1-2\mu)]^{1/2}$

b = $2/(1+H/R)$

S_{u1}, S_{u2}, C_{p1}, C_{p2} = Beredugo-Novak coefficients defined on Table G.2

Table H.2

Beredugo-Novak Coefficients

Coefficient	Restrictions		Frequency Dependent	Constant
	μ	a		
C_{u1}	0	<2	$4.571-4.653a+89.09a/(a+19.14)$	4.30
		>2*	3.694	
	0.5	<2	$5.333-1.584a+10.39a/(a+6.552)$	5.10
		>2*	4.595	
C_{u2}	0	<2	$2.536a-0.1345a/(a+1.923)$	2.70
		>2*	$5.003+2.502(a-2)$	
	0.5	<2	$2.923a-0.1741a/(a+1.927)$	3.15
		>2*	$5.757+2.879(a-2)$	
C_{p1}	0	<1.5	$2.654+0.1962a-1.729a^2+1.485a^3-$	2.50
			$0.4881a^4+0.03498a^5$	
		>1.5*	1.865	
C_{p2}	0	<1.5	$0.00802a+0.01583a^2+0.2035a^3+1.202a^4-$ $1.448a^5+0.4491a^6$	0.43
		>1.5*	$0.9394+1.0179(a-1.5)$	

(Continued)

Table H.2 (Continued)

Beredugo-Novak Coefficients

Coefficient	Restrictions		Frequency Dependent	Constant
	μ	a		
S_{u1}	0	<0.2	$24.577a-52.74a^2$	3.60
		0.2<a<1.5	$0.2328a+3.609a/(a+0.06159)$	3.60
		>1.5*	3.816	
	0.25	<0.2	$-1.468a^{1/2}+5.662a^{1/4}$	4.00
		0.2<a<1.5	$2.474+4.119a-4.320a^2+2.057a^3-0.362a^4$	4.00
		>1.5*	4.042	
	0.4	<0.2	$-1.796a^{1/2}+6.539a^{1/4}$	4.10
		0.2<a<1.5	$2.824+4.776a-5.539a^2+2.445a^3-0.394a^4$	4.10
		>1.5*	3.783	
S_{u2}	0	<1.5	$7.334a+0.8652a/(a+0.00874)$	8.20
		>1.5*	$11.86+7.336(a-1.5)$	
	0.25	<1.5	$0.83a+41.59a/(a+3.90)$	9.10
		>1.5*	$12.80+6.964(a-1.5)$	
	0.4	<1.5	$0.95a+56.55a/(a+4.68)$	10.60
		>1.5*	$15.166+8.50(a-1.5)$	
S_{p1}	All	<1.5	$3.142-0.4215a-4.209a^2+ 7.165a^3-4.667a^4 + 1.093a^5$	2.50
		>1.5*	1.895	
S_{p2}	All	<1.5*	$0.0144a+5.263a^2-4.177a^3+1.643a^4-0.2542a^5$	1.80
		>1.5*	$4.153+3.3276(a-1.5)$	

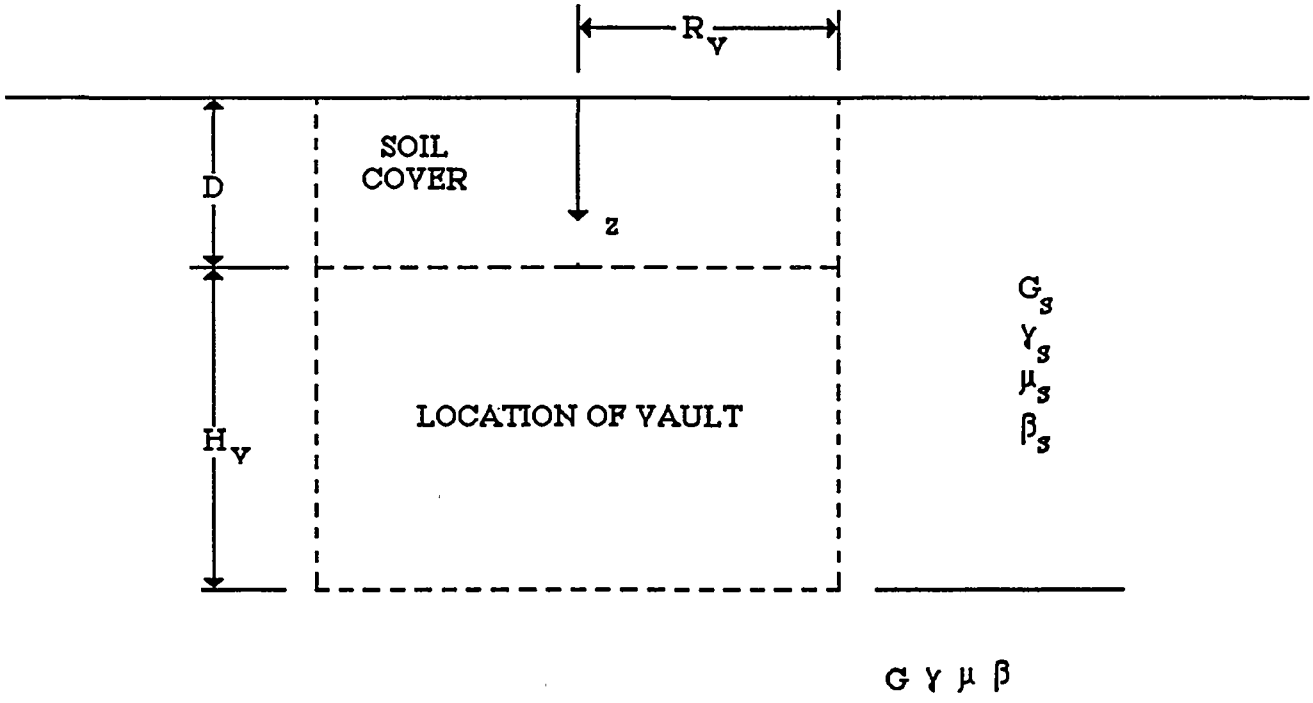

(a) Cavity Geometry and Soil Properties

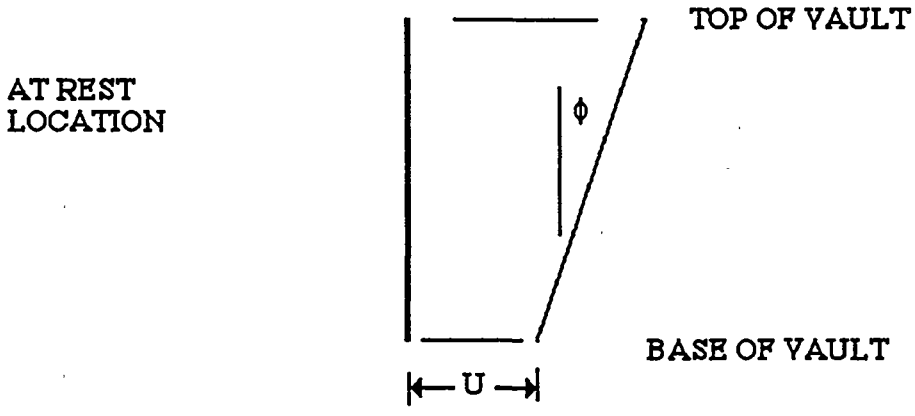

(b) Deflections

Figure H.1 Free Field Geometry and Deflections

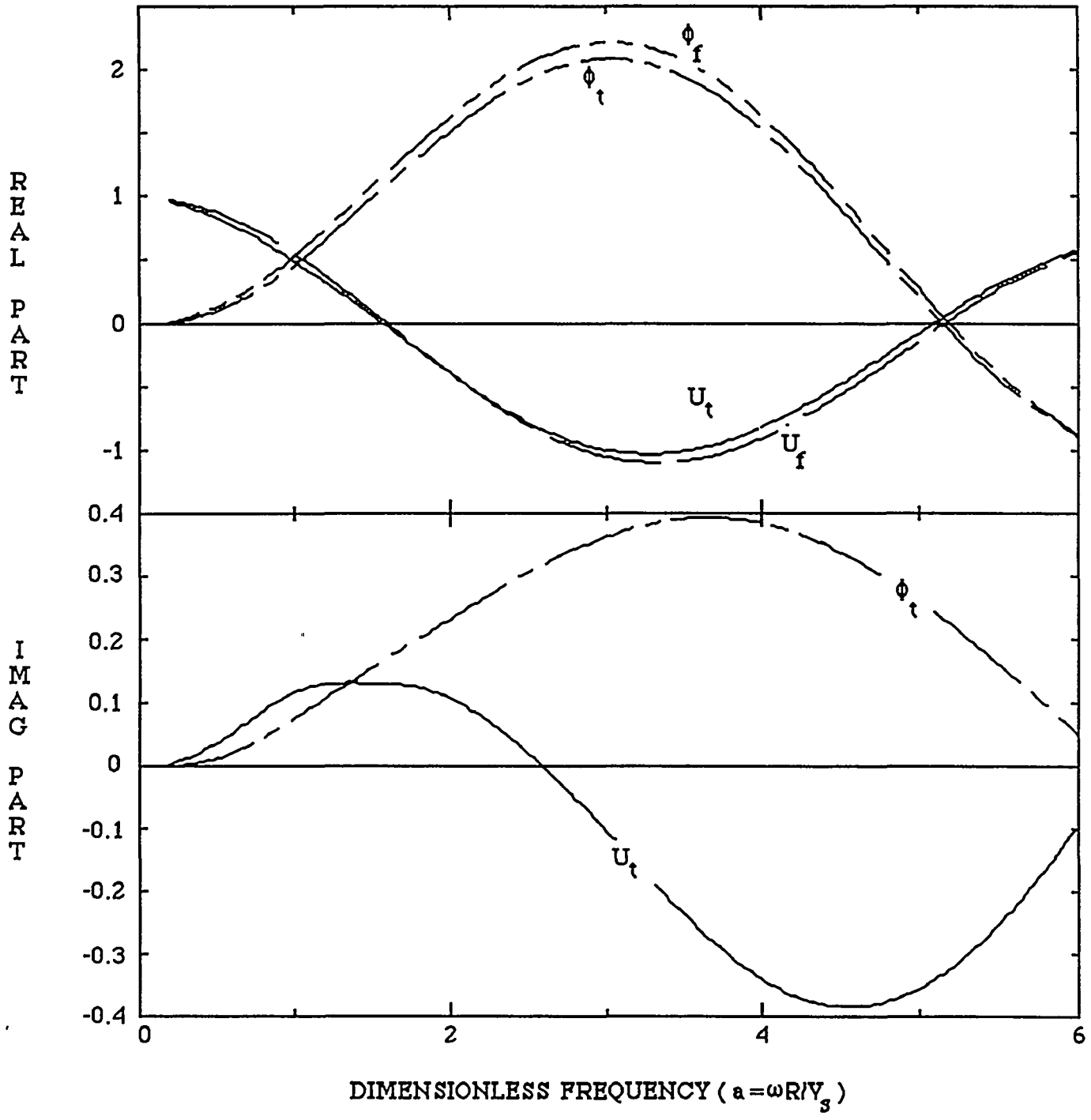

Figure H.2 Kinematic Interaction Effects on Fourier Components of Free Field Displacements - H/R = 1; D/R = 0; Beta = 0%

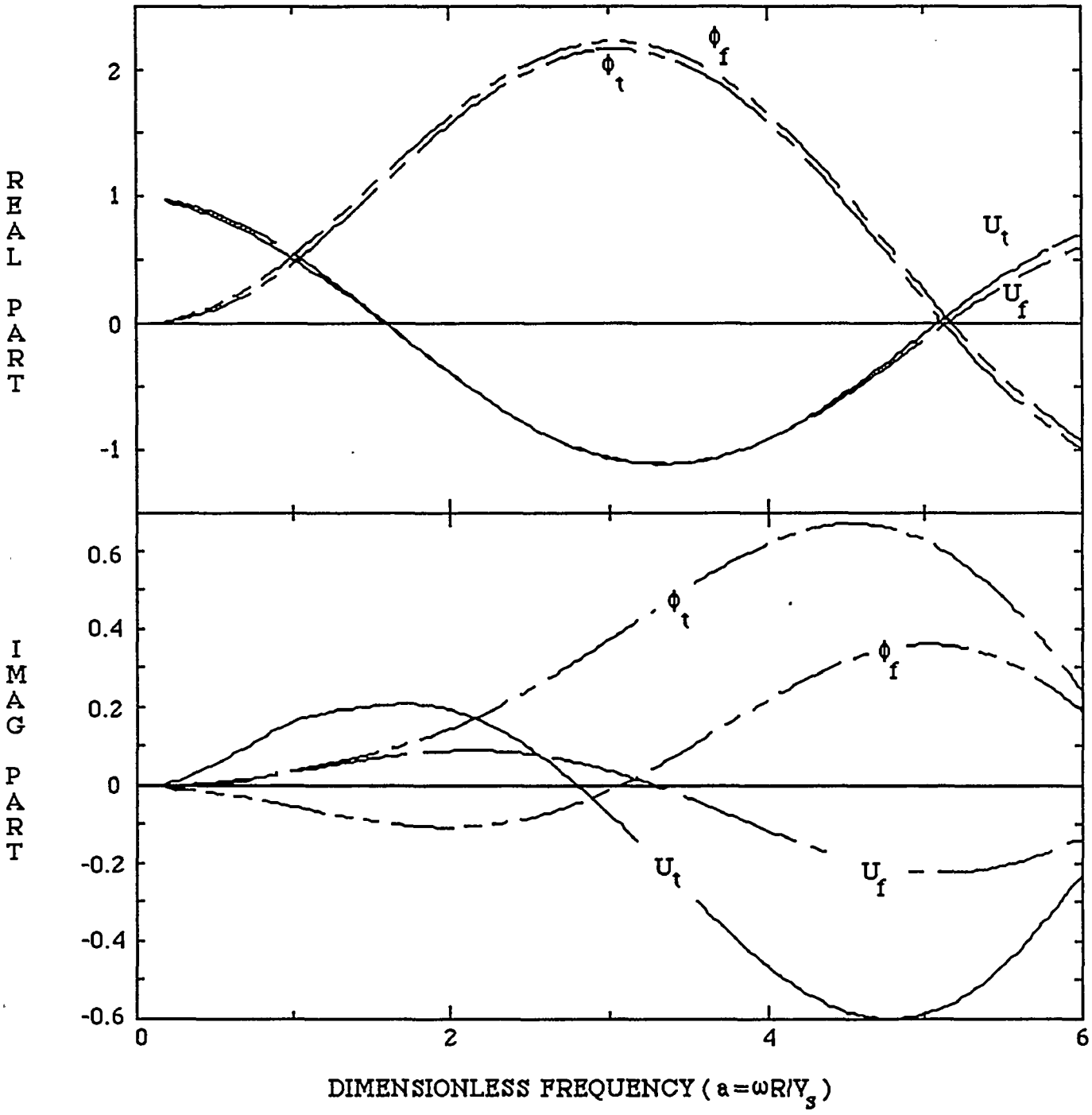

Figure H.3 Kinematic Interaction Effects on Fourier Components of Free Field Displacements - H/R = 1; D/R = 0; Beta = 0.05%

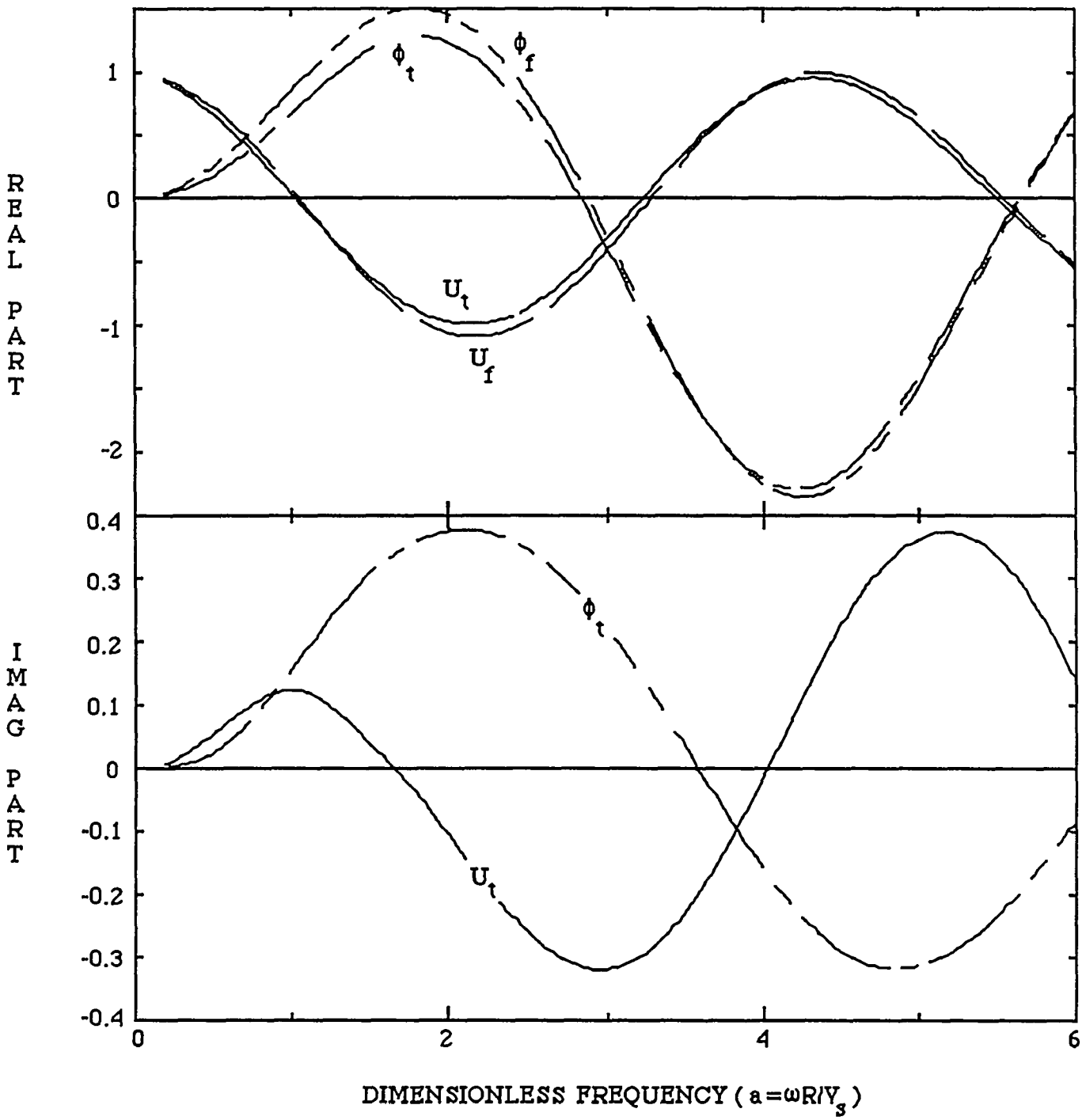

Figure H.4 Kinematic Interaction Effects on Fourier Components of Free Field Displacements - H/R = 1; D/R = 0.5; Beta = 0%

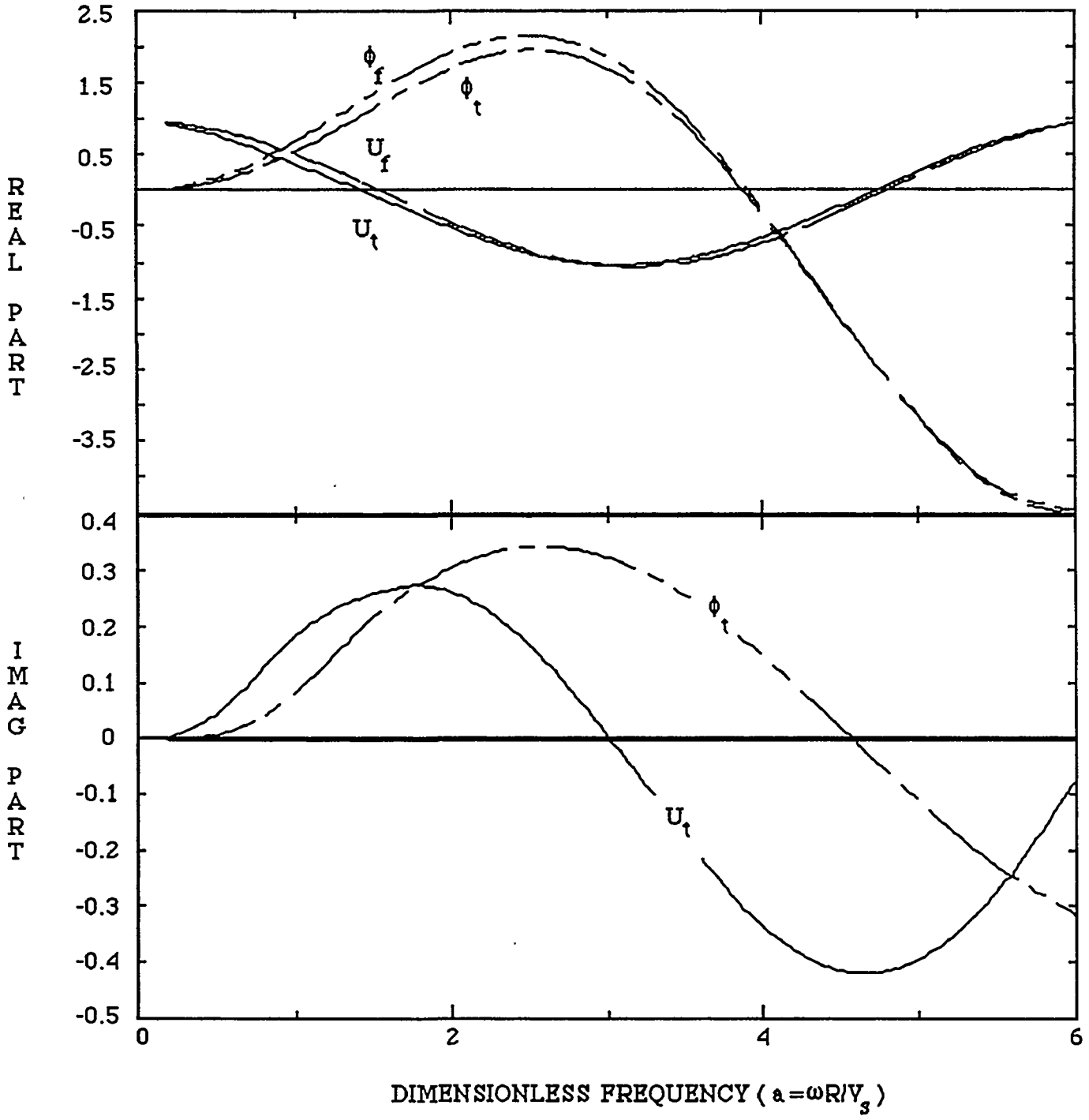

Figure H.5 Kinematic Interaction Effects on Fourier Components of Free Field Displacements - H/R = 0.5; D/R = 0.5; Beta = 0%

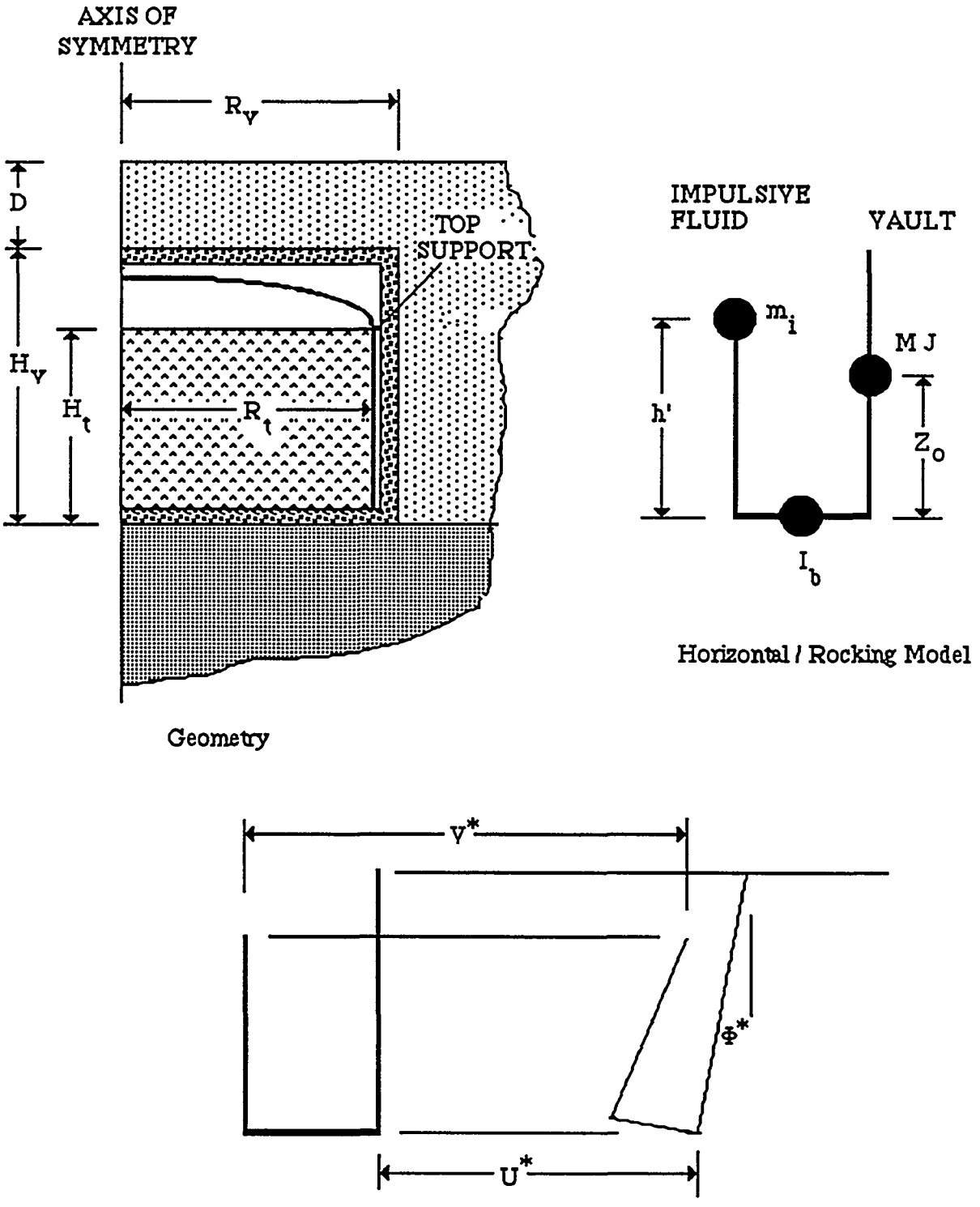

Figure H.6 Horizontal/Rocking SSI Model

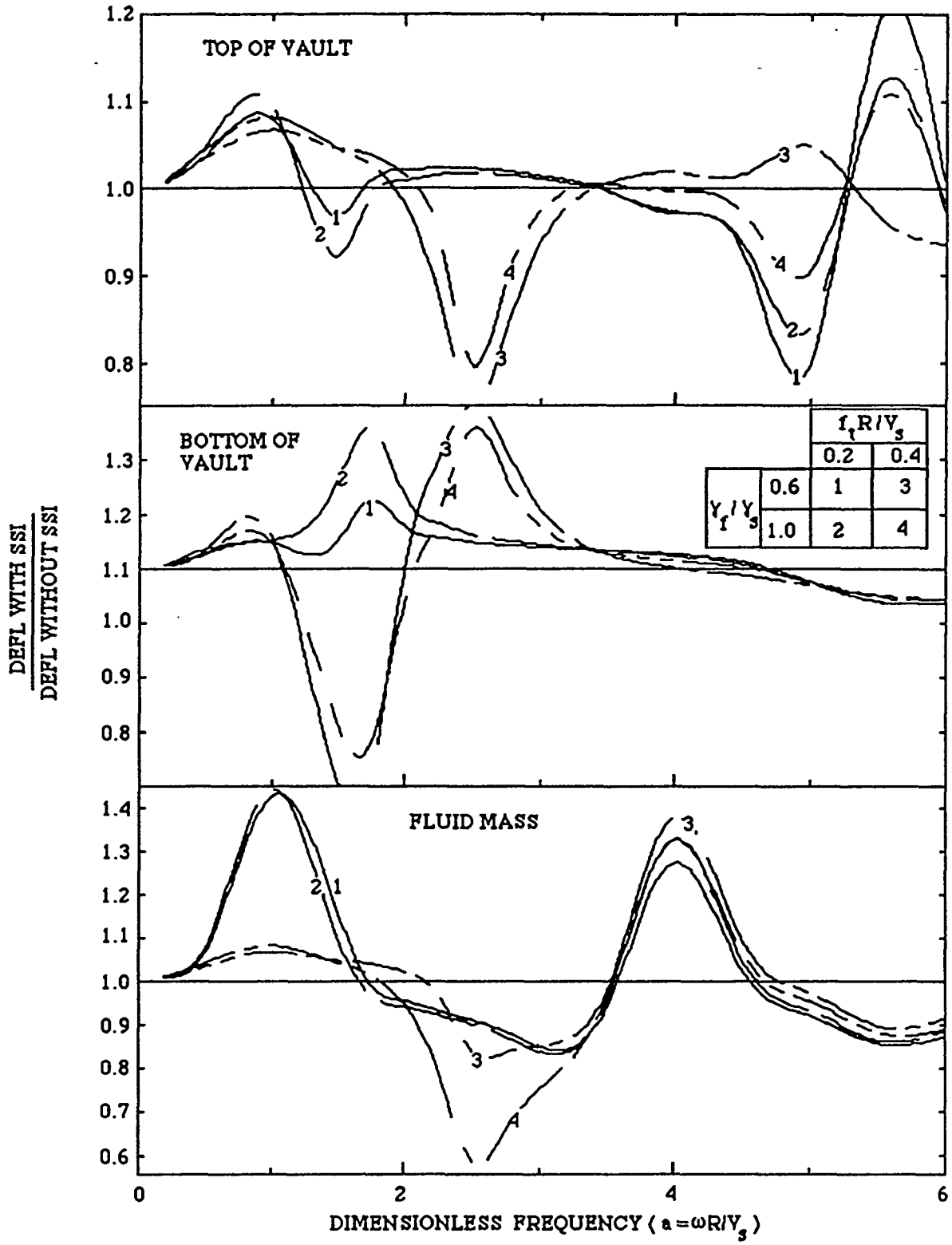

Figure H.7 Comparison of Vault and Fluid Displacements With and Without SSI Effects - $H_v/R_v = 1$; $D/R_v = 0$; Concrete Volume/Vault Volume = 0.3

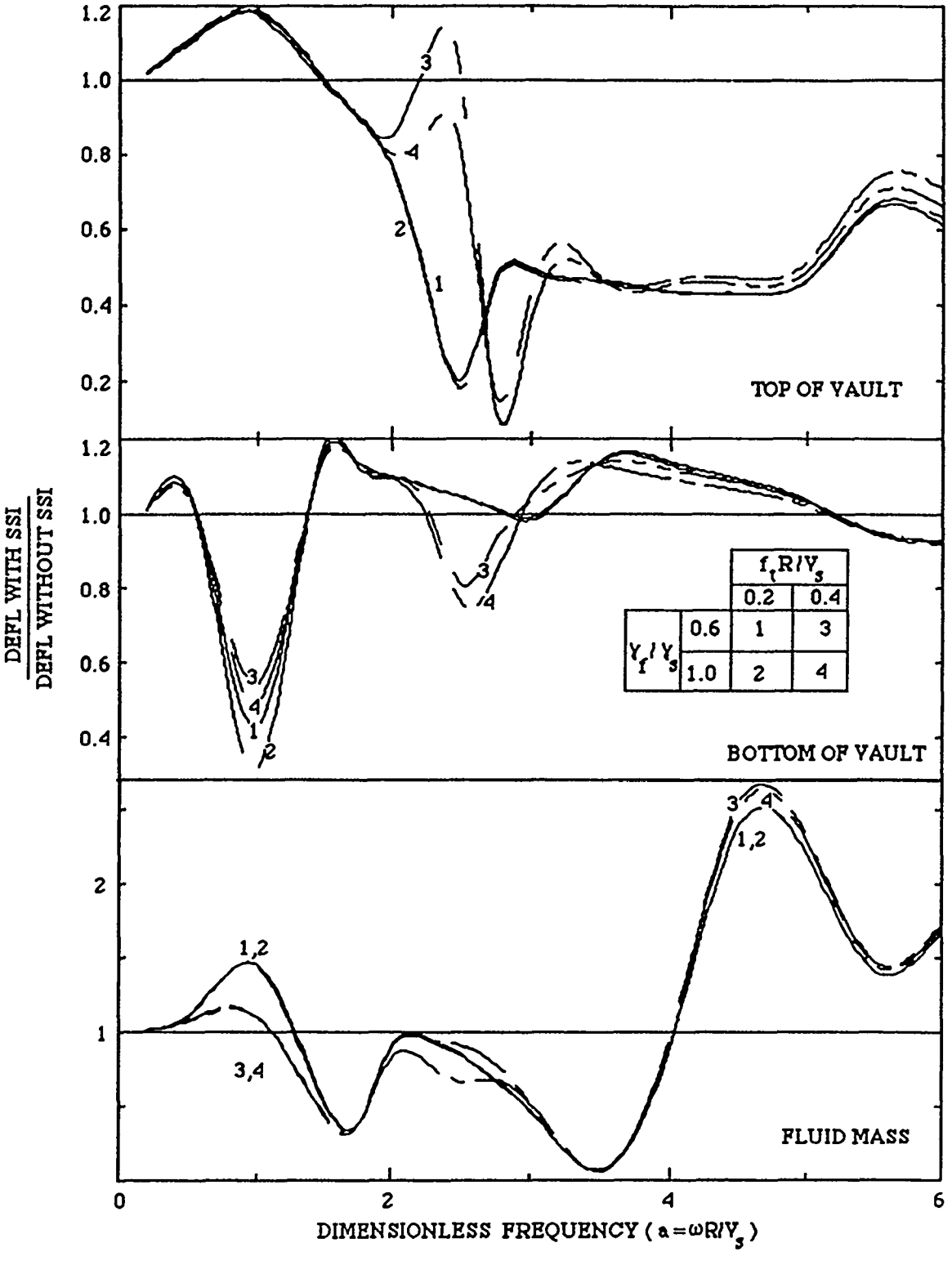

Figure H.8 Comparison of Vault and Fluid Displacements With and Without SSI Effects - $H_v/R_v = 1$; $D/R_v = 0.5$; Concrete Volume/Vault Volume = 0.3

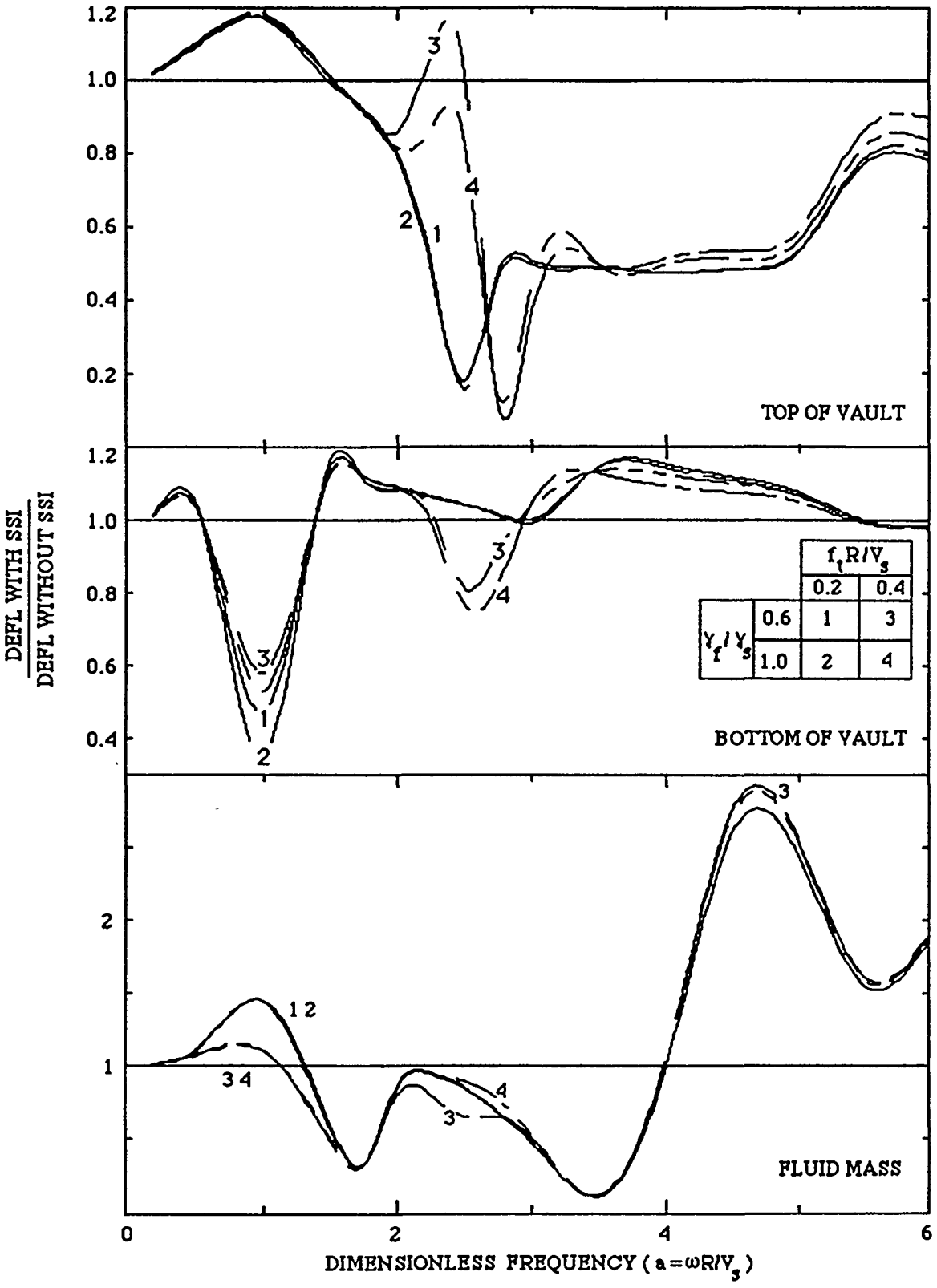

Figure H.9 Comparison of Vault and Fluid Displacements With and Without SSI Effects - $H_v/R_v = 1$; $D/R_v = 0.5$; Concrete Volume/Vault Volume = 0.2

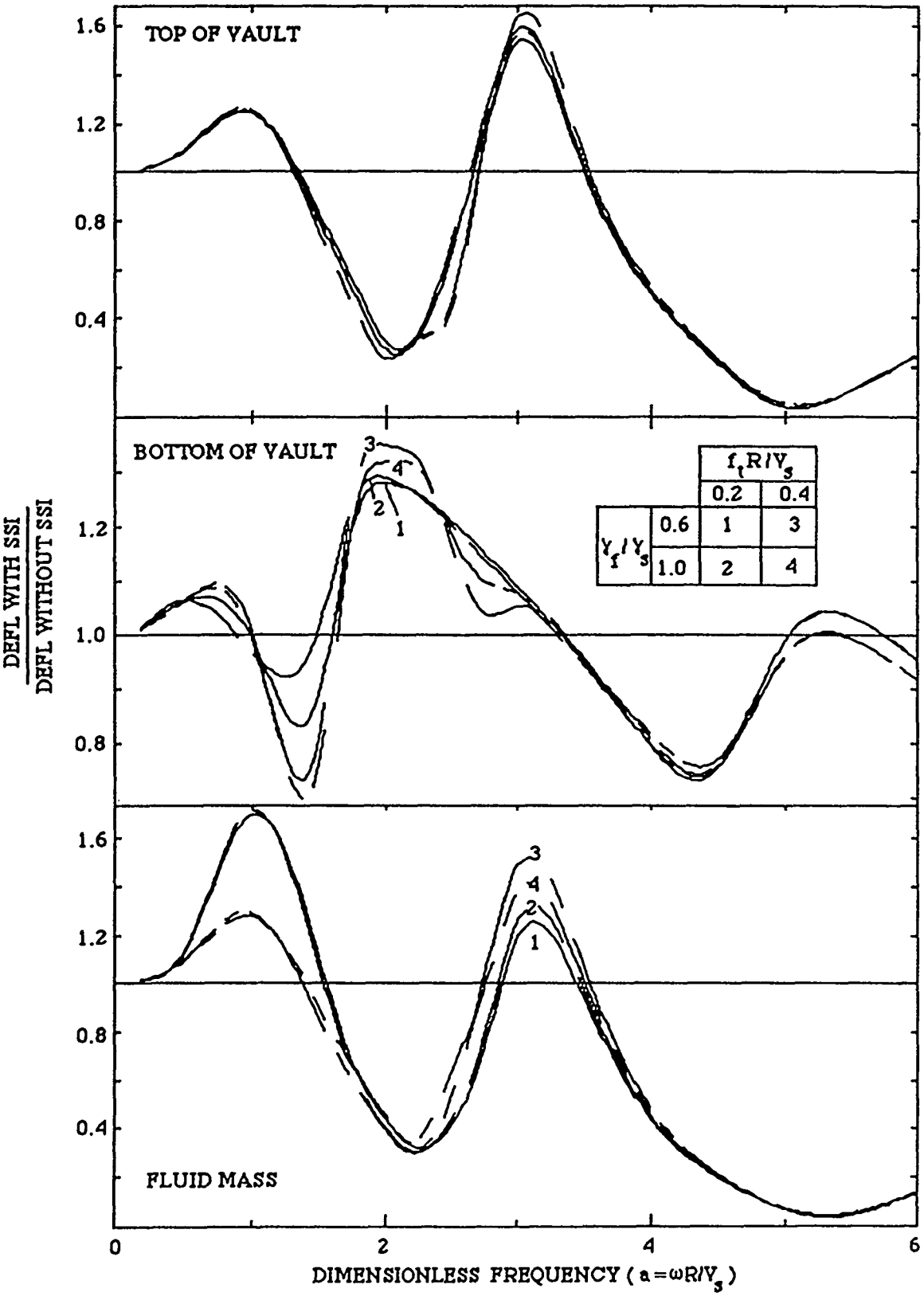

Figure H.10 Comparison of Vault and Fluid Displacements With and Without SSI Effects - H_V/R_V = 0.5; D/R_V = 0.5; Concrete Volume/Vault Volume = 0.3

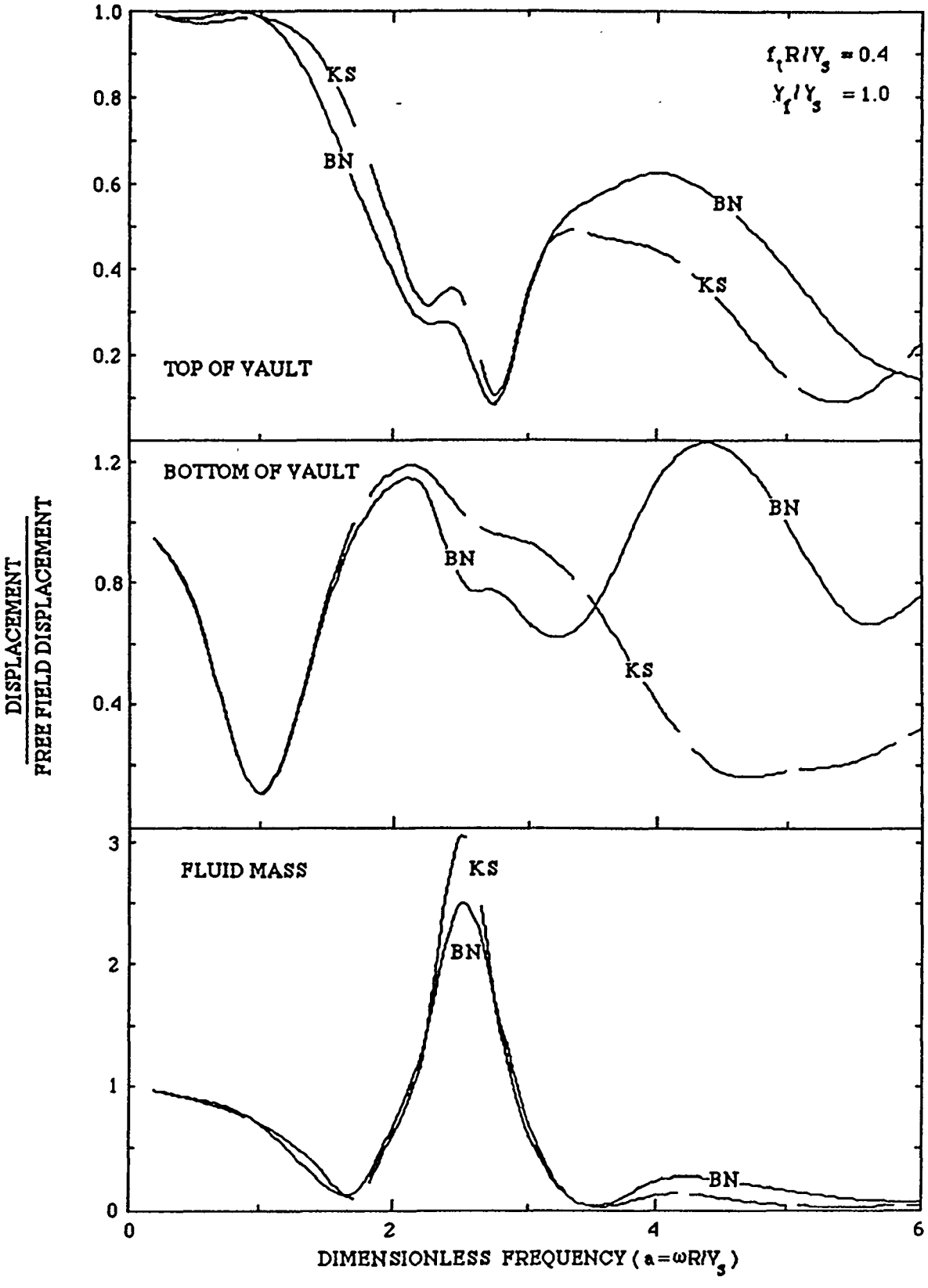

Figure H.11 Comparison Fluid Displacements Using Beredugo-Novak (BN) and Kausel (KS) SSI Models - $H_v/R_v = 1$; $D/R_v = 0.5$; Concrete Volume/Vault Volume = 0.3

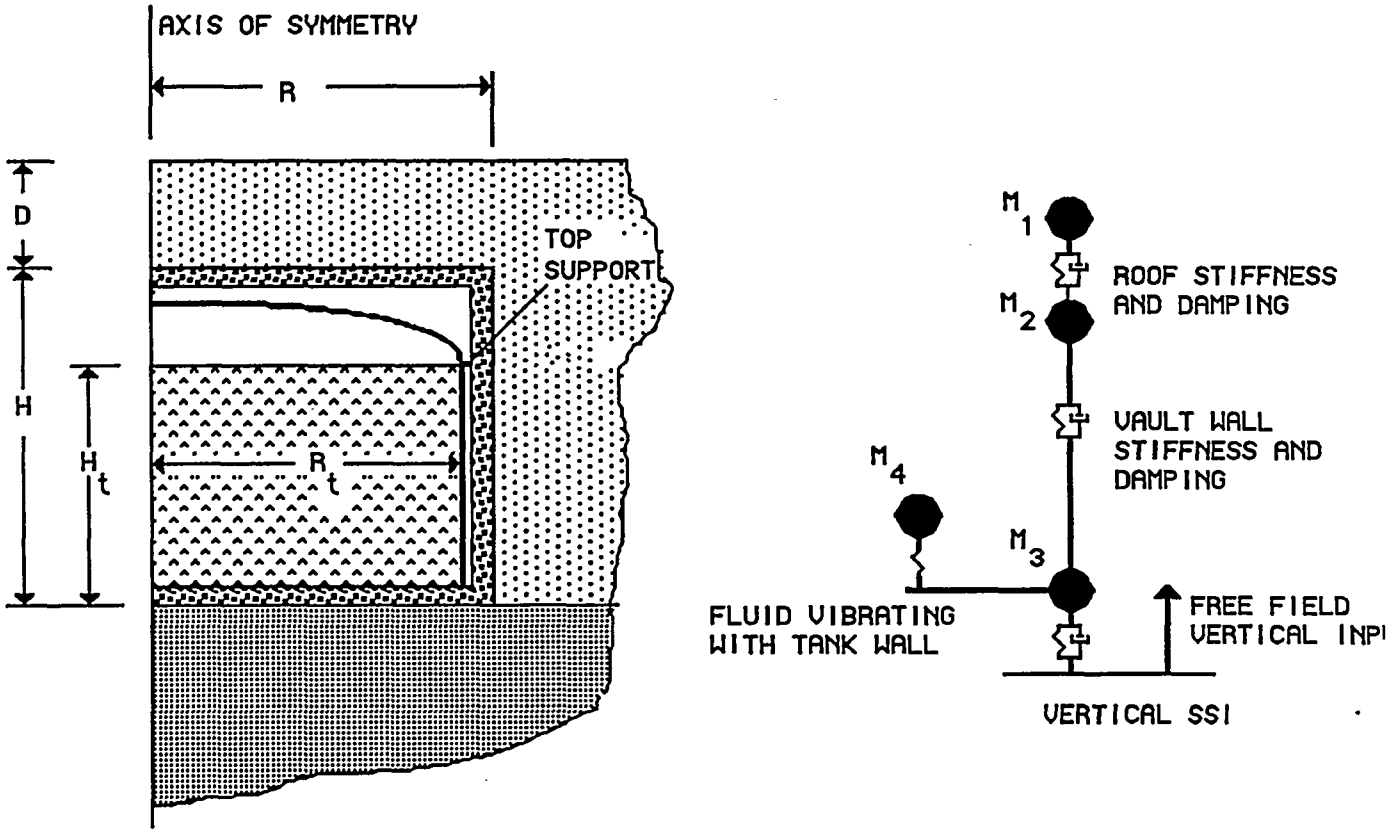

Figure H.12 Vertical Vault/Tank/Fluid Soil-Structure-Interaction Model

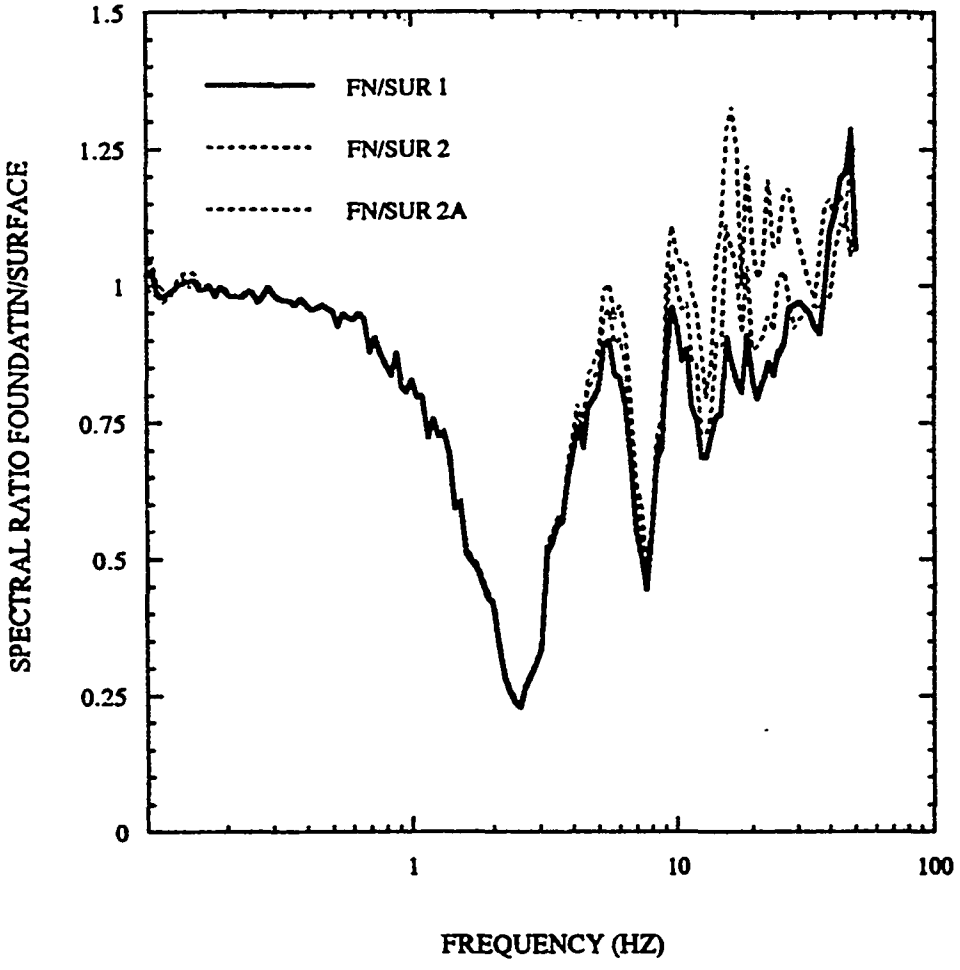

Figure H.13 Spectral Ratios Stiff Upper Soil Layer

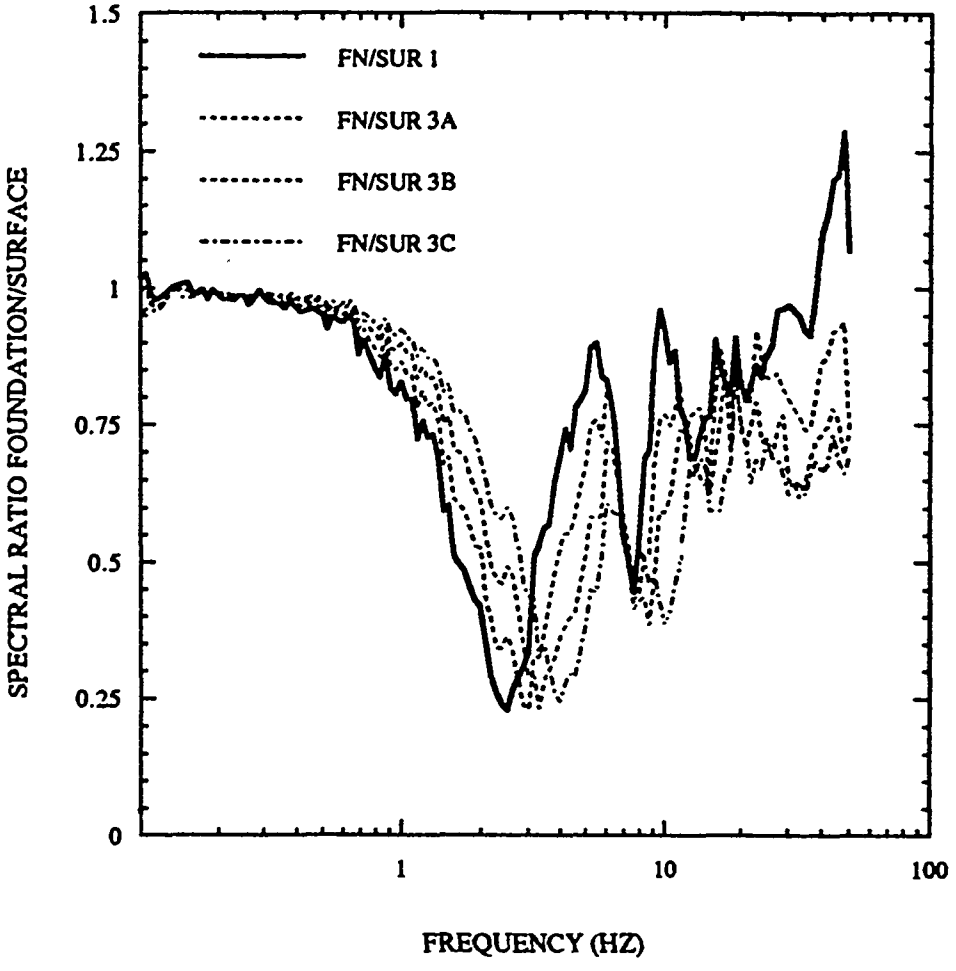

Figure H.14 Spectral Ratios Stiff Lower Soil Layer

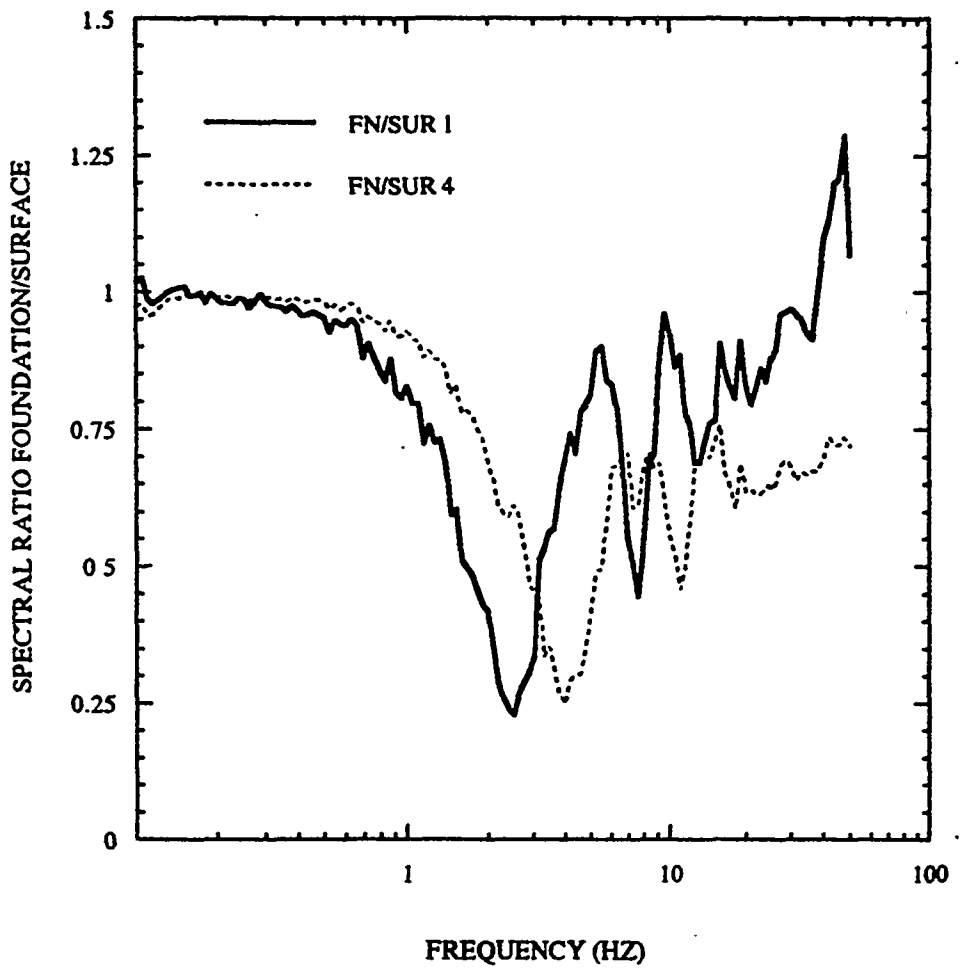

Figure H.15 Spectral Ratios Stiff Sands

APPENDIX I

EXAMPLE SEISMIC ANALYSIS OF AN UNDERGROUND DOUBLE-CONTAINMENT PIPING SYSTEM

I.1 SYSTEM DESCRIPTION

I.1.1 Layout

A buried pipe is designed to transfer hazardous fluids from tank A to tank B, as illustrated in Figure I.1. The pipe routing follows a straight line between the two tanks with expansion loops to accommodate potential expansion and contraction during its service lifetime.

Due to the hazardous nature of the fluid conveyed, the system consists of a double containment piping. The fluid is conveyed in an inner (core) pipe contained within an outer (jacket) pipe. The outer pipe is intended to contain the hazardous fluid in case of leakage from the inner pipe.

The system is sloped down from tank A towards tank B. The slope would allow hazardous fluids, which may leak into the outer pipe, to flow by gravity to collection and monitoring boxes placed at regular intervals along the buried line.

I.1.2 Support Configuration

The pipe and support configuration assumed for this example is illustrated in Figure I.1 with typical supports for the outer and inner pipes as shown in Figure I.2. The outer pipe is supported from piers on concrete pedestals. If the outer pipe is rigidly connected to the pedestal, the support may be considered an anchor. If the pipe is free to move longitudinally on the pedestal, the support may be considered a bilateral support. The piers are spaced to support the combined weight of the inner and outer pipe, prior to backfill. The soil bedding is placed and compacted such that negligible stress and

sag of the outer pipe occur under the normal dead weight of the backfill and surface line loads.

The inner pipe is supported by the outer pipe through cross bars (providing vertical downward restraint) and spacers (providing vertical and lateral restraints). At regular intervals, the inner pipe is anchored to the outer pipe (six degrees of freedom link between inner and outer pipe). These anchors control the differential axial position and growth of the inner pipe relative to the outer pipe.

I.1.3 Design Parameters

The general pipe configuration is typically selected based on the following procedure. The inner pipe diameter is selected on the basis of flow rate. The inner pipe wall thickness is selected on the basis of fluid pressure. The outer pipe diameter is then selected on the basis of diameter and thermal growth of the inner pipe. The outer pipe wall thickness is selected on the basis of soil backfill and surface live and dead loads, and fluid pressure which may develop from leakage of the inner pipe. The design parameters assumed for this example problem are summarized in Table I.1.

I.2 STRESSES FROM NONSEISMIC LOADINGS

In performing evaluations of the components of the buried piping system, stresses induced from all load conditions applied to the system in addition to seismic loads must be incorporated into the evaluation. Such typical loads include:

- dead load due to the weight of the piping system itself,
- static load applied to the outer piping due to soil cover and applied surface loads,

- deformations induced from long term ground deformation due to consolidation effects,
- applied pressures to the inner and outer piping (if any),
- temperature changes.

The methods of analyses for incorporating these effects into an evaluation are considered beyond the scope of this example problem. Stresses induced by soil cover and applied surface loadings can be estimated from procedures such as those described in Reference 7.4, while long term consolidation effects can be estimated by the appropriate methods of foundation engineering. Stresses from these various load components have, therefore, been assumed for purposes of this example to help clarify the stress combination procedures.

I.3 STRESSES FROM SEISMIC LOADINGS

I.3.1 Analysis Method

In this example, the piping system has been modeled using the configuration shown in Figure I.1 and the parameters listed in Table I.1. The gap between the two pipes is computed to be 1.28 inches. Using the spacer definitions shown in Figure I.2, the inner pipe is constrained by the outer pipe in the vertical downward direction by the vertical spacers and in both the horizontal and vertical directions by the bilateral spacers. At these spacer locations, the inner pipe is assumed to move axially with the outer pipe, which assumes that friction provided by the spacers is not overcome. The analysis procedure typically assumes axial continuity of displacement from which the axial and normal forces developed between the members can be determined. Using an appropriate friction factor (as described in Reference 7.32), the adequacy of this assumption can be checked. In this problem, a coefficient of friction at the spacers of 0.74 has been assumed (mild steel on mild steel with

little relative displacement).

At anchor points, the outer pipe is assumed to be fully constrained to the soil against all 6 degrees of freedom. At ordinary pedestal supports, the outer pipe is assumed to be constrained laterally as well as vertically downward to the soil. If a tiedown is used, the pedestal can be made to provide full vertical support.

As described in Section 7.5, the Winkler spring parameters are determined from site specific studies of the surrounding soil conditions. For this example, the Winkler spring stiffnesses were all selected as varying from 400 to 600 pounds per inch of length per inch of deflection.

The system characteristic parameter β is calculated using equation 7.13:

$$\beta = \left[\frac{k_o}{4\,E_b\,I_b}\right]^{1/4}$$

$$with \quad k_o = 400 \text{ to } 600 \text{ lb/in per in} \qquad \text{(I.1)}$$

$$E_bI_b = 28E6 \times 28.1 = 787E6 \text{ lb-in}^2$$

$$or \quad \beta = 1.89E\text{-}2 \text{ to } 2.09E\text{-}2/in$$

From the parameter β, the bearing span is calculated using equation 7.14 as

$$L_b = 125 \text{ in. to } 113 \text{ in.} \qquad \text{(I.2)}$$

As discussed in Section 7.5.5.2.5, the Winkler springs are spaced at a distance of approximately 1.5 diameters in the bearing span of length L_b on either side of each elbow, designated "Zone 1" in Figure I.3. Away from Zone 1, the spacing of the springs is increased to 20 diameters, as indicated by "Zone 2" of Figure I.3.

I.3.2 Seismic Wave Propagation

The analysis of the effects of seismic wave propagation on the buried system is performed in four steps:

Step 1: Calculation of maximum strain imposed by the seismic wave on the outer pipe.

Step 2: Calculation of the soil forces which react to the pipe displacements.

Step 3: Application of the free-field seismic displacements to the inner and outer piping model, and computation of the resulting forces, moments and stresses throughout the system.

Step 4: Comparison of results to allowables.

I.3.2.1 Strain In Outer Pipe

I.3.2.1.1 Axial Strain Due To Axial Force In Pipe

I.3.2.1.1(a) Theoretical Strain in Pipe

The maximum strain that can be transmitted to the buried pipe through shear from the surrounding soil is limited to $(\epsilon_a)_{sh}$ as indicated in Equation (7.3):

$$(\epsilon_a)_{sh} = \frac{F_{max} L_w}{4 E_{sct} A_p}$$

$$with \quad L_w = 750 \; ft \qquad (I.3)$$

$$E_{sct} = 28{,}000 \; ksi$$

$$A_p = 5.58 \; in^2$$

The maximum force per unit length F_{max} is calculated as indicated in Equation (7.4):

$$
\begin{aligned}
F_{max} &= (\pi D)[C_a + \sigma_n \tan(\phi_a)] \\
where\ \sigma_n &= [\gamma H(1 + K_o)/2] + (W_p/\pi D) \\
with\ \gamma &= 120\ lb/ft^3 \\
H &= 5\ ft \\
K_o &= 0.5\ to\ 1.0 \\
W_p &= (19.42 + 10.96)\ lb/ft \\
D &= 6.625\ in
\end{aligned}
\qquad \text{(I.4)}
$$

Hence

$$
\begin{aligned}
\sigma_n &= 3.2\ to\ 4.2\ psi \\
and\ F_{max} &\simeq 60\ to\ 70\ lb/in \\
Therefore\ (\epsilon_a)_{sh} &= 0.08\%\ to\ 0.10\%
\end{aligned}
$$

I.3.2.1.1(b) Maximum Strain In Soil

For this example, the maximum axial ground strain is calculated using Equation 7.1 for a dominant shear wave:

$$
\begin{aligned}
(\epsilon_a)_{max} &= \pm(PGV)/\alpha_\epsilon C \\
with\ PGV &= 15\ to\ 25\ in/\text{sec} \\
\alpha_\epsilon C &= 2.0\ x\ 2000\ fps\ (\alpha_\epsilon = 2.0\ from\ Table\ 7.1) \\
therefore\ (\epsilon_a)_{max} &= 0.03\%\ to\ 0.05\%
\end{aligned}
\qquad \text{(I.5)}
$$

I.3.2.1.1(c) Maximum Strain In Pipe

The maximum strain in the pipe (0.08% to 0.10%) cannot exceed the maximum strain in the soil (0.03% t 0.05%) as indicated by Equation I.5:

$$
(\epsilon_a)_{max} \leq (\epsilon_a)_{sh} \qquad \text{(I.6)}
$$

and therefore

$$
(\epsilon_a)_{max} = 0.05\%
$$

I.3.2.1.2 Axial Strain Due To Bending Of Pipe

The maximum curvature of the ground due to wave propagation is provided by Equation 7.5:

$$(\kappa) = \pm PGA/(\alpha_\kappa C)^2$$
$$with \quad PGA = 80\ in/\sec^2 \qquad (I.7)$$
$$(1/\alpha_\kappa C)^2 = 1E\text{-}7\ \sec^2/in^2\ (\alpha_\kappa = 1.0\ from\ Table\ 7.1)$$
$$therefore \quad \kappa = 8E\text{-}6\ 1/in$$

For this example, assuming no structural discontinuities in the deflected shape of the pipe, the axial strain in the pipe top and bottom fibers due to the curvature is:

$$\epsilon_b = (\kappa)(D/2) = (8E\text{-}6)(6.625/2) \simeq 0$$

I.3.2.1.3 Total Axial Strain

The total axial strain in the outer pipe due to wave axial and bending effects is

$$\epsilon_t = \epsilon_{max} + \epsilon_b = 0.05\%$$

I.3.2.2 Thermal Simulation Of Seismic Wave

The piping and soil stiffness are modeled as described in Section 7.5.5. A pseudo temperature increase $dT_{seismic}$ is applied uniformly to the outer pipe to simulate the seismic wave strain $(\epsilon_a)_{max}$ imposed by the soil. This is done to simplify the analysis and generally leads to conservative estimates of pipe loads.

$$dT_{seismic} = (\epsilon_a)_{max}/\alpha$$
$$dT_{seismic} = 0.05\%/6.3E\text{-}6\ in/in/^\circ F$$
$$= 79^\circ F$$

I.3.3 Seismic Inertia

As a result of the dynamic loadings, the inner pipe is subjected to inertial forces. The effect of the inertial forces on the piping can be calculated in several ways.

I.3.3.1 Upper Bound Estimate

The inertial movement of the inner pipe is limited to the gap between inner and outer pipe. An upper bound of seismic inertia stresses can be obtained when the stiffest span of inner pipe is deflected by an amount equal to the gap.

I.3.3.2 Inner Pipe Model

A model of the inner pipe, excluding the outer pipe, may be analyzed subjected to the 5% damped ground response spectra. Inner pipe spacers are treated as supports to ground. The three directional responses are combined by SRSS to obtain the resultant inertial response.

I.3.3.3 Inner and Outer Pipe Model

The combined model of the inner and outer pipe, as described in Section I.3.1 and used earlier to compute seismic wave effects, may be subjected to the 5% damped ground response spectra. The results of the analysis with the combined model are valid if the outer pipe displacements (which are constrained by the soil stiffness springs) are practically zero.

The combined inner-outer pipe model was used for this example. The 5% ground response spectra used in this example is based on NRC Regulatory Guide 1.60, anchored at 0.20g in the horizontal and vertical directions. Three directional responses are combined by SRSS to obtain the resultant inertial response.

I.3.4 Seismic Anchor Motion

I.3.4.1 Short Term Oscillatory Effect

The seismic event generates oscillatory vibration of the tanks, with respect to the ground, as illustrated in Figure I.4(b). For this example, the maximum differential oscillatory movement between the tanks and the adjacent supports of the outer pipe is assumed to be ±0.2" in both horizontal directions.

The oscillatory vibration is applied as a 0.2" lateral displacement at the terminal anchor points (tanks A and B) of the combined pipe-soil model, and a zero displacement at the outer pipe anchor points. The two directional responses are combined by SRSS to obtain the resultant anchor motion response.

I.3.4.2 Long Term Settlement Effect

The seismic event may be followed by a gradual settlement of soil which results in differential movement between the tanks and the adjacent outer pipe supports, as illustrated in Figure I.4(c). For this example, the absolute settlement is assumed to be 6" down at the tanks and 4" down along the buried pipe. This differential settlement is therefore 2" down at the tanks relative to the buried pipe. This differential settlement is applied as a 2" downward vertical displacement at the terminal anchor points (tanks A and B) of the combined pipe-soil model.

I.4 EVALUATION OF RESULTS

I.4.1 Individual Load Cases

Table I.2 summarizes the maximum stresses for the individual load cases.

I.4.2 Combined Stresses and Allowables

Table I.3 summarizes the combined primary and secondary

stresses. The combined stresses are then compared to the corresponding allowables.

Table I.1 Design Parameters

	Inner Pipe	Outer Pipe
Material	A312-304L Stainless Steel	A106-Grade B Carbon Steel
Size	3" Sch. 40	6" Sch. 40
Diameter	3.500"	6.625"
Thickness	0.216"	0.280"
Linear Weight	10.96 lb/ft with fluid	19.46 lb/ft empty
Internal Pressure	200 psi	Atmospheric
Operating Temperature	180°F	50°F
Construction Code	ASME B31.3	ASME B31.3
S_y Ambient	25,000 psi	35,000 psi
S Ambient	15,700 psi	15,000 psi
E	28.3E6 psi	29.5E6 psi
α	9.3E-6 in/in/°F	6.3E-6 in/in/°F

Table I.2 Maximum Axial Stresses for Individual Load Cases (ksi)

Load Case	Example Section	Inner Pipe	Outer Pipe
Pressure	I.2	$pD_0/4t_n$=0.8 ksi	1.2 ksi
Deadweight	I.2	$0.75iM_{DW}/Z$=2.4 ksi	3.0 ksi
Thermal Expansion	I.2	iM_c/Z=12.8 ksi F_C/A=0.0	0.4 ksi 0.0
Long Term Soil Settlement	I.2	0.0	0.0
Wave Passage (Pseudo-Thermal)	I.3.2.2	iM_{WP}/Z=1.7 ksi F_{WP}/A=0.0	7.7 ksi 0.5 ksi
Seismic Inertia	I.3.3	$0.75iM_I/Z$=5.3 ksi	0.8 ksi
Short Term Oscillatory SAM	I.3.4.1	iM_{O-SAM}/Z=5.0 ksi F_{O-SAM}/A=0.0	14.4 ksi 0.0
Long Term Settlement SAM	I.3.4.2	iM_{DISP}/Z=3.9 ksi F_{DISP}/A=0.0 ksi	6.7 ksi 0.0

Table I.3 Combined Primary and Secondary Stresses and Corresponding Allowables (ksi)

$PDo/4t_n + .75i(M_{DW} + M_I)/Z \leq \min(2S, 2S_y)$ $0.8 + 2.4 + 5.3 = 8.5 < \min(3 \times 15.7, 2 \times 25.0)$ inner pipe $1.2 + 3.0 + 0.0 = 4.2 < \min(3 \times 15.0, 2 \times 35.0)$ outer pipe
$\epsilon_t = K_S\ \sigma e/E < 2\%$ (SS), 1% (CS) $6.6 \times 8.5/28.3E3 = 0.2\% < 2\%$ inner pipe $5.0 \times 4.2/29.5E3 = 0.07\% < 1\%$ outer pipe
$(F_{DISP} + F_c)/A + i\ (M_{DISP} + M_c)/Z \leq \min(3S, 2Sy)$ where DISP represents the SRSS of WP and O-SAM $(0.0^2 + 0.0^2)^{1/2}+0.0+(1.7^2+5.0^2)^{1/2}+12.8=18.1<\min(3x15.7,2x25.0)$ inner pipe $(0.5^2+0.0^2)^{1/2} +0.0+(7.7^2+14.4^2)^{1/2}+0.4=17.2<\min(3x15.0,2x35.0)$ outer pipe
$(F_{DISP}+F_c)/A+i(M_{DISP}+M_c)/Z \leq \min(3S,2Sy)$ Where DISP represents the post-wave settlement SAM $0.0+0.0+3.9+12.8=16.7<\min(3x15.7, 2x25.0)$ inner pipe $0.0+0.0+6.7+14.4=21.1<\min(3 \times 15.0, 2 \times 35.0)$ outer pipe
$\epsilon_t = K_s\ \sigma_e/E < 4\%, 2\%$ (branch, tee) $6.6 \times 3.9/28.3E3 = 0.09\% < 4\%$ inner pipe $5.0x6.7/29.5E3 = 0.1\% < 4\%$ outer pipe

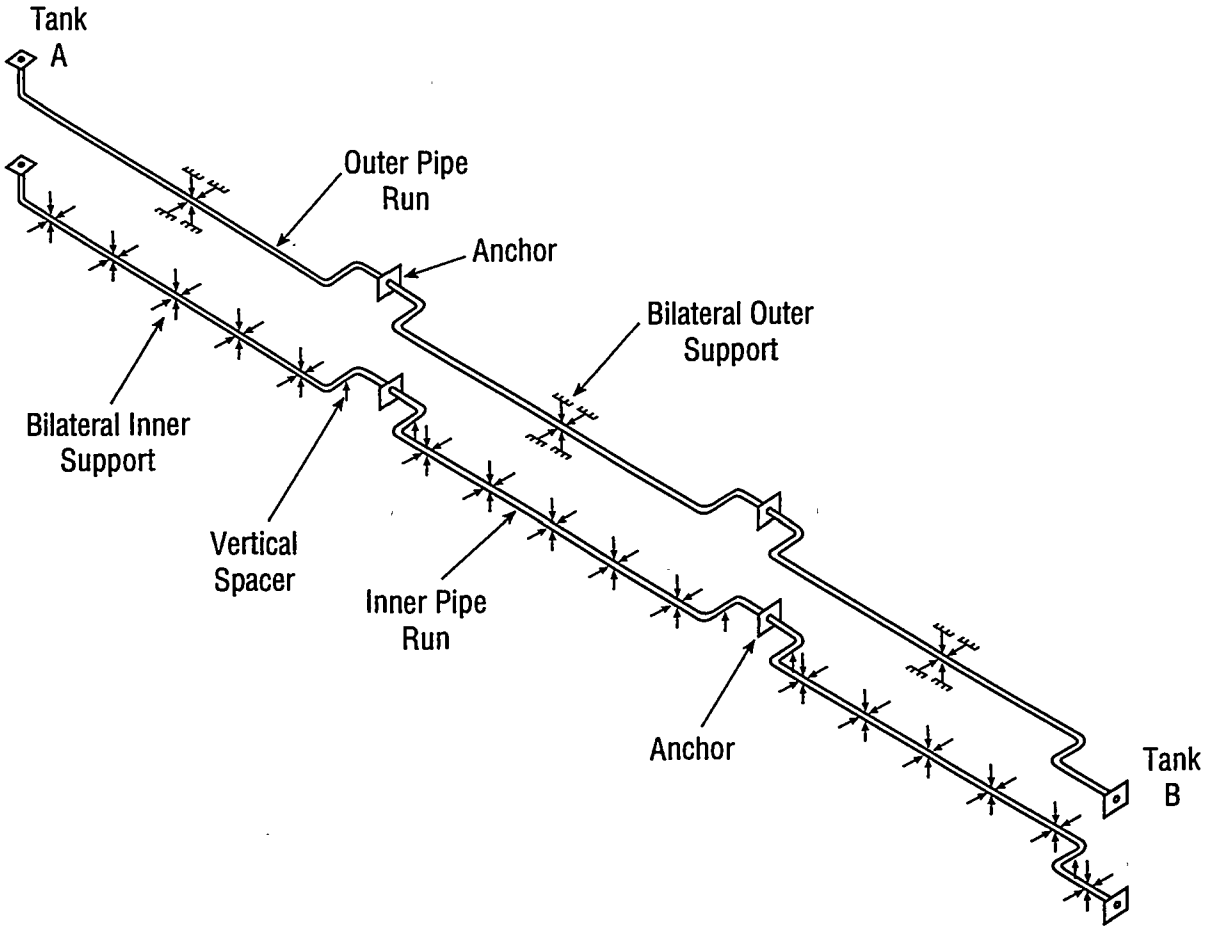

Figure I.1 Layout of Buried Double Containment Transfer Line (Inner and Outer Pipe are Shown Side-By-Side for Clarity)

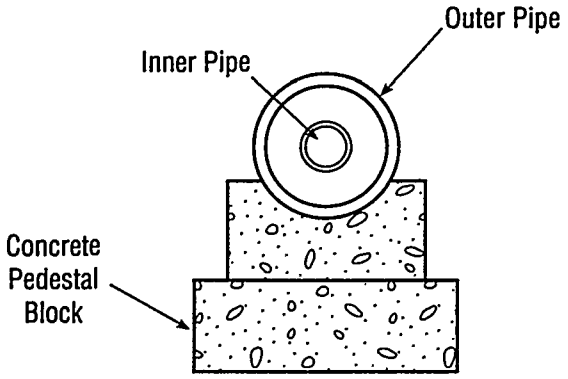

(a) Concrete Pedestal Support

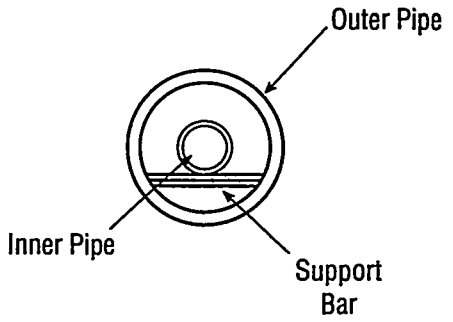

(b) Vertical Spacer for Support of Inner Pipe

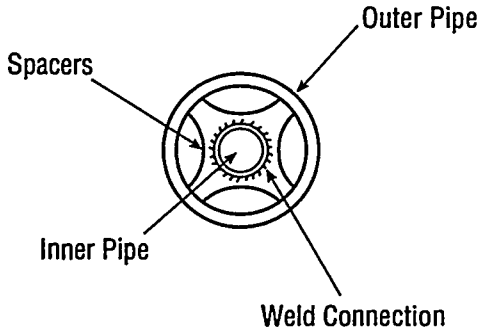

(c) Bilateral Support of Inner Pipe

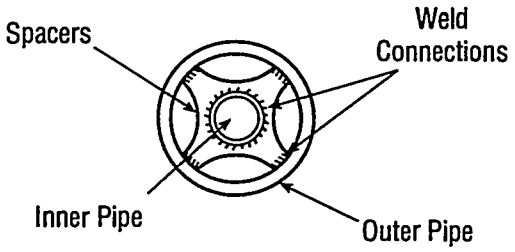

(d) Anchor Support of Inner Pipe

Figure I.2 Typical Support Systems for Inner and Outer Pipe

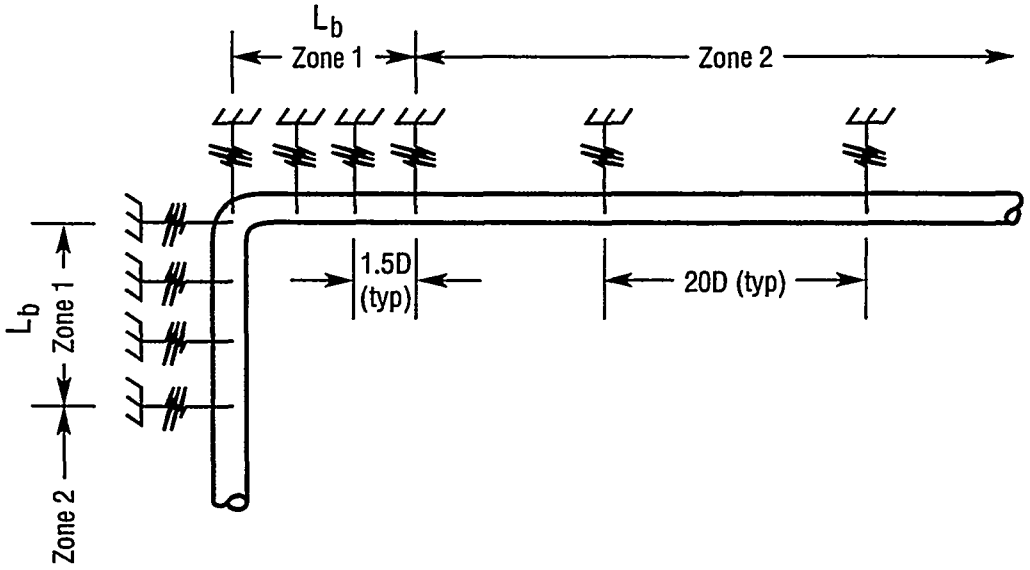

Figure I.3 Modeling of Soil Stiffness (Each Spring Depicts a Stiffness in Three Directions: Two Lateral and One Axial)

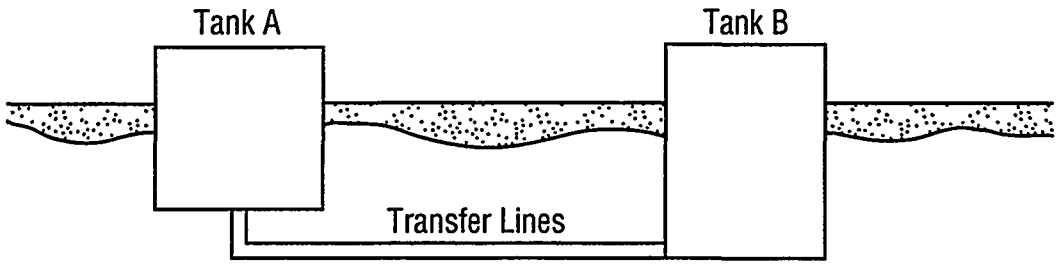

(a) Original Positions

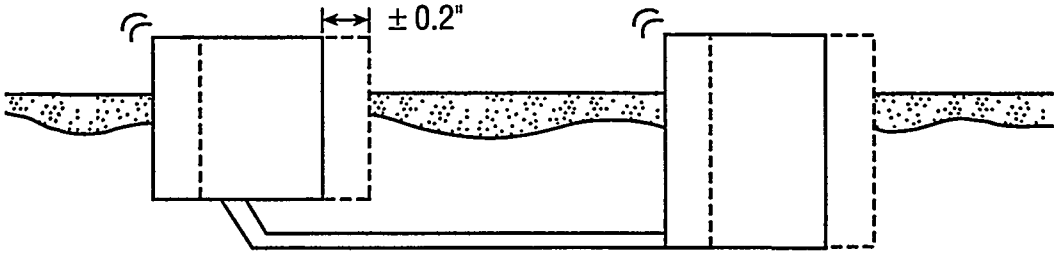

(b) Oscillatory Effects

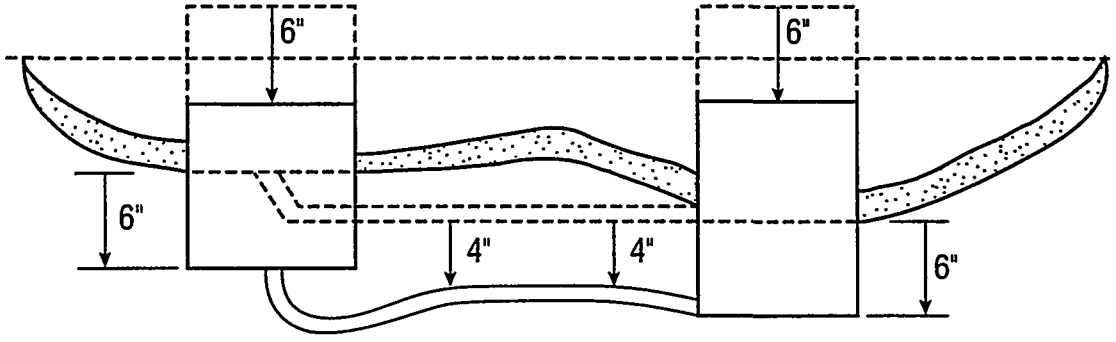

(c) Settlement Effects

Figure I.4 Soil Oscillatory and Settlement Effects